University of Ferrara
University of Bologna - University of Brescia - University of Parma

PH.D. DEGREE IN GEOTECHNICAL ENGINEERING (XXVII)
January, 2015

DETERMINATION of CYCLIC RESISTANCE of CLEAN SANDS FROM CONE PENETRATION TEST BASED ON STATE PARAMETER

A thesis presented by:

Chiara Prearo

Approved by:

Prof. Vincenzo Fioravante
Supervisor

Daniela Giretti, Phd
Co-Supervisor

Prof. Alberto Mazzucato
Head of the Ph.D. Programme in Geotechnical Engineering

To my family and to Enrico

I've learn a lot about myself, as well as about sand, along the way

SUMMARY

LIST OF FIGURES

LIST OF TABLES

Abstract

Cyclic liquefaction is a phenomenon during which granular uncemented saturated soils (gravel, sand and low plasticity silt) lose much of its strength and stiffness for a short interval of time, but long enough to cause significant failures.

The occurrence of liquefaction depends on the cyclic shear loading induced by an earthquake and on the cyclic resistance of the soil; the latter, due to the difficulties in obtaining undisturbed samples of most liquefiable soils, is deduced from field test results interpreted via empirical correlations which provide the link between cyclic resistance and various test indices. CPT based methods of liquefaction assessment are the most used in practice engineering

The cone penetration resistance q_c and the cyclic resistance CRR of a soil depend on the material properties and the state of the soil (stress level and density). The latter two quantities can be expressed by the state parameter ψ, which is an indicator of the direction of volumetric strains (dilation or contraction) during shearing; the amount of the volumetric strains govern the stress variation respect to the initial level of stress.

In these thesis a link between the cone resistance and the cyclic resistance has been defined using the results of centrifuge CPT tests and cyclic undrained triaxial tests carried out using two well none Italian and Japanese sands: Ticino (TS4) and Toyoura (TOS).

The results of cone penetration tests evidenced the existence of a simple relationship between the normalised cone resistance, Q_p and the state parameter ψ (Jefferies and Been, 2006).

The cyclic triaxial test results have been interpreted to define a correlation between the state parameter and the cyclic resistance ratio CRR at a given number of cycles N, for the two studied sands.

Finally results of centrifuge and triaxial tests have been combined to deduce a direct relationship between the normalised cone resistance and the cyclic resistance ratio.

Chapter 1

1 Litterature Review

1.1 Introduction to undrained soil behavior

After Niigata earthquake in 1964, which caused a lot of building damages due to liquefaction, a lot of studies were performed by many authors in order to understand cyclic behavior of sands [Seed and Lee, 1966; Ishihara, 1996; Hyodo, 1991;Yoshimi, 1984; Vaid, 1985, 1995; Sladen, 1985; Tatsuoka, 1984; Toki, 1986, 1993].

Hystorically the ″liquefaction″ of saturated sand was defined as a loss of strenght caused by cyclic loading and it was usually related to geological considerations and surface evidances (sand boils, large deformation or fracture of the ground, etc.).

Castro (1969) defined liquefaction as the strain-softening and collapse of a loose sand to an ultimate state of constant effective stress and deformation. Seed at al. (1983), using the results of an extensive laboratory testing, defined liquefaction as essentially the condition of zero effective stress due to cyclic loading. At zero effective stress a granular soil becames very soft and develops large deformations during cyclic loading. Ishihara (1993) suggests that liquefaction can be defined in terms of the magnitude of cyclic stress ratio required to produce a given level of strain.

Macking reference of the soil behavior in undrained shear, the following definitions of liquefaction are suggested [Robertson, 1994]:

(i) flow liquefaction requires strain-softening behavior response in undrained loading and the trigger to cause collapse can be either monotonic or cyclic.

This type of failure seldom occurs in level ground, as it requires that in-situ shear stress is greater than undrained residual or steady-state shear strength. Cases in which flow liquefaction can arise, are slope or retaining walls: in these situations fast failure occurs when the dynamic load is larger than the static shear stress; on the contrary, with smaller static shear stress, a large excitation is needed in order to start flow liquefaction.

Flow liquefaction occurs in loose sands submitted to high stresses and it is associated to a fast failure with a rapid increase of both deformations and pore pressures.

(ii) cyclic liquefaction and cyclic mobility [Castro, 1975; Casagrande, 1976] might succeed in sands with strain-hardening behavior; in these conditions the failure mechanism will be mainly the consequence of an accumulation of strains as a result of pore pressure increasing.

The cyclic liquefaction requires undrained cyclic loading where stress-reversal or zero shear stress can develop (i.e. in-situ gravitational shear stress is low compared to cyclic shear stress) with a sufficient cyclic load to allow the effective confining stress to essentially reaches zero (Figure 1.1 a).

When the effective stress is zero no shear stress exists and a soft initial stress-strain response can progress, resulting in large deformations. Soil will strain-harden with the increase of shear strain and the failure condition is only a temporary state.

Cyclic liquefaction can occur in sands provided size and duration of cyclic loading is sufficiently large. The more the sand is dense the more the size and duration of cyclic loading will be large and hence, the condition of zero effective confining stress may not always be achieved. Generally, deformations are large when the effective stress is zero but they tend to stabilize when cyclic loading stops; on the contrary, a pore pressure redistribution can occur in soil deposit and sand might experience strain-softening behavior.

Cyclic mobility requires undrained cyclic loading where stress is always greater than zero (i.e. no stress-reversal) and zero effective stress cannot develop (Figure 1.1 b).

It is usually associated to the development of small deformations that tend to stabilize during cyclic loading. It can occur in (i) all sands provided size and duration of cyclic

loading is sufficient large and no stress-reversal occurs or (ii) in dense sands with shear stress-reversal provided cyclic loading is not sufficient to cause zero effective stress. Robertson et al (1994) proposed to use a schematic flow chart reported in Figure 1.2, where cyclic behavior is firstly linked to monotonic behavior of sands.

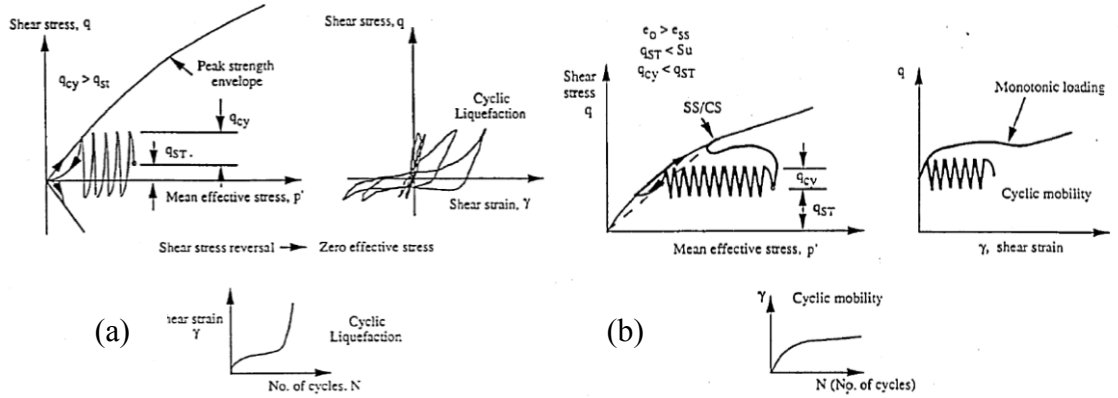

Figure 1.1- Schematic illustration of (a) cyclic liquefaction and (b) cyclic mobility

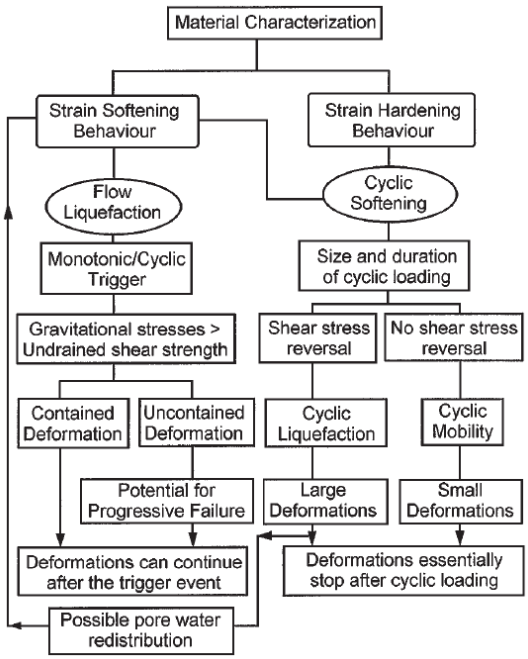

Figure 1.2- Suggested flow chart for evaluation of soil liquefaction [Robertson, 1994]

1.2 Introduction to in-situ static and dynamic penetration tests

1.2.1 Cone penetration tests

Since being developed in early ‘30s as a geological tool for stratigraphic purposes, the cone penetration test has attracted attention from the geomechanics point of view. The main advantage of the CPT is the interesting combination of a continuous data record with excellent repeatability and accuracy at relatively low cost.

The first cone penetrometers were built by Barentsen in 1932, at the Department of Public Works in Netherlands while the electric cone penetrometer was most likely developed in Berlin during the Second World War and, after, implemented during ‘80 in Netherlands [Lunne et al., 1997; Broms 1988]. The improvement in the instrumentation was continued in Canada by Campanella and his students [Campanella et al., 1983; Robertson and Campanella, 1983; Robertson et al., 1986; Robertson and Wride, 1998; Robertson, 2009].

The cone penetration test is conducted by pushing a penetrometer with a conical tip attached to the end of a series of rods into the ground at a constant rate (20 mm/s). The standard electronic cone penetrometer has a conical point with 60° apex angle and a projected cone base of 10 cm^2. The cone tip resistance and sleeve friction resistance are the basic readings of CPT results; the excess pore water pressure (u) can be obtained through a piezometer placed on or behind the cone tip. Commonly, the piezo-element of 5 mm is arranged above the cone and the pore pressure recorded at this location is denoted by u_2.

The tip recorded force Q_c divided by the projected area of the cone, A_c, produces the tip resistance q_c that must be corrected for the effect of the net area ratio, *a.* The tip resistance q_t is defined as:

[1.1] $$q_t = q_c - u_2(1-a)$$

Where: q_t is the tip resistance; it is equal to q_c in coarse-grained soil due to low pore water pressures generated during penetration around the cone;

$q_c = Q_c/A_c$ is the measured tip resistance;

a is the net area ratio function of the geometry of the cone areas.

Friction resistance, f_s, is obtained dividing the lateral measured force, F_s, by the surface area of the friction sleeve, A_s. The normalized friction ratio is defined as follow:

[1.2] $$F_R = \frac{f_s}{q_t - \sigma_{v0}} 100 \quad (\%)$$

Since f_s is measured about 10 cm behind the cone tip, the values of f_s and q_t are not recorded at the same depth, i.e. f_s should be shifted down in order to consider the distance between the cone tip and the center of the friction sleeve.

The location of the various sensors placed on standard cone penetrometer is illustrated in Figure 1.3.

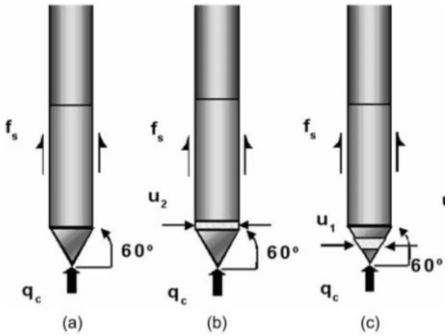

Figure 1.3- Types of cone penetrometers and measurements location: (a) eletric cone penetrometer, (b) piezocone penetrometer (filter behind the tip), (c) piezocone penetrometer (mid face filter)

1.2.2 Standard penetration tests

The test originated in the la 1930s in the USA and was first standardized in 1958 under ASTM D 1586-58T. It is currently covered by several national and regional standards that fully comply with the ISSMGE IRTP published in 1988 at the 1st International Symposium on Penetration Tests [Decourt et al. 1988].

The equipment uses a thick-walled tube that is driven into the ground at the bottom of a borehole by blows from a slide hammer that weighs 63.5 kg falling through a distance of 76 cm, yielding a maximum energy of 474 J. The spoon was attached to the drill rods and lowered to the bottom of the drill hole after the hole had been cleaned. After the spoon reached the bottom, the number of blows of the hammer was counted to achieve three successive penetrations of 15 cm.

The number of blows for the first 15 cm was disregarded because of the disturbance likely to exist at the bottom of the drill hole; the numbers for the second and third 15 cm increments were added and designated the standard penetration resistance, N.

The fall is inhibited to some extent by the residual friction between the rope and cathead and also by friction in the sheave or pulley at the top of the derrick. The ratio of the

energy actually transmitted to the rods to that delivered by the hammer depends primarily on the efficiency of the anvil which, in turn, is a function of its weight. It varies from about 60% for heavy anvils to about 80% for light ones.

The combined efficiency, representing the ratio of the energy that reaches the rod to the available potential energy of the hammer, ranges from about 45 to 78% [Skempton 1986]. In general, most correlations are based on N-values corresponding to a combined efficiency of about 60%. N-values corresponding to this efficiency are designated as N_{60}.

The range of acceptable dimensions for the SPT split-spoon sample have an average external diameter of D_e = 5.1 cm, an internal diameter of D_i = 3.5 cm and a length greater than 45.5 cm.

There are still significant differences between the drilling technique and tests procedures used in different country an the hammer design varies significantly, as well as the rod stiffness.

1.3 Liquefaction susceptibility of soil deposits

The liquefaction susceptibility of soil deposits may be estimated by employing the following methods:

(a) comparison of resistances profiles (i.e. SPT blow count or CPT tip resistance with depth) with critical values;

(b) estimation of a safety factor FS_{Liq} = ″Resistance″/″Action″, which is evaluated as a function of depth.

The ″Action″ can be obtained using either (i) an estimation based on the maximum acceleration at the ground surface using a semi-empirical equation, or (ii) a dynamic calculation including the reduction of soil stiffness due to built-up of pore pressure.

The ″Resistance″ of the soil can be assessed from (i) cyclic undrained laboratory tests on undisturbed or reconstituted specimens or from (ii) correlations with the resistance measured by in-situ tests (i.e. SPT or CPT).

1.3.1 Cyclic stress definition

The cyclic stress ratio, CSR, was originally defined with a simplified procedure because the input motion and its effects on the sand were not always known for a specified case history. The deposit that experience ground motion was approximated to a rigid column (Figure 1.4), where the maximum shear stress was computed as the product of its mass and the horizontal surface acceleration:

[1.3] $$\tau_{\max,r} = \frac{\gamma \cdot z}{g} a_{\max} = \sigma_v \frac{a_{\max}}{g}$$

Where: a_{max} is the maximum acceleration evaluated at the surface of the soil column;

γ is the averaged total unit weight of the soil column;

σ_v is the total vertical pressure.

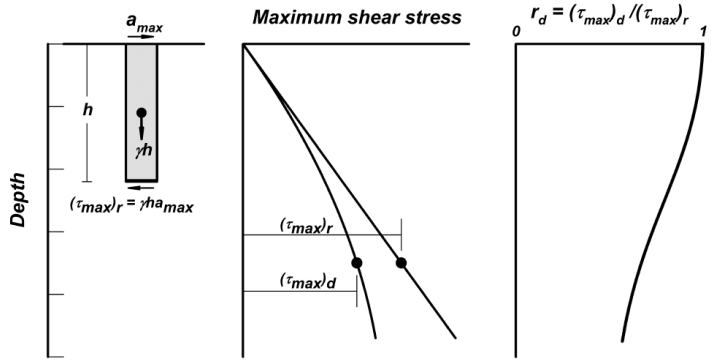

Figure 1.4- Method for determining maximum shear stress, τmax, and the stress reduction coefficient, r_d [Seed et al. 1971]

In order to take into account the deformability of the column, the maximum shear stress was reduced by a factor r_d, determined with a site response analysis. The maximum shear stress evaluated for deformable body was defined as follow:

[1.4] $$\tau_{\max,d} = r_d \cdot \tau_{\max,r}$$

Where r_d is the stress reduction factor, accounting 1 on the ground surface and decreasing with depth [Blake, 1996; Youd, 2001].

Various studies have shown that an irregular earthquake acceleration-time series can be approximated by a uniform cyclic stress time series with an equivalent number of uniform cycles that depends on the uniform cyclic stress amplitude. Seed and Idriss (1971) chose to represent earthquake-induced cyclic stresses by using a representative value equal to 65% of the peak cyclic stress. The corresponding earthquake-induced cyclic stress ratio CSR is therefore computed as follows:

[1.5] $$CSR = \frac{\tau_{ave}}{\sigma'_v} = 0.65\frac{\tau_{\max,d}}{\sigma'_v} = 0.65\frac{a_{\max}}{g}\frac{\sigma_v}{\sigma'_v}r_d$$

Where: CSR is the cyclic stress ratio;

σ'_v is the effective vertical stress;

τ_{av} is the averaged amplitude of cyclic stress considering the deformability of the soil column and using an equivalent uniform cyclic stress amplitude for earthquake.

1.3.2 Resistance from laboratory tests

The liquefaction of saturated sands can be triggered by different combinations of uniform cyclic shear stress ratio using laboratory apparatus, as cyclic triaxial test, simple cyclic shear test and torsional test.

Generally, the cyclic stress ratio CSR required to reach liquefaction in a specified number of loading cycles may also be called the sand's cyclic resistance ratio CRR.

The relationships between the CRR and N can generally be approximated with a power function as $CRR = a \cdot N^{-b}$, where the parameters *a* and *b* are determined by a regression against the experimental data. The dependence of the CRR on N means that any reference to a sand's CRR must specify N.

The ″liquefaction″ of a sample from laboratory test is usually defined as the point at which the soil experience large deformations with zero effective stress; commonly, 5% double-amplitude axial strain in triaxial condition is the criteria employed. In loose of critical sand the adopted liquefaction condition is easily identify by the rapid blow up of deformation and pore water pressure; in contrast, for dense state, the specimen slowly develop 5% double-amplitude axial strain without achieving the rapid deformation associated with essentially zero effective confining stress.

1.3.3 Resistance correlations with in-situ tests

A possible methodology useful to establish a correlation between the cyclic strength and tip resistance is to collect a large numbers of cyclic laboratory tests data from undisturbed soil samples recovered from deposits of known penetration resistance.

In order to correlate the in-situ cone resistance to the cyclic resistance of sands, numerous cyclic tests have been performed in recent years, both on reconstituted and undisturbed samples of sandy soils (usually recovered from alluvial deposits by advanced techniques of sampling).

One of the first correlations to evaluate the cyclic resistance from in-situ tests was proposed by Tatsuoka et al. (1978). He used (i) cyclic triaxial test results conducted on undisturbed samples and (ii) the N-values from SPT carried out at various depths nearby sampling sites. Due to in-situ variability of sand's grain-size, it has been proposed a

general correlation also introduced in Japanese Code of Brides, which allowed for the effects of the average particles dimensions D_{50}:

[1.6]
$$CSR^{TX}{}_{20} = 0.0676\sqrt{N_1} + 0.225 \cdot \log\left(\frac{0.35}{D_{50}}\right) \quad 0.04 \le D_{50} \le 0.6mm$$
$$CSR^{TX}{}_{20} = 0.0676\sqrt{N_1} - 0.05 \quad 0.6 \le D_{50} \le 1.5mm$$

Where: $CSR^{TX}{}_{20} = \sigma_d/(2\cdot\sigma'_{v0})$ is the cyclic triaxial resistance ratio estimated for 20 equivalent earthquake cycles;

σ_d is the amplitude of dynamic stress;

$N_1 = 1.7/(\sigma'_v + 0.7)$ is the normalized N-value;

σ'_v is the effective vertical stress in (kg/cm^2).

This correlation was based on a linear dependence of cyclic triaxial resistance with relative density (i.e. $D_R = 16\cdot N_1{}^{0.5}$), so it is applicable in loose to medium sands (i.e. $N_1 \le 20$).

Other similar formulations were established by Kokusho et al. (1983) and by Ishihara (1990) for clean sands, as a result of a comprehensive series of laboratory tests.

Instead, Porcino et al. (2009) deduced a correlation between (i) tip resistance of CPT performed in large calibration chamber and (ii) cyclic resistance obtained from simple shear tests; the latter two quantities were related to each other introducing the relative state parameter concept [Idriss and Boulanger, 2004].

The circle points in Figure 1.5 are the Porcino's results and they were consistent with the literature CPT-field based correlations (i.e. Idriss and Boulanger, 2004 and the correlation proposed by NCEER Working Group).

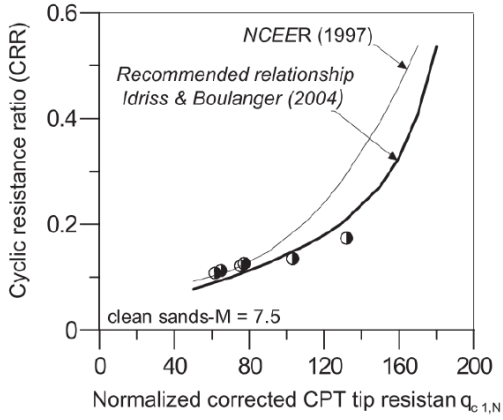

Figure 1.5- The dots represent data from the correlation of cyclic shear test and calibration chamber test results for Ticino sand [Porcino et al. 2009]

1.4 Liquefaction charts

The first semi-empirical methodology proposed in the ’60s by Barkeley’s researches for liquefaction assessment, was defined as ″Geological Criteria″ since liquefaction definition was linked to the observed or non-observed phenomena at the ground surface (i.e. sand boils, important settlements or soil fractures). These ″yes or no″ observations were then related to two estimated quantities: (i) cyclic shear stress ratio experienced at the ground level during a specific earthquake event and (ii) the in-situ tip resistance adequately averaged with depth and normalized for overburden stress.

The in-situ tests that have been used mostly as indices for evaluating liquefaction characteristics includes SPT and CPT tests.

- *N from SPT*

Seed and Idriss (1971) published one of the first liquefaction chart based on ″Geological Criteria″. In this earlier work the authors used mainly in-situ results from SPT, as CPT database was in short supply. In Figure 1.6 is reported the first published liquefaction chart for clean sands based on some further data updates after ‘71. The definition of $N_{1,60}$ is describe hereafter, while the definition of CSR was introduced in the Equation 1.5.

The normalized resistance $N_{1,60}$ blow value is defined as follow:

[1.7] $$N_{1,60} = \frac{N_{60}}{(\sigma'_v)^n}$$

The number of blow $N_{1,60}$ was corrected accounting for an energy dissipation occurring along the drill rods of about 60% of the theoretical free fall energy of the SPT hammer. The stress normalization exponent, *n*, was suggested by Seed and Idriss (1984) to be equal to 0.45 for sands having relative density from 60% to 80% and equal to 0.55 for sands with relative density from 40% to 60%; these last recommendations were based on SPT calibration chamber tests.

It is remarkable that the case histories in Seed’s chart are evaluated for only sands with small fine content (FC < 5%). Charts with data from sites where sands presented a high fine content were also published, but not examined in this paragraph.

Seed and Idriss correlation has been verified and revised along the years as well as the database of case histories increased with time and, for example, CSR and $N_{1,60}$ definitions

were differently evaluated. Anyway, the various suggested curves always represent the division between ″non-liquefaction″ from ″liquefaction″ observations in the field [see i.e. Shibata, 1981; Tokinatsu and Yoshimi, 1983; Kokusho, 1983].

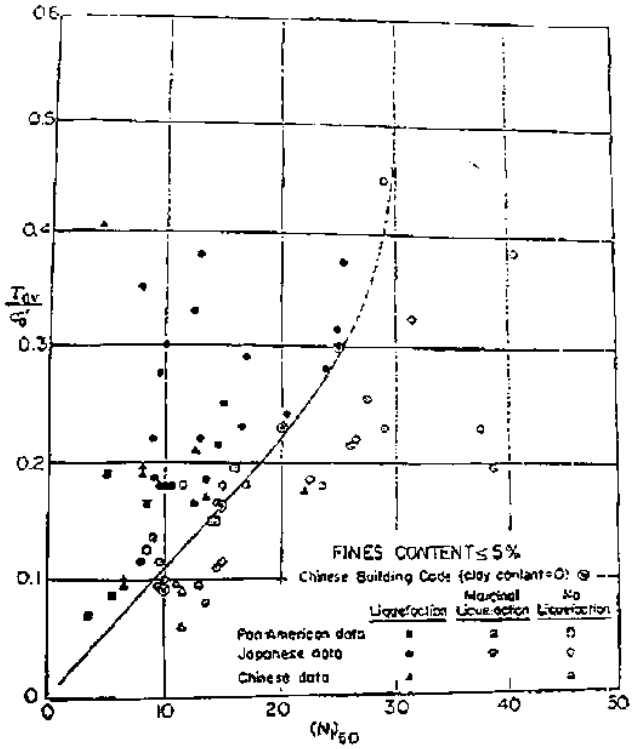

Figure 1.6- Correlation between cyclic strength ratio (τave/σ'0) and normalized blows count from SPT, $N_{1,60}$ for sand with FC < 5% [Seed et al. 1984]

- *q_c from CPT*

With the growing contribution of case histories from all around the world (reported in the proceeding of NRC 1985 and NCEER 1996 workshops), several attempts have been made to establish correlation between field cyclic performance and CPT results.

Based on field tests data, Robertson and Campanella (1985) proposed the correlation shown in Figure 1.7, where the value of q_{c1} represented the in-situ normalized tip resistance evaluated for a reference confining pressure of 98 kPa and cyclic stress ratio was evaluated as in Equation 1.5. This chart was based on CPT tests results and on Seed's SPT database, in which N-values were converted to an equivalent q_c tip resistance.

The cyclic resistance curves were defined by Robertson and Campanella both for clean and silty sands (FC = 15%) and similar correlations proposed by various researches were superimposed on the same graph. The relation gathered from the comprehensive study conducted by Shibata and Teparaska (1988) correlated well with Robertson and Campanella relationships, in particular for clean sand case.

These correlations are however limited in coverage to uncemented, holocenic age and sandy soils and caution must be taken when they are applied to different materials.

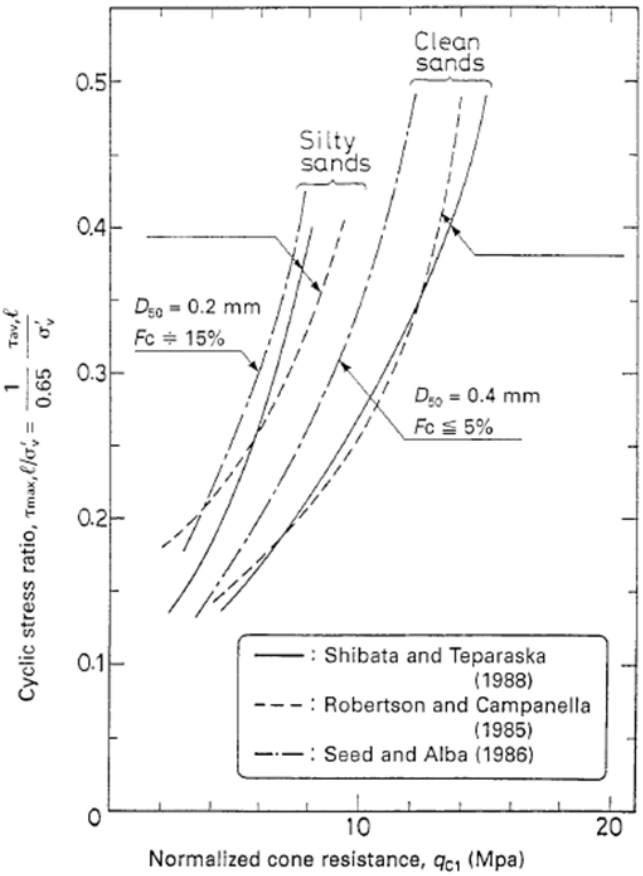

Figure 1.7- Summary chart for the cyclic strength evaluation of sands based on the normalized CPT value q_{c1} [Robertson and Campanella, 1985]

In literature were published a lot of different type of correlations based on in situ measures, for example Shibata and Teparaska (1988), Stark and Olson (1995), Suzuki et al. (1995), all employed a limited database of field case histories in respect to Robertson and Wride (1998) ones. Mitchell and Tseng (1990) presented a theoretical correlation based on cavity expansion analyses, validated with laboratory cyclic simple shear and cyclic triaxial tests data. Recently, works by Juang et al. (2000, 2003) present correlations based on a probabilistic analysis of case histories.

Only a few of the most reliable procedures used to estimate cyclic resistance ratio from in-situ test are described in detail in the follow paragraphs.

1.4.1 Robertson's liquefaction approach (1998, 2004, 2010)

In order to estimate cyclic liquefaction resistance of sand, Robertson and Campanella (1985) published one of the first liquefaction chart where the limited data available were plotted in CSR – q_{c1} plane; this chart was updated and revised after the discussions emerged in NCEER workshop in 1996 and, above all, after the published case histories by Stark and Olsen (1995) and Suzuki et al. (1995). The new curves (determined with only CPT data) are represented in Figure 1.8: CRR – q_{c1N} (later defined) correlations were proposed for different observed superficial deformations, γ_l.

Field deformations used to upgrade liquefaction database were based on the following common conditions: holocene age, clean sand deposits (i.e. FC ≤ 5%), level or gently sloping ground, magnitude M_w = 7.5 earthquakes, ″liquefiable″ depth range from 1 to 15 m (84% were data from depths less than 10 m) and representative average q_c values for the layer that was considered to have experienced cyclic liquefaction. The curve represented in Figure 1.8 for γ_l = 3% was taken as reference, inasmuch it was the most preventive for clean sand.

Dealing with q_c measures usually related to sand with different fine content, Robertson and Wride (1998) proposed to estimate an equivalent clean sand normalized penetration resistance $q_{c1N,cs}$ introducing a correction factor for tip resistance, K_c, later defined.

The cyclic liquefaction resistance curve CRR – $q_{c1N,cs}$, evaluated for an equivalent magnitude earthquake with M_w = 7.5, is reported in Figure 1.8 (for γ_l = 3%):

[1.8] $$CRR_{7.5} = 93 \cdot \left(\frac{q_{c1N,cs}}{1000} \right)^3 + 0.08 \qquad \text{if } 50 \le q_{c1N,cs} \le 160$$

[1.9] $$CRR_{7.5} = 0.833 \cdot \left(\frac{q_{c1N,cs}}{1000} \right) + 0.05 \quad \text{if } q_{c1N,cs} < 50$$

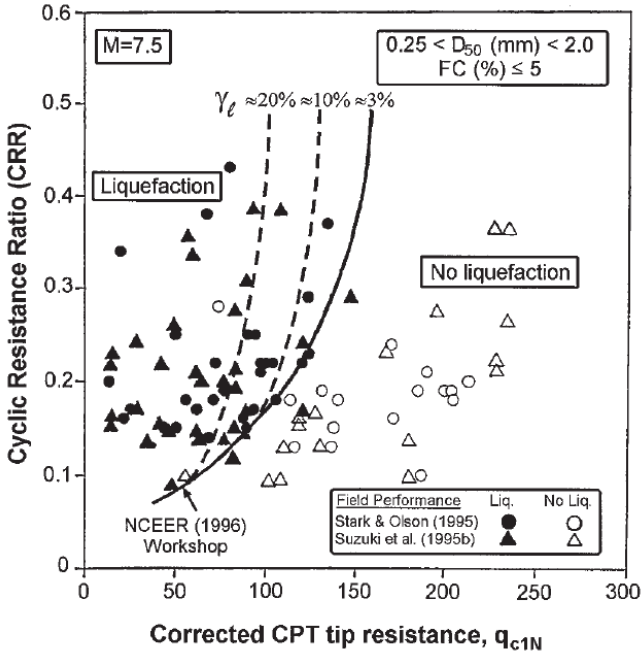

Figure 1.8- Cyclic resistance ratio (CRR) for clean sands vs normalized and dimensionless tip resistance q_{c1N} based on CPT [Robersone and Campanella, after 1996 updated]

If thin layers are present, tip resistance corrections are appropriated.

In the following, it will be explain the quantities introduced in the liquefaction chart and in Equation 1.8 and 1.9.

Cone penetration resistance for clean sand was proposed to be, not only just corrected for overburden stress (resulting in the term q_{c1}), but also properly normalized in order to result in a dimensionless quantity; so q_{c1N} was given by:

[1.10] $$q_{c1N} = \frac{q_{c1}}{p_{atm}} = C_Q \cdot \left(\frac{q_c}{p_{atm}} \right) = \left(\frac{p_{atm}}{\sigma'_{v0}} \right)^n \cdot \left(\frac{q_c}{p_{atm}} \right)$$

The correction factor for overburden stress was defined only for $C_Q \leq 2$ and the stress exponent *n* was originally taken equal to 0.5 for clean sand only [Liao and Whitman, 1986; Robertson, 1998].

Managing with in-situ data, which ones were likely to find a high fine content, Robertson and Fear (1995) recommended operating an average correction on the tip resistance depending on the ″apparent fines content″, in order to report the normalized tip resistance of silty sand to the normalized tip resistance of equivalent clean sand. This type of correlation was supported by the idea that the tip resistance of silty sand had a lower value when compared to the tip resistance of a clean one. This was evidently only a simplification, as well as it was shown that fines content and soil plasticity brought out an

increasing of friction ratio rather than tip resistance [Olsen and Malone 1988; Olsen and Koester 1995; Robertson and Campanella 1988; Robertson 1990].

The unknown grain-size characteristics of in-situ soils, such as fines content, can be initially estimated directly from CPT data using, for example, the soil behavior charts proposed in Figure 1.9 [Robertson, 2010 modified from Robertson 1990 and 1998], where soil type in $Q_{tn} - F_R$ plane are subdivided by I_c curves.

Jefferies and Davies (1993) suggested that the boundaries between soil behaviors type zones 2 to 7 (in Figure 1.9) can be approximated as concentric circles: the value of the radius of each circle can be used as a soil behavior type index. Using the CPT chart by Robertson (2010), where the originally $Q = (q_t - \sigma_{v0})/\sigma'_{v0}$ (from Robertson, 1998) was updated with new values of Q_{tn} (as suggested also by Zhang et al., 2002), the soil behavior type index, I_c, can be defined as follows:

[1.11] $$I_c = \sqrt{(3.47 - \log Q_{tn})^2 + (\log F_R + 1.22)^2}$$

Where: $$Q_{tn} = \left(\frac{q_t - \sigma_{v0}}{p_{atm}}\right) \cdot \left(\frac{p_{atm}}{\sigma'_{vo}}\right)^n$$

$$n = 0.381 \cdot I_c + 0.05 \cdot \left(\frac{\sigma'_{v0}}{p_{atm}}\right) - 0.15 \leq 1$$

$$F_R = \left(\frac{f_s}{q_t - \sigma_{v0}}\right) \cdot 100\ (\%)$$

The I_c value is determined with an iterative procedure and the new definition of the stress exponent *n* was defined by Robertson (2009) as a function of soil type.

Along the normally consolidated region in Figure 1.9 soil behavior type index increases with increasing of fines content and soil plasticity; in order to determine an estimation of the apparent fines content, the following simplified relationships were suggested:

[1.12] if $I_c < 1.26$ apparent fines content FC (%) = 0

[1.13] if $1.26 \leq I_c \leq 3.5$ apparent fines content FC (%) $= 1.75 \cdot I_c^{3.25} - 3.7$

[1.14] if $I_c > 3.5$ apparent fines content FC (%) = 100

The recommended relationship between I_c and the correction factor K_c is defined as:

[1.15] if $I_c \leq 1.64$ $K_c = 1.0$ (for clean sand)

[1.16] if $I_c > 1.64$ $K_c = -0.403 \cdot I_c^4 + 5.58 \cdot I_c^3 - 21.63 \cdot I_c^2 + 33.75 \cdot I_c - 17.88$

From the proposed correlation it is evident that K_c value decreasing with the increasing of apparent fine content.

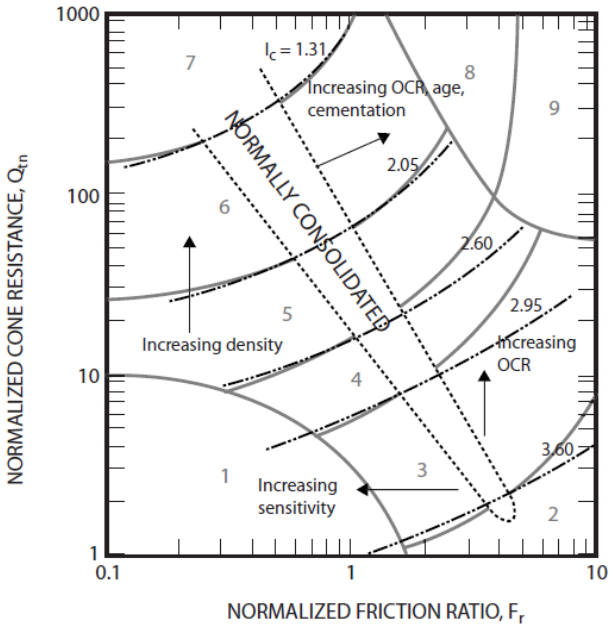

Soil behaviour type index, I_c	Zone	Soil behaviour type (see Fig. 8)
$I_c < 1.31$	7	Gravelly sand to dense sand
$1.31 < I_c < 2.05$	6	Sands: clean sand to silty sand
$2.05 < I_c < 2.60$	5	Sand mixtures: silty sand to sandy silt
$2.60 < I_c < 2.95$	4	Silt mixtures: clayey silt to silty clay
$2.95 < I_c < 3.60$	3	Clays: silty clay to clay
$I_c > 3.60$	2	Organic soils: peats

Figure 1.9- Normalized CPT soil behaviour type chart and boundaries of soil behaviour type [Robertson, 2010]

The equivalent clean sand normalized tip resistance was determined as a function of both the measured penetration resistance and the grain-size characteristics of the soil, as below:

[1.17] $$q_{c1N,cs} = K_c \cdot q_{c1N}$$

Where K_c is iteratively deduced from I_c values.

Factor K_c is only an approximation, since the CPT is susceptible to many factors, such as soil plasticity, mineralogy and shape particles, soil sensitivity and stress history: however, for small projects or for initial screening of larger ones, the above correlation provides a useful guide.

It must be underlined that a particular caution must be taken in applying the proposed relationship to sands that plot in the region defined by $1.64 < I_c < 2.36$ and $F_R \leq 0.5\%$: in this area silty sand must not be confused with very loose clean sands.

In this case, it is suggested to set the correction factor K_c to a value of 1.0 (i.e., assume to have clean sand).

Robertson suggested that it was reasonable to assume that soils with $I_c > 2.6$ were ″non-liquefiable″ and that the correction factor K_c could be so large that no representative values were deducible. Anyway, soils that fall in the lower left region of the CPT soil behavior chart, with $I_c > 2.6$ and $F_R \leq 1.0\%$, can be yet very sensitive to dynamic loading and, hence, possibly susceptible to both cyclic and flow liquefaction.

Cyclic stress ratio CSR reported in the Robertson's chart, for each analyzed case history, was define as Seed's originally suggested (see Equation 1.5).

Stress reduction factor, r_d, was considered as originally evaluated by Seed (1971), with an average value of:

[1.18]
$$\begin{cases} r_d = 1.0 - 0.00765 \cdot z & z < 9.15\ m \\ r_d = 1.174 - 0.0267 \cdot z & z = 9.15 < z < 23\ m \end{cases}$$

Robertson (2004) defined the factor of safely against liquefaction as:

[1.19]
$$FS_{liq} = \frac{CRR_{7.5}}{CSR} MSF$$

Where MSF is the magnitude scaling factor to convert the $CRR_{7.5}$ for $M_w = 7.5$ to the equivalent CRR for the design earthquake. The recommended MSF [Youd et al., 2001] was given by:

[1.20]
$$MSF = \frac{174}{M_w^{2.56}}$$

1.4.2 Idriss and Boulanger's liquefaction approach (2004)

The CPT liquefaction correlation and some case histories were re-evaluated also by Idriss and Boulanger (2003), using data collected by Shibata and Teparaksa (1988), Kayen et al (1992), Boulanger et al (1995, 1997), Stark and Olson (1995), Suzuki et al (1997) and Moss (2003). The Moss's work was particularly valuable in providing the most comprehensive compilation of field data and associated interpretations.

The re-evaluation of the CPT-based procedure incorporated adjustments and parameters revision: cyclic stress ratio CSR was improved to reflect the number of equivalent cycles that had occurred up to the time when liquefaction was triggered, in order to consider that the stronger is the motion, the earlier liquefaction occurs.

The quantities deduced by in-situ evaluations were calculated using the revised r_d and MSF factors, for cyclic stress conditions, and C_N, for tip resistance; a stress correction factor for cyclic resistance was also introduced, K_σ.

Each case history was characterized by the cyclic stress ratio for an equivalent earthquake of magnitude $M_w = 7.5$ and by the normalized and dimensionless tip resistance.

Cyclic stress ratio was defined as follow:

[1.21] $$CSR_{M_w=7.5} = \frac{CSR}{MSF} \cdot \frac{1}{K_\sigma} = \frac{0.65\left(\frac{a_{\max}}{g}\right)\left(\frac{\sigma_{v0}}{\sigma'_{v0}}\right) r_d}{MSF \cdot K_\sigma}$$

Indeed, normalized tip resistance was established with the following formulation:

[1.22] $$q_{c1N} = \frac{q_{c1}}{p_{atm}} = C_N \frac{q_c}{p_{atm}}$$

In Equation 1.21 the stress reduction factor r_d was evaluated using a revised database. Idriss (1999), extending his initial work conducted in 1971 and referring to Golesorkhi's research (1989), performed several parametric site response analyses. He concluded that the parameter r_d could be adequately expressed as a function of depth, z, and earthquake magnitude, M_w, for the most practical interest case, with the following equations:

[1.23]
$$\begin{cases} z \le 34m & \ln(r_d) = \left[-1.012 - 1.126\sin\left(\frac{z}{11.73} + 5.133\right)\right] + \\ & \left[0.106 + 0.118\sin\left(\frac{z}{11.28} + 5.142\right)\right] \cdot M_w \\ z > 34m & r_d = 0.12 \cdot e^{0.22 M_w} \end{cases}$$

Magnitude scaling factors, MSF, was derived by combining correlations obtained by both (i) relating number of equivalent uniform cycles with earthquake magnitude and (ii) using laboratory-based relations between the cyclic stress ratio required to cause liquefaction and the number of uniform cycles. Idriss (1999) derived MSF using cyclic test results from high quality samples; the proposed equation is defined below:

[1.24]
$$MSF = 6.9 \cdot e^{-M_w/4} - 0.058 \le 1.8$$

Some difference has been observed between the last proposed correlation and the original Seed and Idriss (1982) MSF's formulation base on reconstituted specimens results; the scatter was attributed to the difference in samples quality, as reconstituted specimens had always a lower cyclic strength. Besides, various authors proposed different equation for MSF definition, with relevant dispersion in the results, especially for smaller magnitude earthquake events [i.e. Arango (1996) and Ambraseys, 1988].

Lastly, for the CSR determination was introduced the effect of overburden stress for cyclic stress behavior [Boulanger, 2003, Boulanger and Idriss 2004]. The authors demonstrated that overburden stress effects for cyclic stress ratio could be taken into account in either two different ways: (i) through the additional normalization of penetration resistances introducing a relative state parameter, thereby producing the corrected quantity $q_{c1\xi}$, or (ii) through a K_σ factor.

The first approach is useful as it eliminates the necessity to use K_σ factor, as the relative state parameter for sand ξ_R (explained in Chapter 2) was found to be useful in combining the effects of relative density, D_R, vertical effective stress, σ'_{v0}, and the cyclic resistance ratio CRR.

In spite of this potentiality, the second approach (ii) has been the standard approach since the last years. The recommended K_σ curves are expressed as:

[1.25] $$K_\sigma = 1 - C_\sigma \cdot \ln\left(\frac{\sigma'_{v0}}{p_{atm}}\right) \leq 1$$

The factor C_σ is related, trough relative state parameter, to the normalized tip resistance and it is evaluated as:

[1.26] $$C_\sigma = \frac{1}{18.9 - 17.3 \cdot D_R} = \frac{1}{37.3 - 8.27 \cdot (q_{c1N})^{0.264}} \leq 0.3$$

Regarding tip resistance, it was normalized introducing a factor C_N, both theoretically and experimentally determined. Boulanger proposed a linear exponential trend for stress normalization factor, expressed in the following form:

[1.27] $$C_N = \left(\frac{p_{atm}}{\sigma'_{v0}}\right)^m$$

The exponent was defined as $m = 0.784 - 0.521 \cdot D_R$. For as much as, in practice problems, D_R is the unknown quantity, C_N and m values were progressively adjusted on the base of some SPT's results from calibration chamber tests [Marcuson and Bieganousky, 1977]; m stress exponent was adequately estimated using a least squares, weighted, non-linear regression analysis of the data.

Go one step further and introducing relative state parameter index ξ_R, the relative density D_R, for a given q_{c1N} value, could be estimated with the following suggested equation:

[1.28] $$D_R = 0.478 \cdot (q_{c1N})^{0.264} - 1.063$$

Consequently, Boulanger and Idriss (2004) obtained the following implemented expression for C_N:

[1.29] $$C_N = \left(\frac{p_{atm}}{\sigma'_{v0}}\right)^\beta = \left(\frac{p_{atm}}{\sigma'_{v0}}\right)^{1.338 - 0.249 \cdot (qc1N)^{0.264}} \leq 1.7$$

The C_N upper limitation is necessary for the uncertainties in its evaluations at shallow depth.

Tip and cyclic resistance correction factors, C_N and K_σ, are iteratively defined, as both depending on normalized tip resistance, q_{c1N}.

The revised CRR – q_{c1N} relation, considering all factors introduced above, is shown in Figure 1.10 for only clean sand, together with liquefaction and non-liquefaction case

histories considered for the evaluation of the boundary recommended curve; the equation proposed was so defined as:

$$CRR = e^{\left\{\frac{qc1N}{540}+\left(\frac{qc1N}{67}\right)^2-\left(\frac{qc1N}{80}\right)^3+\left(\frac{qc1N}{114}\right)^4-3\right\}} \quad [1.30]$$

It is useful to underline that correlation resulting from Boulanger's analysis was derived for clan sand only, it referred to an equivalent earthquake of M_w = 7.5 earthquake and reference vertical stress of σ'_{v0} = 101 kPa.

The derived relation is comparable to the curve proposed by Shibata and Teparaksa (1988) and by Suzuki et al. (1997) for clean sands but it is more conservative than the corresponding curve proposed by both Robertson and Wride (1998) and Seed et al (2003), for almost the entire range of q_{c1N}.

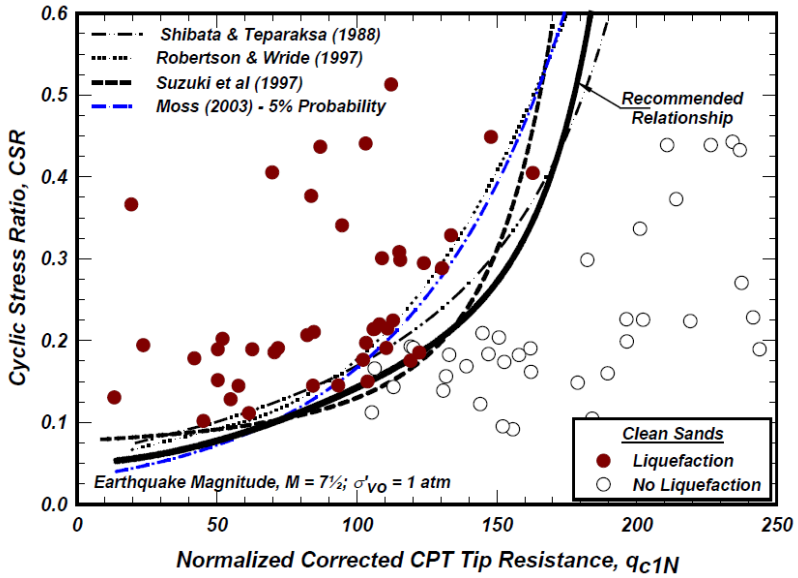

Figure 1.10- CPT-based case histories and recommended relation for clean sands (FC < 5%) [Idriss and Boulanger, 2004]

Chapter 2

2 Critical State of Sand and State Parameters

2.1 Introduction

Monotonic and cyclic behavior of sand depends on its initial physical state, since the tendency to generate excess pore pressure or volumetric deformation (in dependence of drainage conditions) is strongly influenced by both density and initial effective stress.
From the historically point of view the pioneering work of Casagrande (1936) has been the cornerstone of modern understanding of soil strength behavior: with his strain-controlled triaxial drained tests he demonstrated that specimens, with the same confining effective pressure, approached the same ″critical″ density when sheared to large strains despite the initial density. Loose specimens always contracted during shearing while dense ones first exhibited a little contraction, then they began to dilate very quickly. At large strains, all specimens approached the same density and continued to deform with constant shearing resistance under constant effective stress. The consequently related void ratio linked to large strains behavior was named the ″critical void ratio″.
Performing tests at different effective confining pressures, Casagrande found out that the ″critical void ratio″ was uniquely related to the effective confining pressure, and all critical values belong to the same locus called ″critical void ratio line″ in e – p’ plane.

2.1.1 Determination of Steady State of Deformation

Castro (1969) continued and extended the Casagrande's researches; he performed static and cyclic triaxial tests on isotropically consolidated specimens, besides several static tests on anisotropically consolidated ones. Undrained tests were for the first time conducted with a load-controlled system, the only one capable to adequately simulate the so called ″flow failure″ mechanism. Three different types of stress-strain behaviors were observed in monotonic undrained test as reported in Figure 2.1, from a qualitative point of view.

Very loose specimens at low effective confining pressure (specimen ″A″) exhibited a peak undrained strength at a small shear strain and then ″collapsed″ to flow rapidly with large strains. This type of behavior, called ″liquefaction″ by Castro, is now defined as ″flow liquefaction″ and correspond to a rapid loss of strength. Dense specimens (type ″B″) initially contracted but then dilated until a relatively high and constant effective pressure was reached, and large strains and strengths were experienced.

At intermediate densities (specimen ″C″) the achievement of peak strength at low strains was found to be followed by a limited period of softening behavior; after this loss in strength, further loading produced continues dilation to high effective confining pressures and, consequently, higher strains and strengths. This type of failure was termed ″limited liquefaction″ and Ishihara (1975) defined the transition behavior from contractive to dilative as ″phase transformation″. The points at which this changing in behavior was observed, were plot in e – p' plane and they were interpolated with a line called ″quasi-steady state line″.

The state in which the soil flowed continuously under (i) constant shear stress, (ii) constant effective pressure, (iii) constant volume and (iv) constant velocity was defined as the ″steady state of deformation″ in undrained condition [Ishihara, 1975; Castro and Poulos, 1977; Poulos, 1981]. The locus of points describing the relationship between void ratio and effective confining pressure in failure conditions was called the ″Steady State – Line″ (SS – Line), and it was defined as a projection of the three dimensional curve uniquely determined in e – p′ – q space.

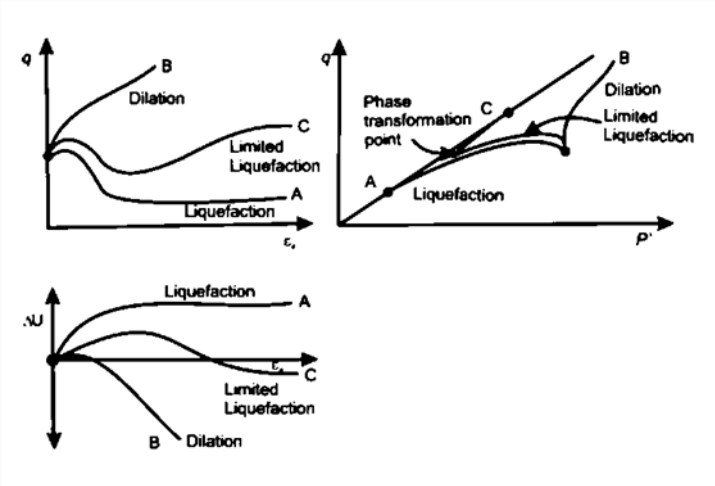

Figure 2.1- Qualitative behaviour of triaxial anisotropically specimens results of stress – controlled tests. ″A″: liquefaction, ″B″: limited liquefaction and ″C″: dilation [Castro, 1969]

The Castro's testing program showed that there was a unique relationship between void ratio and effective confining pressure at large strains. Graphically this function was defined as a line, roughly parallel to the critical line obtained from drained strain-controlled tests conducted by Casagrande. In Figure 2.2, failure conditions derived by various type of tests, were plotted in void ratio *e* versus the minimum effective stress at the end of consolidation, σ'_3: the difference in strength at failure using load (e_f line in the graph) or strain controlled test (e_s line in the graph) were caused by essentially the rate of strains. The constant driving force of a stress-control test produced effectively a rate of stain about 20000 times faster than that observed in the strain-control tests. The slow development of stains in Castro's tests produced in the samples ″groups″ of sand's grains to lose temporary their structure and so phase transformation was observed.

In Figure 2.2 is shown that the failure condition of a sand always ended up along a fairly e_f line, indifferently from the drainage condition, type and the magnitude of consolidation pressure applied to sample, or whether it was cyclically or monotonically loaded.

Since the steady state of deformation is reached only at large strains beyond which the effects of initial conditions such as (i) soil fabric, (ii) stress and strain history and (iii) loading conditions have been obscured, the effective confining pressure, in an element of soil at failure, was considered dependent only by its initial density.

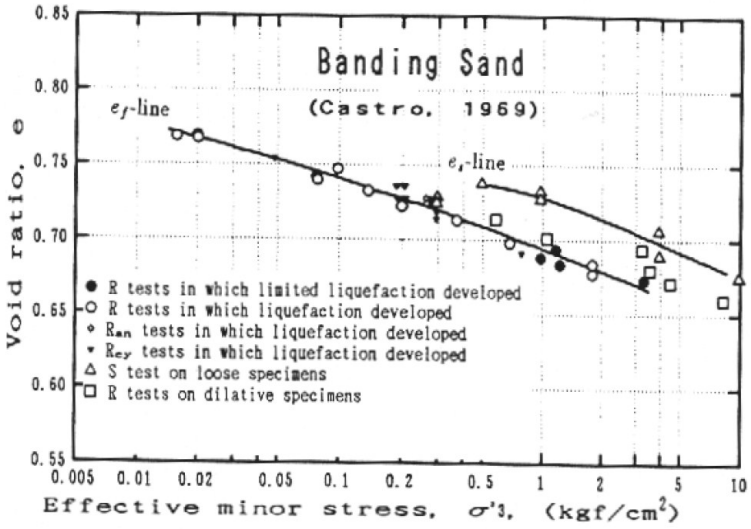

Figure 2.2- Triaxial tests on Banding sand. ″es line″ from strain-controlled tests, while ″e_f line″ from dead-load increments and cyclic loading [Castro 1969]

Relatively recently it has been shown that the steady state conditions is different for compressive and extensional stress paths [Vaid et al., 1990; Reimer and Seed, 1992; Vaid and Thomas, 1995], particularly when the soil is deposited with inherently anisotropic structure. Otherwise, the location of the SS – Line in e – p' plane is strongly influenced by gradation of sand and, its slope, by particle angularity, as illustrated in Figure 2.3, where different curves are associated to different type of sands.

Furthermore, Poulos (1981), Vaid et al. (1990), Hird and Hassona (1990) suggested that the critical-state line, obtained from drained tests, and steady-state line, obtained from undrained tests, were not the same line but they were stress path dependent.

The majority of the researches demonstrated that a unique curve at failure in e – p' plane exists and this leads to think that mechanical properties of sand could be determined by critical soil mechanics approach, therefore knowing where the sand will move to at large strains, it might be possible to relate some characteristics of sand to its in-situ state.

Generally, a soil which physical states plot below the SS – Line is not susceptible to ″flow liquefaction″ but ″cyclic mobility″ could occur; on the contrary, a soil which states stand above the SS – Line, will be susceptible to ″flow liquefaction″, in particular when the static shear stress exceeds the steady-state (or residual) strength. The distinction in soil behavior is usually related to the position of the current state in respective to its steady state condition.

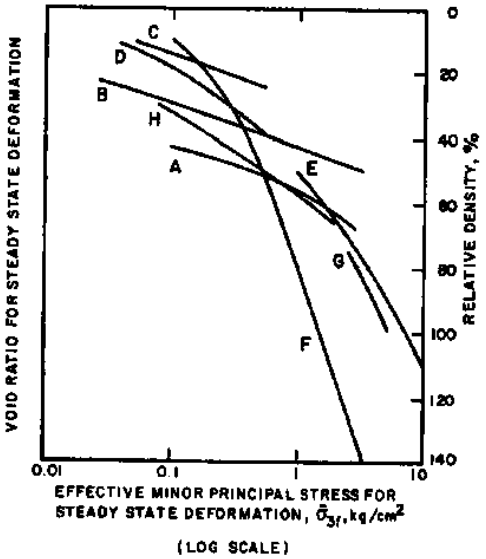

Sand Designation	Grain Size Distribution D_{60} mm	C_u	% Finer Than 0.074 mm %	Grain Shape	Specific Gravity	Maximum Density pcf (5)	Minimum Density pcf (5)	Method of Specimen Preparation	Remarks
A	0.40	3.1	5	Subangular to Angular	2.72	110	84	(2)	Contains shell fragments
B	0.17	1.8	0	Subrounded	2.65	110	90	(2)	
C	0.33	2.3	1	Angular	2.87	108	90	(2)	
D	0.90	5.6	0	Subangular	2.71	114	96	(2)	
E	0.17	2.1	8	Angular	2.87	101	79	(2)	Slightly micaceous
F	0.23	2.0	0	Angular	2.50	73	56	(2)	Contains platey-shaped grains
G	0.15	-	26	Angular	2.79	-	-	Undisturbed	
H	0.85	~17	13	Subangular	2.71	124	98	(2)	
L	0.74	2.5	0	Subrounded	2.66	121	104.8	(3)	
M	0.20	-	44	Angular	2.77	122 (1)	-	(4)	Micaceous, PI = 11
P	0.33	4.7	11	Subrounded to Subangular	2.66	122	98.3	(3)	
Q	1.6	~32	12	Subrounded to Subangular	2.84	145	121.2	(3)	
R	0.60	2.1	0	Subrounded to Subangular	2.69	116	96.5	(3)	

(1) ASTM D1557 Compaction Test
(2) Tamping, moist soil, in layers
(3) Vibration, dry soil, in layers
(4) Kneading, moist soil, in layers
(5) To convert pcf to specific gravity, divide by 62.5

Figure 2.3- State diagram showing steady state lines for various sand with different index properties [Castro and Poulos, 1977]

2.2 State Parameters

Schofield and Wroth (1968) demonstrated that sand behavior is highly depending on the initial state of soil: they took critical state line, defined originally by drained triaxial tests, as a reference ultimately sand condition in effective stress and volume space. Been and Jefferies (1985) agreed that critical state line (calculated from drained tests) and steady state line (calculated from undrained tests) identified the same critical condition of sand. In a work conducted by Been and his co-workers (1991) , the critical state of sands has been examined by carrying out extensive triaxial tests on Erksak 330/0.7 sand and they evaluated that a unique critical-state line existed regardless of the specimen preparation method, drainage, initial condition and stress path effects.

The state parameter ψ defined originally by Been (1985) is used in this research, but a briefly discussion of state index I_s and relative state parameter ξ_R are given in next sections.

The following definitions inherently assume that the critical-state line and steady-state line are equivalent and the subscripts are associated to what kinds of tests are used in the determination of failure condition: ″SS″ from undrained tests and ″CS″ from drained tests.

2.2.1 State Parameter, ψ

Critical state soil mechanics [Roscoe, 1963] based on clay material behavior is applicable also to cohesionless soil, bypassing the obsolete idea that density governs sand behavior. Been (1985) introduced the first-order state parameter for soil as a quantity that potentially governed stress-strain behavior of cohesioless materials.

The state parameter was defined by analyzing drained test results from different type of sands, as:

[2.1] $$\psi = e_c - e_{cs}$$

Where: e_c is the void ratio at the end of consolidation at mean effective stress p'_c;

e_{cs} is the void ratio on the critical state at the same mean effective stress p'_c.

In Figure 2.4 the meaning of state parameter is graphically reported, together with both the linear approximation of critical state line in e – ln(p') and the normal consolidation lines for A e B points.

For positive state parameter (point A), the soil exhibits contractive behavior and flow liquefaction is highly possible, for negative state parameter (point B) soil behavior is dilatant and flow liquefaction cannot happen, but cyclic mobility might occur in cyclic loading conditions.

Considering a specimens with an initial state B in Figure 2.4, with a negative state parameter; if it is shared with constant mean effective stress (i.e. $\delta p' = 0$ to failure, in drained condition), the stress path in e – p' can be represented with a straight vertical line from point B to critical state condition.

The vertical effective stress-path might be seen as an approximation of a triaxial drained complexion test, where the amount of contraction approached in the sample before the dilation started, is not considered.

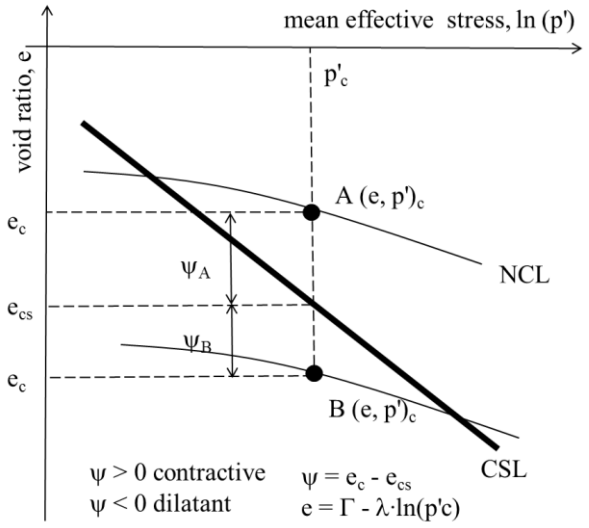

Figure 2.4-Definition of state parameter with linear approximation of critical state line in e – ln(p') plane

The total volumetric strain from point B to critical state can be evaluated as follows:

[2.2] $$\varepsilon_v = -\frac{\Delta e}{1+e_c} = -\frac{e_{cs}-e_c}{1+e_c} = \frac{\psi}{1+e_c}$$

The dilative total volumetric strain ε_v is linearly related to initial state parameter and inversely related to void ratio at the end of consolidation.

Consequently, the average dilation D can be defined as a state parameter dependent:

[2.3] $$D = \frac{\varepsilon_v}{\varepsilon_q} = \left(\frac{\psi}{1+e_c} \right) \cdot \frac{1}{\varepsilon_q}$$

Where $\varepsilon_q = \frac{2}{3}(\varepsilon_a - \varepsilon_r)$ is the deviatoric strain in triaxial conditions, simply deduced during drained tests.

The average dilation D in drained test is independent from mean effective stress p' and slightly dependent from void ratio at the end of consolidation, as well as deviatoric strain.

It must be underlined that, while the mean dilation D is easily relatable to state parameter and total deformations, from the stress-dilatancy theory the dilation of a sheared sample is linked to $\eta_i = q_i/p_i'$, which ratio change during sample deformation. Due to variation of dilation during the test, the minimum dilation D_{min} is usually chosen to be related to the state parameter ψ, as well as to the difference between peak and critical state shear angle $(\phi_p - \phi_{cs})$.

The idea that dilation controls sand behavior was evidenced by many triaxial test results conducted on Kogyuk sand (Erksak sand) with different silt contents [Been, 1985]. The reliability of the relation between mechanical properties of sand and state parameter increased after some considerations emerged from the comparison of test results came from various types of sands, grouped together in a unique database.

The catalogue summarized the main mechanical characteristic of both standard and natural mixed sand [from Golder Associates studies with the support of Canadian oil industry], as well as the digitalized collection of the majors data taken from various published researches.

In Figure 2.5 (a) and (b) are reported the results of the interpretation of drained triaxial tests conducted on reconstituted specimens (with moist tamping, air pluviated and water sedimentation methodology) from 20 different sands. On the right (a) the minimum dilatancy D_{min} and on the left (b) the difference between peak and critical shear angle $(\phi_p - \phi_{cs})$ are represented in dependence of the initial state parameter ψ.

The scatter in the results in Figure 2.5 (b) is important since the difference between the two considered angles (ϕ_p and ϕ_{cs}) is strongly affected by the mineralogy and grain shape of sand's particles. In Figure 2.5 (a) the trend between minimum dilatancy D_{min} and state parameter ψ seems to be more consistent and the scatter is sensibly reduced, even if the comparison is done between very different sands and silty sands.

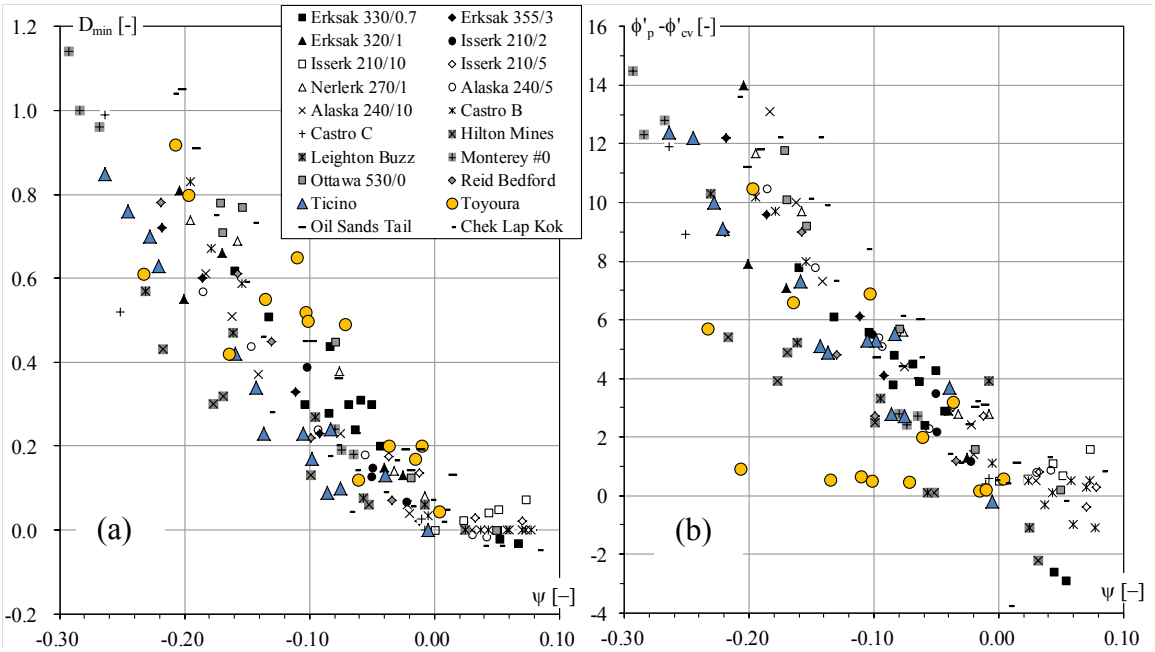

Figure 2.5- a) peak dilatancy vs state parameter; b) stress-dilatancy component of peak strength vs state parameter for 20 different soils in standard drained triaxial compression tests [Jefferies and Been, 2006]

Even if state parameter was formulated focusing on drained behavior of sand in triaxial tests, the volumetric deformation at peak strength during drained shear of a sample could be useful in the understanding of the undrained behavior of sand.

When in a drained test the volumetric strain at peak is compressive, than in undrained test the pore pressure would be positive: in many cases positive pore pressure at peak strength would correspond to rapid flow failure and the undrained strength of sand results smaller than the drained resistance. In contrast, when total volumetric strain at peak is negative (dilative samples), pore pressure would be negative in undrained tests, leading to a greater strength in undrained than in drained conditions.

It must be underlined that, unfortunately, the volumetric deformations at peak stress are influenced by the depositional method used for the reconstituted samples, as well as by the stress path; the consequence is that a unique correlation with state parameter is not deductible.

As can be noted from the test results in Figure 2.5 the majority of sand's physical states present negative state parameter; additionally, when the state parameter reduces (in its modulus value), the dilation of a sample is less pronounced until $\psi = 0$ and the void ratio at the end of consolidation is equal to the void ratio at critical state.

The prevailing dilatant behavior leads to suppose that in-situ sand's states tend to develop negative pore pressure.

State parameter seems to be extremely useful for the soil behavior determination both in drained and undrained condition and, despite its simplicity, the possibility to determinate its value from in-situ or laboratory tests is interesting for geotechnical engineering purposes. The accuracy with whom the state parameter can be determined, however, is influenced by the accuracy with whom the position of the critical state line can be evaluated.

2.2.2 State Index, Is

Ishihara (1993) reported that ψ was a very good ″first-order″ parameter when it was used to quantify the behavior of medium-to-dense sand under relatively high mean effective stress, but it was not reliable for the description of mechanical behavior of very loose sand with low mean effective stress (i.e. physical states closely above or below the steady state line).

According to what Been demonstrated in his researches, two samples with different initial state (e, p') but similar state parameter, would have similar mechanical behavior if monotonically sheared: it did not seems to be true for sand with very low mean effective stresses.

Ishihara demonstrated that under a small well-defined void ratio (e_0), determined by the intersection of the quasi-steady state line (QSS – Line) with zero mean effective stress in e – p' plane, the strength of the sand decreased rapidly to very low values even if the tests were conducted on samples with similar state parameters. This result was related to the fact that as void ratio increase, the behavior of sand became more sensitive to small variation in void ratio.

In order to solve this problem, Ishihara proposed an upper reference line as a combination of the threshold void ratio line and the segment of isotropically consolidated line, IC – Line, considering only the part below the threshold void ratio line.

It is possible to define state index parameter, I_s [Ishihara, 1993], as follows:

[2.4] $$I_S = \frac{e_0 - e_c}{e_0 - e_{QSS}}$$

Where: e_0 void ratio at corresponding upper reference line ($I_s = 0$) for a given mean effective stress p'_c;

e_{QSS} void ratio at a quasi-steady state, QSS, at the same mean effective stress p'_c;

e_c void ratio at the end of consolidation.

State index is graphically explained in Figure 2.6 below.

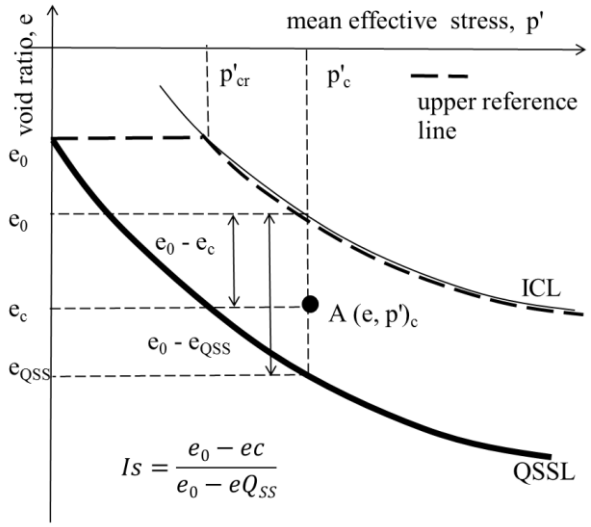

Figure 2.6- Definition of state index I_s in e – p‘ plane [Ishihara, 1993]

In order to capture the essence of sand behavior in the medium strain range, in the general definition was assumed the quasi-steady state condition as a reference state.

Physical implications of state index are given below:

$I_s < 0$ zero residual strength;

$I_s = 0$ zero residual strength for an initial mean effective stress less than p'_{cr}, or non-zero residual strength for an initial mean effective stress greater than p'_{cr};

$I_s = 0 \div 0.72$ occurrence of the QSS condition, with minimum deviatoric stress coupled with moderately large strains;

$I_s \geq 0.72$ occurrence of the steady state at large strains.

In Figure 2.7 (a) are plotted the I_s curves, determined by fitting the initial physical states derived from an extensive triaxial tests program on Toyoura sand. It is evident that the lines of equal I_s extends outwards from point P in the Figure 2.7 (a), where the effective confining stress is zero and the void ratio is the threshold one (e_0 = 0.93 for Toyoura sand). In Figure 2.7 (b) are reported, as an example, the good applicability of I_s parameters: the stress-strain behavior together with stress-path for three specimens with I_s = 0.6 – 0.7, are effectively similar.

The main problem with I_s parameter is that the QSS – Line, taken as reference line, is strongly affected by the preparation method adopted for reconstituted sand samples, as well as from the initial mean effective stress.

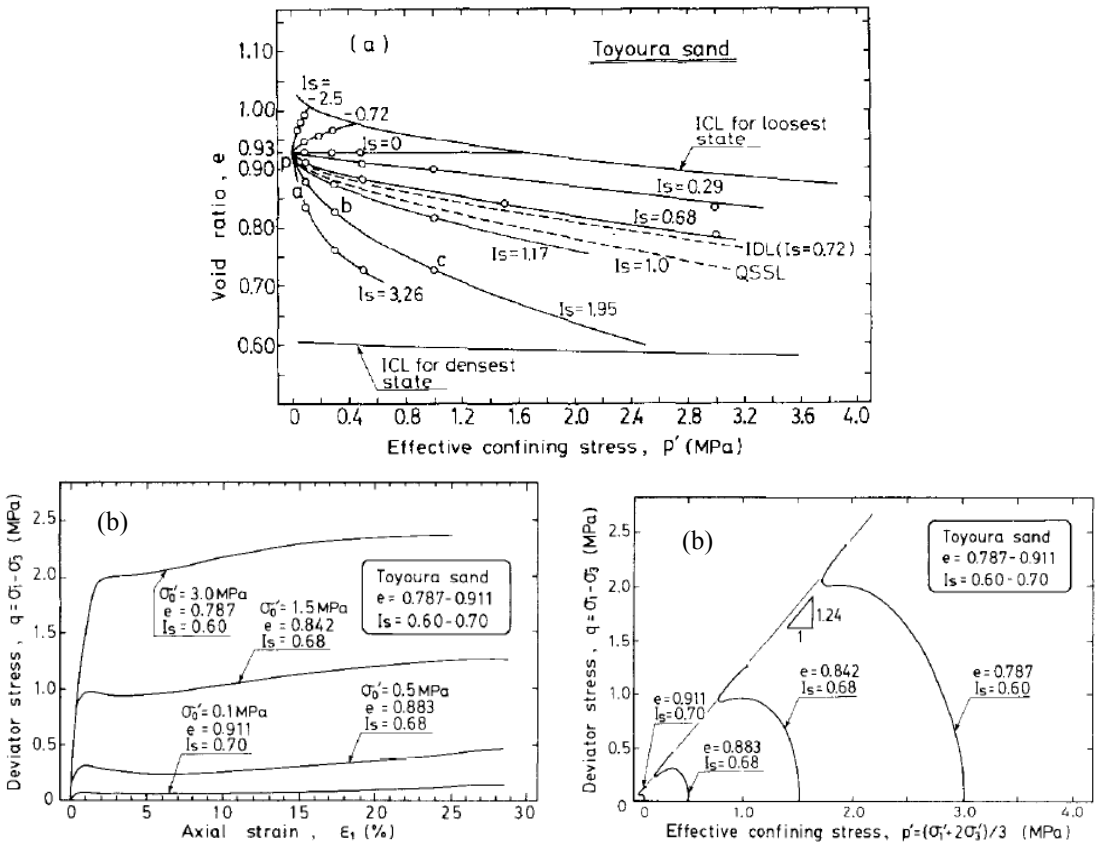

Figure 2.7- (a) a family of curves with equal I_s, value in e-p'plane: circles indicate the I_s values for each set of tests; (b) behavior of Toyoura sand with Is ~ 0.68 [Ishihara, 1993]

2.2.3 Relative state parameter, ξ_R

Bolton (1986) proposed for the first time the relative dilatancy index I_{RD} as a quantity useful to estimate strength and volume change of sands with reasonable accuracy for practice; I_{RD} was defined as:

[2.5] $$I_{RD} = D_R \cdot \left(Q - \ln \frac{100 \cdot p'}{p_{atm}} \right) - R$$

Where: D_R is the relative density;

Q is an empirical constant and determines the value of p' at which dilatancy is suppressed; it depends on grain-size and mineralogy, for quartz sand is 10;

R is a fitting parameter taken equal to 1 and function of $(\phi_{cv}-\phi_{\mu})$.

Even if I_{RD} is empirically derived, it was found that the Equation 2.5 correlates quite well with relative density, confining pressure and dilatancy characteristics of sand.

For the particular case of zero dilatancy index, it was defined a critical relative density $D_{R,CS}$:

[2.6] $$D_{R,CS} = \frac{1}{Q - \ln \frac{100 \cdot p'}{p_{atm}}}$$

The critical state line, in D_R – p' plane, is empirically derived by Bolton's law with Q represents the value at which the curve sharply downwards, consequently to the beginning of particles crushing.

Konrad (1988) introduced a relative state parameter, ξ_R, using concepts defined in Bolton's work and normalizing the state parameter ψ with respect to the void ratio difference ($e_{max} - e_{min}$); the parameter was previously used by Hird and Hassona (1986) and after by Idriss and Boulanger (2004). The relative state parameter was derived as a difference in relative density:

[2.7] $$\xi_R = D_{Rc} - D_{R,CS}$$

Where D_{Rc} is the relative density for p'_c (end of consolidation condition) and $D_{R,CS}$ is the relative density at the critical state for the same mean effective stress (see Figure 2.8).

Relative state parameter was found to be connected to the behavior of sand and its positive value was associated to contracted behavior in triaxial tests. Contrary to ψ parameter, ξ_R takes into account sand physical properties, i.e. Q or e_{max} and e_{min}, but considers relative density as one of the state variables.

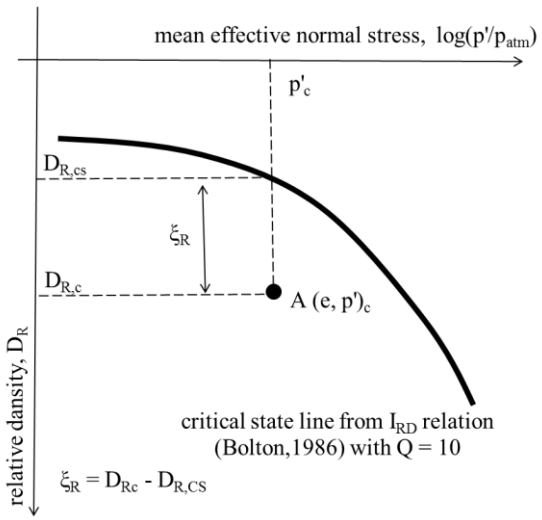

Figure 2.8- Definition of relative state parameter ξ_R [Idriss& Boulanger,2004] in e – p' plane

2.3 Physical state of sand from penetration resistance

The direct determination of void ratio by in-situ testing is still a challenge, like sampling of cohesioless material, which is often unreliable or expensive technique.

The tempting idea, grown up in the last twenty years, is looking for the solution of an inverse boundary problem by determining the resistance of soil with a standardized instrument. From the measured resistance the state parameter would be determined and possibly related with other strength and stiffness characteristic of tested sand.

Considering an in-situ domain with an unknown physical state and with a not well-defined boundaries conditions (stress distribution or drainage conditions), we know the ″answer″, i.e. measured q_c, but we want to identify the state and the properties of the material: this is called an ″inverse boundary problem″ resolution.

Historically, the state of in-situ soil is determined using SPT (standard penetration test) or CPT (cone penetration test) results but the penetration resistance could be also determined by results of centrifuge or calibration chamber tests, where boundaries conditions (i.e. stresses and strains), initial physical state and characteristics of the material are known.

Here after are reported some of the most used formulation used for the in-situ physical state determination. They were determined using both:

(i) ″reference approach″, where physical state of sand means mainly relative density linked with stress;

(ii) ″dimensionless approach″, where physical state of sand is mainly related to critical state line through the definition of a state parameters.

2.3.1 Reference approach

It has been customary to associate the penetration resistance with the relative density using q_c and f_s to classify type and behavior of sand.

Penetration testing, meant for many years, the standard penetration test (SPT), extensively used up through ‘90s; because of its economic benefit and simplicity, this test was, and still is, widely used to evaluate the spatial variability of a soil deposit.

Meyerhof (1957) proposed one of the first formulation published in literature; he determined a correlation between the relative density to the in-situ resistance:

[2.8] $$D_R = \sqrt{\frac{N}{a + b\frac{\sigma'_v}{98}}}$$

Where parameters a = 17 and b = 24 are sand dependents values and N is the SPT blow count. The Equation 2.8 seems to underestimated the relative density of fine and silty sands when compared to relative density deduced from undisturbed samples of normally consolidated deposits [Tatsuoka et al. 1978]: generally *a* and *b* parameters decrease with the decreasing of mean diameter D_{50} or with the increasing of fine content [Skempton, 1986].

Recently Cubrinowski and Ishihara (1999) used data of high-quality undisturbed samples (ground freezing) of clean sand, silty sands and gravelly soils, in order to establish an empirical correlation between SPT blow count and relative density of granular soils, introducing steady-state line in the general defined equation. The relationship between N, the maximum variation in void ratio ($e_{max} - e_{min}$) and the vertical effective stress where combined together as illustrated in Figure 2.9 for rounded grained (a) and for angular (b) sands. It can be noted that the biggest is the void ratio excursion, the biggest is the N blow count associated to flow liquefaction. For a defined stress level and void ratio range, when the N value exceeded N_s limit ones, there cannot be flow behavior of sand.

In dependence of the type of mixture, authors proposed the curves $N_1 - D_R$ illustrated in Figure 2.10.

The equations derived for different sands, silty sands and gravelly sands are defined below:

[2.9] $$D_R = \sqrt{\frac{N_1}{C_D}} = \sqrt{\frac{C_N}{C_D} N} = \sqrt{\left[\frac{N \cdot (e_{\max} - e_{\min})^{1.7}}{9} \sqrt{\left(\frac{98}{\sigma'_v} \right)} \right]}$$

Where: C_N is function of stress level defined as $(98/\sigma'_v)^{1/2}$;

C_D is an empirical parameter representing the grain-size effects, defined as $[9/(e_{max} - e_{min})^{1.7}]$.

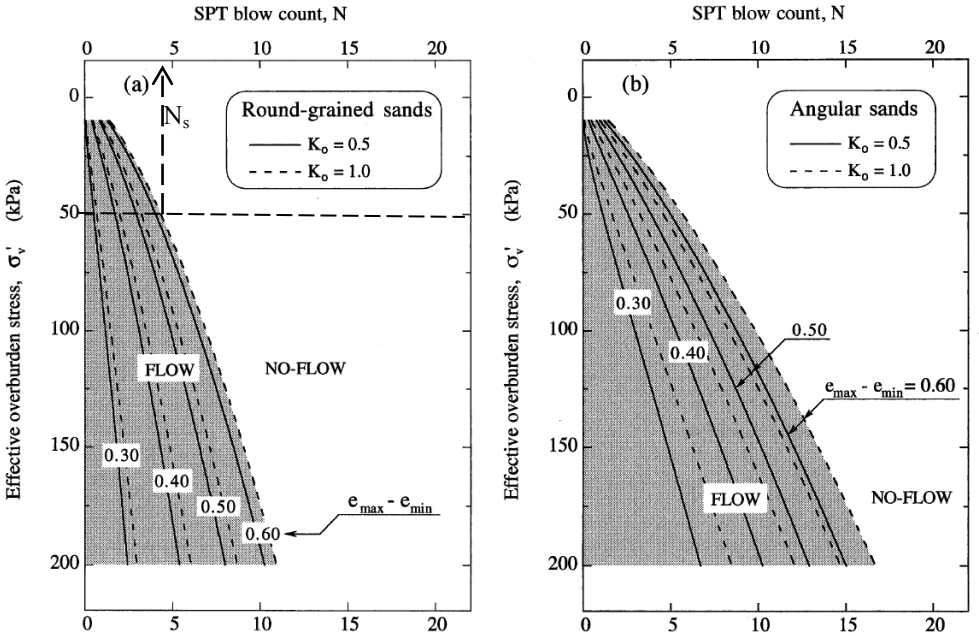

Figure 2.9- SPT boundaries differentiating between flow and no flow conditions for a range of $(e_{max} - e_{min})$ values: (a) rounded-grained sands; (b) angular sands [Cubrinowski and Ishihara, 1999]

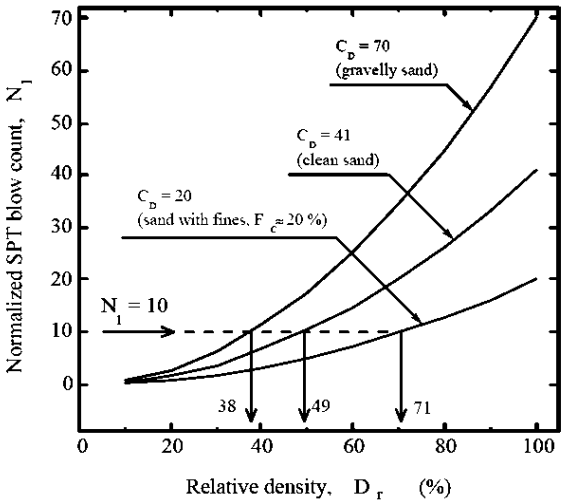

Figure 2.10- N_1 - D_R relationships for three sandy soils with different grain-size characteristics [Cubrinowski and Ishihara, 1999]

During the last twenty years, SPT has been progressively replaced by the CPT tests. The change of direction in geotechnical in-situ testing practice was also supported by some perplexity about the real quality of relative density deduced from SPT samples, as errors

in it evaluations was determined in the range of +20/-45% [Holtz, 1973; Tavenas et al. 1993; Hatanaka and Feng, 2006].

The first pioneering work aimed to determinate a relationship between cone penetration resistance q_c and D_R considering also stresses (σ'_h and σ'_v) was done by Schmertmann (1976); he linked the measured q_c in calibration chamber tests conducted under known boundary stress conditions, with the medium initial relative density of the reconstituted tested sample. The equation was defined fitting tests results conducted on medium, fine, unaged and normally consolidated sands:

[2.10] $$D_R = \frac{1}{C_2} \ln \left[\frac{q_c}{C_0 \cdot \sigma'^{C_1}} \right]$$

Where: q_c is the measured tip resistance corrected for chamber size effect;

D_R is the relative density expressed as decimal;

σ' is the initial vertical geostatic (considering NC deposits) or invariant (considering NC + OC deposits) stress;

C_0, C_1, C_2 sand's dependent coefficients.

Baldi et al. (1986) determined the coefficients of the Equation 2.10 with a best regression analysis, considering results from CC tests on normally-consolidated Ticino sand:

[2.11] $$D_R = \frac{1}{2.41} \ln \left[\frac{q_c}{157 \cdot \sigma'_v{}^{0.55}} \right]$$

Slightly different coefficients were proposed by Jamiolkowski et al. (2001) because they were derived from CC tests results of three sands (Ticino, Toyoura and Hukksund). They were reported in Figure 2.11, together with the $q_c - \sigma'_v$ or $q_c - \sigma'_h$ curves for different D_R values.

Lancellotta (1983) introduced in the elaboration the compressibility of sand and he proposed the following equation:

[2.12] $$D_R = A_0 + B_0 \ln \frac{q_c}{\sigma'_{v0}{}^{\alpha}}$$

Where: q_c, D_R and σ'_{v0} have the same meaning seen in Equation 2.10.

The A_0, B_0 and α coefficients were obtained with a best regression analysis of the CC tests results conducted on Ticino, Toyoura and Hukksund sands (Figure 2.12).

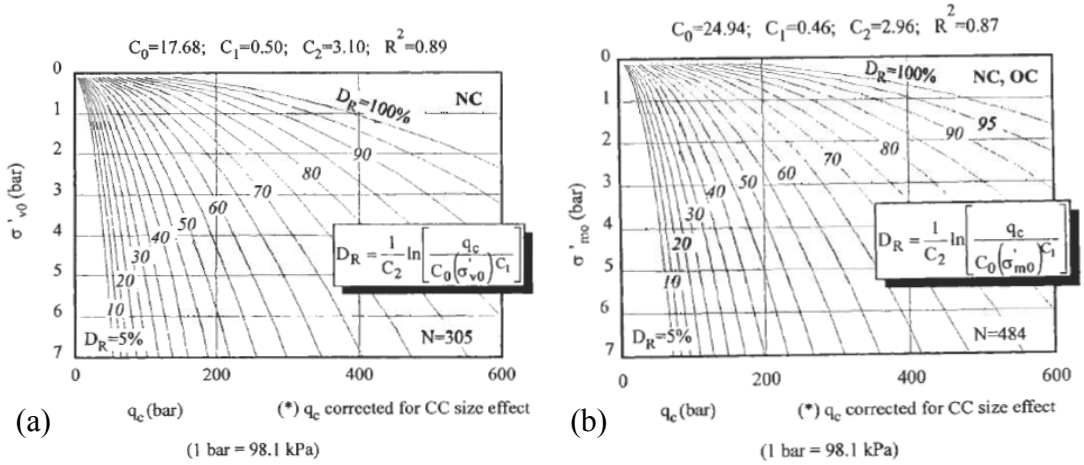

Figure 2.11- Relative density of NC (a) and NC+OC (b) sands from calibration chamber tests [Jamiolkowski, 2001]

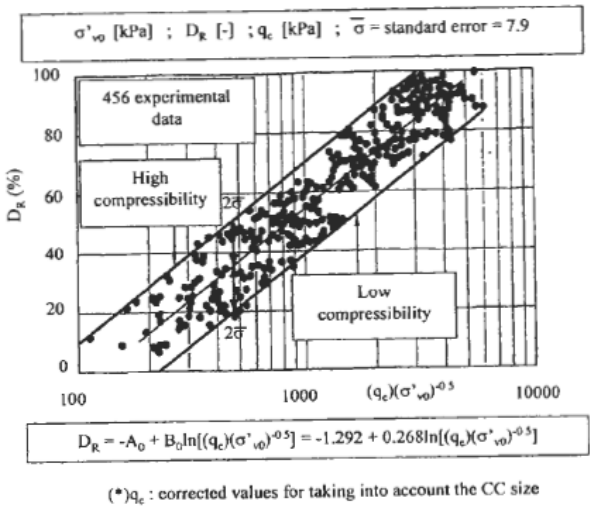

Figure 2.12- Experimental correlation between D_R –q_c -σ'_{v0} for mainly NC sands of different compressibility [Lancellotta, 1983; Garizio, 1997]

Comparison between different correlations leads to determine different relative density, as the relationships proposed are sand's dependents.

Some implementation in physical state determination was done after the introduction of state parameters and steady-state line concepts in the analysis.

2.3.2 Dimensionless approach

Been (1985, 1986; 1987) defined an exponential correlation between normalized tip resistance and state parameter ψ using a large numbers of CC test results conducted on different type of sands and silty sands, with known steady state lines.

Normalized tip resistance was defined using a dimensionless approach:

[2.13] $$Q_p = \frac{q_c - p'}{p}$$

Where: $q_c - p'$ is the net tip resistance;

p is the total mean effective stress (in drained condition p' = p).

Been demonstrated that it can be determined an exponential correlation between Q_p and ψ:

[2.14] $$Q_p = k \cdot e^{-m \cdot \psi}$$

Where *m* and *k* are sand's parameters dependents and are respectively defined as the slope of the curve in $Q_p - \psi$ plane and as the minimum value of Q_p for $\psi = 0$. From the measured normalized tip resistance it is possible to deduce the physical state of sand, as a combination of *e* and p' as follow:

[2.15] $$\psi = -\frac{\ln\left(Q_p / k\right)}{m}$$

Concurrently with the growing of CC data, it has been possible to compute the $Q_p - \psi$ curves for different type of sands, as can be seen in Figure 2.13 [database published by Jefferies and Been, 2006].

The simplified equation imposes a substantial restrain, as the evaluation of state parameter was based on a linear equation of critical state line in semi-logarithmic plane and it suggests that the contours of normalized tip resistance must be parallel to the steady state line, in an e – ln(p') plot.

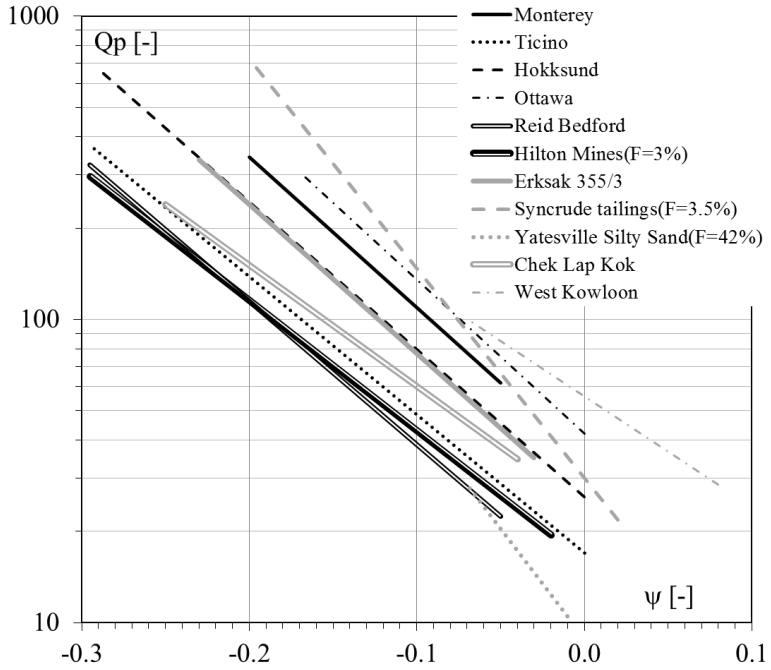

Figure 2.13- Comparison of log(Q_p) - ψ curves obtained by the best fitting of CC tests results [after Been, 1986]

Sladen (1989) stated that the Q_p - ψ relationships were stress dependent as can be noted from Figure 2.14, where are reported Ticino's sand CC test results, grouped together for constant mean effective stress. The medium fit curve deduced by Been (1986) tends to underestimate state parameter for small value of p' and overestimate state parameter for medium-to-high p' (error of $\Delta\psi = \pm 0.2$).

Shuttle and Jefferies (1998) determined numerically that there wasn't a unique relationship between dimensionless tip resistance and state parameter and that changing the stress level, keeping a constant G_0 value, (i.e. G_0 = 64 MPa for p' = 100 – 1000 kPa) arose to a stress level bias in the results. It was recognized that the state parameter is uniquely related to normalized tip resistance only if it was considered a constant value of the dimensional group G_0/p' in the Q_p – ψ determination.

Indeed, the complete formulation of the general dimensionless inverse problem must take into account six parameters (G_0/p', M, N, H, λ, ν), all of which could affect the relationship between Q_p and ψ. The influence of each parameter on the results was numerically and ″separately″ studied (Figure 2.15 from a to f): it is evident that the relationship between tip resistance and state parameter is mainly influenced by shear modulus (G_0/p'), shear strength (M parameter), dilatancy (N parameter) and hardening (H parameter) of sand.

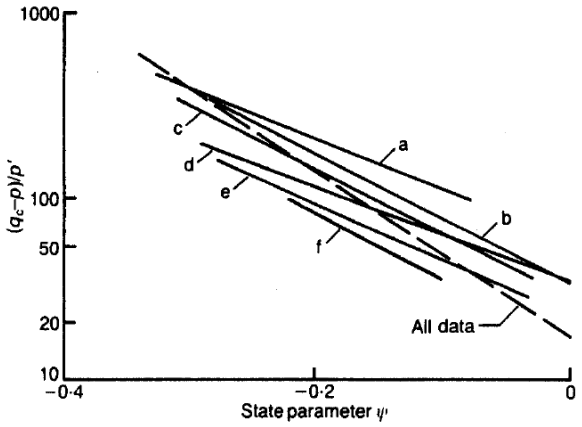

Figure 2.14- Linear regression relationships between the $\log(Q_p)$ and ψ for various mean stress levels. Comparison from (a) p' = 25 – 28 kPa to (f) p' = 442 - 458 kPa [Sladen, 1989]. It is shown the relationship published by Been et al (1987) as a mean trend of the results

The numerical simulation done by Shuttle and Jefferies leaded to determine the correction for m^* and k^* in order to take into account sand rigidity, but it was noted that this procedures was accompanied by a very small progress in the uncertainties in ψ determination. It must be underlined that cavity expansion solution, used in the numerical analysis, returns an half normalized tip resistance value when compared to measured value in CC tests, if the same state parameter is considered.

Actually, the rigidity dimensional group, $I_r = G_0/p'$, is indeed not considered in the simplified curve deduced by Been and Jefferies and the scatter in CC results might be conducted to this missing variable as one of the most influencing in the results.

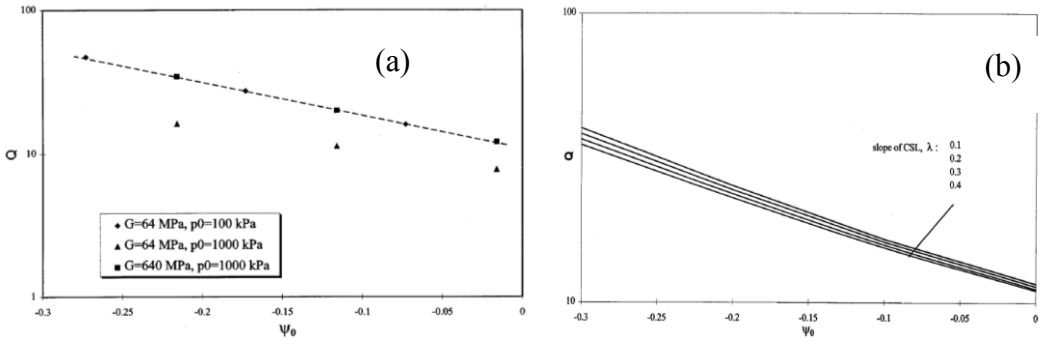

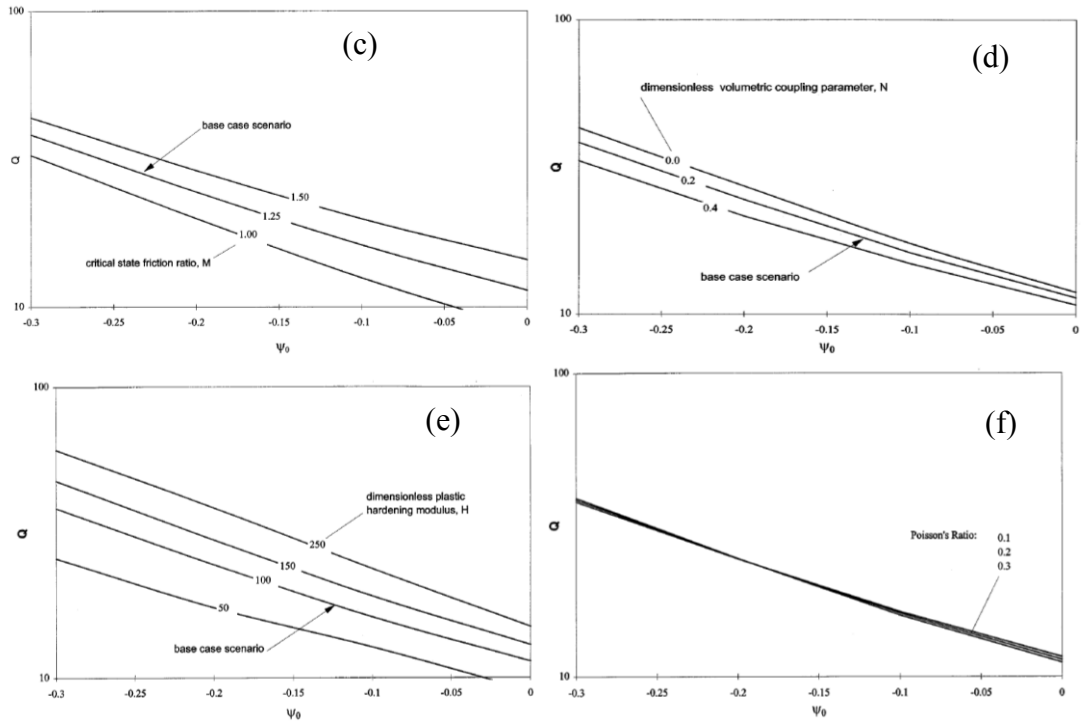

Figure 2.15- Effect of stress level on drained spherical cavity expansion in Ticino sand for different initial condition [Shuttle and Jefferies, 1998]

Another dimensionless approach has recently proposed Idriss and Boulanger (2004).

Boulanger (2003, 2004) introduced in the normalization of the tip resistance the factor C_ξ as he formulated that a uniform deposit of sand with the same D_R over all depth would be expected to have the same normalized q_{c1} values at all depth. The sand in such a deposit would become, however, less dilatant with the increasing depth. The corrected penetration resistance could be further normalized to an equivalent relative state index ξ_R value at $\sigma'_v/p_{atm} = 1$, introducing the state normalization factor C_ξ as:

[2.16] $$q_{c1\xi} = C_\xi \cdot q_{c1N} = C_\xi \cdot C_N \frac{q_c}{p_{atm}}$$

A uniform deposit of sand at the same D_R would therefore have $q_{C1\xi}$ values that slowly decrease with depth, whereas a uniform deposit of sand at the same ξ_R over all depths would have D_R increasing with depth, q_{c1} values that increases slightly with depth and $q_{C1\xi}$ values that are constant with depth.

The state normalization factor was defined by firstly finding the difference in D_R that would give the same ξ_R at an equivalent $\sigma'_v = 1$ atm. This corresponds to the difference between the critical state $D_{R,CS}$ at the in situ σ'_v and at the reference σ'_v of 1 atm:

[2.17] $$\Delta D_{R,CS} = \frac{1}{Q - \ln\left(100\frac{p'}{p_{atm}}\right)} - \frac{1}{Q - \ln\left(100\frac{p'_{rif}}{p_{atm}}\right)}$$

The p'_{rif} is usually taken equal to p_{atm}. In most situations, the values for Q and k_0 can reasonably be set at 10 and 0.45 respectively; in this case, the expression can be simplified to:

[2.18] $$\Delta D_{R,CS} = \frac{1}{5.85 - \ln\left(\frac{\sigma'_v}{p_{atm}}\right)} - 0.171$$

The C_ξ derivation can then be completed by determining how $\Delta D_{R,CS}$ affects the q_{C1} values. For the CPT, the derivation uses Equations 1.28 to get:

[2.19] $$C_\xi = \left(\frac{D_R - D_{R,CS} - 1.063}{D_R + 1.063}\right)^{3.788}$$

Using Equation 2.19 and 1.28 introduced in Chapter 1, the state normalization factor is defined as:

[2.20] $$C_\xi = \frac{\left(q_{c1N}{}^{0.264} - \frac{2.09}{5.85 - \ln\left(\sigma'_v / p_{atm}\right)} + 0.358\right)^{3.788}}{q_{c1N}}$$

Where $q_{c1N} \leq 254$.

The resulting curves are reported in Figure 2.16 (a) and (b).decreasing with depth and are slowly dependents to both q_{c1N}, k_0 and Q values.

Robertson (2010) recently re-evaluated some flow liquefaction case histories (static or dynamically induced) in order to link the behavior of sand with soil behavior chart. Using calibration chamber tests with defined state parameter and resistance, it was possible to define curves of equal state parameter in soil behavior chart $Q_{tn} - F_R$ [Robertson, 1998]. The author determined an equivalent clean sand curves in $Q_{tn} - F_R$ plane using Olsen (2001) and Olsen and Stark (2002) database of case histories, observing that $Q_{tn,cs}$ curves in Figure 2.17 (b) had the same trend observed in ψ curves in Figure 2.17 (a).

Robertson suggested that boundaries between dilative and contractive soil behavior could be determined at an equivalent normalized clean sand tip resistance $Q_{tN,CS} \sim 70$, in

correspondence to the limitation of state parameter ψ = - 0.05 proposed by Jefferies and Been).

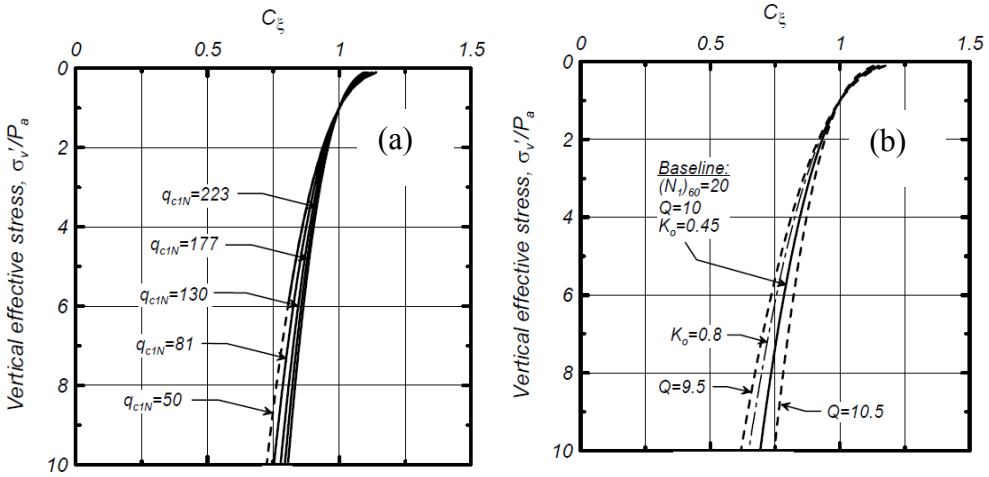

Figure 2.16- (a) state normalization factor C_ξ for range of q_{c1N} and (b) sensitivity of C_ξ to variations in k_0 and Q [Boulanger, 2004]

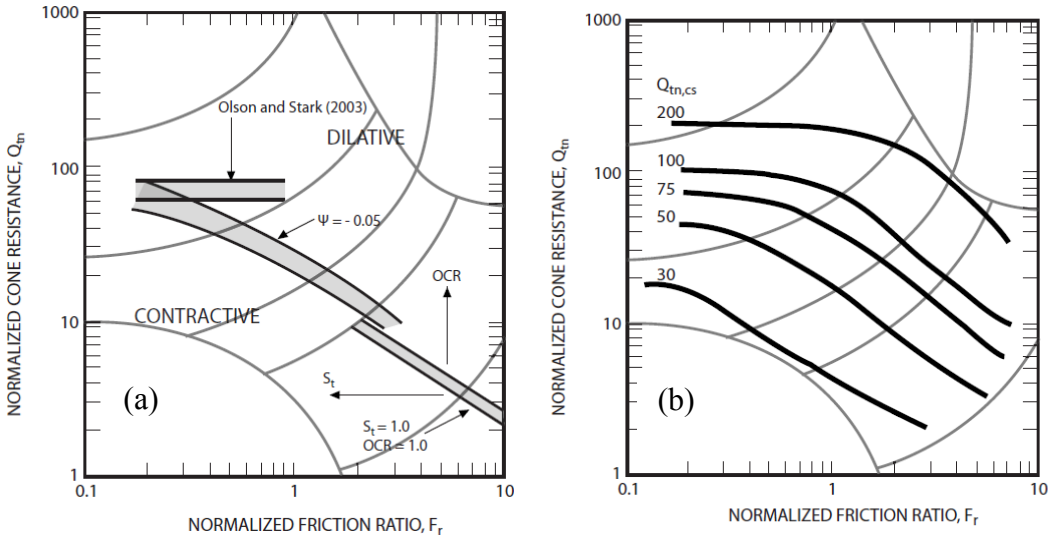

Figure 2.17- (a) approximate boundary between dilative and contractive soil response using normalized CPT parameters using CC tests and CSSM theory; (b) contours of equivalent clean sand normalized cone resistance, Qtn,cs, based on in situ evidence of seismic caused liquefaction [Robertson and Wride, 1998; Robertson 2010]

2.4 Evaluation of state of sands from laboratory tests

Here after are introduced some of the most used test apparatus for liquefaction analysis in the laboratories, with particular attention on triaxial test.

2.4.1 Cyclic simple shear tests

In cyclic simple shear test, the specimen is initially k_0 consolidated to a mean confining stress $p' = [(1 + 2 \cdot k_0)/3] \cdot \sigma'_{v0}$; the initial principal stress conditions are shown in Figure 2.18 (a), together with the relative Mohr's circle.

After consolidation, a cyclic horizontal shear stress of peak magnitude τ_h is applied in undrained condition at the top and at the bottom of the sample. The condition of non-volume change is obtained by forcing axial deformation to be zero ($\varepsilon_r = 0$ during all test); the change in total vertical stress in such a constant volume test equals the pore pressure which would developed in an equivalent undrained test. The effective stress condition and Mohr's circle are illustrated in Figure 2.18 (b). The CSR = τ_h/σ'_{v0}, where the vertical effective stress at the end of consolidation is the major of the principal stresses and the only one always precisely known.

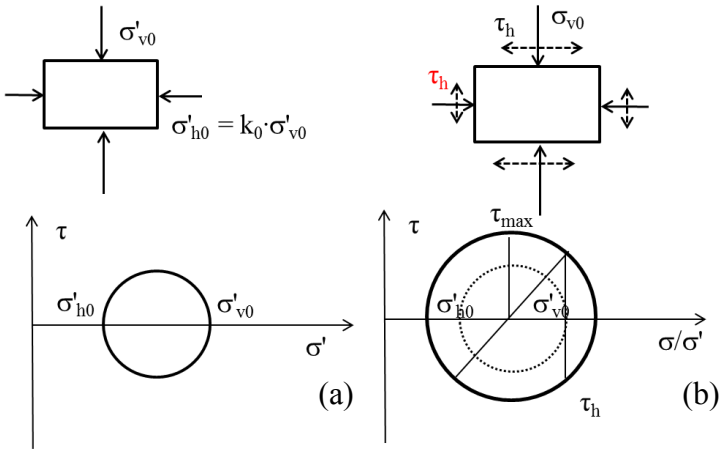

Figure 2.18- Mohr'r circle for cyclic simple shear test

There are currently two designs of simple shear apparatus: one developed at Cambridge University and the other at the National Geotechnical Institute (NGI) in Oslo; the last one is commonly used also in academic and commercial laboratories.

The sample in NGI apparatus (80 x 10 cm) is contained in a special membrane reinforced with iron wires that prevent lateral deformation, but allows uniform vertical deformation

and rotation of vertical sides of sample. Cambridge apparatus contains a rectangular prism (10 x 10 cm) laterally confined by smooth side platens that allows vertical displacements but they not provides complementary shear stresses on the vertical plane.
The cyclic simple shear is considered the test apparatus that batter reproduced the in situ condition under cyclic loading [Boulanger, 1993, 2004, 2006, 2007; Sancio, 2003; Ghionna and Porcino, 2003].

2.4.2 Torsional cyclic test

At the beginning of 70's Ishihara and Li developed one of the first torsional triaxial test device. The whole setup is almost identical to the triaxial test apparatus except for the new features consisting of a piston with the same diameter as the sample, which permits the condition of no lateral strain of the specimen. Therefore, it became possible to apply torsional cyclic shear while preventing lateral movements of the specimen (i.e. simulation of k_0 condition) and simulate the field condition during earthquake.
When a full cylindrical specimen with a circular cross section is subjected to a twisting moment, the distribution of torsional shear stress in a plane perpendicular to the axis is not uniform, so the choice of a representative shear stress in not a simple task. Usually the average shear stress deduced from plastic distribution of stress in the sample and the corresponding strain are the quantities utilized in the analysis.
In order to step ahead from the non-uniformity of stress and strain valuation, hollow sample are usually preferred. The hollow cylinder test allows testing on both isotropically and anisotropically consolidated specimens. This instrumentation is capable to simulate field's stresses conditions, including principal stress axis rotation. As it is possible to control all principal stresses applied on the specimen, tests result are used to calibrate constituted model using different stress path.
The four components of stress σ_z, σ_r, σ_θ e $\tau_{z\theta}$ induced the four components of deformation ε_z, ε_r, ε_θ e $\varepsilon_{z\theta}$ (Figure 2.19) and all of these quantities are directly measured.
Vertical stress is assumed to be uniformly distributed across the cross section, while the others quantities are obtained by averaging stresses over the volume of the specimen assuming soil to be linear elastic.

Failure due to cyclic loading is usually defined by the development of a specific level of strain; the shear strain in the sample is defined below considering the principal strains in triaxial condition is $\gamma = 2/3 \cdot (\varepsilon_1 - \varepsilon_3)$.

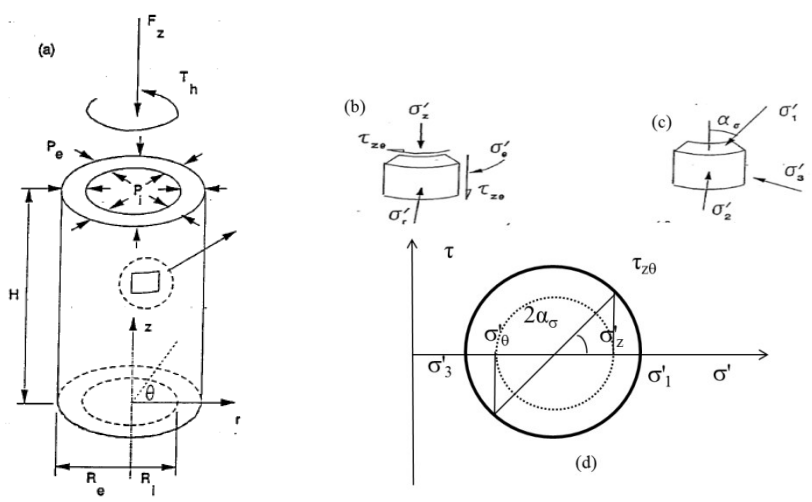

Figure 2.19- Mohr's circle for cyclic torsional shear test; hollow cylinder case

Using a triaxial torsional shear test apparatus two type of strain-controlled tests were carried out. In the first type the principal stress ratio was maintained unaltered during cyclic loading and the changes in torque, pore pressure and vertical displacement were measured. The results showed that the liquefaction did not occur and the pore pressure ceasing to increase after reaching a certain level, but the vertical displacement continued to increase indefinitely suggesting some failure of the sample. In the second type of tests, the water can't entry in the cell during the torsional test. After anisotropical consolidation, it was observed that in this type of test liquefaction could easily set up, concurrently with a lateral increase of lateral stress. Pore pressure was generated both by cyclic loading and by the change in principal stress rotation.

Ishihabi and Sherif, (1974) adopted a device that summarized the qualities of torsional and simple shear. The instrumentation was capable to eliminate the effect of wall friction coupled with the fact that the magnitudes of the horizontal stresses were known as in torsional shear device. For the particular geometry of the container, the shear strains through the sample were uniformly defined as well as the shear stresses. The authors demonstrated how the CSR – N curves were dependent both on the type of shear stress and on the type of normalization chosen for cyclic stress ratio definition. Furthermore, comparison from torsional and simple shear tests were not comparable, even if the same k_0 value was adopted. In fact, authors found that $(\Delta\tau_{max}/\sigma_{oct})$ – N curves were independent

of k_0 values while Seed and Peacock's (1971) work revealed a decrease of ($\Delta\tau_{max}/\sigma_{oct}$) with decreasing k_0 for a constant number of cycles N, a well contradictory result.
The torsional device is not always available in laboratory and specimen's preparation procedure could be very difficult due to placement of two membranes on the specimen. Lastly, the interpretation of the test is not immediate and is difficult to be correlated with other test results.

2.4.3 Triaxial cyclic test

The triaxial cyclic apparatus is certainly the most used equipment for cyclic liquefaction analysis of sand.
Cyclic stress and deformation of an in situ finite element is reproduced, in approximately way, by cyclic triaxial compression tests. In order to demonstrate the analogy, in Figure 2.20 (column 1) are shown three stress conditions at different stages of loads while in the column 2 the three correspondents Mohr's diagrams. In case (a, column 1) the stress applied to an infinite element is isotropic and the Mohr circle is a point. In condition (b, column 1) the vertical stress is increased by an amount of $\sigma_{dp}/2$ while the horizontal stress is decreased by the same quantity; by the Mohr circle is deducible that on the plane XX acts again the initial isotropical stress σ_3, as well as a shear stress equal to $\sigma_{dp}/2$. Finally, in condition (c, column 1) the vertical stress is reduced by $\sigma_{dp}/2$ and the horizontal stress is increased by the same amount. Again, the resulting stress on the XX plane is the same of case (b, column 1) but with revers sign. Thus, the stress acting on a plane XX cycling a sample as (b) and (c) is considerably the same as the stress acting on a horizontal plane in situ. In (column 3) there is a decomposition of the applied stresses represented in (column 1); it is clear that applying an all-around pore water pressure does not change the effective stress and the deformation of the specimen so it might be neglected.
The stress acting on in situ elements for saturated sand is so easily obtainable in triaxial test apparatus applying to the specimen the stress in (column 4), correcting the water pressure by a factor equal to $\sigma_{dp}/2$.

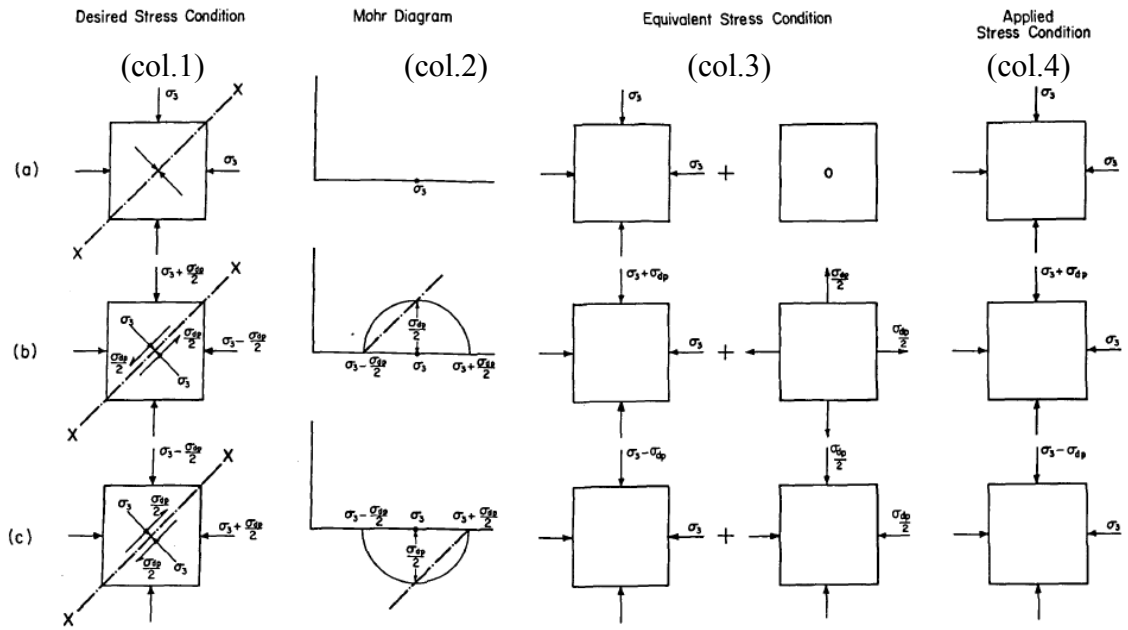

Figure 2.20- Stress condition for triaxial test on saturated sand under simulated earthquake loading condition [Seed and Lee, 1966]

Garca and McKay grouped together many cyclic triaxial tests results of more than 30 different type of soils, 13 of which were sand and silty sand; tests were analyzed with ″limiting strain criteria″ ($\Delta\varepsilon_a$ = 5% for isotropically consolidated tests and ε_a = 2.5% in compression for anisotropically consolidated tests) in order to determinate the number of cycles causing liquefaction. Sample tested were reconstituted in laboratories or collected from thin-wall tube sampler, so they presented different relative density and type of particle arrangement.

In Figure 2.21 are reported some test results conducted on tailing sand in $CSR_{DR=50\%} - N$ plane. The cyclic resistance of the samples were corrected in order to be representative of a sample with D_R = 50%. While results in Figure 2.21 (a) seem to have a reasonably unique trend, the same conclusion is not deduced from the Figure 2.22 (b) for non-tailing sands results.

The scatter in the cyclic resistance is considerably high such as the sands compared were different; the trend in the mean curves is evident, as the number of cycles to liquefaction increases with the decreasing of the normalized cyclic stress.

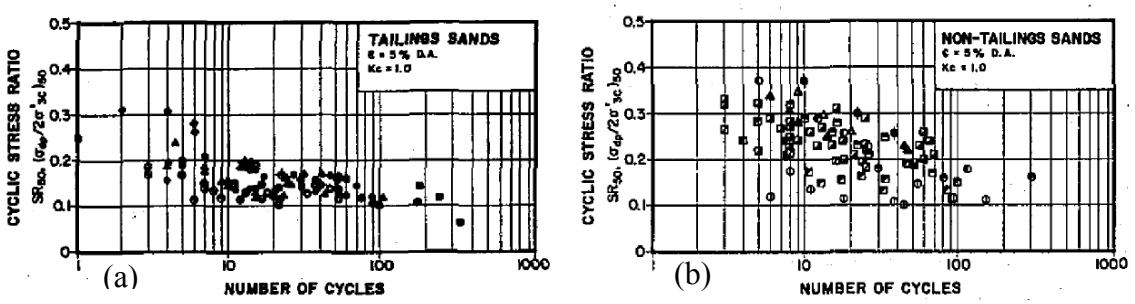

Figure 2.21- (a) cyclic stress ratio vs number of cyclic for tailings sand and (b) for non – tailing sands where CSR is normalized to an equivalent CRR(D_R = 50%) [Garga and McKay; 1984 database]

The main consideration and doubt about CSR – N curves is how cyclic resistance, for a particular number of cycles, is related to state of sand throughout critical soil mechanics.

It has to be considered that cyclic resistance should be related to critical friction angle trough parameter M and critical state theory also leads to expect that the undrained behavior of sand is related to the ratio between elastic and plastic modulus of the sand [Jefferies and Been, 2000]. In any case, the most important factor affecting cyclic behavior of sand is considered to be grain contact and intrinsic arrangement of the particle of sand, together with initial void ratio and mean effective stress.

Boulanger (2003) determined that the CRR of sand for both triaxial and simple shear tests could be expressed as an approximately unique function of relative state parameter ξ_R, as illustrated in Figure 2.22 (a). He used data from tests conducted on Fraser river sand [after Vaid and Sivathayalan, 1996] on specimens with D_R = 30 ÷ 70%, consolidated under effective stress from 50 to 400 kPa. CRR was determined in correspondence to the development of 3% shear strain in 10 uniform loading cycles. This data suggest that ξ_R parameter can reasonably represents the combined effects of D_R and σ'_v on the cyclic resistance, but are profoundly dependent from the type of test condition as can be noted from the difference between triaxial and simple shear tests.

In Figure 2.22 (b) are illustrated the interrelations among K_σ , ξ_R, CRR, D_R and σ'_v. The CRR – D_R relationship, for a given consolidation stress, upwards with increasing D_R, but cyclic resistance ratio decreases with the decreasing of ξ_R value.

Increasing the consolidation stress from 100 kPa to some higher value, it results in the same decrease in ξ_R for all values of D_R.

This ξ_R changes the CRR by amounts that depend on the initial D_R, because of the curvature of the CRR versus ξ_R relationship (which applies to all values of D_R and consolidation stresses). Thus, the reduction in the CRR, as expressed through the K_σ

factor, depends on the initial D_R. The K_σ relationships derived from the CRR versus ξ_R relationship match the relationships resulting directly from the experimental results, as expected. State normalization approach seems to be an alternative methodology for the computation of CRR, instead of using K_σ. Porcino et al. (2009) correlated CRR for Ticino sand and relative state parameter using results from simple shear device deducing a unique function between CRR – ξ_R, deducing the same correlation as introduced by Boulanger.

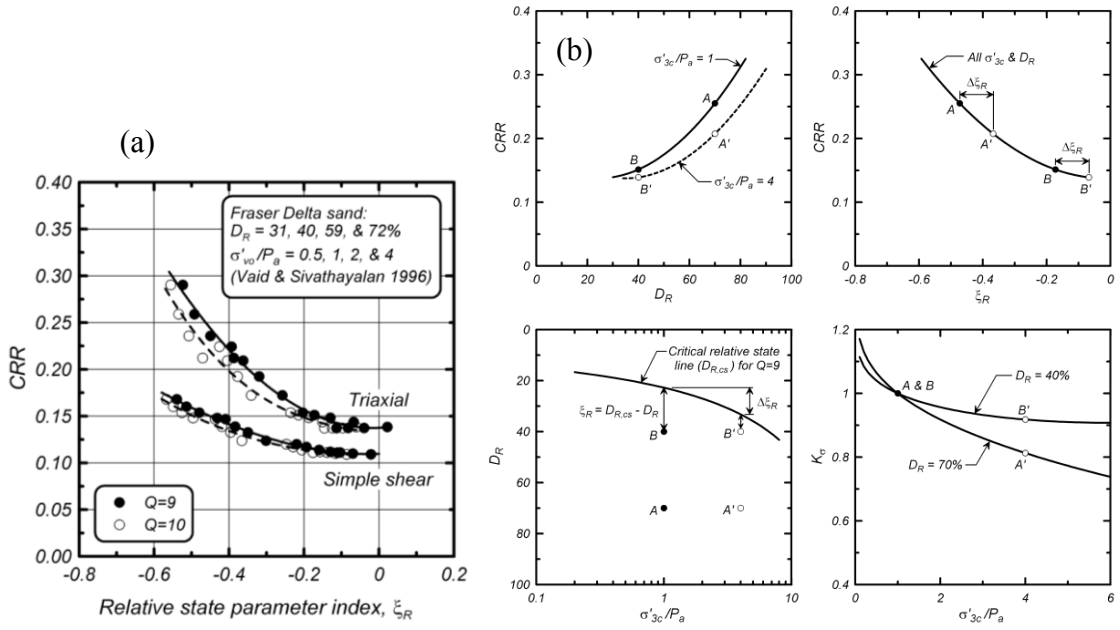

Figure 2.22– (a) CRR versus ξ_R for reconstituted specimens of Fraser Delta sand (b) correlating K_σ and ξ_R values [Boulanger 2003]

In Figure 2.23 are reported some results grouped together and derived by different experimentations; the plot represents the CRR (for 15 cycles) versus the initial state parameter ψ as defined by Been (1985). As determined for the CRR – ξ_R graph, also in this kind of representation the decreasing of cyclic resistance with state parameter is evident, but a unique trend is not determinable as the sands were tested in different conditions.

The results derived all from cyclic triaxial isotropically consolidated tests (with p'_c = 100 kPa), but the inner characteristics of sands were different. Methods adopted for reconstituting samples were dissimilar from research to research, furthermore some state parameter values were referred to void ratio before the consolidation; inasmuch some data were not available.

From the Figure 2.23 is deduced that state parameter alone does not capture the anisotropy of the sand and here's why it was observed an important scatter in the results.

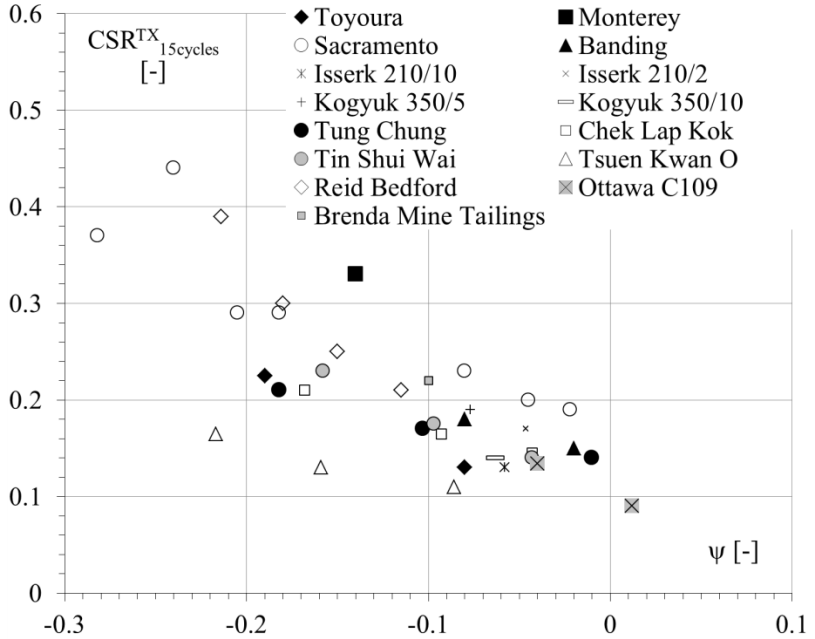

Figure 2.23- Cyclic liquefaction resistance versus state parameter for different type of sands (p'_c = 100 kPa for all tests) [after Jefferies and Been, 2010]

2.4.3.1 Triaxial cyclic test apparatus

In this research the ISMGeo triaxial apparatus is used for the estimation of cyclic behaviour of Ticino sand.

The cell for cyclic triaxial testing is the result of an improvement in its construction details. This cell can stand pressure up to 1000 kPa and is designed to easily allow the removal of the only lateral chamber, rather than the whole top part.

The top platen and the bottom platen are perfectly aligned, providing better contact between the specimen and the platens. On the other hand, being the two platens interchangeable, the cell can accommodate specimens of variable diameter, from 38.1 to 100 mm.

The cell is equipped with special ball valves and fitting for sealing, if necessary, the cell during the test. A vertical lock mechanism is also provided to maintain axial pressure. Thanks to this features, the cell may be disconnected from the compressed air generation system, and moved without disturbing the specimen. Thus, it is possible, for example, to consolidate in a laboratory room and to test in another part, where loading and acquisition equipment are located.

The cell is constructed of high-strength stainless steel; it requires no maintenance, and may be used with corrosive soils and brackish water.

The heart of the cell consists of a piston and a bearing system, especially designed to eliminate friction phenomena which have in the past compromised the results of the triaxial tests. An O-ring is used during the static consolidation phase to maintain lateral pressure in cell.

During the dynamic loading or static shear testing, the ring is disengaged: thus a small volume of air is allowed to pass around the load rod. The resulting friction on the rod is virtually zero. This feature is very important, since in the cyclic triaxial test, even a small amount of friction involves improper measurements of forces acting on the specimen and consequently of test results. This drawback takes a special significance during tests on slight-strength materials, or still, when loads of small amount are to be applied.

The system is electro-pneumatic: the signal produced by an electrical function generator is converted into a pneumatic signal, which may be used to control pneumatic actuators applicable to any type of soil test equipment.

The system producers not only signal for applying dynamic loads but also for static loads, under stress-controlled conditions. The latter are used both to consolidate specimens and for shear testing. In addition, static and dynamic combined loads may be applied.

The amplitude and frequency of loading may be varied by programming the function generator which is incorporated into the system. All the necessary pneumatic controls are included in the system, as well as a digital counter to display the number of loading cycles.

The double acting pneumatic cylinders are designed to be used with electro-pneumatic cyclic load generator and make it possible to apply static or repeated loads, at controlled amplitude, to a variety of different test equipment.

The cylinders are available in a variety of size, so as to achieve the loading system that better suits test requirements. For example, for cyclic testing on small-size or soft specimens, small loading cylinders are available. For other specimens which require the application of higher stress, larger cylinder are available, which make it possible to develop static or cyclic forces of about some hundreds of daN. These actuators use Bellofram sealing membranes and bearings on the load rod to minimize friction.

Chapter 3

3 Monotonic Behavior of Saturated Sand

3.1 Monotonic resistance of saturated sand in undrained condition

The mechanical behavior of granular soil mainly depends on its initial physical state, as introduced in the previous Chapters [see i.e. Poulos, 1981 and Been, 1985]. It was also found that, in the e – p' plane, exists an ultimate curve corresponding to the steady state of a cohesionless material defined when continuous deformation of soil, at constant volume and constant stresses occurs [Castro, 1975; Poulos, 1981].

The region above steady-state curve corresponds to the contractive behavior of soil, which means that the pore pressure in sand built up if it is sheared in undrained condition. The region below steady-state curve corresponds to a dilative behavior of sand with the developing of negative pore pressure during shearing.

In undrained tests, it is useful to define three different sand's ″behaviors″ associated to different levels of deformations. The definitions of the steady-state, the quasi-steady state and the phase transformation state are shown in Figure 3.1, for a monotonically triaxial undrained test result.

It can be seen that the steady-state is associated to large deformations and corresponds to a state of residual undrained strength at ″C″ condition. The state of transient minimum

strength in ″A″ corresponds to the phase-transformation state in q – p’ plane or to the quasi-steady state in e – p’ plane [Ishihara et al., 1975].

Experimental evidences suggest that a single line, usually named PT – Line in the q – p’, plane would exist as a fitting line of the phase-transformation states plotted. Identically in the e – p’ plane the quasi-steady state line could be determined.

More precisely, Ishihara (1993) determined a line in e – p’ plane (called Initial Dividing line) that separated the initial state $(e, p')_c$ that could present quasi-steady state behavior from that ones that couldn’t. Samples with physical state that hung on the plane region above the ID – Line will manifest the quasi-steady state when sheared; on the contrary, below the ID – Line no drop in shear will occur and the sand approaches steady state with a hardening behavior.

Furthermore, as can be seen in Figure 3.2, the curve that interpolates the quasi-steady (or phase transformation) state condition is stress dependent: two samples of Toyoura sand reconstituted with the same void ratio but consolidated with two different mean effective stresses manifest the quasi-steady state condition for different deformation values.

Finally, instable behavior of very loose sand has received particular attention, as at failure a quasi-zero shear resistance is observed; mechanical behavior of such loosely packed sand has been called ″flow liquefaction″ or ″static liquefaction″ [Castro, 1969; Poulos, 1981; Sladen et al., 1985; Ishihara, 1993; Yamamuro and Lade, 1997].

Two approaches were commonly used to interpret the location of the occurrence of static liquefaction in the q − p ' plane by establishing different lines: (i) collapse line [Sladen et al., 1985] and (ii) instability line [Lade et al., 1988] or flow liquefaction line [Vaid et al., 1990]. The first was a straight line locus of points triggering liquefaction that passes through the steady-state points with the same void ratio at different confining pressures, while the second was a straight line locus of points triggering liquefaction passing through the origin point and was regardless of stress path, initial void ratio and confining pressure.

Some discussions have proven that flow liquefaction line is not exclusively determined but variable with state of sands [Yang, 2002] and researches are still in progress.

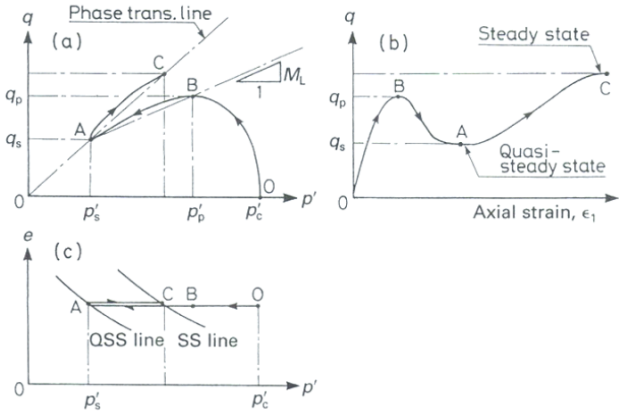

Figure 3.1- The definition of various states of sand subject to undrained loading [Ishihara, 1996]

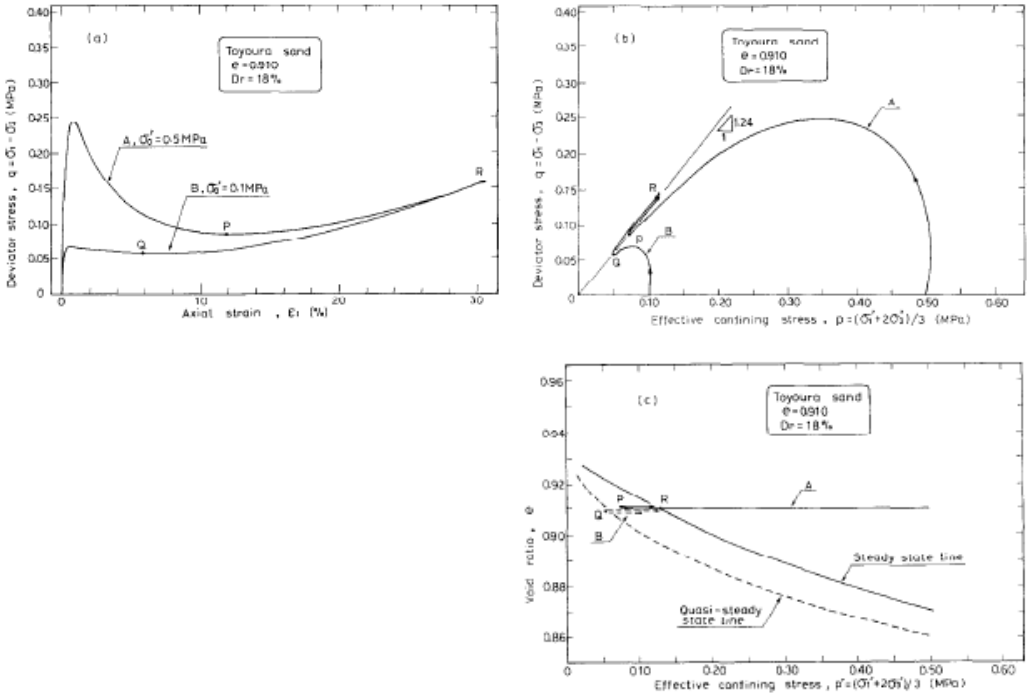

Figure 3.2- Position of QSS – Line in dependence of the mean effective stress and ubiquity of SS – Line. Results from two CIU tests on Toyoura sand with the same void ratio (e = 0.91) but different consolidation mean effective stress (p'_c = 100 – 500 kpa) [Verdugo, 1992; Ishihara, 1993]

3.2 Monotonic resistance of saturated sand in drained condition

As was mentioned in the previous sections, both the initial void ratio and the level of effective confining pressure have an influence on the stress-strain and volume change responses of sand, even in drained load conditions [Lee and Seed, 1967; Miura et al.; 1984; Tatsuoka et al., 1986].

In Figure 3.3 (a, loose state) and (b, dense state) are reported some triaxial drained tests conducted by Lee (1967) on reconstituted air pluviated samples of Sacramento River sand. In dense specimens the mechanical behaviour was dilative until high stress $\sigma'_{3c} \leq 10$ atm was approached. Overtook the very high consolidation stress of $\sigma'_{3c} \geq 19$ atm, a dense sand looks like a loose sand at medium pressure, as it contracted to critical state. The behaviour of dense sand for very high confining pressures was associated to the continuous breakage of sand particles: during shearing grains tend to packages differently in conjunction with the increasing of fine content in the original grain size distribution [Bandini and Coop, 2011; Ghafghazi, 2014].

Loose sand (Figure 3.3 b) sheared at low confining pressure (σ'_{3c} = 1.0 – 1.9 atm) behaves nearly like a dense sand sheared at medium effective confining pressure, and a slightly dilation is observed; with the increasing of confining pressure the loose sand approaches the critical state with a contractive behavior.

It is well known that shear bands form in dense sand samples sheared under drained conditions and the deformations are herein localized. The post-peak brittleness is anticipated and the magnitudes of drop in shear seem sample-size dependent: the smaller sample shows a small decline in strength with strain after peak, whereas the larger samples show a more rapid drop to a stable residual strength. [Jefferies et al., 1990; Scott, 1987]. The void ratio at critical state condition may be not fully representative of in-situ condition and an underestimation of volumetric strains could be important for a correct evaluation of critical state line [Oda, 1972, Desrues et al., 1996, Frog and Jang, 2000].

Results in Figure 3.4 demonstrated that the distribution of void ratio within the specimens deformed beyond peak stress, were not uniform and their middle part showed an higher void ratio than the top and bottom of the specimens.

The tests were conducted by Oda (1972) on dense specimens reconstituted by air depositional method (P series) and wet tamping method (T series); he established that a

deformed sample could be subdivided into three statistically homogenous sections in regard to void ratio distribution:

- dead domain: the formation of this domain at the end of specimens was due to the restraining effect of radial friction forces at the end plated, by which little fabric reconstruction occurred during deformation;
- dilated domain: this domain was characterized by a great void ratio (dilation occurred in specimen) occurring in a narrow bonds in the central part of the specimens. With the increasing of deformation dead domain became smaller and the final volumetric deformation must be determined, not only by the initial narrow void ratio, but by the extent of the final expansion of its domain;
- shear domain: this domain had also large void ratio, but smaller of that one in dilated domain.

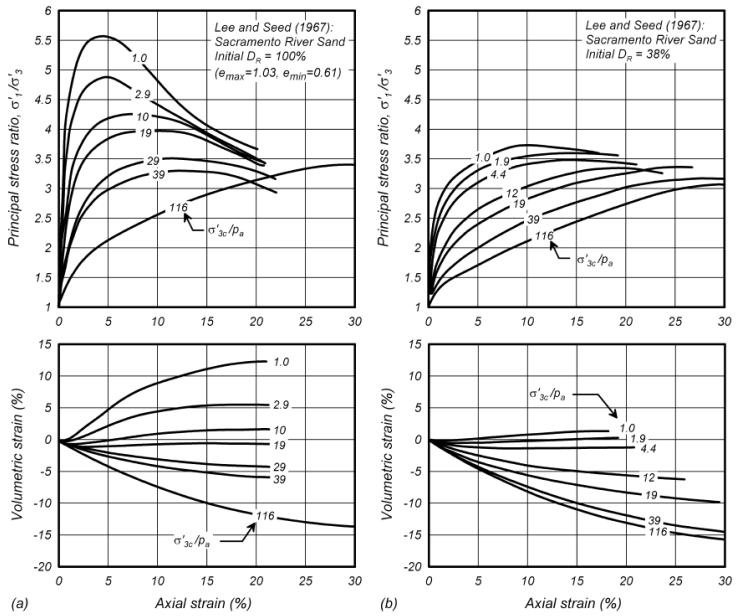

Figure 3.3- Drain triaxial tests on (a) dense and (b) loose samples of Sacramento River sand. Stress strain behavior on σ'_1/σ'_3 - ε_a and ε_a - εv plane [Lee and Seed, 1967]

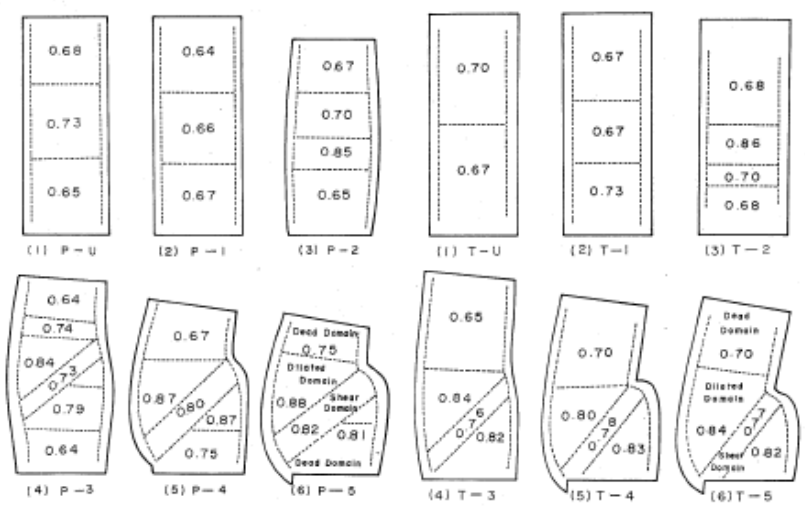

Figure 3.4- Evolution of internal void ratio during a compression triaxial test from start to the end of test. ″P″ sample reconstituted with air pluviation method ″T″ sample reconstituted with wet tamping method [Oda, 1972]

3.3 Factors affecting the resistance of a sand

3.3.1 Depositional methods

Laboratory tests conducted on granular soils are usually performed on reconstituted specimens as well as obtaining samples of these materials in their undisturbed state is very difficult and sometimes not representative (especially for loose sand).

Various samples preparation methods have been developed based on (i) the moisture condition of the soil, (ii) the method of soil placement (i.e. pluviation, spooning or flowing) and (iii) medium through which the soil is placed (air or water).

These procedures were developed in order to correctly reproduce both in situ orientation of sand's particles and in order to reconstitute the widest range of void ratio.

Pluviation in water is one of the most used reconstituted method; it has been shown to resemble the alluvial deposition process because the fabric that ensues upon water pluviation has been found to be similar to that of the naturally deposited alluvial and hydraulic fill sands [Vaid et al., 1999; Kuerbis and Vaid, 1988; Chaney and Mulilis, 1978]. Also, the air depositional method [Oda et al., 1978; Oda and Koishikawa, 1978] has been used as ones of the easier and trusty procedures available for reconstituted samples.

Even if the problem posed by sampling is overtaken by introducing different samples reconstructions techniques, the complicatione is that different depositional methodologies used in specimens preparation cause different mechanical behavior of tested sands [Vaid et al., 1999; Ishihara, 1993; Wood and Yamamuro, 1999; Della, 2009].

In Figure 3.5 is shown the effect of fabric on the behavior of Synclude sand in a constant volume simple shear device. Three specimens were formed at approximately the same void ratio e_c = 0.76 and consolidated at a vertical stress of σ'_v = 200 kPa, only depositional method was varied (air pluviation, water pluviation and moist tamping).

The specimens show completely different patterns of behavior: the moist-tamped sample (c) is brittle in undrained shear and shows a tendency to easily collapse; the water pluviated sample (a) is ductile and mobilizes a large undrained strength and the air pluviated sample (b) shows an intermediated pattern of behavior.

The first sample reconstruction methodology (c) is usually associated to a drop in shear resistance due to the honeycomb particles configurations, which seems particularly collapsible and phase-transformation is difficulty observed [Casagrande, 1975]; moreover, the moist-tamped methodology allows to reconstituted very loose samples but a great non-uniformity is always observed [Castro, 1969].

Deposition through water, indeed, produces very uniform samples [Vaid and Negussey, 1988]; on the other head, very loose states are very difficultly reproduced.

Air depositional method seems the most reliable because, with standard procedures, uniformity of the sample is easily achieved [Lo Presti, 1993] and different densities are obtained varying easily the height of fall or the sieves opens from witch the sand come out [Vaid and Nagussy, 1984; Lo Presti, 1993].

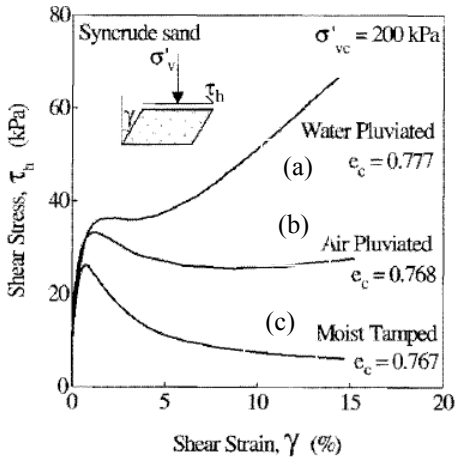

Figure 3.5-Influence of different depositional methods on the mechanical behavior of Synclude sand in simple undrained shear test [Vaid et al, 1995]

3.3.2 Loading direction and loading type

A similar range in behavior as observed in sample formed with different depositional methods is shown in Figure 3.6 [Uthayakumar and Vaid, 1998], where differences in stress-strain behaviors are related to consequence of anisotropy produces during the shear stress application.

The samples of loose Fraser river sand were reconstituted with the same depositional methodology and with the same void ratio, but were sheared with different modes; actually the samples were sheared with different direction of the principal stress.

Loading direction of the shear stress applied to the sample is usually associated to α parameter:

[3.1] $$\alpha = \frac{\sigma_1}{\sigma_2}$$

This parameter defines the grade of the major applied stress σ_1 with respects to the intermediate stress σ_2.

In multi-axial general stress condition is useful to define also the *b* parameter, capable to consider the influence of the intermediate stress on the result of the test:

[3.2] $$b = \frac{\sigma_2 - \sigma_3}{\sigma_1 - \sigma_3}$$

The major, the intermediate and the minor stress are respectively σ_1, σ_2 and σ_3.

For example, in triaxial compression tests $\alpha = 0$ e $b = 0$ while in triaxial extension tests $\alpha = 90°$ e $b = 1$.

Introduced the α and *b* factors, it can be deduced from Figure 3.6 that the strongest stress-strain response is associated to a shear stress applied with σ_1 perpendicular to the bedding (i.e. triaxial condition with $b = 0$ and $\alpha = 0°$) and the weakest one when σ_1 is parallel to the bedding (i.e. $b = 1$ and $\alpha = 90°$). The α and *b* parameters rule response of sand: in triaxial compression conditions a strain-hardening behavior is observed while in triaxial extension test a soften behavior with a collapse in strength is experienced in the sample; in simple shear tests an intermediate stress-strain behavior with a limited phase-transformation condition were detected.

Different monotonical behavior of sand is surely linked to the anisotropy of sand's particles. Usually, the methodologies used in laboratories always take the vertical depositional direction as the most representative of in situ condition [Bishop, 191; Oda et al, 1978; Hanzawa, 1980, Miura e Toki, 1982; Vaid et al., 1990].

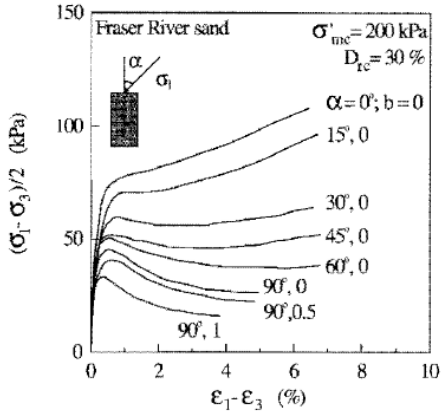

Figure 3.6-Different mechanical stress-strain behavior for triaxial undrained test on Fraser River sand for various α and b values

3.4 Critical state from triaxial tests

Critical state line definition was historically associated to the interpretation of medium to high density drained tests, while steady state line definition was associated to undrained triaxial tests results deduced from loose samples.

A lot of discussions occurred in the last decades on the difference between the two failure lines obtained from drained and undrained tests; the questioning about the uniqueness and equivalence of the two curves in e – p' were usually linked to an incorrect evaluation of critical state condition [Casagrande, 1975; Poulos, 1971; Sladen, 1985; Alarcon, 1988, De Gregorio, 1990]. This misleading might be related to some confusion between ultimate critical and phase transformation state; this last temporary condition can't be confused with an ultimate failure situation, because, if the sample is continuously loaded, it presents some extra resistance.

Laboratory experiences have indicated that the most reliable method for the determination of critical (or steady) state line is based on a series of triaxial compression tests on loose samples.

Working with soften specimens, Castro's approach is usually employed and a series of undrained triaxial tests (in stress-controlled apparatus) are always recommended as a starting point for critical state line determination. In fact, loose samples don't develop shear bands localization and an accurate evaluation of critical state condition is possibly determined because, for a small starting deformation, occurs a fast pore pressure build up. Indeed, specimens with a loose of critical state approach to failure with fast deformations that are in the range of triaxial tests apparatus.

Sometimes, undrained tests are usually replaced by drained tests conducted on loose samples because they approach failure with a lower rate of displacements, even though they take more than $\varepsilon_a > 20\%$ before critical condition becomes established.

This change in laboratory practice is linked to some limitations encountered in the determination of soften samples; in order to obtain loose of critical states a very high consolidation pressure ($p'_c > 2$ MPa) must be applied to the specimens. Such high pressures are inconvenient for most commercial triaxial equipment as well as they often involves grain crushing effects.

The critical state line is considered to be correctly defined when the following cautions are considered:

- uniform samples are prepared with a reliable technique;
- samples must be fully saturated ($B \geq 0.95$);
- void ratio must be accurately calculated before, during and after the test ($\Delta e = \pm 0.003$);
- apparatus system must be capable to measure very low pressures, as well as very high pore pressures generation;
- number of triaxial tests must be sufficient to have an adequately confidence on critical state line determination.

Been suggested to determine the critical state line from at least 5 tests, in two phases:

- 3 undrained tests on very loose samples ($e_1 > e_2 > e_3$) consolidated to a medium value of mean confining stress (for example $p'_c = 350$ kPa equal for all samples). 2 others drained tests on very loose samples with a void ratio similar to e_2 from the first set data, and consolidated with two different mean effective stress, one higher and one smaller than $p'_c = 350$ kPa (say i.e. 200 and 800 kPa);
- others 3 or more tests in order to correctly define the critical state line slope.

In the present thesis critical state line and steady state line are considered uniquely determined by drained and undrained triaxial tests interpretation [Castro, 1975; Been, 1991].

In the following paragraphs are reported the procedures adopted for the determination of critical state of sand.

3.4.1 Critical state from triaxial undrained tests

Critical state condition in undrained test is extrapolated from the experimental stress-stain and stress-path graphs, as explained below.

For each test the deviatoric stress q_{cs}, the overburden pressure Δu_{cs}, the mean effective stress p'_{cs} and the void ratio e_{cs} at critical state conditions were determined as follows:

- deviatoric stress at critical state condition q_{cs} is derived interpreting the test results in η_i - $\varepsilon_{a,i}$, where stress ratio is defined as $\eta_i = q_i/p'_c$. At large axial deformation the stress-stain curves approach to the same critical stress ratio $\eta_{cs} = M_{tc}$ and consequently q_{cs}:

[3.3] $$q_{cs} = M_{tc} \cdot p'_c$$

- overburden pressure Δu_{cs} is graphically defined as the asymptotic value of pore pressure in $\Delta u - \varepsilon_a$ plane but it must satisfied simultaneously $\delta u/\delta\varepsilon_a = 0$ and $\delta q/\delta\varepsilon_a = 0$;

- the mean effective stress at critical state is deduced from the following equation:

[3.4] $$p'_{cs} = \frac{3 \cdot p'_c - q_c - 3 \cdot \Delta u_{cs}}{3 - \eta_f}$$

Where the subscript ″c″ is associated to the end of consolidation condition, ″f″ to the end of test condition, ″cs″ to the critical state condition and ″tc″ to triaxial compression test condition.

Note that the values of $M_{tc} = \eta_{cs} = \eta_f$ are coincident for undrained tests and the void ratio at critical state is defined as $e_{cs} = e_c$.

3.4.2 Critical state from triaxial drained tests

In drained tests the critical state is extrapolated considering that the failure condition is easily deduced when both mean dilatancy D and its rate variation, $\dot{D}$, are zero: the last condition is the most important one in order to correctly determine critical state line.

Generally, the dilatancy $\dot{D}$ is defined as an increment of principal strains:

[3.5] $$\dot{D} = \frac{\delta\varepsilon_v}{\delta\varepsilon_q}$$

Where ε_v an ε_q are the volumetric and deviatoric deformations; dilation is conventionally negative for dilatant samples after the peak value η_p.

The mobilized dimensionless stress is defined as:

[3.6] $$\eta = \frac{q}{p'}$$

Where q and p' are the deviatoric and mean effective stresses.

The critical states of all tests involved in this research are extrapolated as summarized hereafter:

- using the Stress-Dilatancy method (described below) the deviatoric stress q_{cs} at the critical state is defined, linearly extending the end-path of each test's graph in q – Ḋ plane until Ḋ = 0;
- the mean effective stress at failure p'_{cs} is defined as follows:

[3.7] $$p'_{cs} = p_{cs} = p'_c + \frac{q_{cs} - q_c}{3}$$

- the critical void ratio value e_{cs} is defined by considering the total volumetric variation of the sample, extrapolating $\varepsilon_{v,cs}$ from $\varepsilon_a - \varepsilon_v$ plot:

[3.8] $$e_{cs} = e_f - (\varepsilon_{v,f} - \varepsilon_{v,cs}) \cdot (1 - e_c)$$

The subscript ″f″, ″cs″ and ″c″ have the same meaning already reported for undrained tests.

The critical state angle of shear resistance ϕ_{cs} appears to be constant for a particular soil under triaxial compression conditions; however, there is no agreement on the most accurate method to determine its value. Ghafghazi and Shuttle (2006) suggested that the (i) Bishop and (ii) Stress-Dilatancy methods are the most reliable procedures for the determination of ϕ_{cs} from triaxial compression test.

Bishop's method (1972) is based on the interpretation of dense of critical drained tests. For each test the value of the total minimum dilatancy D_{min} ($\delta\varepsilon_v / \delta\varepsilon_1$) at peak strength is computed neglecting the zero elastic strain (from compression to extension strains) and the total and plastic strains increments are considered identical.

This method relies on the experimental observation that dilatancy and hence peak angle of shear resistance, increase with density; for sand that reaches the critical state directly (contractive behavior) the peak stress ratio corresponds with the critical state value, where $\eta_{cs} = M_{tc}$ and $D_{min} = 0$. For convenience, this method is used to interpret the results in η_{max} – D_{min} plane, instead of using the peak shear angle.

After plotting the drained tests values in η_{max} – D_{min}, it is possible to determine M_{tc} extrapolating linearly the fitting line until D = 0. The slope of this line, (N–1), has been

used by some researchers as a material parameter [Nova 1982; Jefferies, 1993]; N is called the volumetric coupling parameter.

Stress-Dilatancy method, involves extrapolating the plot of the only post-peak stress ratio η versus dilatancy D data to zero.

This provides good predictions when shear localizations are not involved after the post-peak strength value. At larger strains (above 15%) other problems such as a higher effect of membrane penetration, tilting or bulging of the sample could occur, hence the data should be used very carefully especially after the post-peak data.

For known stress conditions the angle of shear resistance is directly related to the stress ratio at the critical state; in triaxial compression tests:

[3.9] $$\eta_{cs} = M_{tc} = \frac{6 \cdot \phi_{cs}}{3 - sen\phi_{cs}}$$

Where M_{tc} is the stress ratio and ϕ_{cs} is the angle of shear resistance at the critical state and under triaxial compression conditions.

3.5 Physical and mechanical characteristics of Toyoura Sand

The Japanese Toyoura sand has been widely studied by various authors [Yoshimi, 1977; Oda, 1978; Tatsuoka, 1986; Hyodo, 1991; Yamashita, 1993; Hyodo, 1994; Verdugo, 1992; Ishihara, 1993; Georgiannou, 2008; Chiaro, 2012].

It is a uniform fine sand having sub-angular grains with a high content of quartz (90%) and a small content of feldspar (7%) and chert (3%) [Fioravante et al., 1992].

The two grain size distributions are reported in Figure 3.7.

Toyoura sand used in monotonic and cyclic triaxial tests (called Toyoura 180) is compared to the one used in calibration and centrifuge tests (called Toyoura 220); a small difference is observed between the two sands in both uniformity and grains distribution.

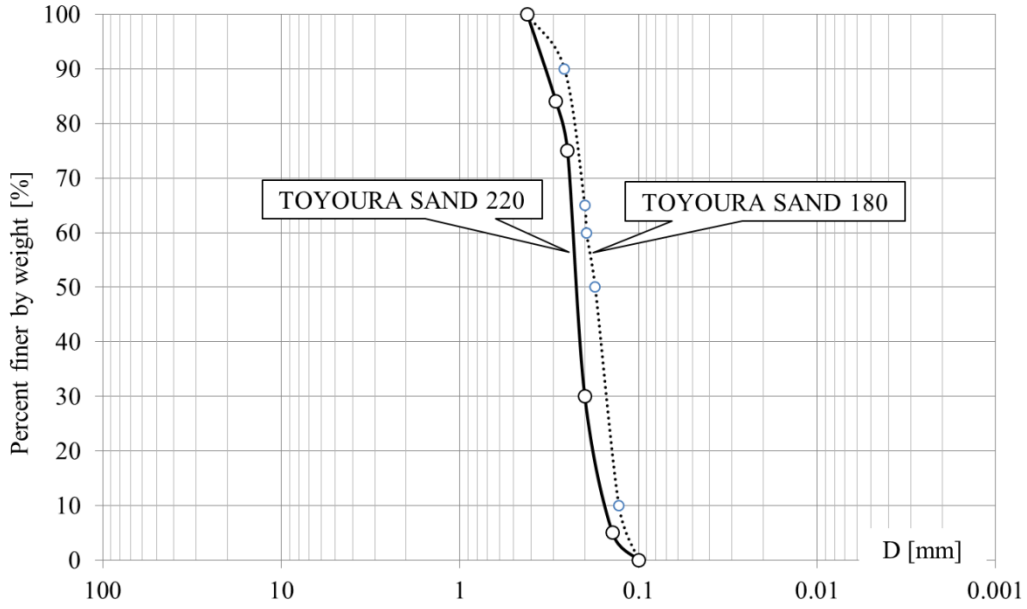

Figure 3.7- Grain size distribution of Toyoura Sand

Critical state line adopted in this thesis is the one obtained from a great number of triaxial isotropically consolidated tests [Verdugo, 1992; Ishihara, 1993]. The samples were reconstituted with different depositional methods (i.e air depositional, wet-tamping and water sedimentation methods), in order to study the widest range of possible physical state, varying both relative density (D_R = 7 ÷ 65%) and mean effective stress (p'_c = 100 ÷ 3000 kPa).

Critical state points are reported in Figure 3.8, together with the critical state line obtained by a non-linear regression fitting calculation; it is defined as [Verdugo, 1992; Li and Dafalias, 2004]:

[3.10] $$e_{cs} = \Gamma - \lambda \cdot \left(\frac{p'}{p_{atm}} \right)^{n} = 0.934 - 0.019 \cdot \left(\frac{p'}{101} \right)^{0.7}$$

Where:

Γ is a sand property, defined as the void ratio for p' = 1 kPa;

λ is a sand property, linked with the compressibility of the sand;

n is a sand property, defined as the stress exponent;

p_{atm} is the reference atmospheric pressure usually equal to 101 kPa.

In Figure 3.8 is also evident how the critical state line is independent from the samples preparation method.

In Table 3.1 are summarized the physical and mechanical characteristics of Toyoura sand: grain-size, physical properties, critical state line parameters and angle of shear resistance [see Jefferies and Been, 2006] of Toyoura 220 and Toyoura 180 have small variations and only ″Toyoura sand″ will be used in the future, as they will be considered equal.

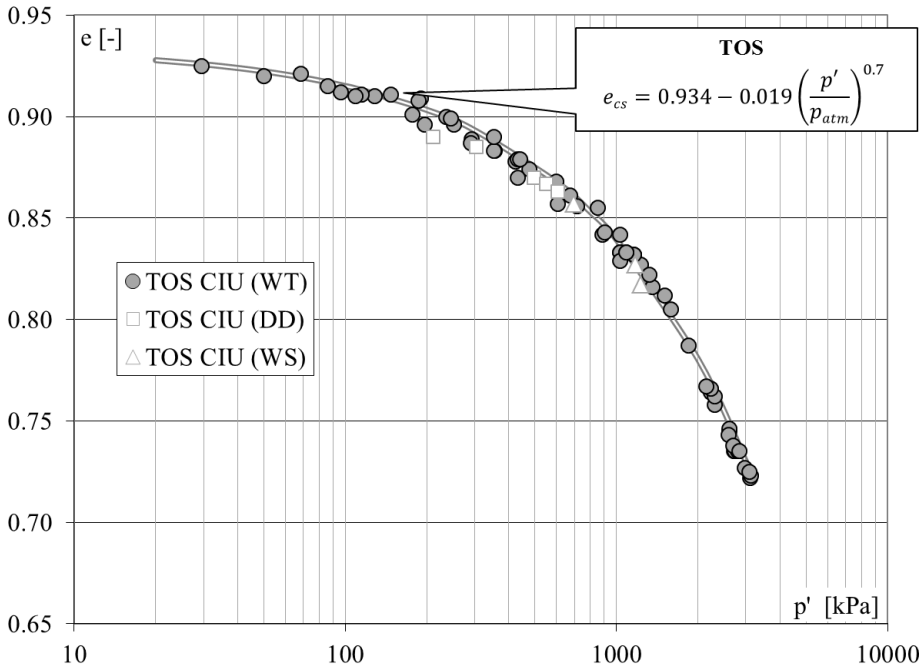

Figure 3.8- CS – Line for Toyoura sand in e – p' plane. ″WT″ water-tamping method; ″DD″ dry depositional method; ″WS″: water sedimentation method [Verdugo and Ishihara, 1993].

Physical properties							
	γ_{min}	γ_{max}	e_{min}	e_{max}	G_s	D_{50}	C_u
	kN/m^3	kN/m^3	-	-	-	mm	-
TOS 220	13.09	16.13	0.611	0.986	2.65	0.22	1.31
TOS 180	13.15	16.28	0.597	0.977	2.65	0.18	1.52

Mechanical properties				
Γ	λ	n	M_{tc}	ϕ_{cs}
[-]	[-]	[-]	[-]	[°]
0.934	0.019	0.7	1.24	31

Table 3.1- Physical and mechanical characteristics for Toyoura sand

3.6 Physical and mechanical characteristics of Ticino Sand

All triaxial tests on Ticino sand belong to the database of ISMGeo (Istituto Sperimentale Modelli Geotecnici, formerly ISMES, Seriate – BG – Italy). Ticino sand is a uniform mainly feldspathic (65%) sand, with quartz (30%) and minor mica content (5%) [Jamiolkowski, 2003].

Its particles have high sphericity, small roundness and its angularity is defined as sub-angular-to-sub-rounded [Baldi, 1982; Bellotti, 1989]. The grain-size distribution is reported in Figure 3.9, while the physical characteristics in Table 3.3.

The critical state parameters are derived interpreting triaxial drained and undrained compression tests. The samples were prepared by air depositional method and they were both isotropically and anisotropically consolidated. These tests are integrated with some triaxial tests carried out on wet-tamped samples conducted by Been (1986) [source Golder Associates]. In order to cover the widest range of the physical states of sand, mean effective stress range between 50 kPa to almost 800 kPa.

In Table 3.2 are summarized the main data with respect to the tests used for the critical state line definition: type of tests and load conditions, tougher with the physical state both at the end (e_c, p'_c, q_c) and at the critical state (e_{cs}, p'_{cs}, q_{cs}) conditions are reported.

The extrapolated critical state points deduced from drained and undrained tests as described in Paragraphs 3.4.1 and 3.4.2, are shown in Figure 3.10 in e – p' plane; even though the general trend seems clear, the scatter in data points for the drained tests is much more significant than for the undrained tests, which seems preferable for evaluating the critical state. Although, tests lead to the determination of the critical state line with a non-linear shape as proposed by various authors [Been, 1991; Ishihara, 1993; Li and Wang, 1998]. Critical state line for Ticino sand is defined as follows:

[3.11] $$e_{cs} = \Gamma - \lambda \cdot \left(\frac{p'}{p_{atm}} \right)^{n} = 0.923 - 0.046 \cdot \left(\frac{p'}{101} \right)^{0.5}$$

Where Γ, λ, n and p_{atm} are defined as in Equations 3.10.

For undrained tests the calculated state parameter is slightly minor or greater than zero (ψ = -0.01 ÷ 0.03) and the overburden pressure were positive in the samples until phase-transformation occurs; after the drop in shear resistance and with the decreasing of confining pressure, the samples tend to developed a change in pore water pressure from positive to slightly negative. It is noticed that the quasi-steady state is associated to an axial deformation ranging from 3 % to 10 % [Ishihara et al., 1975; Alarcon-Guzman et al., 1988; Ishihara, 1993; Verdugo, 1992].

Drained tests have negative state parameters (ψ = -0.02 ÷ - 0.15) so dilatant behaviors ware always observed.

Angle of shear resistance at critical state is also deduced from triaxial tests, interpreting the data with both (i) Stress-Dilatancy and (ii) Bishop's methods.

The first methodology consists in the linear extrapolation of the critical ratio η_{cs} for zero dilatancy reporting the data in $\eta_i - D_i$ graph; this procedure is used for the determination of critical state conditions in drained triaxial tests, assuming that axial and deviatoric deformation are similar. In Figure 3.11 are reported the extrapolated critical state values in the q – p' plane using the methodology proposed in Paragraph 3.4.2 (Stress-Dilatancy method). The slope of the fitting line leads to determine $\eta_{cs} = M_{tc} = 1.36$ and the critical angle of shear resistance is $\phi_{cs} = 34°$.

The second methodology considers that a linear fitting curve is determinable in $\eta_{max} - D_{min}$ plane. In Figure 3.12 are reported the values deduced from each drained triaxial tests and the linear trend with the black fitting line. For zero dilatancy the critical ratio is deduced as $\eta_{cs} = M_{tc} = 1.33$ and the critical angle of shear resistance is defined as $\phi_{cs} = 33°$.

The two methodology used for the determination of the critical angle of shear resistance are compared in Figure 3.13. The experimental data are reported in $\eta_i - D_i$ for the only drained 172 test as an example: the dotted black line is extended until D = 0 and $\eta_{cs} = M_{tc} = 1.38$ (″Stress-Dilatancy″ method) while the white circle symbol represents the point where the maximum stress ratio η_{max} and the minimum dilation D_{min} occurs in the same moment (Bishop's method).

The angle of shearing resistance at the critical state is considered equal to $\phi'_{cs} = 34°$, as the analysis with the two proposed methodology hang over a very small difference in its evaluation ($\Delta\phi = 1°$)

All triaxial tests and their critical state evaluation are reported in Appendix A, while in Table 3.3 are summarized the physical and mechanical Ticino sand characteristics.

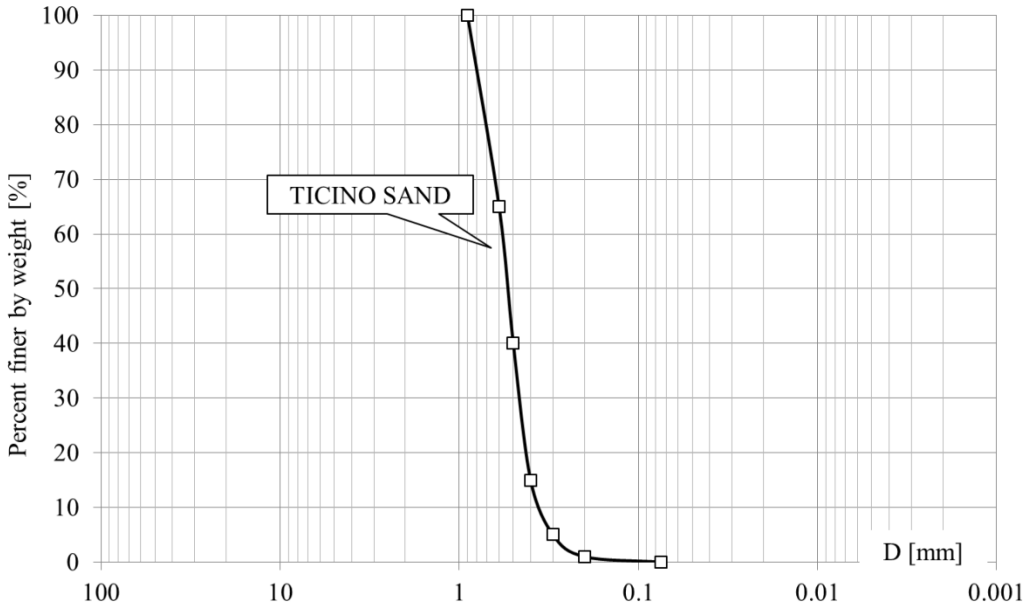

Figure 3.9- Grain size distribution of Ticino Sand

Test	Type	Stress path	Sourse	e_c	σ'_{vc}	σ'_{hc}	p'_c	q'_c	ψ	OCR/R	e_{cs}	p'_{cs}	q_{cs}	η_{cs}
				[-]	[kPa]	[kPa]	[kPa]	[kPa]	[-]	[-]	[-]	[kPa]	[kPa]	[-]
171	CK0D	σ_3=cost	ISMES	0.759	500	235	324	265	-0.082	1.2	0.810	439	610	1.39
172	CK0D	σ_3=cost	ISMES	0.773	401	221	281	180	-0.074	1.5	0.824	397	530	1.33
CK5	CK0D	σ_3=cost	ISMES	0.790	877	370	539	507	-0.028	1	0.809	677	921	1.36
K6	CK0D	σ_3=cost	ISMES	0.730	1447	581	870	866	-0.059	1	0.770	1061	1440	1.36
K8	CK0D	σ_3=cost	ISMES	0.798	774	341	485	433	-0.025	1	0.827	620	837	1.35
M32	CID	σ_3=cost	ISMES	0.640	800	800	800	0	-0.154	1	0.678	1543	2230	1.44
R14	CK0D	p' cost	ISMES	0.698	1200	507	738	693	-0.102	1	0.778	726	980	1.35
U21	CK0D	σ_3=cost	ISMES	0.756	301	298	299	3	-0.088	4	0.814	525	680	1.30
U22	CK0D	σ_3=cost	ISMES	0.796	125	124	124	1	-0.076	4	0.856	212	265	1.25
U24	CK0D	σ_3=cost	ISMES	0.760	125	118	120	7	-0.112	4	0.827	205	260	1.27
U36	CK0D	σ_3=cost	ISMES	0.751	200	246	231	-46	-0.103	6	0.785	420	521	1.24
U38	CK0D	σ_3=cost	ISMES	0.760	50	59	56	-9	-0.129	6	0.852	102	130	1.27
U50	CK0D	σ_3=cost	ISMES	0.785	75	94	88	-19	-0.095	8	0.847	164	210	1.28
V9	CK0D	σ_3=cost	ISMES	0.687	1155	437	676	718	-0.118	1	0.761	810	1119	1.38
CID_C262	CID	σ_3=cost	GOLDER	0.851	200	200	200	0	-0.008	1	0.819	324	374	1.16
CID_C263	CID	σ_3=cost	GOLDER	0.781	200	200	200	0	-0.078	1	0.796	337	407	1.21
LIQ_1101	CIU	σ_3=cost	GOLDER	0.867	308	308	308	0	0.024	1	0.867	147	155	1.05
LIQ_1103	CIU	σ_3=cost	GOLDER	0.877	302	302	302	0	0.033	1	0.877	95	103	1.08
LIQ_1105	CIU	σ_3=cost	GOLDER	0.898	279	279	279	0	0.051	1	0.898	36	38	1.05
LIQ_1106	CIU	σ_3=cost	GOLDER	0.850	504	504	504	0	0.029	1	0.850	278	334	1.20
H0	CIU	σ_3=cost	ISMES	0.810	800	800	800	0	0.015	1	0.810	845	1126	1.33
H1	CIU	σ_3=cost	ISMES	0.831	400	400	400	0	-0.001	1	0.831	486	649	1.34
H2	CIU	σ_3=cost	ISMES	0.827	500	500	500	0	0.005	1	0.827	582	788	1.35
H3	CIU	σ_3=cost	ISMES	0.826	600	600	600	0	0.014	1	0.826	687	921	1.34
H4	CIU	σ_3=cost	ISMES	0.812	700	700	700	0	0.009	1	0.812	728	983	1.35
H5	CIU	σ_3=cost	ISMES	0.808	800	800	800	0	0.013	1	0.808	751	1022	1.36
H6	CK0U	σ_3=cost	ISMES	0.816	750	341	477	409	-0.008	1	0.816	781	1079	1.38
H7	CK0U	σ_3=cost	ISMES	0.844	750	367	495	384	0.022	1	0.844	571	764	1.34
H8	CK0U	σ_3=cost	ISMES	0.846	750	360	490	391	0.024	1	0.846	561	753	1.34
H10	CK0U	σ_3=cost	ISMES	0.839	600	286	391	315	0.006	1	0.839	530	703	1.33
H11	CK0U	σ_3=cost	ISMES	0.842	750	344	479	406	0.019	1	0.842	527	699	1.33
H12	CK0U	σ_3=cost	ISMES	0.841	900	428	585	473	0.028	1	0.841	641	849	1.32
H13	CK0U	σ_3=cost	ISMES	0.825	1050	479	669	572	0.019	1	0.825	682	911	1.34
H14	CK0U	σ_3=cost	ISMES	0.826	1200	556	770	644	0.029	1	0.826	717	962	1.34
H15	CK0U	σ_3=cost	ISMES	0.812	750	358	489	392	-0.011	1	0.812	692	944	1.36
H16	CK0U	σ_3=cost	ISMES	0.813	750	359	489	391	-0.009	1	0.813	639	868	1.36

Table 3.2- Main characteristics for triaxial tests carry out on Ticino sand's samples

Physical properties

γ_{min}	γ_{max}	e_{min}	e_{max}	G_s	D_{50}	C_u
[kN/m^3]	[kN/m^3]	[-]	[-]	[-]	[mm]	[-]
13.64	16.67	0.574	0.923	2.68	0.53	1.3

Mechanical properties

Γ	λ	n	M_{tc}	ϕ_{cs}
[-]	[-]	[-]	[-]	[°]
0.923	0.046	0.5	1.37	34

Table 3.3- Physical and mechanical characteristics for Ticino sand

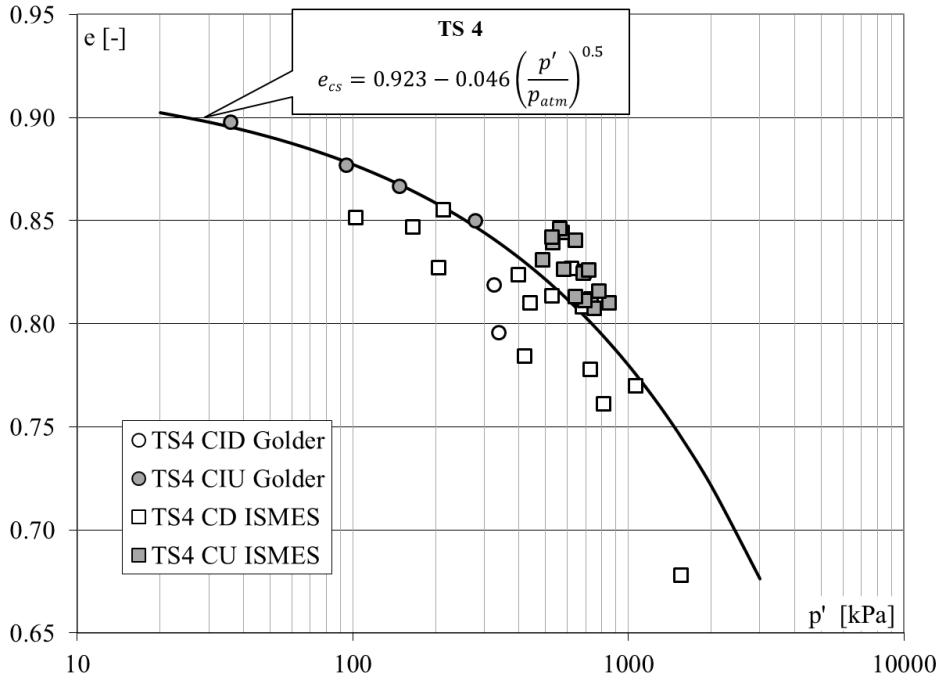

Figure 3.10- CS – Line for Ticino sand in e – p' plane

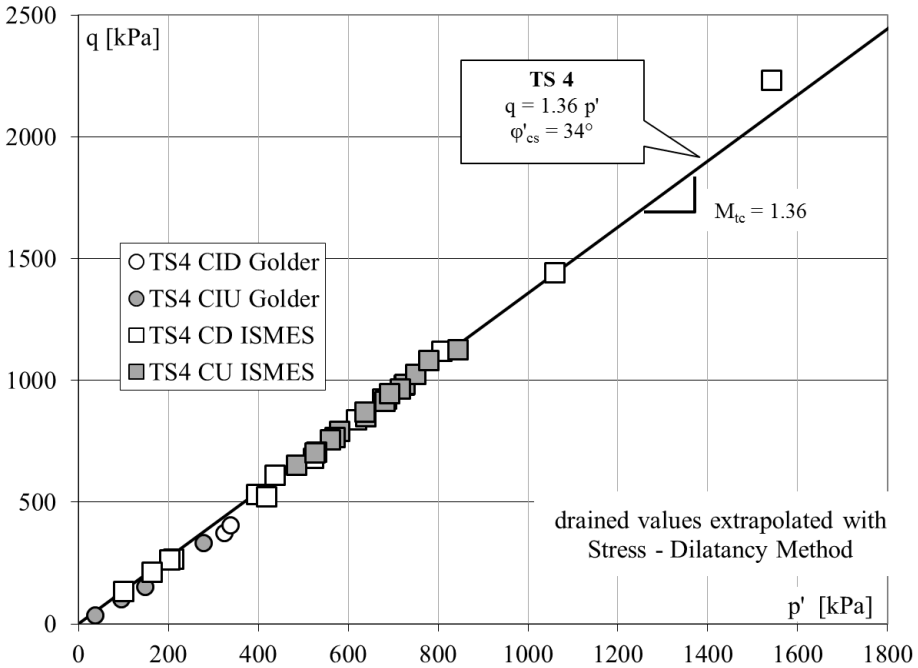

Figure 3.11- Determination of critical shear angle ϕ_{cs} in q – p' plane. Critical state for drained tests deduced with ″Stress-Dilatancy″ method.

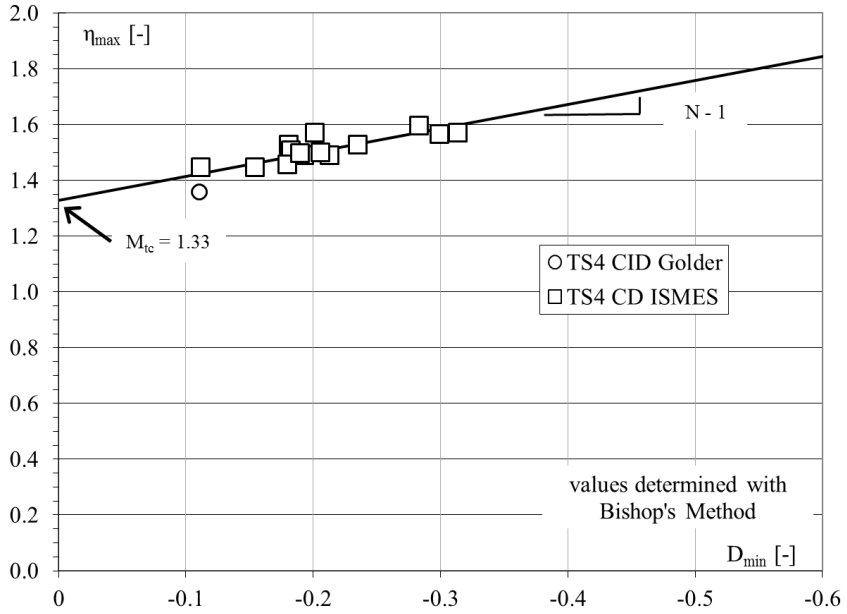

Figure 3.12- Determination of critical shear angle ϕ_{cs} with Bishop's method in $\eta_{max} - D_{min}$ plane

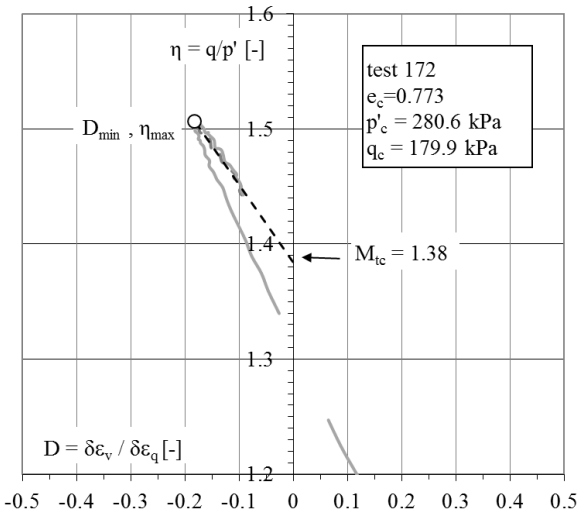

Figure 3.13- Interpretation of drained 172 test in $\eta_i - D_i$ plain for M_{tc} determination. ″Stress-Dilatancy″ method (black dot line) and Bishop's method (white circle)

Chapter 4

4 Cyclic Behavior of Saturated Sand

4.1 Cyclic resistance from reconstituted sample

Dynamic behavior of saturated sand has been widely studied by using results from reconstituted samples tested by triaxial, simple shear and torsional shear apparatus.
Test results evidence that cyclic resistance of sand is mainly influence by (i) initial condition state (e_c, p'_c), (ii) intensity and shape of the dynamic stress, (iii) number of cycles imposed and (iv) level of deformation [Yoshimi et al, 1977; Seed, 1979].
Some in-depth elements influencing cyclic resistance to liquefaction are discussed here after.

4.1.1 Void ratio and initial effective stress

The major parameter influencing cyclic behavior of sand is the relative density, D_R, or, better, initial void ratio, *e*. Indeed, while relative density takes into account the maximum and minimum packages of sand, it does not predict the possibility of liquefaction condition, because even medium to dense sands may present loss of resistance due to dynamic loading. Actually *e* controls the type of failure mechanism in sand and influence

the cyclic strength, as well as the liquefaction resistance increases with the increasing of void ratio as can be notice in Figure 4.1 [Tatsuoka, 1986].

The effect of initial confining pressure p'_c is also important on dynamic behavior of sand as two samples, with the same void ratio, have different mechanical comportments. Worse luck, the effect that confining pressure has on the test results is a controversial argument in literature.

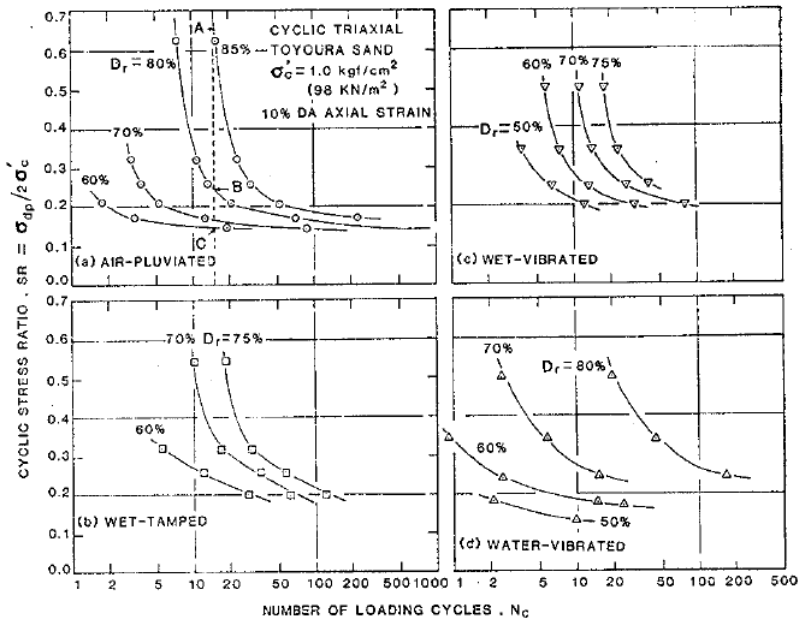

Figure 4.1- Stress ratio versus N_c to 10% DA axial strain by triaxial tests on Toyoura sand for different initial density and sample preparation [Tatsuoka, 1986]

Benahmed (2001) shown that the more the confining pressure σ'_{3c} increasing the more the cyclic strength was high: in fact, very loose specimens subjected to the same cyclic stress ratio, request more cycles to liquefaction when consolidation pressure increases. On the contrary, Hyodo et al. (2002) performed cyclic isotropical consolidation triaxial tests on dense sand and obtained a decrease of cyclic strength up to very high pressure, more than 1 MPa (see Figure 4.2). This last evidence is confirmed by other authors, which tested also samples with smaller consolidation pressure and higher void ratio [Vaid, 1985; Vaid and Sivathayalan, 1995].

The influence of stating stress conditions of the specimen, i.e. anisotropical or isotropical, has also been studied by many researchers [Seed, 1979; Ishihara, 1996; Hyodo, 2002; Ghionna and Porcino, 2006; and so on].

They all agreed that the initial stress condition influences the cyclic behavior of sand.

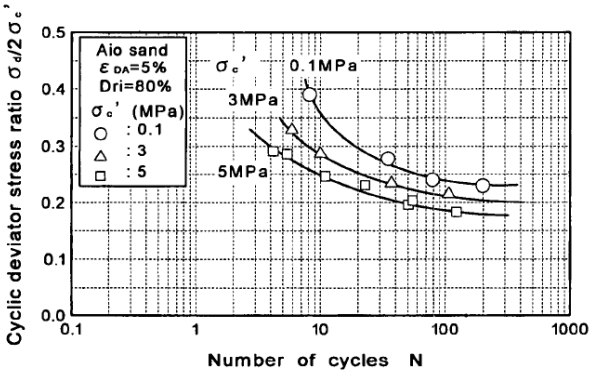

Figure 4.2- Isotropic cyclic strength curves for different consolidation pressures in triaxial conditions [Hyodo, 2004]

4.1.2 Depositional methods

Specimens tested in research are usually reconstituted by various depositional methods in order to better reproduce the anisotropy and fabric of in-situ conditions.

Mulilis (1977) conducted a large number of triaxial tests on specimens reconstituted with various methods in order to quantify the influence that the depositional methods might have on the cyclic behavior of sand. The results are reported in Figure 4.3, where the resistance curves, $\sigma'_d/(2\cdot\sigma'_0)$ – N, belong to the samples with the same initial physical states but reconstituted with different methods: vibratory compaction methods (a) or compaction methods (b).

Air pluviation technique leaded to the lowest liquefaction resistance, while moist tamping technique the strongest ones. This result is in agreement with other researches, as far as these two methods determine the lower and the upper limits for cyclic resistance determination for reconstituted specimens [Yoshimi, 1984; Tatsuoka, 1989].

As liquefaction evaluation depends on depositional methods, the aim in each research is to choose the methodology capable to better assessment the arrangement of in-situ particles. It seems essential the comparison between results from undisturbed and reconstituted samples subjected to cyclic loading.

Yoshimi et al. (1984) conducted tests on (i) in-situ freezing and (ii) in-situ triple tube samples, (iii) reconstituted sample changing the depositional method in air pluviation (PA) and moist tamping (MT). The results, summarized in Figure 4.4, shown the clear difference between the cyclic resistance to liquefaction obtained by the in-situ freezing (FS) and triple-tube sampling (TS) technique. In particular TS method tended to underestimate the cyclic resistance to liquefaction, because of a probably variation in

structure and void ratio during sampling. Air pluviated samples seem more convenient instead triple-tube technique, also because the tests results were found to be comparable [Ishihara, 1985]. Furthermore, neither MT nor AP methods reproduce correctly the real cyclic behavior of undisturbed sand (FS sample); they all tended to underestimate the cyclic resistance.

Ghionna et al. (2006) tested Gioia Tauro sand in triaxial cell and deduced that specimens reconstituted with water sedimentation method have very similar cyclic resistance if compared with that of undisturbed samples.

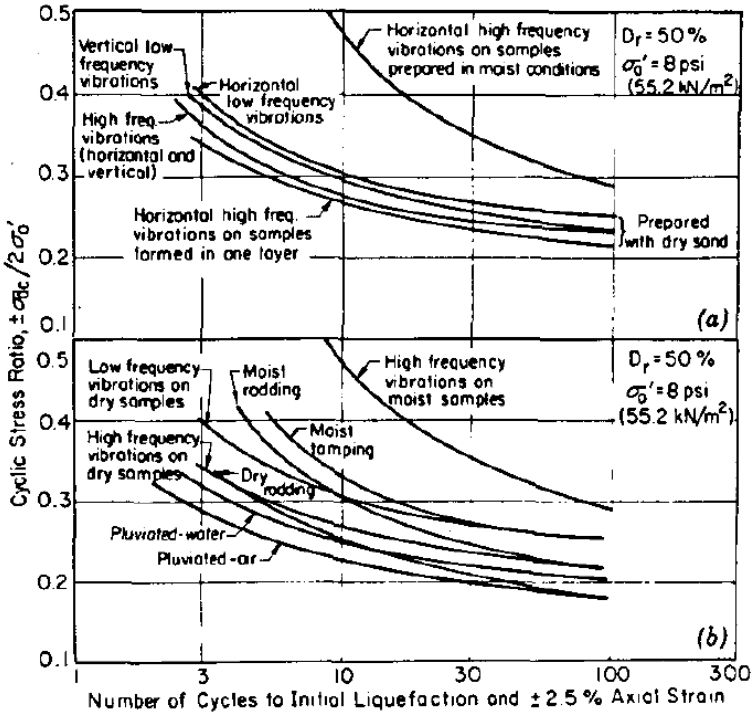

Figure 4.3-Cyclic stress ratio versus number of cycles for different: a) vibratory compaction procedure, b) compaction procedure [Mulilis, 1977]

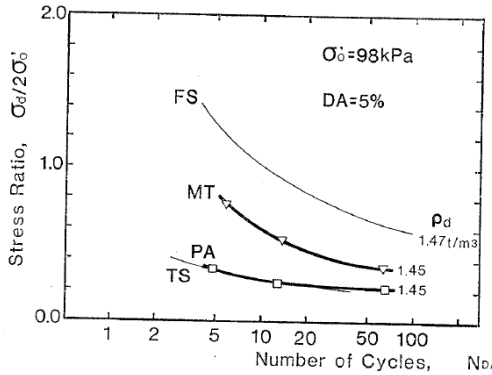

Figure 4.4-CSRs required to cause 5% double-amplitude axial strain of in-situ frozen samples (FS), conventional "undisturbed" tube samples (TS), samples reconstituted by air pluviation (AP), and samples reconstituted by moist tamping (MT) [after Yoshimi et al. 1984]

4.1.3 Initial stress conditions

Depositional environment and stress history of the deposit affected the anisotropy of sand, but how the initial particle configuration influences the cyclic liquefaction resistance has some contradictory results in literature. It is wildly recognize that (i) the initial physical state and (ii) stress/non-stress reversal of dynamic loads are the mains influencing factors.
For Seed (1979) and Ishihara (1979, 1996), liquefaction resistance increased with the increasing of stress ratio k_0 ($k_0 = 0.5 \div 1.5$). Ghionna and Porcino (2006) establish a small increasing of resistance with the increasing of k_0, for only samples prepared with air depositional method; opposite results have been reached for samples prepared with water sedimentation method, which shown a decreasing of resistance with the increasing of k_0 values (with k_0 values from 0.59 to 1).
Hyoda (2002) demonstrated that the increase or decrease of cyclic resistance was related to the stress reversal of dynamic stress applied to the specimens. In Figure 4.5 is reported a summary of the cyclic triaxial isotropically and anisotropically consolidated tests results of Aio dense sand ($D_R = 80\%$). In the case of isotropically consolidated tests always stress reversal happens: considering a constant number of cycles to liquefaction, the resistance to liquefaction decreasing with the increasing of confining pressure.
When a static shear is imposed on the sample two different behaviors were observed: (i) for low consolidation pressures cyclic resistance increased with the decreasing of k_0 value (with k_0 values from 0.5 to 1) because stress-reversal always occurred, (ii) tendency of decreasing resistance with increasing of k_0 values, when pressures are very high and stress-reversal did not occur.
Different results are obtained from of a series of torsional and laterally constrain tests reported in Figure 4.6 [Ishihara, 1979] in the $(\tau_d/\sigma'_{v0}) - N$ ($\gamma = 2.5\%$) space. For constant density and consolidation pressure the resistance of samples with $k_0 > 1$ is greater in comparison with sample with $k_0 < 1$. This type of behavior is confirmed also from simple shear test results [Tatsuoka and Silver, 1980, 1982].

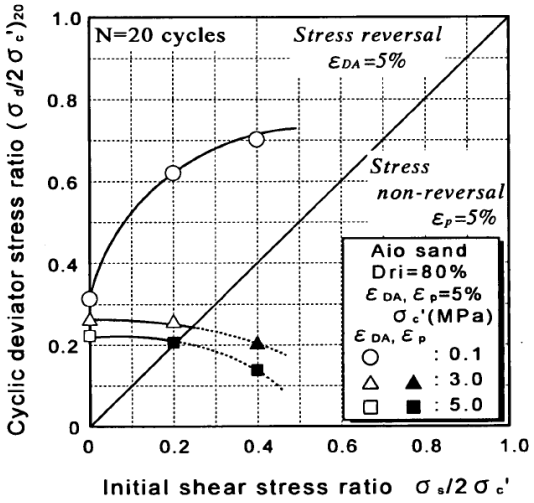

Figure 4.5-Variation of cyclic strength at N = 20 cycles with initial shear stress ratio in triaxial stress condition [Hyodo et al., 2002]

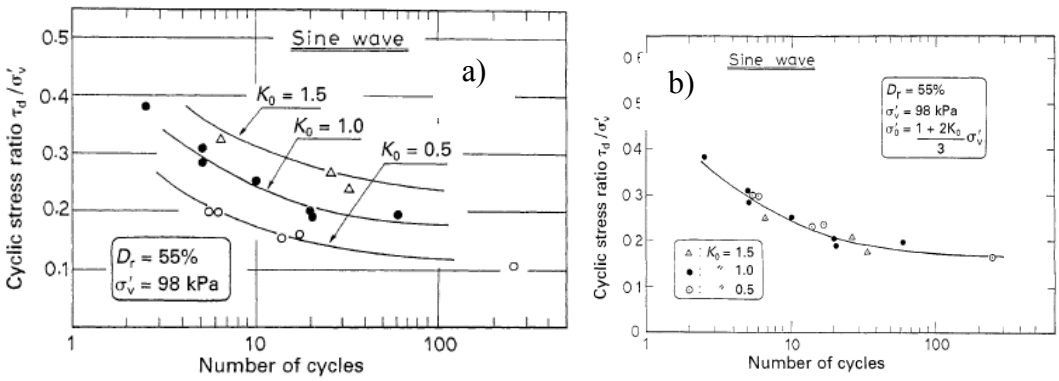

Figure 4.6-a) Effects of k_0 consolidation on cyclic strength under the condition of lateral constraint.b) Cyclic stress ratio versus the number of cycles for the ACOT tests with different k_0 conditions. Results from torsional tests on Fuji River sand [Ishihara, 1979]

As can be deduced from the above considerations, cyclic resistance would be also related to the particular apparatus used. In effect, considerably discrepancy between the various ″started-stresses″ conditions and principal stress direction, are not negligible and a direct comparison between results from various tests are not possible.

Ishihara (1972, 1977, 1985) suggests a correction factor for cyclic liquefaction resistance in order to consider the different results raise from isotropically and anisotropically consolidation conditions. The research, based on torsional tests, provided that the cyclic resistance from anisotropically consolidated test is linearly related to cyclic resistance from isotropical consolidation tests, by a factor enclosing the stress ratio k_0:

[4.1] $$CRR_{k_0 \neq 1} = \frac{1+2 \cdot k_0}{3} \cdot CRR_{K_0=1}$$

This consideration brought up by the observation that, normalized the shear stress by p'_c instead of σ'_{v0}, the cyclic resistance of a sand with different k_0 values is defined only by number of cycles (Figure 4.6 b), for the case of torsional test results with lateral strains prevented.

Similarly, the CRR from the simple shear tests can be related to the results of triaxial tests as follows:

[4.2] $$CRR^{SS} = \frac{1+2\cdot k_{0,ss}}{3} CRR^{TX}$$

For normally consolidated sand the reduction factor coefficient is nearly 0.65. This relationship is found to be consistence with the range of results obtained by various researcher [De Alba, 1976; Tatsuoka, 1986], although it seems to vary with density and depositional method [Tatsuoka, 1986].

4.1.4 Rotational effects of principal stress

Characterized earthquake loading only by stress ratio CSR = τ_d/σ'_{v0}, in some cases can be restrictive as it does not link the liquefaction potential with the changes in principal stress directions; this last consideration is probably the main cause of liquefaction problems [Arthur et al., 1980; Wong e Arthur, 1986].

Ishihara and Towata (1993) studied the effect of variation in principal stress direction using cyclic simple shear device. Loose Toyoura sand was drainelly subjected to reversal stresses from 0° to ± 45°, keeping constant deviatoric and mean effective stress (p'_c = 300 kPa). Even if invariants ware unchanged during tests, principal stress rotation on its own caused the irreversible volumetric strains accumulation; q and p' gradually decreased as number of cycles increased pointed out a hardening response of sample.

Cyclic rotational of principle stress directions in sand which causes strain, radically alters the behavior of material from that presents in shear under constant direction of principal stress [Wong and Arthur, 1986].

In triaxial test condition, direction of principal stress changes from + 90° to – 90° leading the largest excursion in variation of α parameter introduced in Chapter 3. On the contrary, simple shear test with lateral constrained strains brings a limited excursion of principal stress directions, which continually re-orientating during shearing.

4.2 Influence of criteria used in liquefaction estimation

Seed and Lee (1966) concluded that the larger the stress or stain, the lower the number of cycles required to induce liquefaction; also, the more the number of stress cycles to which the sand is subjected, the more likely the liquefaction failure will occur. These two factors are directly related to the magnitude of cyclic loading.

Generally, volumetric cyclic threshold shear strain γ_{tv} is the limit shear strain after which significant permanent volume changes or permanent development of excess pore water pressure occurs in the soil. Its values seems to be independent from relative density, initial effective stress and fabric, and it is defined approximately at a shear deformation level of $\gamma_{tv} \sim 10^{-4}$ for most sands and silty sands [Dobry et al., 1982].

For cyclic strain below γ_{tv} there is no permanent microstructural change, on the contrary a permanent volumetric strain and high excess pore water pressure developments cause a stiffness degradation effect on sand.

The load applied produces a cyclical stress (and so strain) reversal and two events might occur in the sand with the increasing of cycles: (i) the generation of plastic deformations under stress-controlled cycles and (ii) excess pore water pressure increases in undrained condition.

In cyclic liquefaction tests the excess pore water pressure is usually expressed as:

[4.3] $$R_u = \frac{\Delta u}{\sigma'_{3c}}$$

The pore pressure measure Δu is normalized by the minor initial effective stress σ'_{3c}.

The Equation 4.3 is useful to determine the start of liquefaction, as well as when $R_u = 1$ sand does not have any shear resistance. It must be noted that in tests with no stress-reversal, great strains may occur but $R_u = 1$ could not be reached.

Seed (1979) proposed to use as failure criteria the threshold pore pressure value R_u = 100% but, due to limitation of applicability (i.e. R_u = 100% not always reached for all sands and silty sands), the specimen is said to be ″fully liquefied″ when a certain value of axial strain amplitude is reached. Different values of ε_a are used in literature as a liquefaction criteria, almost the choice of which ones depending on the serviceability limit the project wants to achieve. The more the tested sand is dense, the more the difference in cyclic resistance curves are important if different strain conditions are used for

″liquefaction definition″. This is due to the fact that, after the initial liquefaction, the increase in the strain amplitude with each subsequent cycle is much more smaller in the case of dense sand than for loose one [Lee and Seed, 1967]. On the contrary, for loose sand the initial and fully liquefaction are nearly coincident and the strain criteria used doesn't influence the final CSR – N curves.

A definition based on threshold strain level seems appropriate for laboratory test. Ishihara (1996) proposed to assume as reference deformation level ε_a (DA) = 5% for triaxial test (where DA: double amplitude, i.e. distance between minimum and maximum value of load).

4.3 Linking monotonic and cyclic behavior

Relating cyclic with monotonic behavior of sand seems to be a good approach in order to understand how resistance of a granular material changes in dependence of the loading type. Researches from Chen (1985), using triaxial tests results, and Alarcon-Guzman et al. (1988), using torsional test results, were the first that try to link monotonic and cyclic behavior of loose sand. As a conclusion, Vaid and Chen (1985) mentioned that in cyclic tests, the flow deformation initiated when the stress-path reached the peaks envelope line (herein called CSR). On the other hand, Alarcon et al. stated that flow liquefaction occurred when the stress state during cyclic loading reached the effective path from monotonic tests, in compression or in extension.

Using results from some undrained triaxial test on very loosely samples, Sladen (1985) shown the existence of a surface in e – p' – q space that separated stable from unstable behavior of loose sand (Figure 4.7). In q – p' plane this surface is a straight line that interpolate the maximum peaks resistance q_p and p'_p and is usually called ″collapse line″ [Ishihara, 1993] or ″instability line″ [Lade, 1983]; this line is unique for a given void ratio and independent of consolidation pressure. In the space the ″collapse surface″ is an envelope of all peaks of stress, after which a drastic decay of resistance is observed in monotonic tests [Castro et al, 1982; Sladen et al., 1985; Sasitharan, 1992, Ishihara, 1993].

In Figure 4.8 is reported the result of a cyclic torsional test conducted on loosely reconstituted specimens of Fontainebleu Sand [Georgiannou, 2008], where the monotonic and cyclic behaviors are compared. With the continues application of cycles, pore water

pressure rise up slowly until the effective stress-path reach the I – Line (IL in graph, on the basis of Lade definition) in correspondence of point (4) in τ – p' plane. From point (4) to point (5) the shear deformation increase rapidly in spite of increment of stress is small. Until point (6) pore water pressure accumulation during shear increases, than decreasing up to point (7) because effective stress path overtakes the PT – Line and the mechanical behavior from contractive became dilatative.

If sample is reloaded the pore pressure again builds up and cause a quasi- zero effective stress and so liquefaction of sand. This state, generally, is momentary and sand continues to carry on loads and manifests cyclic mobility. Usually, collapse of sand always happens in the extension zone when a stress reversal load is applied.

De Gennaro (2004) evidenced that sand behavior is controlled by the same characteristics lines when it was monotonically and cyclically stressed: the phase-transformation line (PT – Line), the critical state line (CS – Line) and the collapse/instability line (I – Line), the last one function of void ratio and type of load (i.e. compression or extension).

Instead the different ideas propose in literature there is a good agreement in asserting that flow deformation is very likely to occur when stress path is in the range between PT – Line and I – Line.

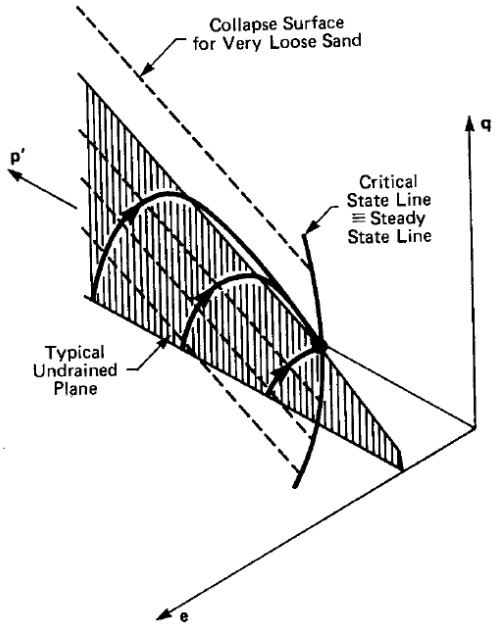

Figure 4.7- The collapse surface in p' – q – e space showing typical stress – void ratio path followed by samples in triaxial undrained compression tests [Sladen et al., 1985]

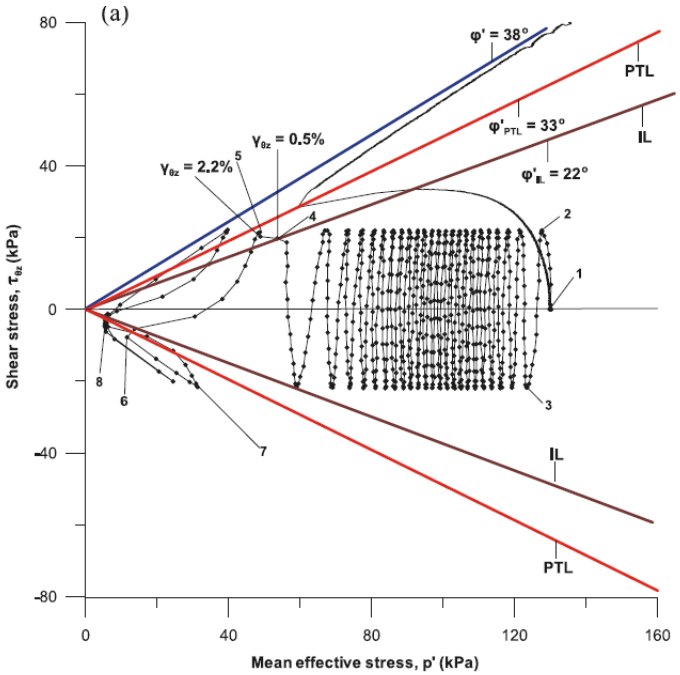

Figure 4.8- Effective stress path of undrained cyclic torsional hollow cylinder test conducted on loose Fontainebleau Sand [Georgiannou, 2008]

4.4 Method of liquefaction evaluation in triaxial tests

The assessment of liquefaction susceptibility using the cyclic ″stress-approach″ follows three steps:

- characterization of earthquake loading converting an irregular motion of known moment magnitude into an equivalent cyclic loading of regular amplitudes and certain number of cycles;
- characterization of cyclic liquefaction of soil using the simplifying concept of cyclic stress ratio CSR: usually the resistance is consider at a given number of cycles and for different initial state of sand;
- evaluation of safety factor FS, considering the ratio between CRR required to cause liquefaction and the CSR equivalent to earthquake-induced shear stress.

Usually, several cyclic tests with different stress amplitudes are conducted on a given sand varying both void ratio and mean effective stress at the end of consolidation. The number of cycles to liquefaction decreases with the increasing of the cyclic amplitude stress; commonly the test results are represented in a plot where cyclic stress ratio is a function of number of cycles that produce liquefaction.

Focusing on triaxial isotropically consolidated tests results, cyclic stress ratio CSR is cyclically applied to the specimens with a stress-controlled device, and is defined as follows:

[4.4] $$CSR^{TX} = \frac{q_{\max}}{2 \cdot \sigma'_{3c}}$$

Where q_{max} represents the maximum deviatoric stress applied to the sample and σ'_{3c} the minimum effective stress at the end of consolidation phase.

CSR is supposedly uniquely related to the number of cycles at failure for a given void ratio and pressure and the criterion for failure individuation is usually based on strain-amplitude or pore pressure considerations.

Worldwide used criteria is highly recommended in liquefaction analysis because CSR is very sensitive, not only to initial physical state of tested sample, but also to depositional method, OCR, aging [Dobry et al., 1982], shape of particles [Vaid et al., 1985; Benahmed, 2001; Geogiannou, 2008], as well as type and intensity of load; furthermore,

is well known that resistance to liquefaction is higher for tests without stress-reversal (only q > 0) that for tests with stress-reversal [Benahmed, 2001; De Gennaro, 2004].

The common practice is to consider soil liquefied when the development of 5% double-amplitude axial strain is reached. It must be underlined that for very dance sand the CSR – N curves, depends strongly on the strain criteria chosen (i.e. ε_a from 2.5 to 10%). In contrast, cyclic resistance curve for medium-to-loose sand is almost independent from the strain amplitude adopted to quantify liquefaction [Yoshimi, 1984; Toki et al., 1986].

From cyclic triaxial tests are possibly definable the cyclic resistance ratio CRR fulfilling a given failure criterion in a certain number of cycles N; this means that for different CSR – N curves, defined for different physical state of sand, the number of cycles need to be specified in the constant-amplitude uniform cyclic loading

In Figure 4.9 is reported a correlation proposed by Idriss (1999), representing the number of equivalent cyclic for different earthquakes magnitude; usually, the cyclic resistance ratio is considered for an equivalent number of cycles of N = 15 (earthquake magnitude M_w = 7.5), in view of typical number of significant cycles being presents in many of actual and past time histories of accelerations record [Seed and Idriss, 1982, Ishihara, 1996].

Most of the tests data concerning liquefaction used in this thesis have been obtained using the cyclic triaxial test and the difference between in-situ and laboratory tests was taken into account applying to the cyclic stress ratio from triaxial tests results the correction factor proposed in Equation 4.1

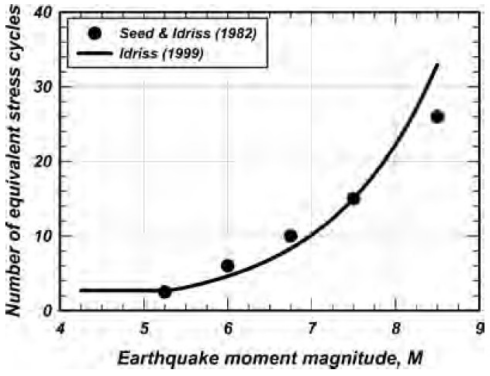

Figure 4.9- Mean number of equivalent uniform cycles at 65% of the peak stress versus earthquake magnitude [Idriss, 1999]

4.5 Cyclic behavior of Toyoura Sand

Cyclic resistance to liquefaction of Toyoura sand has been widely examined by many authors using different test apparatus (triaxial, simple shear and torsional apparatus) [Miura and Toki, 1982; Toki et al., 1986; Yomashita and Toki, 1993; Ishihara, 1993; Chiaro, 2012].

In this research results from triaxial cyclic test published by Toki et al. (1986) have been considered.

The maximum and the minimum densities of sand used by Toki in its experimentation were determined by JSSMFE methodology and resulted as $\rho_{d,max}$ = 1.645 g/cm^3 (e_{min} = 0.977) and $\rho_{d,min}$ = 1.335 g/cm^3 (e_{max} = 0.605) while the mean diameter was defined as D_{50} = 0.18 mm.

The samples were reconstituted by air depositional method and tested by five different laboratories in Japan. The slenderness of the specimens was kept constant (H/D = 2 ÷ 2.5) while the height, the diameter, the cyclic stress ratio and the void ratio were varied in order to determine their influence on cyclic resistance ratio.

The difference in results from samples with different dimensions (i.e. D = 7 – 10 cm) were found to be negligible, even if the more the sample diameter was great the more the error in the measure resulted in less accuracy [Tatsuoka et al., 1986].

The results of the extensive series of the cyclic triaxial isotropical consolidated tests (with p'_c = 98.1 kPa) are presented in Figure 4.10 in CSR^{SS} – N plane, where cyclic stress ratio deduced from triaxial condition is reduced by a quantity that keeps into account in-situ state and N is defined when axial deformation ε_a(DA) = 5% [Toki et al., 1986]. In the normally useful range of N values adopted for cyclic resistance determination, it has been demonstrated that for loose to medium Toyoura sand the CRR is not influenced by the deformation values assumed as reference for liquefaction definition; on the contrary for high relative density the choose of 1 to 10 % DA deformation might produces some little cyclic resistance differences.

In this thesis the results are grouped in two families with two different void ratio and state parameter: the set with higher and lower density have respectively a mean void ratio and a mean state parameter equals to e_c = 0.684 (ψ = - 0.231) and e_c = 0.788 (ψ = - 0.127).

Results from another research conducted by Hyodo (1994) are superimposed on the same graph; the tested samples of dry pluviated loose Toyoura sand have D_R = 35% and p'_c = 100 kPa. The differences of the cyclic resistance behavior between loose-to-medium density is small if compared to the bigger one obtained between medium-to-dense sand.

State parameters are deduced considering the non-linear critical state line obtained by Verdugo (1992), already reported in Chapter 3.

The curves that interpolates data are defined as CSR^{ss} (ψ = -0.231) = $0.331 \cdot N^{-0.302}$ and CSR^{ss} (ψ = -0.127) = $0.11 \cdot N^{-0.149}$.

Cyclic resistance of sand is clearly state parameter dependent: with the increasing of dilatancy the cohesionless material has a greater resistance to liquefaction. The cyclic resistance ratio is defined for a reference earthquake of magnitude M_w = 7.5, namely CRR^{ss} is defined for 15 numbers of cycles. It results:

[4.5] $$CRR^{ss}_{15} = 0.146 \quad \text{for } \psi = -0.231$$

[4.6] $$CRR^{ss}_{15} = 0.073 \quad \text{for } \psi = -0.127$$

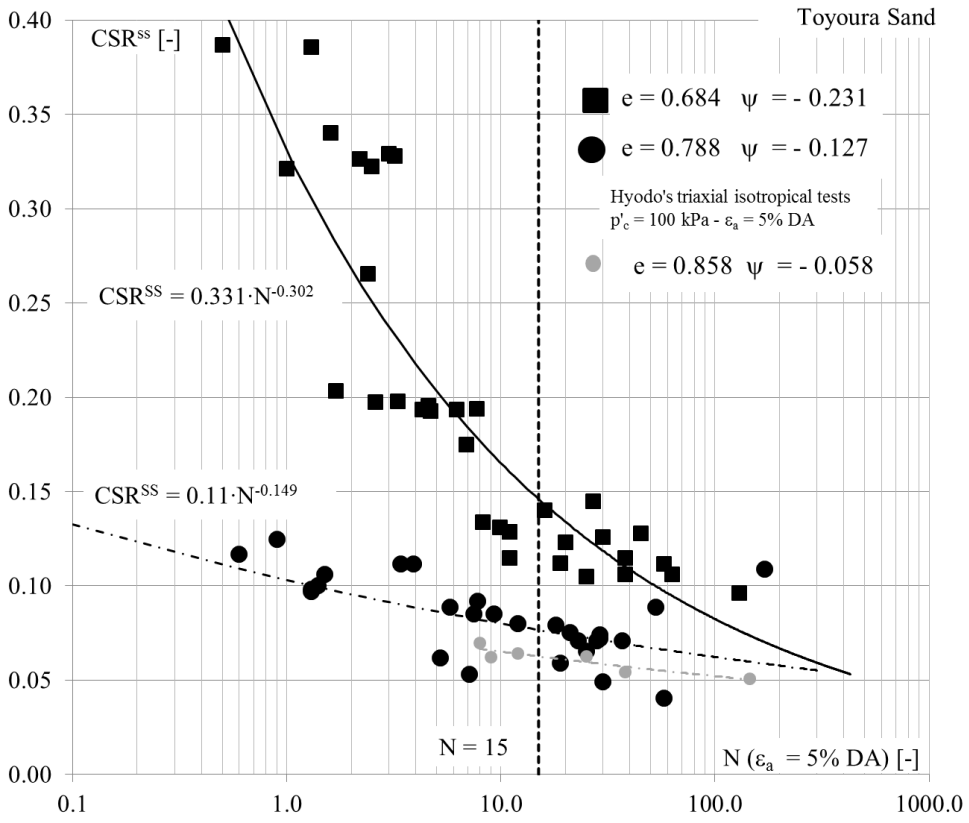

Figure 4.10-Cyclic stress ratio CSR^{SS} versus number of cycles N, where CSR is reduced by a factor (1 + 2 k_0)/3 and N is defined at axial deformation ε_a = 5% DA [Toki, 1986, Hyodo, 1994]

4.6 Cyclic behavior of Ticino Sand

The cyclic behavior of Ticino sand has been deduced by cyclic triaxial isotropical consolidated tests conducted on specimens reconstituted with air depositional method.
Main characteristics of tests are reported in Table 4.1, where are summarized the source and the type of test, the initial state conditions (e_c, p'_c, ψ) and the initial cyclic stress ratio CSR^{TX} applied in triaxial condition. As can be seen from the table below, all samples are tested varying the initial void ratio and the cyclic deviatoric stress, keeping a constant mean effective stress at the end of consolidation, with the exception of TS4_13_12 test which is consolidated to a mean effective stress of p'_c = 200 kPa.

Test	Sample B x H [cm x cm]	Type of test	Sourse	Depositional Method	e_c * [-]	σ'_{vc} [kPa]	σ'_{hc} [kPa]	p'_c [kPa]	ψ [-]	CSR^{TX} ** [-]
TS4_13_1	5 x 10	CYC ISO	ISMGeo	AP	0.740	100	100	100	-0.137	0.234
TS4_13_4					0.730	100	100	100	-0.147	0.183
TS4_13_6					0.700	100	100	100	-0.177	0.181
TS4_13_7					0.700	100	100	100	-0.177	0.336
TS4_13_8					0.640	100	100	100	-0.237	0.304
TS4_13_9					0.640	100	100	100	-0.237	0.243
TS4_13_11					0.760	200	200	200	-0.099	0.285
TS4_13_13					0.760	100	100	100	-0.117	0.253
TS4_13_14					0.730	100	100	100	-0.147	0.207
TS4_13_15					0.730	100	100	100	-0.147	0.162
TS4_13_17					0.700	100	100	100	-0.177	0.330
TS4_13_20					0.644	100	100	100	-0.233	0.198
TS4_13_23					0.707	100	100	100	-0.171	0.244
TS4_14_01					0.586	100	100	100	-0.291	0.414
TS4_14_02					0.580	100	100	100	-0.297	0.288
TS4_14_03					0.581	100	100	100	-0.297	0.208
TS4_14_04					0.582	100	100	100	-0.295	0.391

* e_{max} = 0.923; e_{min} = 0.574 **initial cyclic stress ratio TX condition

Table 4.1- Characteristics of cyclic isotropical triaxial tests on Ticino sand

Tests are grouped together considering samples with similar initial state parameter; three main groups are obtained with mean state parameter equal to ψ = - 0.132, - 0.201, - 0.295, representing samples from medium to high initial density. State parameter is deduced using the critical state line introduced in Chapter 3.
In specimens with a medium density it is not uncommon that cyclic stress ratio manifests some drop in values (as observed also in Toyoura sand cyclic tests), especially when both the specimen approaches the initial liquefaction and small cyclic stress is applied.
All specimens exhibits cyclic mobility after liquefaction started because the physical state are well below the critical state line in e – p' plane. Figure 4.11 is reported a test result

that evidenced cyclic liquefaction. In the first cycles the stress-strain hysteresis are narrow and nearly linear in q – ε_a plane; when the liquefaction starts the curves run parallel to ε_a = 0-axis over a wide range of strains, implying that the soil does not mobilize any shear resistance. Once both a certain axial strain is reached and the pore pressure drops due to dilatancy, a shear resistance is regained. In q – p' plane is shown the stress-path of the test: due to the increase in the water pressure and the accompanying decrease in the effective stress p' with the increase of cycles, the stress-path shift to left. During the phase of cyclic mobility the stress path takes a butterfly-like shape.

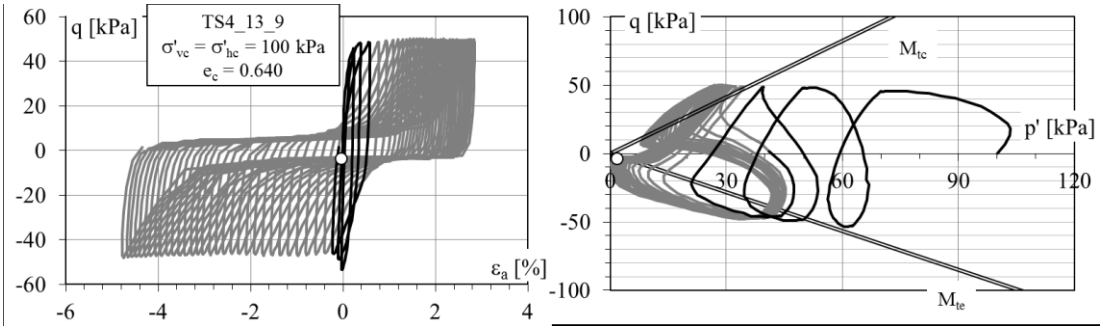

Figure 4.11- Cyclic liquefaction in triaxial test

In medium-to-loose specimens the limiting deformation and the build up pore pressure are typically coincident and N values are uniquely determined, namely the deformation of 5% in double-amplitude is achieved when the pore water pressure ratio is in the range of $R_u = 0.95 \div 1$. In any case liquefaction in samples is reached firstly by the cutch up of the limit deformation.

In very dense specimens pore pressure reaches the mean effective stress value before the axial deformation develops the 5% (DA). The application of cyclic stress develops a peak pore pressure ratio of $R_u > 0.95$ but, subsequently, stress application causes limited strains because the soil dilates and stabilized under the applied loads.

In Figure 4.13 are reported the results of the cyclic triaxial tests in CSR^{SS} – N plane; in this graph cyclic stress ratio, CSR^{TX}, is reduced in order to take into account the in-situ stress and strain conditions and number of cycles to liquefaction N are evaluated when the criterion $\varepsilon_a(DA) = 5\%$ or $R_u > 0.95$ are satisfied.

With the increasing of stress applied the number of cycles to liquefaction decrease with a potential low. The curves that interpolates data are defined as CSR^{ss} (ψ = - 0.132) = $0.171 \cdot N^{-0.139}$, CSR^{ss} (ψ = - 0.201) = $0.271 \cdot N^{-0.211}$ and CSR^{ss} (ψ = - 0.295) = $1.396 \cdot N^{-0.377}$.

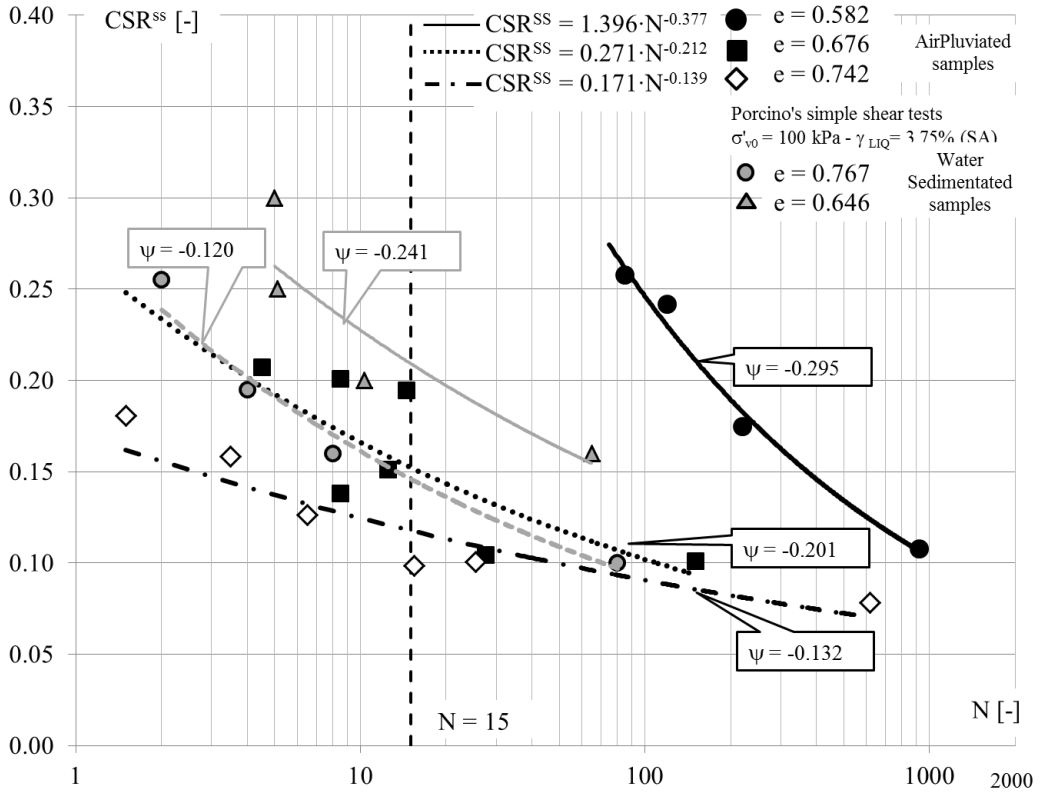

Figure 4.12- Cyclic stress ratio CSR^{SS} versus number of cycles N, where CSR is reduced by a factor $(1 + 2 k_0)/3$ and N is defined at axial deformation ε_a = 5% DA. Simple shear test results based on Porcino's research (2005, 2009)

The cyclic resistance ratio is defined for a reference earthquake of magnitude $M_w = 7.5$, namely CRR^{ss} is defined for 15 numbers of cycles. As cyclic stress ratio and state parameter are related to each other, CRR^{ss} results in:

[4.7] $CRR^{SS}_{15} = 0.503$ for $\psi = -0.295$

[4.8] $CRR^{SS}_{15} = 0.152$ for $\psi = -0.201$

[4.9] $CRR^{SS}_{15} = 0.118$ for $\psi = -0.132$

In the same graph are superimposed the results of a series of simple shear tests conducted on Ticino sand [Porcino et al., 2005, 2009]. Samples ware reconstituted with water sedimentation method and tested with two different void ratio and consolidated to a vertical effective stress σ'_{v0} = 100 kPa (e_c = 0.646, 0.767, with e_{max} = 0.905 and e_{min} = 0.559, sand slightly different from Ticino sand used in triaxial cyclic tests of these research). In order to report the data in CSR^{ss} – N plane, k_0 = 0.44 is assumed in order to determine the state parameter ψ.

The differences in results are mainly assigning to the different depositional method used in the two researches: in particular air pluviation method leads a smaller cyclic resistance ratio if compared with water sedimentation method results, as it can be confirm by the comparison of the two curves with similar state parameter (ψ_{WS} = - 0.120 and ψ_{AP} = - 0.132).

More detailed concerning the tests and the results in q – p', q – ε_a, ε_a – N and Δu – N planes are reposted in Appendix B.

Chapter 5

5 Tip Resistance of Sands from Physical Modelling Tests

5.1 ISMGeo Centrifuge

The ISMES-GEO geotechnical centrifuge (IGC) is a beam centrifuge with a symmetric rotating arm that holds two swinging basket that contain the model and the counterweight (Figure 5.1). An outer fairing, which rotates with the arm, has an aerodynamic purpose of limiting the air friction in reaching the limit speed with low power consumption [Baldi et al., 1988].

The IGC is a medium size centrifuge with a capacity of 240 g-ton, which has designed to reach a limiting speed of 600g with a payload of 400 kg. The particular beam shape is project for (i) minimize the distortion on the model due to centrifugal forces, (ii) simplify the position of the basket and location of the instrumentation, (iii) eliminate Coriolis's acceleration, a_c.

The nominal radius of the model is 2 m, and its maximum dimensions are: length 1000 mm, height 600 mm and width 500 mm. As centrifuge acceleration increases, the swinging baskets rotate from a vertical position at rest to a horizontal one and then move radially to rest against the arm in order to prevent transmitting working loads to the suspension system. The propulsion system is a 300 kW D.C. electric motor.

The centrifuge is equipped with a set of hydraulic slip rings, for the oil at high pressure (250 MPa max), water and air (20 MPa max), and electrical slip rings for the power supply (7 A) and electrical signals.

Special signal conditioners, specifically developed by ISMES, have been mounted in the centre of the arm, and are programmable from the control room in terms of type of transducer to be supplied, transducer supply voltage, offset and sampling frequency; the signal conditioners are equipped with both analogical and digital outputs. A 14 bit A/D converter is employed, with a maximum sampling rate, for digital acquisition, of 100 Hz per channel for a total number of 32 channels. All operations can be completely remote controlled from the centrifuge control room.

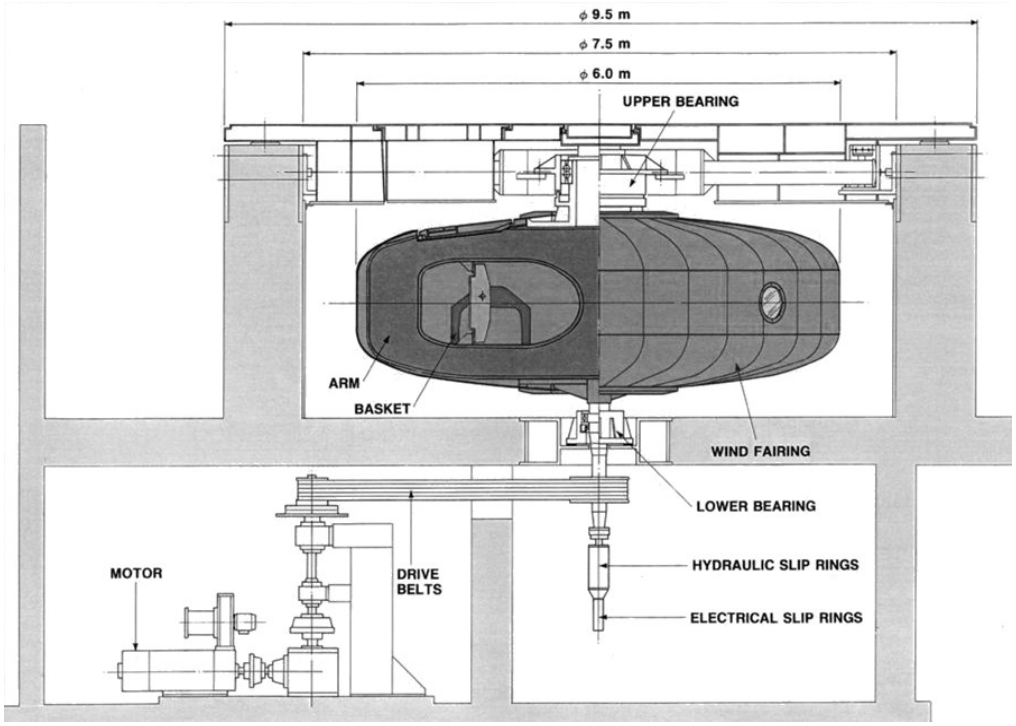

Figure 5.1- Cross section of ISMES – Geo Geotechnical Centrifuge [Fioravante, 1994]

5.1.1 Linear scaling low

In order to extrapolate the observations made on a model to a prototype scale, we need to understand scaling laws. The way we can obtain these similarity rules is through dimensional analysis, which is based on the hypothesis that any physical phenomenon can be described by a dimensionally consistent equation between governing variables.

The tool used in dimensional analysis is Buckingham's ″Pi″ theorem which states that the number of variables to be considered in a dimensional analysis problem, defined by a list (V) of *h* variables, encompassing a total of independent *m* primary dimensions (D), can always be reduced to a number N of dimensionless groups, where N = h - m.

The use of dimensional analysis allows one to identify the variables that are independent and hence important to be reproduced at model scale. Butterfield (1999) demonstrates that Buckingham's theorem is a necessary, but not sufficient condition to establish a general dimensional analysis solution for problems in which time intervenes only to converse mass to force.

The various similarity conditions between models and prototypes that have to be fulfilled in geotechnical model testing have been examined by many researches [e.g. Roscoe, 1968; Rowe et al., 1977; Schofield, 1980; Baldi et al., 1989a, Taylor, 1995; Butterfield, 1999; 2000] and are therefore not discussed here.

For all quantities that describe static and dynamic phenomena in soil mechanics, the following ratio is defined as scale factor:

[5.1] $$X^* = \frac{X_{\text{model}}}{X_{\text{prototype}}}$$

Where X stands for a generic physical quantity (e.g. length, mass, density, or time).

If the length, the mass density, the acceleration field and the strain (or stiffness) are assumed as independent quantities, the other quantities can be expressed as functions of the independent quantities.

The critical similarity relationships between a centrifuge model and a prototype state that if a model in which each linear dimension is reduced by a factor N is subjected to a centrifuge acceleration of N·g (where g is the gravity field), it achieves the equivalent vertical stress as the full scale prototype, on condition that a material with the same unit

weight is used. As the stresses derive from the density of the soil and gravitational acceleration:

[5.2] $$\delta\sigma' = \rho \cdot g \cdot \delta z \Rightarrow \sigma^* = \rho^* \cdot g^* \cdot L^*$$

If g* = N, L* = 1/N and ρ* = 1 hence the Equation 5.2 became:

[5.3] $$\sigma^* = 1$$

If the same soil is used for the model and the prototype, the stress strain behaviour of the model is the same as that of the prototype. This also means that a similarity of strain is achieved (i.e. ε*=1).

The majors scaling lows use in centrifuge analysis are summarized in Table 5.1; they are derived considering the same soil both in prototype and model and they are better examined in the following paragraph.

Parameter	Unit	Scale factor model/prototype
acceleration	m/s^2	N
linear dimension	m	1/N
stress	kPa	1
strain	-	1
density	kg/m^3	1
mass or volume	kg or m^3	$1/N^3$
unit weight	N/m^3	N
force	N	$1/N^2$
bending moment	N m	$1/N^3$
bending moment/unit width	N m /m	$1/N^2$
flexural stifness/unit width	N m^2/m	$1/N^3$
time diffusion	s	N^2
time dynamic	s	N
frequancy	1/s	N

following low $\sigma_v = \rho_m \cdot (N\ g)_m \cdot (z/N)_m = \rho_p \cdot g_p \cdot z_p$

Table 5.1- Scale factors in an artificial gravity field

The maintenance of consistency between a model and a prototype, in terms of stress and strain, is one of the key factors which leads to centrifuge modelling being preferred to unit gravity models, as soil behaviour greatly depends on the stress history and current applied stress.

5.2 Mechanics of centrifuge modelling

The acceleration field in a centrifuge varies through the model depth, as it is a function of the radial distance as follows:

[5.4] $$a_c = N \cdot g = R_t \cdot \omega^2$$

Where: $g = 9.81$ m/s^2 is the earth gravitational acceleration;

$N = a_c/g$ is the ratio between centrifuge acceleration and earth's gravity at free surface;

ω is angular velocity;

R_t is the radial distance between the free surface of the model and the rotational axis.

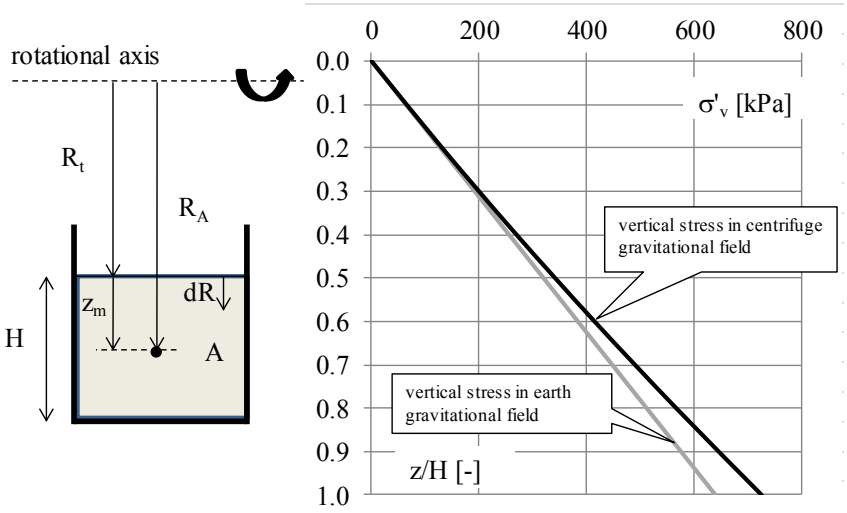

Figure 5.2- Stress distribution with depth in a centrifuge model and in prototype [Taylor, 1995]

The infinitesimal increment of the vertical stress caused by an infinitesimal depth increment dR from the free surface (Figure 5.2) can be expressed through the following equation:

[5.5] $$d\sigma'_v = \rho \cdot g \cdot (N \cdot dR) = \rho \cdot g \cdot \frac{\omega^2 \cdot R}{g} \cdot dR = \rho \cdot g \cdot \omega^2 \cdot R \cdot dR$$

Where ρ is the mass density and R is the radial distance from the rotational axis.

The vertical stress of the point A in the soil model is given by the following integral:

[5.6] $$\sigma'_v = \int_{R_A}^{R_t} \rho \cdot \omega^2 \cdot R \cdot dR = \frac{1}{2} \cdot \rho \cdot \omega^2 \cdot \left({R_A}^2 - {R_t}^2 \right)$$

Where: R_A is the radial distance of soil point A from the rotational axis;

R_t is the radial distance of the free surface of the model from the rotational axis.

As the distance $R_A = R_t + z_m$, where z_m is the model depth that refers to the free surface, and the angular velocity expressed by the relation $\omega^2 = (N \cdot g)/R_t$, the resulting vertical stress at the corresponding prototype depth z_p is:

[5.7] $$\sigma'_v = \int_{R_A}^{R_t} \rho \cdot \omega^2 \cdot R \cdot dR = \rho \cdot g \cdot N \cdot z_m \cdot \left(1 + \frac{z_m}{2 \cdot R_t}\right) = \rho \cdot g \cdot z_p \cdot \left(1 + \frac{z_m}{2 \cdot R_t}\right)$$

Where $z_p = N \cdot z_m$ is the corresponding prototype depth.

In the earth's gravity field, the vertical stress of point at depth z is given by the following equation:

[5.8] $$\sigma'_v = \int_0^z \rho \cdot g \cdot dz = \int_0^z \gamma \cdot dz$$

If soil is considered homogeneous with depth (i.e. soil density constant with depth, the result of the previous integer is:

[5.9] $$\sigma'_v = \rho \cdot g \cdot z$$

It can be seen from Figure 5.2 that the model stress distribution is not linear and tends to slightly diverge from the triangular distribution, as the radial distance from the rotational axis increases.

5.3 In-Flight cone penetration tests: results and interpretations

Centrifuge cone penetration tests have been carried out in dry samples reconstituted by air depositional method. This methodology is widely used to reproduce uniform specimens [Passalacqua, 1991; Lo Presti et al., 1993] and an adequate anisotropy, comparable with that of the alluvial deposit [Oda et al. 1978].

Sand is deposed at 1 g with a travelling sand spreader into a cylindrical container; varying the height of the hopper by keeping constant the fall height of sand and the speed of deposition, it is possible to obtained samples with various initial relative density. The container wall is 5 cm thick in order to prevent radial deformation during accelerated test.

After the deposition phase the container with sand is weighted and then inserted on the swinging basket of the centrifuge. Here in, the model is accelerated until the pre fixed a_c/g acceleration level is reached; during this stage the superficial sand settlement is monitored by an LVDT placed on the free surface of soil: specimen compacts in dependence of its initial relative density and acceleration level. At the end of consolidation phase, the cone advanced in the soil with a constant velocity until the end of test (v = 2 mm/s). The container dimensions and CPT system are illustrated in Figure 5.3.

The ISMES miniaturized piezocone has a diameter of B = 11.3 mm, the driving force acts on both the 60° cone as well as on the shaft behind the tip (areas A = 100 mm^2); the tip and the shaft have two load cells able to record force up to 9.8 kN, while the actuator system is capable to produce a 11.8 kN of trust. If the sample is saturated, the pore pressure transducer located in the mini – cone can measures up to 35 bars.

It is of interest noting that a centrifuge test conduct with the ISMGeo Cone with B = 11.3 mm at a g-level of 50 g represent a prototype cone of 56.5 cm; in spite of the different dimensions in real case and in prototype, the results of these CPT tests can be used for evaluating tip resistance of soil as proved by a great testing program conduct by 5 laboratories in an European research [Renzi et al., 1994; Bolton et al. 1998].

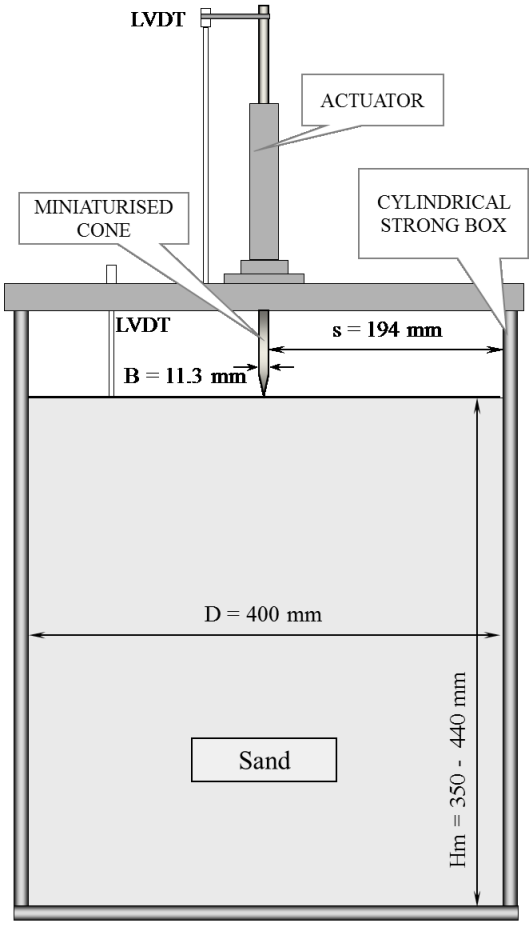

Figure 5.3- ISMES – Geo in flight cone penetrometer

The results of this investigation leaded to evaluate the effects of (i) grain size and scale factors, (ii) stress non uniformity and (iii) boundary conditions.

(i) Grain size and scale factor:

- $B/D_{50} \geq 20$ (grain size effect): soil particle size doesn't affect tip resistance if cone diameter is 20 times greater than mean particle size. This is evident for fine particle (Figure 5.4 c) and for medium course particle (Figure 5.4 d).

(ii) Stress non uniformity:

as proposed by Bolton et al. (1999), in order to overcome the problem of non-linear stress in centrifuge test, all the measurements of depth of penetration recorded by the miniaturized cone, are corrected as follow:

[5.10] $$z_{pc} = N \cdot z_m \cdot \left(1 + \frac{z_m}{2 \cdot R_t}\right)$$

In most cases, centrifuge is design in order to have $h_m/R_e < 0.2$ (h_m is the maximum height of the model) and so the maximum error committable on the evaluation of vertical stress is less than 3% with depth.

(iii) Boundary conditions:

- D/B ≥ 30 (container size effect): as can be seen in Figure 5.4 (a) the influence of the container size D to cone diameter B on the normalized Q cone resistance is negligible if D is almost 30 times greater than cone diameter B. This limitation is particular important for dense sand because the rigid walls increases the confining pressure around the plastic soil zone leading to an overestimation of cone resistance.

- s/B (size boundary effect): it was found that for a circular container, there is no significant deviation in Q, for both s/B = 11 and s/B = 22 for dense sand (Figure 5.4 b).

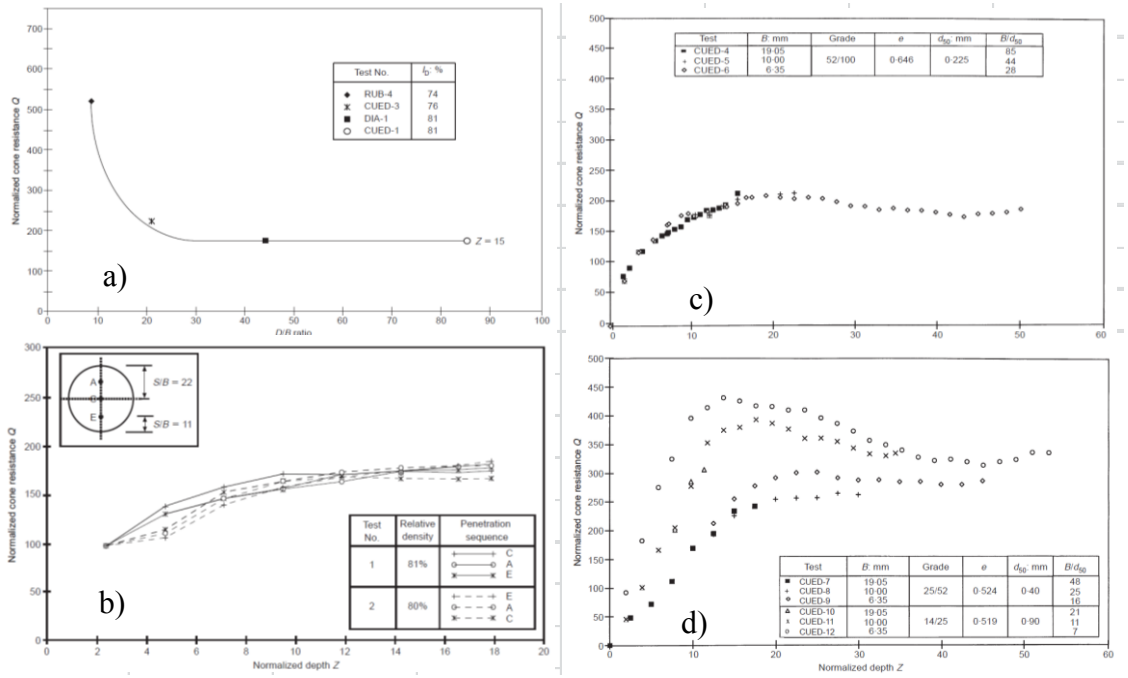

Figure 5.4- Scale effect in centrifuge cone penetration tests in sand. In Figures normalized cone resistance $Q = (q_c - \sigma_v)/\sigma'_v$; normalized penetration depth Z = z/B): (a) D/B - container size effect, (b) s/B – side boundary effect, (c) B/d_{50} – grain size effect (fine particles), (d) B/d_{50} – grain size effect (medium and coarse particles) [Bolton et al., 1999]

The size of the container and of the piezocone used in this research allow concluding that (i) and (iii) conditions are prevent for the two sands, in fact: D/B = 35.4 and s/B = 17.2, for both tested sands, $B/D_{50} = 21.3$, for Ticino sand, and $B/D_{50} = 51.4$, for Toyoura sand. The stress non-uniformity (ii) has also been accounted for.

5.3.1 Tip resistance for Toyoura and Ticino sands

The main data on CPT tests performed on Toyoura and Ticino sand are reported in Table 5.2 and Table 5.3 respectively, where the acceleration factor N and density ρ, void ratio e and height H of the samples at the end of consolidation phase are summarized.

The CPT tests conducted on TOS were performed on specimens with classes of three different void ratio (e ~ 0.778; 0.725; 0.654) and two acceleration levels (N = 30, 80). Considering the height of the samples the maximum investigated depth is almost 25 m.

Identically, the CPT tests conducted on TS4 were performed on specimens with classes of three different void ratio (e ~ 0.819; 0.726; 0.627) and three acceleration levels (N = 30, 50, 80). In this case the maximum investigated height is almost 30 m.

The *e* and ρ data were evaluated at the end of consolidation phase and are medium values. In fact, the angular velocity of the centrifuge has been imposed so that the target ratio a_c/g was reproduced at the surface of the model. The settlement of the sand during the in–flight consolidation is non-linear with depth, thus the relative density increases with depth and is slightly lower at the soil surface and slightly higher at the container bottom, with respect to the average value. The maximum scatter from the average value has been estimated to be about ±5%, therefore it was assumed constant in the presented analysis.

In Figure 5.5 and in Figure 5.6 are reported the tip resistance q_c function of mean effective stress p' (on the left axis) and depth z_{pc} (on the right axis) for TOS and TS4 sands respectively, where all measures are in prototype scale and corrected for distortion produced by radial field.

In the same graphs are superimposed some results from calibration chamber tests conducted by ISMES (Seriate – Bergamo – Italy). A selection of only ″BC3″ boundary condition tests are considered, where vertical stress σ_v is constant with depth and the radial deformation ε_h is zero with depth; instead, cone diameters range between B = 11.3 – 35.7 mm. Generally, the more the cone diameter is smaller the more the tip resistance is greater, keeping the other conditions the same [Fioravante et al., 1992].

All data about tests carried out in calibration chamber are reported in Table 5.4 and Table 5.5 for Toyoura and Ticino sands.

CPT TESTS IN CENTRIFUGE ON TOYOURA SAND					
Side boundary effect		s/B = 17.2	Particle size effect		B/D_{50} = 51.4
Container size effect		D/B = 35.4	Penetration rate		v = 2 mm/s
TEST	Acceleration Level N = a/g	γ_{dry}	e	D_R	Prototype Height H
	[-]	[kN/m^3]	[-]	[%]	[m]
T1/TYC1	30	15.71	0.655	88	10.5
T1/TYC2	30	15.71	0.654	89	10.5
T1/TYC3	80	15.69	0.657	88	27.9
T1/TYC4	80	15.75	0.650	90	27.8
T1/TYC5	80	14.66	0.774	57	27.9
T1/TYC6	80	14.58	0.783	54	27.8
T1/TYC7	80	15.08	0.724	70	27.8
T1/TYC8	80	15.02	0.730	68	28.0
T1/TYC9	30	15.12	0.719	71	10.4
T1/TYC10	30	15.04	0.728	69	10.4

all values are at the end of consolidation e_{max} = 0.986; e_{min} = 0.612

Table 5.2- Tests data of in-flight CPT in Toyoura Sand

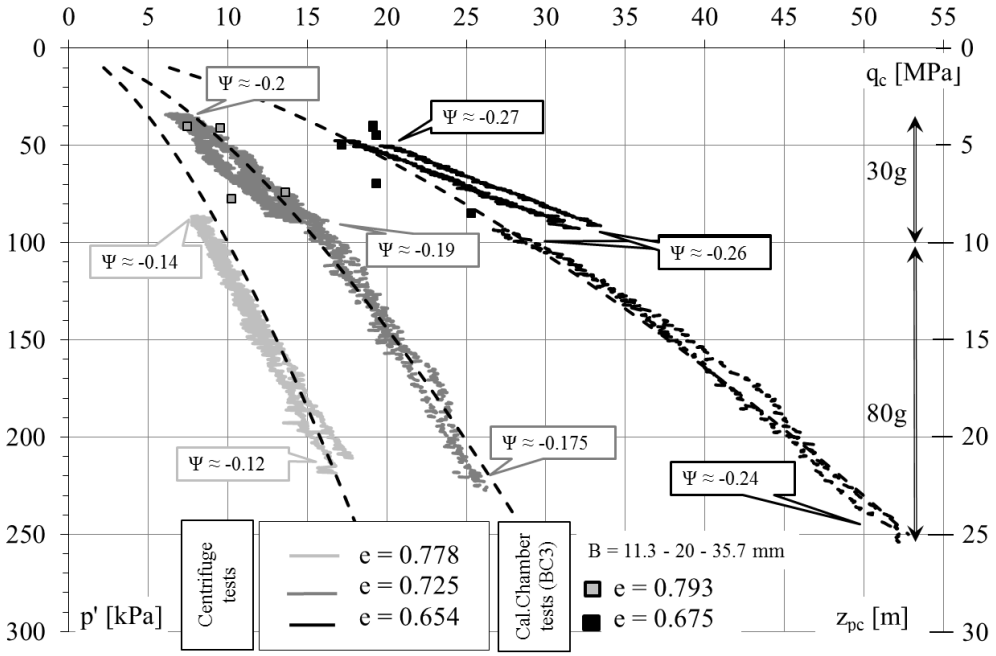

Figure 5.5- Cone tip resistance test results for Toyoura sand. In the graph: tip resistance q_c vs mean effective stress p' for various consolidation void ratio e. Superimposed on the same graph the results of calibration chamber tests [ISMES-Geo]. In dotted black lines evaluation of tip resistance with $q_c = 17 \cdot p_{ref} \cdot (p'/p_{ref})^{0.66} \cdot e^{3.19 \cdot D_R}$. Depth z_{pc} on the right axis is a mean values

CPT TESTS IN CENTRIFUGE ON TICINO SAND					
Side boundary effect		s/B = 17.2	Particle size effect		B/D_{50} = 21.3
Container size effect		D/B = 35.4	Penetration rate		v = 2 mm/s
TEST	Acceleration Level N = a/g	γ_{dry}	e	D_R	Prototype Height H
	[-]	[kN/m^3]	[-]	[%]	[m]
TS4-1	30	14.30	0.834	25.5	10.40
TS4-2	30	14.40	0.822	28.9	10.37
TS4-3	80	14.45	0.815	30.8	27.58
TS4-4	80	14.53	0.805	33.7	27.57
TS4-5	30	16.11	0.629	84.3	10.61
TS4-6	30	15.94	0.646	79.4	10.52
TS4-7	80	16.02	0.638	81.6	27.84
TS4-8	80	16.03	0.637	81.9	27.90
TS4-11	30	14.54	0.804	34.0	13.17
TS4-12	30	14.31	0.834	25.6	13.18
TS4-13	80	14.44	0.816	30.6	35.07
TS4-14	80	14.47	0.813	31.6	35.14
TS4-15	80	15.09	0.738	53.0	35.41
TS4-16	30	15.18	0.728	55.8	13.31
TS4-17	50	15.22	0.724	57.1	22.16
TS4-18	50	15.24	0.721	57.7	22.15
TS4-19	30	16.19	0.620	86.6	13.35
TS4-20	80	16.27	0.613	88.8	35.58
TS4-21	50	16.21	0.619	87.1	22.23
TS4-22	50	16.16	0.623	85.9	22.23
TS4-23	50	14.42	0.819	29.9	22.01
TS4-24	50	14.47	0.813	31.5	22.02
TS4-25	30	14.41	0.821	29.2	13.21
TS4-26	80	14.41	0.821	29.2	35.24
TS4-28	50	16.23	0.617	87.7	22.22
TS4-29	50	15.25	0.720	58.2	22.15
TS4-30	30	14.38	0.824	28.2	13.20
all values are at the end of consolidation			e_{max} = 0.923 e_{min} = 0.574		

Table 5.3- Tests data of in-flight CPT in Ticino Sand

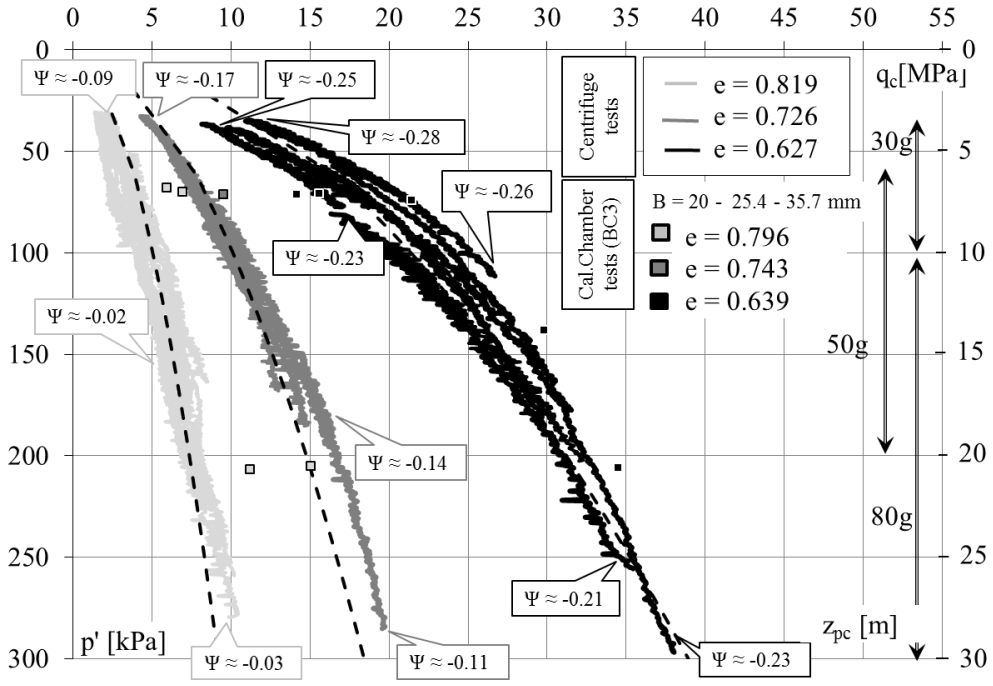

Figure 5.6- Cone tip resistance test results for Ticino sand. In the graph: tip resistance q_c vs mean effective stress p' for various consolidation void ratio e. Superimposed on the same graph the results of calibration chamber tests [ISMES-Geo]. In dotted black lines evaluation of tip resistance with $q_c = 23 \cdot p_{ref} \cdot (p'/p_{ref})^{0.55} \cdot e^{2.63 \cdot D_R}$. Depth z_{pc} on the right axis is a mean values

	end of consolidation			penetration							
Test	σ_v	σ_h	e	σ_v	σ_h	d_c	q_c	p'	k_0	Q_p	Ψ
	[kPa]	[kPa]	[-]	[kPa]	[kPa]	[mm]	[MPa]	[kPa]	[-]	[-]	[-]
392i	62.4	27.3	0.673	63.4	28.5	11.3	17.4	40.1	0.45	432.0	-0.251
405i	62.2	27.6	0.673	63.9	35.4	20.0	19.3	44.9	0.55	429.7	-0.250
408i	62.2	27.1	0.674	63.4	29.7	11.3	19.1	40.9	0.47	466.8	-0.250
409i(a)	117.6	208.2	0.671	111.7	49.0	11.3	20.2	69.9	0.44	288.4	-0.248
412i(a)	75	107.7	0.673	74.2	38.0	11.3	17.2	50.1	0.51	342.0	-0.249
316i	112	49.5	0.690	124.8	65.1	20.0	25.3	85.0	0.52	296.7	-0.227
323i	111.1	53.2	0.803	111.9	60.7	35.7	10.2	77.8	0.54	130.7	-0.115
358i	111.7	52.1	0.776	112.3	55.1	20.0	13.6	74.2	0.49	182.9	-0.143
365i	61.6	29	0.793	62.1	30.9	20.0	9.5	41.3	0.50	230.1	-0.131
394i	61.5	29.2	0.800	61.6	29.5	11.3	7.5	40.2	0.48	184.6	-0.124

dry samples; border condition "BC3"; OCR = 1

Table 5.4- Test data of calibration chamber test on Toyoura sand [ISMES]

	end of consolidation			penetration							
Test	σ_v	σ_h	e	σ_v	σ_h	d_c	q_c	p'	k_0	Q_p	Ψ
	[kPa]	[kPa]	[-]	[kPa]	[kPa]	[mm]	[MPa]	[kPa]	[-]	[-]	[-]
124i	313.5	137.0	0.599	319.4	149.2	20.0	34.5	205.9	0.47	166.5	-0.258
121i	213.9	89.2	0.603	214.8	99.9	20.0	29.8	138.2	0.46	214.9	-0.266
119i	114.1	45.9	0.652	114.4	49.8	20.0	14.2	71.4	0.44	197.8	-0.233
284i	112.2	48.6	0.669	112.8	55.0	20.0	21.4	74.2	0.49	287.6	-0.215
194i	112.0	45.9	0.674	110.8	51.2	20.0	15.6	71.0	0.46	218.5	-0.211
166i	112.0	47.8	0.726	112.5	50.7	25.4	9.5	71.3	0.45	132.5	-0.159
199i	111.4	45.4	0.788	111.5	46.2	20.0	6.0	68.0	0.41	86.6	-0.097
201i	111.1	47.7	0.794	111.8	49.0	20.0	7.0	69.9	0.44	98.7	-0.091
70i	316.4	148.4	0.800	317.9	151.1	35.7	11.2	206.7	0.48	53.2	-0.057
70i	316.4	148.4	0.800	314.7	150.5	35.7	15.1	205.2	0.48	72.3	-0.058

dry samples; border condition "BC3"; OCR = 1

Table 5.5- Test information of calibration chamber test on Ticino sand [ISMES]

It can be seen that, for both sands, there is a good agreement between chamber tests and centrifuge tests results, especially for high density. Indeed, some scatter is evidenced for medium-to-loose state of sand.

In order to take into account the progressive mobilization of the cone resistance from the model free surface [Schmertmann, 1978], the measures registered in the first 10·B of penetration from the surface have been removed.

The test results were also interpreted using a function proposed by Jamiolkowski et al. (2003), where the sand's dependent coefficients are determined with a best-regression analysis based on centrifuge test results. Tip resistance is related with mean effective stress and relative density as fallow:

[5.11] $$q_c = C_0 \cdot p_{ref} \cdot \left(\frac{p'}{p_{ref}} \right)^{C_1} \cdot e^{C_2 \cdot D_R}$$

Where:

q_c is cone resistance;

p_{ref} is atmospheric pressure, p_{atm} = 101 kPa

p' is mean effective stress at cone depth;

D_R is relative density expressed as a number;

C_0, C_1, C_2 are dimensionless empirical correlation factors.

The tip resistances for the two sands are:

[5.12] $$TOS \quad q_c = 17 \cdot p_{ref} \cdot \left(\frac{p'}{p_{ref}} \right)^{0.66} \cdot e^{3.19 \cdot D_R}$$

[5.13] $$TS4 \quad q_c = 23 \cdot p_{ref} \cdot \left(\frac{p'}{p_{ref}} \right)^{0.55} \cdot e^{2.63 \cdot D_R}$$

The functions, despite some scatter, follow the general tendency of the measured data and they are superimposed on experimental results in Figure 5.5 and 5.6, in dotted black lines.

5.3.2 Stress normalization

Been (1991) proposed to normalizing tip resistance as follows:

[5.14] $$Q_p = \frac{q_c - p}{p'}$$

Where (q_c – p') is approximately defined as q_c as the penetration in sands is drained.

In Figures 5.7 and 5.8 are reported the resulting normalized tip resistance Q_p function of mean effective stress p' respectively for Toyoura and Ticino sand; in the graphs are also shown the calibration chamber tests considered for comparison purpose.

It is well noticed that tip resistance normalization, which considers a linear relationships between tip resistance and mean effective stress, is not sufficient to account for the stress effect. This is more pronounced in dense material at the maximum depths reached, where Q_p is not a constant value but reduces with depth as shown in the normalized charts reported in Figures 5.7 and 5.8.

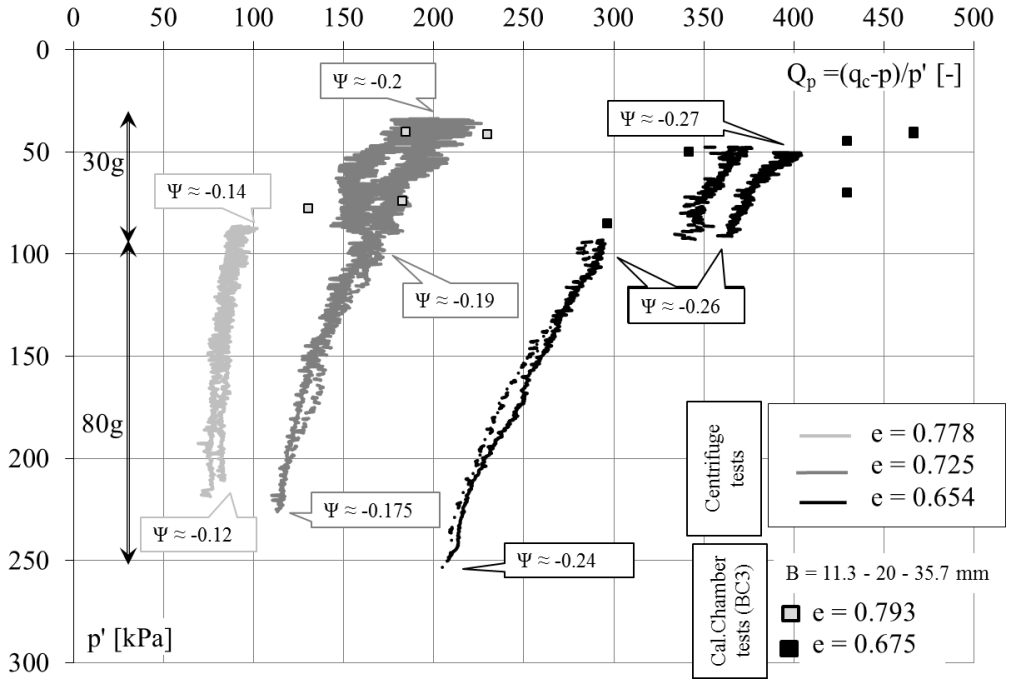

Figure 5.7- Normalized cone tip resistance for Toyoura sand. In the graph: normalized tip resistance Q_p vs mean effective stress p' for various consolidation void ratio e. Superimposed on the same graph results of calibration chamber tests [ENEL - ISMES]

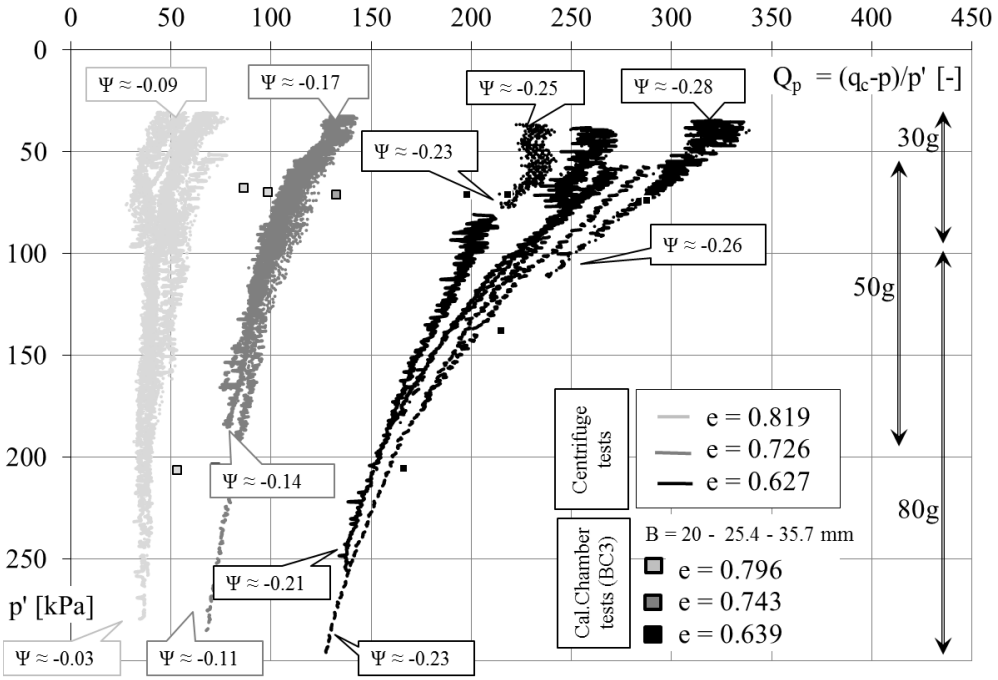

Figure 5.8- Normalized cone tip resistance for Ticino sand. In the graph: normalized tip resistance Q_p vs mean effective stress p' for various consolidation void ratio e. Superimposed on the same graph results of calibration chamber tests [ENEL - ISMES]

Some centrifuge test data are reported in Figure 5.9 (a and b) in $(q_c - p) - p'$ plane; each point is related to a specific void ratio and state parameter value.

In the graphs the data with similar state parameter are interpolated with a linear equation, as proposed by Been (1986). This trend approximation is adequate for high void ratio and for swallow depth; on the contrary, with the increasing of mean effective stress and with the decreasing of void ratio, the net tip resistance tends to increase with a non-linear low with depth (dashed lines).

A different normalization of tip resistance is proposed in Figure 5.10 and 5.11 for both Toyoura and Ticino sands, with the aim to understand how the normalization of q_c is stress dependent. In these graphs, normalized tip resistance Q* are defined as follow:

[5.15] $$Q^* = \frac{q_c / p_{ref}}{\left(p' / p_{ref}\right)^n}$$

Where Q* is a stress dimensionless ratio, p_{ref} is taken as 101 kPa.

The stress exponent *n* was defined from Equations 5.12 and 5.13: n = 0.66 for Toyoura sand and n = 0.55 for Ticino sand.

In the graphs, Q* is constant with depth only for medium-to-high density sand at medium-to-high effective stresses, while Q* increases with depth for low density sand at swallow depth.

The Q_p normalization was adopted here since is largely used, also because a comparison with other researches is appealing.

In both normalized charts proposed Q_p – p' and Q* – p', the dilatancy of sand became the fundamental properties that affected soil behavior.

Dilatancy of a cohesioless material is surly well related with state parameter value (see Chapter 2) inasmuch the more the absolute value of ψ decreases the more the tendency of the sand to dilate is suppressed. Confirmation of what suggested above is proved by the results in Figure 5.7 and 5.8, where values of the state parameter are superimposed in the normalization charts for various mean effective stress and void ratio; it can pointed out that higher values of state parameter leads to higher values of normalized tip resistance.

In the conclusive Chapter 6 will be determine a correlation between tip resistance Q_p and state parameter for the two tested sands.

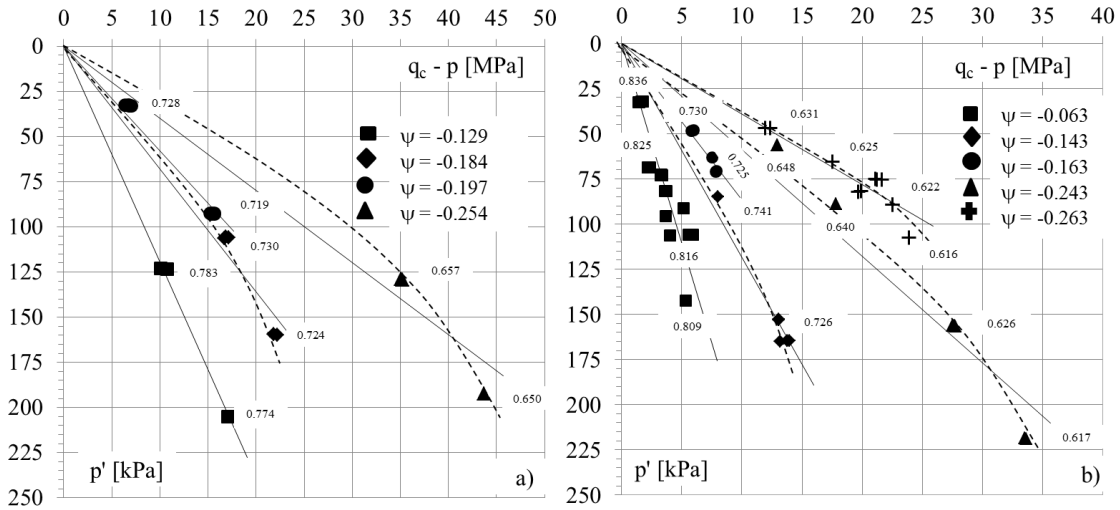

Figure 5.9- Net tip resistance q_c – p' vs mean effective stress p' for various initial state parameter ψ for (a) Toyoura sand and (b) Ticino sand

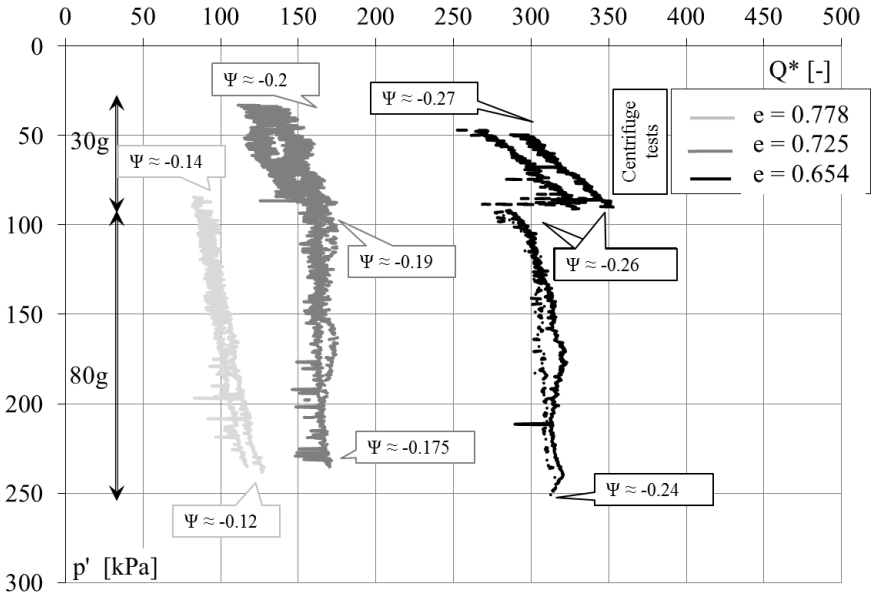

Figure 5.10- Normalized cone tip resistance for Toyoura sand. In the graph: normalized tip resistance Q* vs mean effective stress p' for various consolidation void ratio e.

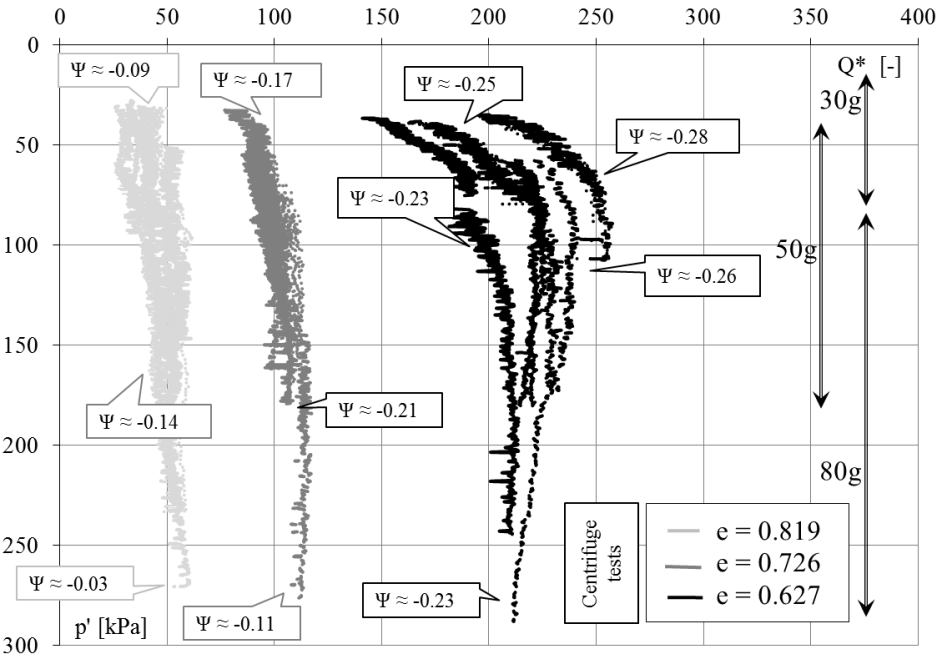

Figure 5.11- Normalized cone tip resistance for Ticino sand. In the graph: normalized tip resistance Q* vs mean effective stress p' for various consolidation void ratio e.

Chapter 6

6 Cyclic Resistance Determination from CPT. A Simplified Relationship

6.1 Introduction

Jefferies and Been (2006) demonstrated that both normalized tip resistance Q_p and cyclic resistance ratio CRR were a function of the state parameter.

In Figure 6.1 are summarized the exponential curves obtained by the fitting procedures of CC test results of different type of sands with 3.5% of maximum fine content. For each sand it was defined a correlation between Q_p and ψ: with the decrease of dilatancy, the normalized tip resistance drops as an exponential function, $Q_p = k \cdot e^{-m \cdot \psi}$, where *k* and *m* parameters are sand dependents.

Jefferies and Been (2006) proposed a mean curve considering the totality of the CC tests and assuming average values of sands mechanical properties (i.e. $M_{tc} = 1.25$, $\lambda_{10} = 0.05$, $\chi_{tc} = 3.5$, $I_r = 600$, $k_0 = 0.7$ and $\sigma'_v = 100$ kPa); the equation, reported in Figure 6.1, was defined as follows:

[6.1] $$Q_p = 31.5 \cdot e^{-9.4 \cdot \psi}$$

Where *k* = 31.5 and *m* = 9.4 were determined as best-fit from all CC tests conducted on different type of sands.

Jefferies and Been (2006) demonstrated that cyclic resistance ratio was state parameter dependents: the more the sand was dilative the more the resistance to liquefaction was higher.

The cyclic resistance ratio is easily derived from CSR^{TX} – N curves which interpolate the experimental values with similar state parameter; considering a reference earthquake of $M_w = 7.5$ (15 equivalent of uniform cycles).

In Figure 6.2 the cyclic resistance ratio in triaxial condition CRR^{TX}_{15} is plotted as a function of ψ and it is observed that each sand have its own liquefaction curve, linked with its intrinsic mechanical and physical characteristics.

In the same graph, a mean exponential curve was determined despite the evident data dispersion due to the differences in samples preparation methodology and in the type of studied sand; the equation was defined as:

[6.2] $$CRR^{TX}{}_{15} = 0.125 \cdot e^{-3.85 \cdot \psi}$$

Hereafter, simplified correlations are going to be proposed for both tip and cyclic resistance; they will be linked with state parameter values in order to determine a function between CRR and Q_p. The analyses are based on high quality tests data in controlled stress and strain conditions described in Chapters 3, 4 and 5.

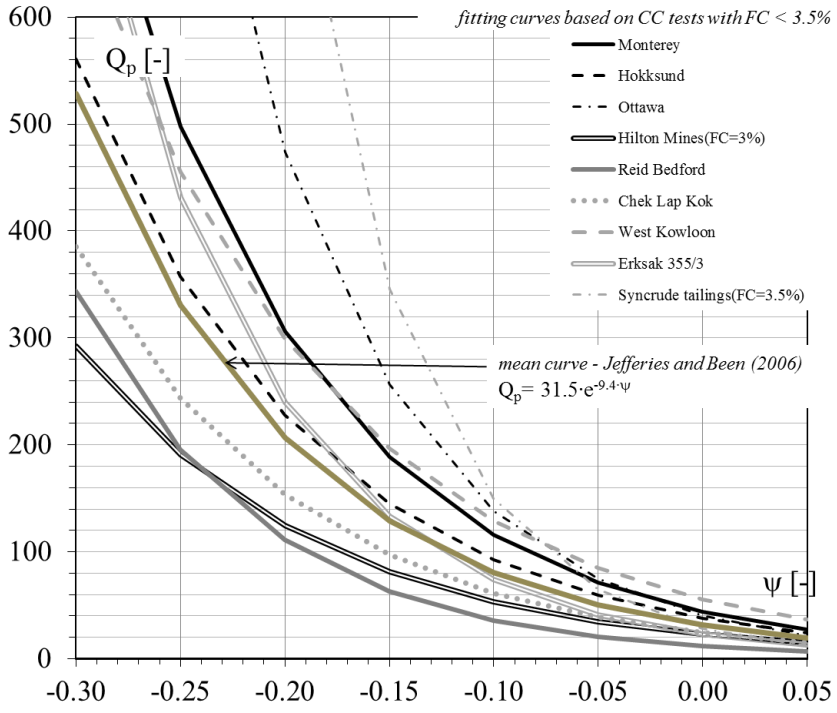

Figure 6.1- Q_p - ψ curves for different type of sands

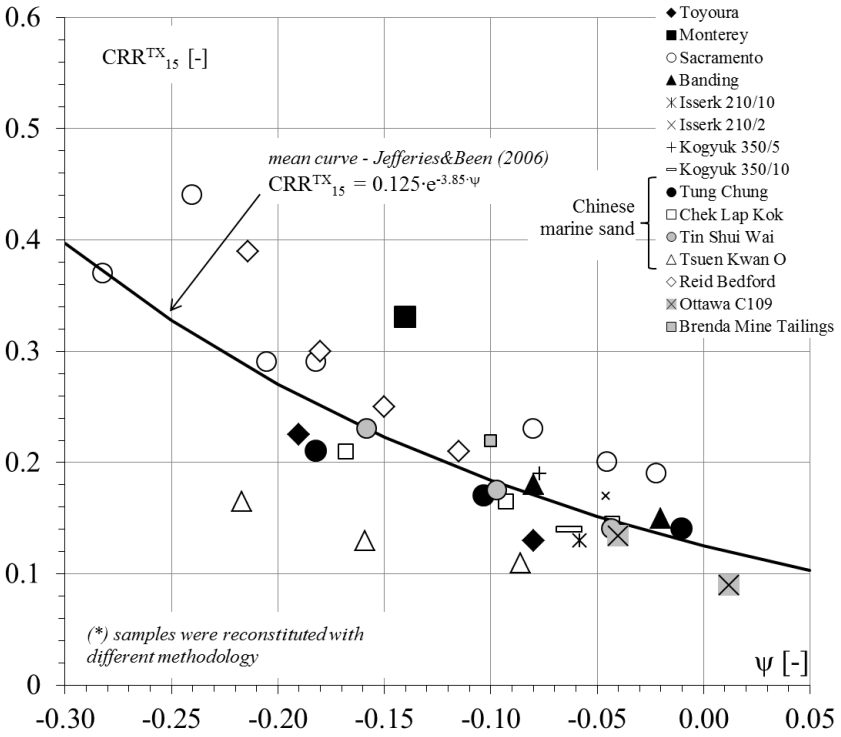

Figure 6.2- CRR - ψ curves for different type of sands

6.2 Q_p - ψ and CRR - ψ curves for Ticino and Toyoura sands

In Chapter 3 the critical state lines of Ticino and Toyoura sands have been defined. In Chapter 4 the cyclic behavior of Ticino and Toyoura sands were analyzed and it has been demonstrated that CSR – N curves were state parameter dependents. In Chapter 5 it has been described how tip resistance was influenced by dilation and state parameter.

In Figure 6.3 the centrifuge tests results performed on Toyoura sand are reported in Q_p - ψ plane. The results have been grouped in three sets of void ratio (i.e. e_c = 0.778, 0.725, 0.654): the measured q_c profile of each test is associated with an initial void ratio value and, so, to a state parameter.

The more the sand is initially ″dense of critical″ the more the normalized tip resistance is high; a unique mean exponential function between normalized tip resistance Q_p and state parameter ψ was deduced, as follows:

[6.3] $$Q_p = 23.94 \cdot e^{-9.78 \cdot \psi}$$

In the equation above k = 23.94 and m = 9.78.

In the same graph, are plotted some results from calibration chamber test conducted on sample with e_c = 0.793 and e_c = 0.675. Penetration tests were conducted in samples with constant vertical stress and zero lateral deformation conditions (BC3); even if it is thought that CC-BC3 test is the best representation of the centrifuge boundary conditions, there is some scatter in results between calibration chamber and centrifuge tests. Data from CC test are shifted above in Q_p – ψ graph and this could be due to an underestimation of state parameter or to an overestimation of tip resistance.

The centrifuge tests results of Ticino sand are reported in Figure 6.4 in Q_p – ψ plane; also in this case an exponential trend between normalized tip resistance and state parameter is observed and the mean curve was deduced as:

[6.4] $$Q_p = 26.37 \cdot e^{-8.44 \cdot \psi}$$

In the equation above k = 26.37 and m = 8.44.

Calibration chamber test results are superimposed in the graph with the aim to compare them with centrifuge ones. Tests were selected so that BC3 conditions were satisfied and void ratio were e_c = 0.796, 0.726 and 0.639. For Ticino sand, a minor dispersion is

observed between CC and centrifuge tests, in comparison to that experienced for Toyoura sand.

It is notably that Ticino and Toyoura sands have a very similar Q_p - ψ curves. So that a mean function is herein proposed, in which *k* and *m* parameters are calibrated with all available centrifuge tests:

[6.5] $$Q_p = 25.6 \cdot e^{-8.9 \cdot \psi}$$

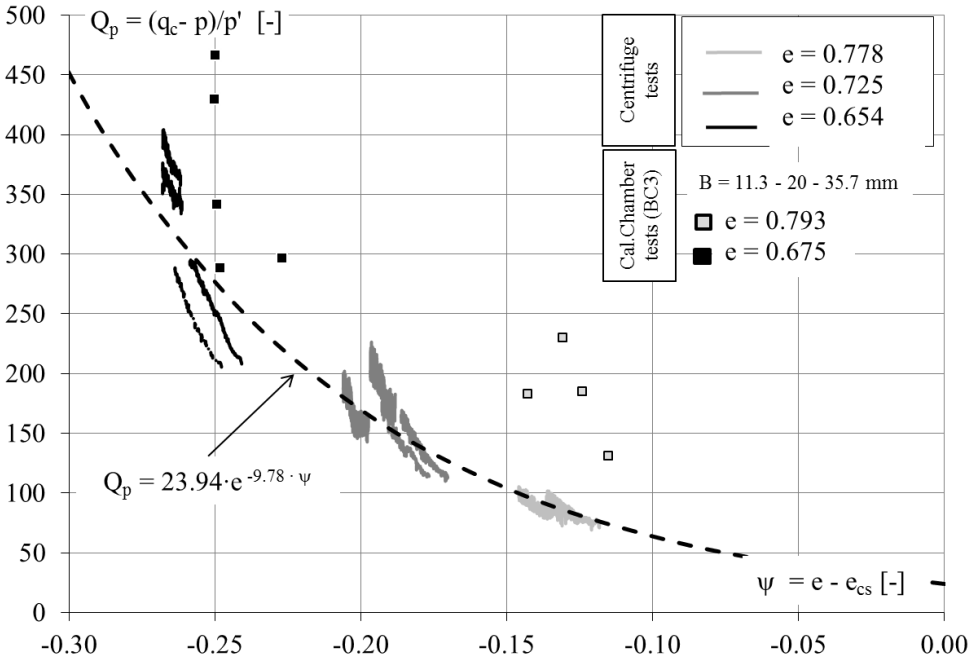

Figure 6.3- Centrifuge penetration test results and calibration chamber tests plot in Q_p - ψ plane for Toyoura sand. In dot black line the mean exponential curve with *m* = 9.78 and *k* = 23.94

As can be noted from the data plotted in Q_p - ψ plains, the more the sand is dense the more the experimental results diverge from the mean trend curves.

Sladen (1986) suggested that the mean exponential curve as deduced by Been et al. in the '80s for different sands would not be so representative for all states (e, p'). He determined that, for Ticino sand, the *m* parameter was reasonably constant for different mean effective stress (m ~ 7.2), but *k* parameter had a significant excursion with stress level variation [k from 63 (p' = 30 kPa) to 16 (p' = 450 kPa)].

In Figure 6.5 (a) and (b) are reported respectively the variation of the coefficients *k* and *m* with mean effective stress p' as deduced by CC tests from Sladen (1989) and for the centrifuge test results used in this research.

The values of the parameters *k* and *m* from this research are deduced by the interpolation of tests results considering the fitting exponential curves in Q_p - ψ plane using data with equal p': the more the mean effective stress is high the less the exponential curve is steep.

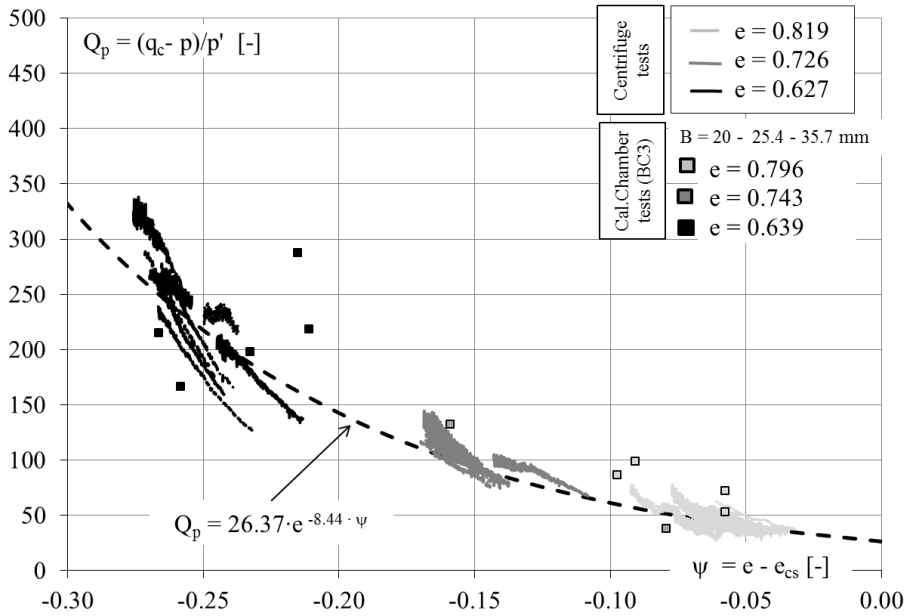

Figure 6.4- Centrifuge penetration test results and calibration chamber tests plot in Q_p - ψ plane for Ticino sand. In dot black line the mean exponential curve with *m* = 8.44 and *k* = 26.37

Analysis conducted on Ticino and Toyoura centrifuge tests evidence that *k* parameter slowly increases with stress: its variation is considerably small for both tested sands and a constant value with mean effective stress is considered a good approximation.

The mean trends are reported with black lines in k – p' plane in Figure 6.5 (a), where k = 26.37 for Ticino sand and k = 23.94 for Toyoura sand.

The variation of *m* parameter is more pronounced with the increasing of stress but it is easy to demonstrate that the difference in using constant or variable *m* parameter results in a small increase of more precise evaluation of state parameter. A mean value of *m* parameter for both Ticino and Toyoura sands is convenient, as the maximum error on state parameter evaluation results in $\Delta\psi_{max} < 0.03$ for only very dense physical states: m = 8.44 for Ticino sand and m = 9.78 for Toyoura sand are reported in black lines in m – p' plane (Figure 6.5 (b)).

It is notice that the trend of *k* and *m* with p' proposed by Sladen is difference if compared to centrifuge tests, especially for low p'.

Finally, the *k* value for zero state parameter represents an ideal separation in $Q_p - \psi$ plane between contractive and dilative soil behavior; they are evaluated as k = 26.37 and k = 23.94 respectively for Ticino and Toyoura sands.

In Figure 6.6 are compared the best-fit trend lines for Ticino and Toyoura sands with others curves deduced from calibration chamber tests results [Been et al. 1987, Baldi et al. 1987; Harman, 1987; Golder Ass., 1987]. The relationships are very different from sand to sand, even if they are derived from tests conducted on specimens reconstituted with air/dry depositional method.

The values of CRR^{ss}_{15} and the associated state parameter are reported in Figure 6.7. The cyclic resistance ratios are deduced from the CSR^{ss} – N curves described in Chapter 4; considering an equivalent number of cycles typical of earthquake with M_w = 7.5 it is possible to define a cyclic resistance for a constant state parameter.

The two curves that interpolate the experimental data are represented in the Figure 6.7; the equations are defined for Toyoura and Ticino sands respectively as:

[6.6] $$CRR^{ss}_{15} = 0.03 \cdot e^{-6.6 \cdot \psi}$$

[6.7] $$CRR^{ss}_{15} = 0.03 \cdot e^{-9.2 \cdot \psi}$$

In the equations above k* = 0.03 and m* = 6.6, for Toyoura sand, and k* = 0.03 and m* = 9.2, for Ticino sand.

When state parameter is zero the sand passes from a dilative to a contractive behavior and Toyoura and Ticino sands for $\psi = 0$ exhibit the same value of $CRR^{ss}_{15} = 0.03$.

It seems of interest to compare curves deduced from laboratories tests with the ones based on case histories and widely used in common practice.

The liquefaction chart proposed by Robertson (1998) linked the cyclic resistance ratio CRR_{15} to the normalized in-situ tip resistance q_{c1N}.

The curve was based on selected case histories based on liquefaction (or non-liquefaction) evidences on sandy soils with a limited range of properties and subjected to a restrict stress variation ($\sigma'_{v0} \sim 100$ kPa). It was assumed here reasonable that the normalized tip resistance q_{c1N} determined by Robertson was very similar to Q_p, inasmuch normalized stress coefficient $C_Q \sim 1$ and mean ratio $k_0 \sim 0.7$. This leaded to determine a Q_p value based on in-situ tip resistance evaluation and, using the inversion function in Equation 6.1, it was possible to define an ″in-situ″ state parameter.

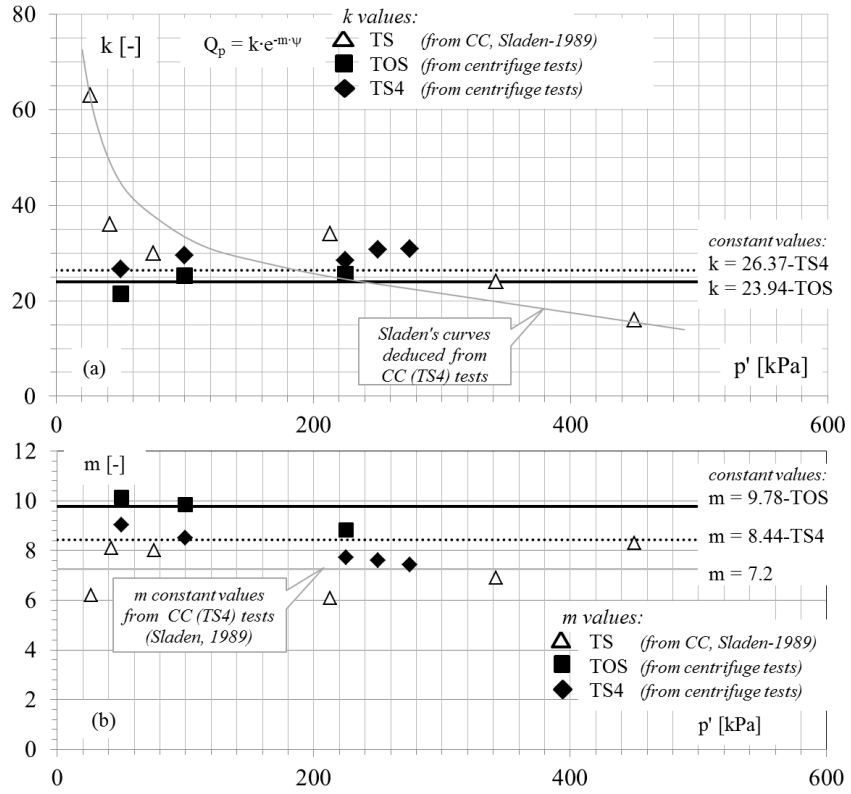

Figure 6.5- Determination of *k* and *m* values from centrifuge tests reported in k – p' and m – p' plane(black symbols and lines) compared with Sladen data determined from CC test (grey symbols and lines)

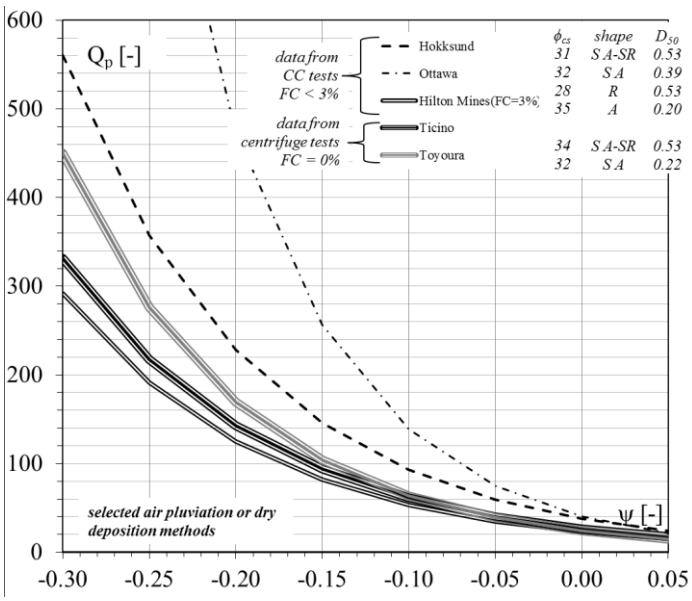

Figure 6.6- Comparison of Q_p - ψ curves derived from samples reconstituted by air/dry pluviated method

Furthermore, the cyclic resistance ratio associated to an equivalent earthquake of magnitude 7.5, was known for each case histories.

In Figure 6.8 data with calculated cyclic stress ratio [by Robertson, 1998] was related to a particular state of sand determined by the inversion of Equation 6.1: the empty symbols

are associated to non-liquefable sites, while the full ones are linked to liquefaction evidence.

The equation in black line in Figure 6.8 represents the demarcation between liquefaction and non-liquefaction occurring and was defined by Jefferies and Been (2006) as:

[6.8] $$CRR_{7.5} = 0.03 \cdot e^{-11 \cdot \psi}$$

Where $k^* = 0.03$ and $m^* = 11$.

The Equation 6.8, calibrated on in-situ tests, together with the Equation 6.2, adequately scaled in order to reproduce the simple shear conditions ($CRR^{ss}_{15} = 0.04 \cdot e^{-3.8 \cdot \psi}$ with mean ratio $k_0 = 0.5$) are superimposed in Figure 6.7.

The curves deduced by laboratory triaxial tests for Ticino and Toyoura sands are in good agreement with the assessed curve resulting by case histories analysis for slightly dilatant soils (i.e. $\psi = 0 \div -0.1$). On the contrary, for higher state parameter values, the curves are strongly divergent and the mean curve deduced from laboratory tests in dotted grey line represents the lowest cyclic resistance.

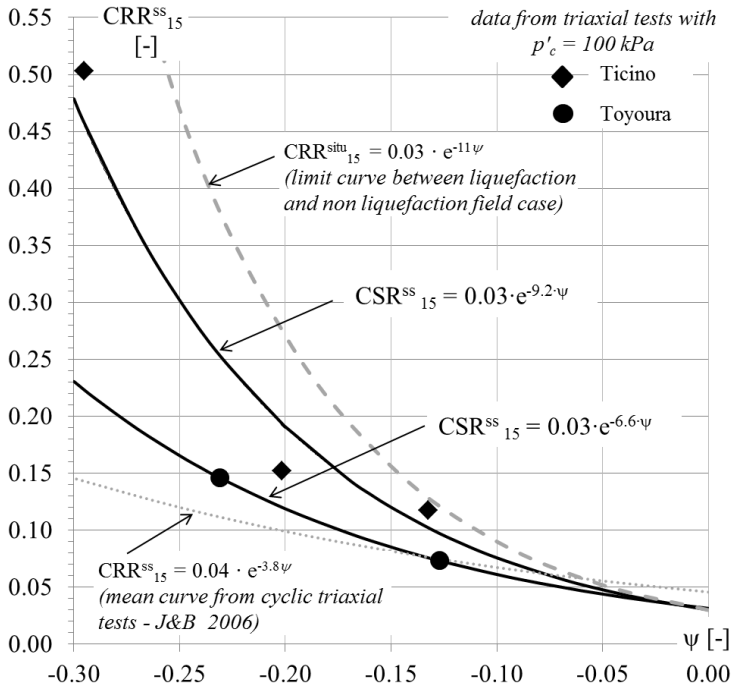

Figure 6.7- Results from cyclic triaxial tests for Ticino and Toyoura sands in CRR^{ss}_{15} - ψ plane; in black lines the mean exponential curve with $m^* = 6.6$ and $k^* = 0.03$, for Toyoura sand, and $m^* = -9.2$ and $k^* = 0.03$ for Ticino sand. In traced and dotted grey lines are represented the curves proposed by Been and Jefferies (2006) deduce from triaxial tests and in-situ case histories

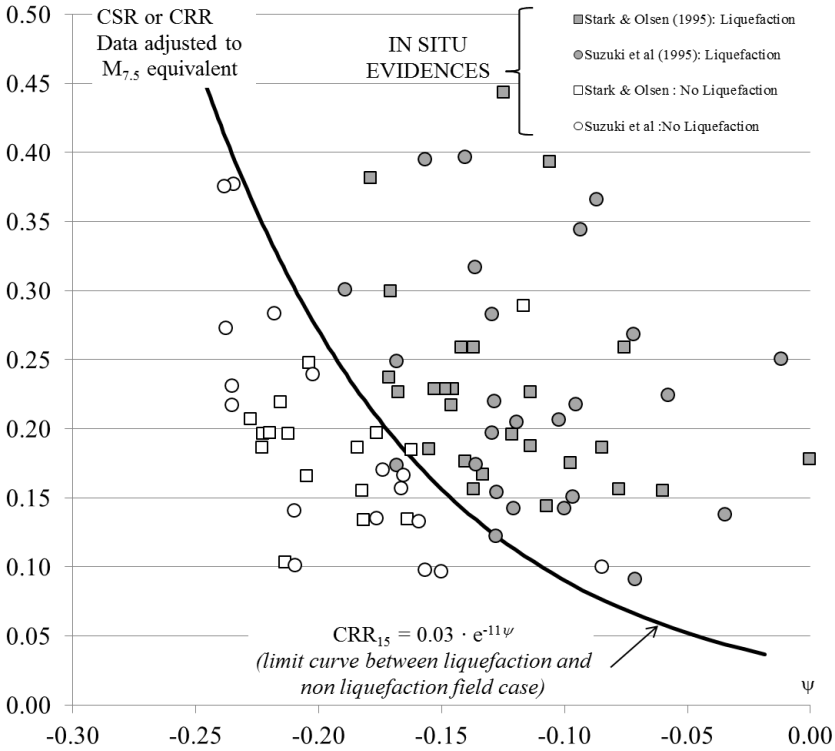

Figure 6.8- Field liquefaction or non-liquefaction case histories from Robertson's database (1998) re-evaluated in terms of state parameter ψ. Inversion procedure involves the approximation of $q_{c1N} \sim Q_p$ and $k_0 \sim 0.7$ [after Jefferies and Been, 2006]

6.3 Simplified CRR – Q_p correlation for liquefaction analysis

It has been demonstrated that the normalized tip resistance and the cyclic stress ratio are both state parameter dependent. The k-k* and m-m* parameters are also calibrated for the two investigated sands in order to determine a best-fit curve in Q_p - ψ and in CRR - ψ planes.

In Figure 6.9 are reported the CRR^{ss}_{15} and Q_p values considering state parameters used in triaxial tests (i.e ψ = -0.132, -0.201, -0.295 for Ticino sand and ψ = -0.231, -0.127 for Toyoura sand).

The cyclic resistance ratio can be linked to normalized tip resistance using the Equations 6.5, 6.6 and 6.7. The resulting inversion curves are reported in Figure 6.9 in $CRR^{ss}_{15} - Q_p$ plane, for Ticino and Toyoura sands:

[6.9] $$CRR^{ss}_{15} = 0.03 \cdot e^{1.03 \cdot \ln\left(Q_p / 25.6\right)}$$

[6.10] $$CRR^{ss}_{15} = 0.03 \cdot e^{0.75 \cdot \ln\left(Q_p / 25.6\right)}$$

In the same graph is reported the CRR – Q_p curve obtained from the, re-analyzed case histories by Jefferies and Been (2006), using the Equations 6.1 and 6.8.

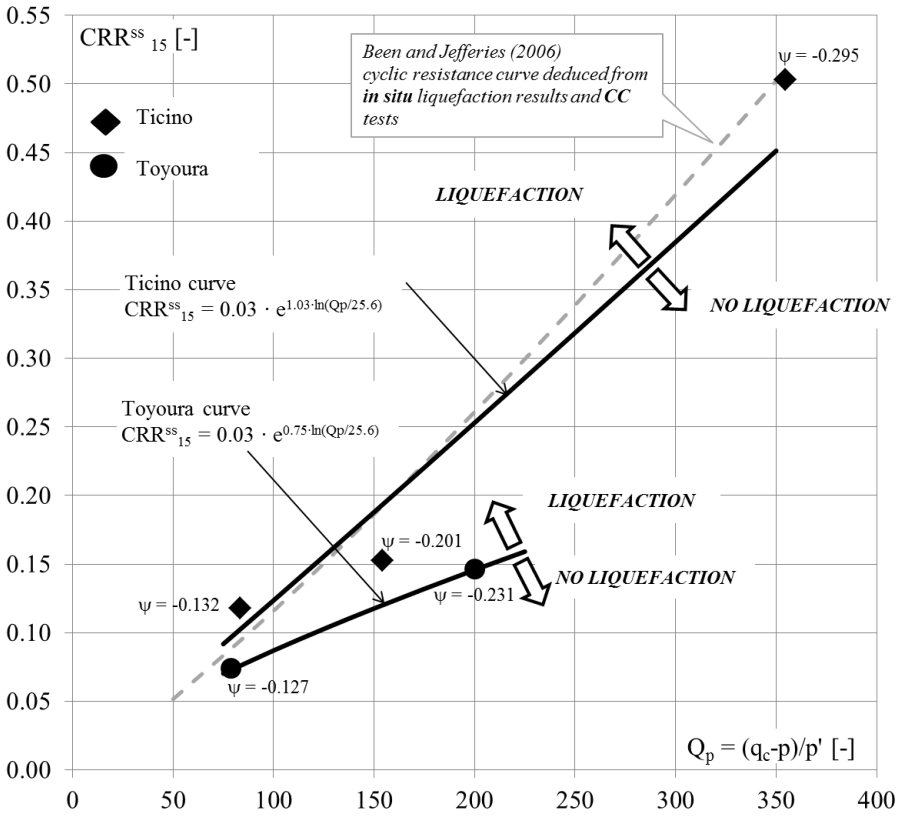

Figure 6.9- Cyclic resistance ratio and normalized tip resistance for Ticino and Toyoura sand

6.4 Conclusion and remarks

Simplified correlations between cyclic resistance ratio and normalized tip resistance for a uniform medium and for a uniform fine sands are proposed in this thesis.

Dense Ticino sand shows smaller values of normalized tip resistance respect to those ones of Toyoura sand; this might be due to the higher compressibility of Ticino sand, where mica minerals are present. Nevertheless, the Q_p – ψ curves for the two tested sands are very similar and it might be said that the curves in Figure 6.9 were not affected from Q_p values.

It is thought that the curves variance in CRR^{ss}_{15} – Q_p plane is mainly related to the cyclic behavior of the sands. In fact, at the same state parameter values, Toyoura sand manifests a lower value of cyclic resistance ratio respect to that of Ticino sand.

The results evidence how the cyclic resistance decreases with the decreasing of the mean diameter D_{50}, leading to a smaller CRR^{ss}_{15} curves for Toyoura sand. Actually,

the reduction of the mean grain size is usually accompanied by a minor drainage condition and the complete loss of strength is achieved for less number of cycles [Lee, 1969; Seed and Idriss, 1971; Dupla and Canou, 2003].

6.5 Recommendation for future research

The scope of this research program was limited to the determination of simplified correlations for liquefaction analysis for only clean and uniform sands.

The evaluation of these curves might be important for also well-graded sands or sands with fines, in order to establish a good affordability of the procedures proposed and to evaluate the variability of the curves with the grain-size distribution.

In the semi-empirical equations are usually considered only the fine content influences on the cyclic resistance ratio, while the gradation and the shape of the particles are neglected: this might lead to an underestimation or an overestimation of the liquefaction potential. Indeed, fine content could be included in the analysis using the state parameter approach, neglecting the corrections factors used for tip resistance in empirical formulations.

At least, some improvements might be useful also in CRR - ψ curves determination as well, in this thesis, they were determined for only a particular value of p'_c. It might be of interest to confirm that a unique cyclic resistance curve is definable varying the mean effective stress at which the sample is consolidated.

References

Ahmadi M.M., Byrne P.M., and Campanella R.G., [1999]. *Numerical simulation of CPT tip resistance in layered soil*. Asian Institute of Technology 40th Year Conference, New Frontiers & Challenges.

Ahmadi M.M., Byrne P.M., and Campanella R.G., [2005]. *Cone tip resistance in sand: modeling, verification, and applications.* Can. Geotech. J., 42, pp. 977 – 993.

Alarcon-Guzman A., Leonards G.A. and Chameau J.L., [1988]. *Undrained monotonic and cyclic strength of sands.* Journal of Geotech. Eng., 114, 11, pp. 1089 – 1109.

Arthur J.R.F., Chua K.S., Dunstan T. and Rodriguez del C. J.I., [1980]. *Principal stress rotation: a missing parameter.* Journal of the Geotech. Eng. Div., 106, 44, pp. 419 – 433.

Arthur J.R.F., Koenders M.A. and Wong R.K.S., [1985]. *Anisotropy in particle contacts associated with shearing in granular media.* Acta Mechanica, 64, pp. 19 – 29.

Bałachowski L. [2006]. *Penetration resistance of Lubiatowo sand in calibration chamber tests.* Archives of Hydro-Engineering and Environmental Mechanics 53, 4, pp. 311–329.

Bałachowski L. [2007]. *Size Effect in Centrifuge Cone Penetration Tests.* Archives of Hydro-Engineering and Environmental Mechanics 54, 3, pp. 161–181.

Bandini V. and Coop M.R. [2011]. *The influence of particle breakage on the location of the critical state line of sands.* Soils and Foundations, 51, 4, pp. 591 – 600.

Battaglio M, Bellotti R. and Pasqualini E. [1979]. *La deposizione pluviale come mezzo per la preparazione dei provini in sabbia*. Rivista Italiana di Geotecnica, 2, pp. 106 – 121.

Been K. and Jefferies M.G. [1985]. *A state parameter for sands*. Géotecnicque, 35, 2, pp. 99 – 112.

Bobei, D. [2004]. *Static Liquefaction of Sand with a Small Amount of Fines.* PhD thesis. The University of New South Wales.

Bobei D.C., Lo S.R., Wanatowski D., Gnanendran C.T. and Rahman M.M. [2009]. *Modified state parameter for characterizing static liquefaction of sands with fines*. Can. Geotech. J., 46, pp. 281 – 295.

Bolton M.D. [1986]. *The strenght and dilatancy of sands*. Géotecnicque, 36, 1, pp. 65 – 78.

Bolton M.D. and Gui M.W. [1993]. *The study of relative density and boundary effects for cone penetration tests in centrifuge*. CUED/D-SOILS/TR256.

Bolton M.D., Gui M.W and Phillips R. [1993]. *Rewew of miniature soil probes for model tests*. Eleventh southeast asian geotechnical conference, Singapore.

Boulanger R.W. and Truman S.P. [1996]. *Void redistribution in sand under post-earthquake loading*. Can. Geotech. J., 33, pp. 829 – 834.

Bolton M.D., Gui M.W., Garnier J., Corte J.F., Bagge G., Laue J. and Renzi R. [1999]. *Centrifuge cone penetration tests in sand*. Géotecnicque, 49, 4, pp. 543 – 552.

Boulanger R.W. [2003]. *Relating K to relative state parameter index*. Journal of geotechnical and geoenvironmental engineering, 129/8, pp. 770 – 773.

Boulanger R.W. [2003]. *High overburden stress effects in liquefaction analyses*. Journal of geotechnical and geoenvironmental engineering, 129/12, pp. 1071 – 1082.

Boulanger R.W. and Idriss I.M. [2004]. *State normalization of penetration resistance and the effect of overburden stress on liquefaction resistance*. Proceedings of the 11th SDEE and of the 3rd ICEGE, Berkeley, CA.

Bucknam M.D. [1981]. *Densification and cyclic triaxial testing of Leighton-Buzzard 120/200 sand*. Master of Sience thesis. Massachusset institute of technoclogy.

Carraro J.A.H., Bandini P. and Salgado R. [2003]. *Liquefaction resistance of clean and nonplastic silty sands from cone penetration resistance*. Journal of geotechnical and geoenvironmental engineering, 129/11, pp. 965 – 976.

Carter J.P., Booker J.R. and Yeung S.K. [1986]. *Cavity expansion in cohesive frictional soils*. Geotechnique 36/3, pp. 349 – 358.

Casagrande A. [1975]. *Liquefaction and cyclic deformation of sands, a critical review*. Harvard soil mechanics series no. 88.

Castro G. [1975]. *Liquefaction and cyclic mobility of saturated sands*. Journal of the geotechnical engineering division 101/6, pp. 551 – 569.

Castro G. and Poulos S.J. [1977]. *Factors affecting liquefaction and cyclic mobility*. Journal of the geotechnical engineering division, pp. 501 – 516.

Cetin K.O., Seed R.B., Der Kiureghian A., Tokimatsu K., Harder Jr. L.F., Kayen R.E. and Moss R.E.S. [2004]. *Standard penetration test-based probabilistic and deterministic assessment of seismic soil liquefaction potential*.

Chang N.Y., Yeh S.T. and Kaufman L.P. [1982]. *Liquefaction potential of clean and silty sands*. International earthquake microzonation conference proceedings 28/06-01/07 Seattle (Usa), 2, pp. 1018 – 1032.

Chen Y. [1995]. *Behavior of a fine sand in triaxial, torsional and rotational shear tests*. PhD thesis. University of California, Davis.

Chen Y.C. and Liao T.S. [1999]. *Studies of the state parameter and liquefaction resistance of sands*. Earthquake geotechincal engineering, pp. 513 – 518.

Chern J. [1968]. *Undrained response of saturated sands with emphasis on liquefaction and cyclic mobility*. PhD thesis. National Taiwan University.

Cheng Y.P., Bolton M.D. and Nakata Y. [2005]. *Grain crushing and critical states observed in DEM simulations*. Powder and grains, pp. 1393 – 1397.

Chiaro G., Kosekic J. and Sato T. [2012]. *Effects of initial static shear on liquefaction and large deformation properties of loose saturated Toyoura sand in undrained cyclic torsional shear tests*. Soils and foundations, 52/3, pp. 498 – 510.

Chiaro G., Kiyota T. and Kosekic J. [2013]. *Strain localization characteristics of loose saturated Toyoura sand in undrained cyclic torsional shear tests with initial static shear*. Soils and foundations, 53/1, pp. 23 – 34.

Cho G.C., Dodds J and Santamarina C. [2006]. *Particle shape effects on packing density, stiffness and strength – natural and crushed sands*. J. Geotech. Environ. Engin., 132/5, pp. 591 – 602.

Collins I.F. Pender M.J. and Yan W. [1992]. *Cavity expansion in sand under drained loading conditions*. International journal for numerical and analitical methods in geomechanics, 16, pp. 3 – 23.

Collins I.F. and Yu Y.S. [1996]. *Undrained cavity expansions in critical state soils*. International journal for numerical and analitical methods in geomechanics, 20, pp. 489 – 516.

Colombi A. [2005]. *Physical modeling of an isolated pile in coarse grained soils.* PhD thesis. University of Ferrara, University of Parma, University of Bologna, University of Brescia.

Crova R., Jamiolkowski M., Lancellotta R. and Lo Presti D.C.F. [1993]. *Geotechnical characterization of gravelly soils at Messina site: selected topics*. Predictive soil mechanics, 16, pp. 199 – 218.

Cubrinowski M. and Ishihara K. [1998]. *State concept and modified elastoplasticity for sand modelling*. Soils and foundations, 38/4, pp. 213 – 225.

Cubrinowski M. and Ishihara K. [2000]. *Flow potential of sandy soils with different grain compositions*. Soils and foundations, 40/4, pp. 103 – 119.

Cubrinowski M. and Ishihara K. [2001]. *Correlation between penetration resistance and relative density of sandy soils*. 15th ISSMGE Istanbul, Turkey, pp. 393 – 396.

Cubrinowski M. and Ishihara K. [2002]. *Maximum and minimum void ratio characteristics of sands*. Soils and foundations, 42/6, pp. 65 – 78.

De Alba P., Bolton Seed H. and Chan C.K. [1976]. *Sand liquefaction in large-scale simple shear tests*. Journal of the geotechnical engineering division, 102/9, pp. 909 – 927.

De Gennaro V., Canou J., Dupla J.C. and Benahmed N. [2004]. *Influence of loading path on the undrained behavior of medium loose sand*. Can. Geotech. J., 41, pp. 166 – 180.

Di Prisco C., Wood D. M., [2012]. *Mechanical behavior of soils under environmentally induced cyclic loads.* International center for mechanical sciences – Course and lecturer - -No 534, ISBN 978 – 3 – 7091 – 1067 – 6, pp. 1 – 137.

Dupla J.C and Canou J. [2004]. *Cyclic pressumeter loading and liquefaction properties of sands*. Soils and foundations 43/2, pp. 17 – 31.

Colliat-Dangus J.L., Desrues J. and Foray P. [1988]. *Triaxial testing of granular soil under elevated cell pressure*. Special technical publication 977, pp. 290 – 310.

Dobry R. and Abdoun T. [2011]. *An investigation into why liquefaction charts work: a necessary step toward integrating the states of art and practice*. Proceedings of the 5th int. conf. on Earthquake Geot. Eng., pp. 13 – 45.

Erickson R.P.C. [2012]. *State normalization of cone penetration resistance*. ECI 284: theoretical geomechanics professor Boris Jeremić.

Frost J.D. and Jang D.J., [2000]. *Evolution of sand microstructure during shear*. Journal of geotechnical and geoenvironmental engineering, pp. 116 – 130.

Garga V.K. and McKay L.D., [1984]. *Cyclic triaxial strength of mine tailings*. Journal of geotechnical engineering, 110/8 pp. 1091 – 1105.

Garnier J., Gaudin C., Springman S.M., Culligan P.J., Goodings D., Konigv D., Kutterv B., Phillipsv R., Randolph M.F., and Thorel L., [2007]. *Catalogue of scaling laws and similitude questions in geotechnical centrifuge modeling*. International Journal of Physical Modeling in Geotechnics, 3, pp. 01 – 23.

Georgiannou V.N. and Tsomokos A. [2008]. *Comparison of two fine sands under torsional loading*. Can. Geotech. J., 45, pp. 1659 – 1672.

Ghafghazi M. [2011]. *Towards comprehensive interpretation of the state parameter from cone penetration testing in cohesionless soils*. PhD thesis. University of British Columbia.

Ghafghazi M., Shuttleb D.A., DeJong J.T. [2014]. *Particle breakage and the critical state of sand.* Soils and foundations, 54/3, pp. 451 – 461.

Ghionna N. and Porcino D., [2006]. *Evolution of sand microstructure during shear*. Journal of geotechnical and geoenvironmental engineering, 132/2, pp. 194 – 202.

Giretti D. [2009]. *Modeling of piled raft foundations in sand*. PhD thesis. University of Ferrara.

Gui M.W. and Bolton M.D., [1998]. *Geometry and scale effects in CPT and pile design*. Geotechincal site characterization, pp. 1063 – 1068.

Gui M.W., Bolton M.D., Garnier J., Corte J.F., Bagge G., Laue J. and Renzi R. [1998]. *Gudelines for cone penetration tests in sand*. Centrifuge 98, pp. 155 – 160.

Gui M.W. and Jeng D.S.. [2009]. *Application of cavity expansion theory in predicting centrifuge cone penetration resistance*. The Open Civil Engineering Journal 3, pp. 1 – 6.

Hanzawa H., Nutt N., Lunne T, Tang Y.X. and Long M. [2007]. A comparative study between the NGI direct simple shear apparatus and the Mikasa direct shear apparatus. Soils and foundations, 47/1, pp. 47 – 58.

Hatanaka M. and Geng L. [2006]. *Estimating relative density of sandy soils.* Soils and foundations, 46/3, pp. 299 – 313.

Hosono Y. and Yoshimine M. [2004]. *Liquefaction of sand in simple shear condition*. Cyclic behavior of soils and liquefaction phenomena: proceedings of the international conference, Bochum, Germany, pp. 129-136.

Houlsby G.T. and Hitchman R. [1988]. *Calibration chamber tests of a cone penetrometer in sand*. Geotecnique, 38/1, pp. 39 – 44.

Huang A.B. [1992]. *Calibration chamber testing*. Proceedings of the first international symposium on calibration chamber testing.

Hyodo M., Tanimizu H., Yasufuku N. and Fujii T. [1991]. *Undrained cyclic shear strength and residual shear strain of saturated sand by cyclic triaxial tests*. Soils and foundations 31/3, pp. 60 – 76.

Hyodo M., Tanimizu H., Yasufuku N. and Murata H. [1994]. *Undrained cyclic and monotonic triaxial behavior of saturated loose sand*. Soils and foundations 34/1, pp. 19 – 32.

Hyodo M., Hyde A.F.L., Aramaki N. and Nakata Y. [2002]. *Undrained monotonic and cyclic shear behavior of sands under low and high confining stress*. Soils and foundations 42/3, pp. 63 – 76.

Idriss I.M. and Boulanger R.W. [2004]. *Semi-empirical procedures for evaluating liquefaction potential during earthquakes*. Proceedings of the 11th SDEE and of the 3rd ICEGE, Berkeley, CA.

Idriss I.M. and Boulanger R.W. [2008]. *Soil liquefaction during earthquakes*. Monograph by EERI, Oakland, California.

International symposium on cone penetration testing [1995]. Linkoping, Sweden, Vol. 1, 2, 3, 4.

Ishiara K., [1985]. *Stability of natural deposits during earthquakes*. Proceedings of the 11th international conference on soil mechanics and foundation engineering, San Francisco, pp. 321 – 376.

Ishiara K. [1993]. *Liquefaction and flow failure during earthquakes*. Geotecnique 43/3, pp. 351 – 415.

Ishiara K. [1996]. *Soil behavior in earthquake geotechnics.* Clarendon Press, Oxford.

Ishiara K. and Li S.I. [1972]. *Liquefaction of saturated sand in triaxial torsion shear test*. Soils and foundations 12/2, pp. 19 – 39.

Ishiara K., Tatsuoka F. and Yasuda S. [1975]. *Undrained deformation and liquefaction of sand under cyclic stresses*. Soils and foundations 15/1, pp. 29 – 44.

Ishiara K. and Takatsu H. [1979]. *Effects of overconsolidation and K_0 conditions in the liquefaction carachteristics of sands*. Soils and foundations 19/4, pp. 59 – 68.

Ishiara K., Shimizu K. and Yamada Y. [1981]. *Pore water pressures measured in sand deposit during an earthqake*. Soils and foundations 21/4, pp. 85 – 100.

Ishiara K., Towhata I. [1983]. *Stress response to cyclic rotation of principal stress directions as induced by wave loads*. Soils and foundations 23/4, pp. 11 – 26.

Ishiara K. and Perlea V. [1984]. *Liquefaction-associated ground damage during the Vrancea earthquake of march 4, 1977*. Soils and foundations 24/1, pp. 90 – 112.

Ishiara K., Yamazaki A. and Haga K. [1985]. *Liquefaction of K_0-consolidated sand under cyclic rotation of principal stress direction with lateral constraint*. Soils and foundations 25/4, pp. 63 – 74.

Ishibashi I. and Sherif M.A. [1974]. *Soil liquefaction by torsional simple shear device*. Journal of the geotechnical engineering division, August 1974 pp. 871 – 888.

Jamiolkowski M, Lo Presti D.C.F and Manassero M. [2001]. *Evalutation of relative density and shear strength of sands from CPT and DMT*. Soil behaviour and soft ground construction, pp. 201 – 238.

Jefferies M. [1999]. *A critical state view of liquefaction*. Physics and mechanics of soil liquefaction, pp. 221 – 235.

Jefferies M. and Been K. [2006]. *Soil liquefaction – a critical state approach*. Taylor & Francis e-Library.

Jefferies M. and Shuttle D. [2011]. *Understanding liquefaction through applied mechanics*. Proceedings of the 5th int. conf. on Earthquake Geot. Eng..

Joseph P.J., Einstein H.H. and Whitman R.V. [1988]. *A literature review of geotechnical centrifuge modeling with particular emphasis on rock mechanics*. M.I.T. Dept. of Civil Eng., Final report.

Juang C.H., Ku C.S. and Chen C.C. [2010]. *Simplified model for evaluating soil liquefaction potential using CPTU*. CPTU-2010.

Konrad J.M. [1997]. *In situ sand state from CPT: evaluation of a unified approach at two CANLEX sites*. Canadian geotechnical journal 34/1, pp 120 – 130.

Kokusho T. [2007]. *Liquefaction strengths of poorly-graded and well-graded granular soils investigated by lab tests*. Earthquake geotechnical engineering, pp. 159 – 184.

Kwong J.S.M. [1995]. *A review of some drained reclamation works in Hong Kong*. Geo Report 63.

Lee K.L. and Bolton Seed H. [1967]. *Dynamic strength of anisotropically consolidated sand*. Journal of the soil mechanics and foundations division 93/SM5, pp. 169 – 190.

Lehane B.M., Schneider J.A. and Xu X. [1967]. *CPT-based design of displacement piles in siliceous sands*., Advances in deep foundations pp 69 – 86.

Ladd R.S. [1978]. *Preparing test specimens using undercompaction*. Geotechnical testing journal 1/1, pp. 16 – 23.

Lagioia R., Sanzeni A. and Coleselli F. [2006]. *Air, water and vacuum pluviation of sand specimens for the triaxial apparatus*. Soils and foundations 46/1, pp. 61 – 67.

Leung C.F., Lee F.H. and Tan T.S. [1994]. Centrifuge 94.

Li X.S. and Wang Y. [1998]. *Linear representation of steady-state line for sand*. Journal of geotechnical and geoenvironmental engineering 124/12, pp. 1215 – 1217.

Li X.S. and Dafalias Y.F. [2000]. *Dilatancy for cohesionless soils*. Geotecnique 50/4, pp. 449 – 460.

Liu Q.B. and Lehane B.M. [2012]. *The influence of particle shape on the (centrifuge) cone penetration test (CPT) end resistance in uniformly graded granular soils*. Geotechnique 62/11, pp. 973 – 984.

Liu J. [2012]. *Liquefaction resistant on Monterey no.0/30 sand*. Master of Sience Thesis, University of Colorado Denver.

Lo Presti D.C.F., Berardi R., Pedroni S. and Crippa V. [1993]. *A new traveling sand pluviator to reconstitute specimens of well-graded silty sands*. Geotechnical testing journal 16/1, pp. 18 – 26.

Lo Presti D.C.F., Puci I., Pallara O., Maniscalco R. and Pedroni S. [2006]. *Experimental laboratory determination of the steady state of sands*. Soils and foundations 40/1, pp. 113 – 122.

Maki I.P., Boulanger R.W., DeJong J.T. and Jaeger R.A. [2013]. *State-based overbunden normalization of cone penetration resistance in clean sand*. Journal of geotechnical and geoenvironmental enigineering.

Miura S. and Toki S. [1982]. *A sample preparation method and its effect on static and cyclic deformation-strength properties of sand*. Soils and foundations 22/1, pp. 61 – 77.

Miura S., and Toki S. [1984]. *Anisotropy in mechanical properties and its simulation of sands sampled from natural deposit*. Soils and foundations 24/3, pp. 69 – 84.

Miura S., Toki S., and Tanizawa F. [1984]. *Cone penetration characteristics and its correlation to static and cyclic deformation-strength behaviors of anisotropic sand*. Soils and foundations 24/1, pp. 58 – 74.

Mohamad R. and Dobry R. [1986]. *Undrained monotonic and cyclic triaxial strength of sand*. Journal of geotechnical engineering 112/10, pp. 941 – 958.

Mooney M.A., Finno R.J. and Viggiani M.G. [1998]. *A unique critical state for sands?*. Journal of geotechnical and geoenvironmental engineering 124/11, pp. 1100 – 1108.

Mortezaie A.R. and Vucetic M. [2012]. *Small-strain cyclic testing with standard NGI simple shear device.* Geotechnical testing journal 35/6, pp. 935 – 948.

Moss. R.E.S. [2003]. *CPT-based probabilistic assessment of seismic soil liquefaction initiation*. PhD thesis. University of California, Berkeley.

Moss. R.E.S., Seed R.B., Kaven R.E., Stewart J.P., Der Kiureghian A. [2006]. *CPT-based probabilistic assessment of seismic soil liquefaction initiation*. PEER Report.

Mulilis J.P. [1977]. *Effects of sample preparation on sand liquefaction*. Journal of the geotechnical engineering division 103/2, pp. 91 – 108.

Murthy T.G., Loukidis D., Carraro J.A.H., Prezzi M. and Salgado R. [2007]. *Undrained monotonic response of clean and silty sands*. Geotecnique 57/3, pp. 273 – 288.

Oda M. [1972]. *Deformation mechanism of sands in triaxial compression tests*. Soils and foundations 12/4, pp. 45 – 63.

Oda M., Koishikawa I. and Higuchi T. [1978]. *Experimental study of anisotropic shear strength of sand by plane strain test*. Soils and foundations 18/1, pp. 25 – 38.

Omarov M. [2010]. *Liquefaction potential and post-liquefaction settlement of saturated clean sands; and effect of geofiber reinforcement*. Master of Sience thesis. University of Alaska Fairbanks.

Onder Cetin K. and Tolga Blige H. [2012]. *Cyclic large strain and induced pore pressure models for saturated clean sands*. Journal of geotechnical and geoenvironmental engineering 138/3, pp. 309 – 323.

Pallara O., Lo Presti D.C.F., Jamiolkowski M. and Pedroni S. [1998]. *Caratteristiche di deformabilità di due sabbie da prove monotoniche e cichliche*. Rivista italiana di geotecnica 1/98, pp. 63 – 83.

Passalacqua R. [1991]. *A sand-spreader used for the reconstitution of granular soil models*. Soils and foundations 31/2, pp. 175 – 180.

Phillips R. and Valsangkar A.J. [1987]. *An experimental investigation of factors affecting penetration resistance in granular soils in centrifuge modeling*. Soils TR 210, pp. 1 – 54.

Pillai V.S. [1991]. *Liquefaction analysis of sands: some interpretation of Seed's Kα (sloping gound) and Kσ (depth) correction factors using steady state concept*. Second Int. Conf. on Recent Adv. in Geotech. Earthquake Engin. and S. Dynam, St. Louis, Missouri, paper n.3.62, pp. 579 – 587.

Pillai V.S. and Byrne P.M. [1994]. *Effect of overburden pressure on liquefaction resistance of sand.* Canadian geotechnical journal 31/1, pp. 53 – 60.

Porcino D. and Caridi G. [2007]. *Pre and post liquefaction response of sand in cyclic simple shear*. Geotechnical Denver Proceeding, pp. 31 – 40.

Porcino D. and Marcianò V. [2009]. *Correlating qc and cyclic liquefaction resistance of sands through calibration chamber tests and simple shear tests*. Performance-based design in earthquake geotechnical engineering, pp. 1307 – 1314.

Porcino D., Marcianò V. and Granata R. [2012]. *Liquefaction and re-liquefaction of a silicate grouted sand due to repeated earthquakes*. Incontro annuale dei ricercatori di geotecnica.

Poulos S.J. [1971]. *The stress-strain curves of soils*. Geotechnical Engineers, Inc.

Poulos S.J. [1981]. *The steady state of deformation*. Journal of the Geotechnical Engineering Division 107/5, pp. 553 – 562.

Pournaghiazar M., Russell A.R. and Khalili N. [2012]. *The cone penetration test in unsaturated sands*. Géotechnique, November 2012.

Puppala A.J., Acar Y.B. and Tumay M.T. [1995]. *Cone penetration in very weakly cemented sand*. Journal of geotechnical engineering 121/8, pp. 589 – 600.

Rahman M. [2009]. *Modelling the influence of fines on liquefaction behaviour*. PhD thesis. University of New South Wales at Australian Defense Force Academy.

Rascol E. [2009]. *Cyclic properties of sand: dynamic behaviour for seismic applications*. PhD thesis. École Polytechnique Fédérale de Lausanne.

Renzi R., Cortè J.F., Rault G., Gui M. and Laue J. [1999]. *Cone penetration tests in the centrifuge: experience of five laboratories*. Centrifuge 94, pp. 77 – 82.

Riemer M.F. and Seed B. [1997]. *Factors affecting apparent position of steady-state line.* Journal of geotechnical and geoenvironmental engineering 123/3, pp. 281 – 288.

Rowe P.W. [1962]. *The stress-dilatancy relation for static equilibrium of an assembly of particles in contact.* Proceedings of the Royal Society of London 269/1339, pp. 500 – 527.

Robertson P.K. [1990]. *Soil classification using the cone penetration test.* Can. Geotech. J. 27, pp. 151 – 158.

Robertson P.K. [1994]. *Suggested terminology for liquefaction – CANLEX (Canadian liquefaction Experiment).*

Robertson P.K. [2004]. *Evaluating soil liquefaction and post-earthquake deformations using the cpt.*

Robertson P.K. [2009]. *Interpretation of cone penetration tests – a unified approach.* Submitted to the Canadian Geotechnical Journal.

Robertson P.K. [2010]. *Evaluation of flow liquefaction and liquefied strength using the cone penetration test.* Journal of geotechnical and geoenvironmental engineering 136/6, pp. 842 – 853.

Robertson P.K. [2010]. *Soil behaviour type from the CPT: an update.* CPT '10 - 2nd International Symposium on Cone Penetration Testing

Robertson P.K., Campanella R.G., Gillespie D. and Greig J. [1986]. *Use of piezometer cone data.* Use of in situ tests in geotechnical engineering.

Robertson P.K., List B.R. and Hofmann B.A. [1994]. *CANLEX (Canadian liquefaction Experiment) – a one year update.*

Robertson P.K. and Wride C.E. [1998]. *Evaluating cyclic liquefaction potential using the cone penetration test.* Can. Geotech. J. 35, pp. 442 – 459.

Robertson P.K. and Cabal K.L. [2010]. *Guide to cone penetration testing for geotechnical engineering.* Gregg Drilling & Testing, Inc.

Russell A.R. and Khalili N. [2002]. *Drained cavity expansion in sands exhibiting particle crushing.* International journal for numerical and analytical methods in geomechanics 26, pp. 323 – 340.

Sadrekarimi A. [2013]. *Influence of state and compressibility on liquefied strength of sands.* Canadian geotechnical journal 50/10, pp. 1067 – 1076.

Salgado R., Boulanger R.W. and Mitchell J.K. [1997]. *Lateral stress effects on cpt liquefaction resistance correlations.* Journal of geotechnical and geoenvironmental engineering 123/8, pp. 726 – 735.

Salgado R., Jamiolkowski M. and Mitchell J.K. [1998]. *Penetration resistance in sands: analysis and applications to liquefaction potential assestment and estimation of pile base resistance.* Rivista italiana di geotecnica 98/4, pp. 5 – 17.

Salgado R., and Randolph M.F. [2001]. *Analysis of cavity expansion in sand.* The international journal of geomechanics 1/2, pp. 175 – 192.

Salgado R., and Prezzi M. [2007]. *Computation of cavity expansion pressure and penetration resistance in sands.* The international journal of geomechanics 7/4, pp. 251 – 265.

Sasitharan S., Robertson P.K., Sego D.C. and Morgenstern N.R. [1993]. *Collapse behaviour of sand.* Canadian geotechnical journal 30/4, pp. 569 – 577.

Schneider J.A. [2007]. *Analysis of piezocone data for displacement pile design*. PhD thesis. University of Western Australia.

Schofield A.N., and Wroth C.P. [1968]. *Critical State Soil Mechanics*. McGraw-Hill, London. Download: http://www.geotechnique.info/.

Seed H.B. and Lee K.L. [1966]. *Liquefaction of saturated sans during cyclic loading.* Journal of the soil mechanics and foundations division 92/6, pp. 105 – 134.

Shen C.K. and Lee K.M. [1994]. *Hydraulic fill performance in Hong Kong.* Geo Report 40.

Shen C.K., Lee K.M. and Li X.S. [1996]. *A study of hydraulic fill performance in Hong Kong – phase 2.* Geo Report 64.

Shibata T. and Teparaksa W. [1988]. *Evaluation of liquefaction potentials of soils using cone penetration tests.* Soils and foundations 28/2, pp. 49 – 60.

Shuttle D. and Jefferies M. [1998]. *Dimensionless and unbiased cpt interpretation in sand.* International journal for numerical and analytical methods in geomechanics 22, pp. 351 – 391.

Silver M.L., Tatsuoka F., Phunkunhaphan A., Avramidis A.S. [1980]. *Cyclic undrained strength of sand by triaxial tests and simple shear test.* Soils and Foundations 32/1, pp. 35 – 38.

Sladen J.A., D'Hollander R.D. and Krahn J. [1985]. *The liquefaction of sands, a collapse surface approach.* Canadian geotechnical journal 22, pp. 564 – 578.

Sladen J.A. [1989]. *Problems with interpretation of sand state from cone penetration test.* Geotecnique 39/2, pp. 323 – 332.

Swidzinski W. and Mierczynski J. [2005]. *Instability line as a basic characteristic of non-cohesive soils.* Archives of Hydro-Engineering and Environmental Mechanics 52/1, pp. 59 – 85.

Stedman J.D. [1994]. *Effects of confining pressure and static shear on liquefaction resistance of frasier river sand*. Master of Sience thesis. University of British Columbia.

Tadesse S. [2000]. *Behaviour of saturated sand under different triaxial loading and liquefaction*. PhD thesis. Norwegian University of Science and Technology.

Tavenas F.A., Ladd R.S. and La Rochelle P. [1973]. *Accuracy of relative density measurements: results of a comparative test program.* Evaluation of relative density and its role in geotechnical projects involving cohesionless soils, pp. 18 – 60.

Tatsukoa F., Iwasaki T., Tokida K., Yasuda S., Hirose M., Imai T. and Kon-no M. [1978]. *A method for estimating undrained cyclic strength of sandy soils using standard penetration resistances.* Soils and foundations 18/3, pp. 43 – 58.

Tatsukoa F., Silver M.L., Phukunhaphan A. and Anestis A. [1980]. *Cyclic undrained strength of sand by simple shear test and triaxial test I (test procedures).* Soils and foundations 26/3, pp. 35 – 38.

Tatsukoa F., Silver M.L., Phukunhaphan A. and Anestis A. [1982]. *Cyclic undrained strength of sand by simple shear test and triaxial test III (test results and discussions).* Soils and foundations 26/3, pp. 209 – 212.

Tatsukoa F., Ochi K., Fujii S. and Okamoto M. [1986]. *Cyclic undrained triaxial and torsional shear strength of sands for different sample preparation methods.* Soils and foundations 26/3, pp. 23 – 41.

Tatsukoa F., Toki S., Miura S., Kato H., Okamoto M., Yamada S., Yasuda S. and Tanizawa F. [1986]. *Some factors affecting cyclic undrained triaxial strength of sand.* Soils and foundations 26/3, pp. 99 – 116.

Toki S., Tatsukoa F., Miura S., Yoshimi Y., Yasuda S. and Makihara Y. [1986]. *Cyclic undrained triaxial strength of sand by a cooperative test program.* Soils and foundations 26/3, pp. 117 – 128.

Uchida K. and Stedman J.D. [2001]. *Liquefaction behaviour of Toyura sand under cyclic strain controlled triaxial testing.* 11Th Int. Offshore and Polar Eng. Conf.

Uthayakumar M. [1992]. *Dynamic properties of sands under cyclic torsional shear*. Master of Sience thesis. University of British Columbia.

U.S.A. Army Corps of Engineers [2000]. Thechnical bases for regulatory guide for soil liquefaction

Vaid Y.P. and Negussey D. [1984]. *Relative density of pluviated sand samples.* Soils and foundations 24/2, pp. 101 – 105.

Vaid Y.P., Chern J. and Tumi H. [1985]. *Confining pressure, grain angularity and liquefaction.* Journal of geotechnical engineering 111/10, pp. 1229 – 1235.

Vaid Y.P., Chung E.K.F. and Kuerbis R.H. [1989]. *Preshearing and undrained response of sand.* Soils and foundations 29/4, pp. 49 – 61.

Vaid Y.P., Fisher J.M., Kuerbis R.H. and Negussey D. [1990]. *Particle gradiation and liquefaction.* Journal of geotechnical engineering 106/4, pp. 689 – 703.

Vaid Y.P. and Sivathayalan S. [1996]. *Static and cyclic liquefaction potential of Fraser Delta sand in simple shear and triaxial tests.* Canadian geotechnical journal 33/2, pp. 281 – 289.

Vaid Y.P. and Sivathayalan S. [2000]. *Fundamental factors affecting liquefaction susceptibility of sands.* Canadian geotechnical journal 37/3, pp. 592 – 606.

Verdugo R. and Ishihara K. [1996]. *The steady state of sandy soils.* Soils and foundations 36/2, pp. 81 – 91.

Wang J. [2005]. *The stress-strain and strength characteristics of Portaway sand*. PhD thesis. University of Nottingham.

Wang Z., Dafalias Y.F., Li X. and Makdisi F.I. [2002]. *State pressure index for modelling sand behaviour.* Journal of geotechnical and geoenvironmental engineering 128/6, pp. 551 – 519.

Wichtmann T. and Triantafyllidis T. [2009]. *On the influence of the grain size distribution curve of quartz sand on the small strain shear modulus Gmax.* Journal of geotechnical and geoenvironmental engineering 135/10, pp. 1404 – 1418.

Wood D.M. and Budhu M. [1980]. *The behaviour of Leighton Buzzard sand in cyclic simple shear test.* Int. symposium on soil under cyclic and transient loading, Swansea, pp. 9 – 21.

Yamashita S. and Toki S. [1993]. *Effects of fabric anisotropy of sand on cyclic undrained triaxial and torsional strengths.* Soils and foundations 33/3, pp. 92 – 104.

Yoshimi Y. and Tokimatsu K. [1977]. *Settlement of building on saturated sand during earthquakes.* Soils and foundations 17/1, pp. 23 – 38.

Yoshimi Y., Tokimatsu K., Kaneko O. and Makihara Y. [1984]. *Undrained cyclic shear strength of dense nigata sand.* Soils and foundations 24/4, pp. 131 – 145.

Yoshimi Y., Tokimatsu K. and Hosaka Y. [1989]. *Evaluation of liquefaction resistance of clean sands based on high-quality undisturbed samples.* Soils and foundations 29/1, pp. 93 – 104.

Youd T.L. and Idriss I.M. [1997]. *Proceedings of the NCEER workshop on evaluation of liquefaction resistance of soils.* Inn at Temple Square, Salt Lake City, Utah.

Yu H.S. and Houlsby G.T. [1991]. *Finite cavity expansion in dilatant soils: loading analysis.* Geotechnique 41/2, pp. 173 – 183.

APPENDIX A

Undrained and Drained Triaxial tests
TICINO SAND

Symbols and abbreviations for triaxial condition:

$q = \sigma'_1 - \sigma'_3 = \sigma_1 - \sigma_3$	deviatorico stress	$[F/L^2]$
$p = (\sigma_1 + 2 \cdot \sigma_3)/3$	mean total stress	$[F/L^2]$
$p' = (\sigma'_1 + 2 \cdot \sigma'_3)/3$	mean effective stress	$[F/L^2]$
$\varepsilon_a = \Delta H/H_0$	axial deformation	[-]
$\varepsilon_v = \Delta V/V_0$	volumetric deformation	[-]
Δu	overburden pressure	$[F/L^2]$

CS critical state condition
AP air pluviation method
MT moist tamping method

UNDRAINED TESTs

A total of 16 undrained triaxial compression tests are performed on Ticino sand on specimens reconstituted with air pluviation method.

The main data about the dimensions and the type of load, together with the initial state of samples are summarized in Table A.1.

The depositional method used was that one proposed by Miura and Toki (1982).

It consists in a simple preparation method of sand's specimen using multiple sieving pluviation apparatus, capable to reproduce from loose to very dense sample without applying vibration or impact on sand.

The dry sand is pluviated trough a conical hopper down in seven layers of sieved in order to insure a uniform material deposition. Changing the height of fall and the nozzle diameter is possible to reproduce a wide range of initial void ratio.

Experimentally it is observed that nozzle diameter has a stronger influence on the variation of relative density, unlike the height of fall and speed of deposition.

The test results are reported from Figure A.1 to A.16 in $q - p'$, $q - \varepsilon_a$, $\varepsilon_a - \Delta u$ and $p' - \Delta u$ graphs.

Test	Sample B x H [cm x cm]	Type	Stress path	Sourse	Depositional Method *	Failure mode	e_c ** [-]	σ'_{vc} [kPa]	σ'_{hc} [kPa]	p'_c [kPa]	q'_c [kPa]	OCR/R [-]
H0	7 x 14	CIU	σ_3=cost	ISMES	AP	load	0.810	800	800	800	0	1
H1		CIU	σ_3=cost	ISMES	AP	load	0.831	400	400	400	0	1
H2		CIU	σ_3=cost	ISMES	AP	load	0.827	500	500	500	0	1
H3		CIU	σ_3=cost	ISMES	AP	load	0.826	600	600	600	0	1
H4		CIU	σ_3=cost	ISMES	AP	load	0.812	700	700	700	0	1
H5		CIU	σ_3=cost	ISMES	AP	load	0.808	800	800	800	0	1
H6		CK0U	σ_3=cost	ISMES	AP	def	0.816	750	341	477	409	1
H7		CK0U	σ_3=cost	ISMES	AP	def	0.844	750	367	495	384	1
H8		CK0U	σ_3=cost	ISMES	AP	def	0.846	750	360	490	391	1
H10		CK0U	σ_3=cost	ISMES	AP	load	0.839	600	286	391	315	1
H11		CK0U	σ_3=cost	ISMES	AP	load	0.842	750	344	479	406	1
H12		CK0U	σ_3=cost	ISMES	AP	load	0.841	900	428	585	473	1
H13		CK0U	σ_3=cost	ISMES	AP	load	0.825	1050	479	669	572	1
H14		CK0U	σ_3=cost	ISMES	AP	load	0.826	1200	556	770	644	1
H15		CK0U	σ_3=cost	ISMES	AP	def	0.812	750	358	489	392	1
H16		CK0U	σ_3=cost	ISMES	AP	def	0.813	750	359	489	391	1

* miura depositional method

** e_{max} = 0.923; e_{min} = 0.574

Table A.1- Undrained triaxial tests on Ticino sand

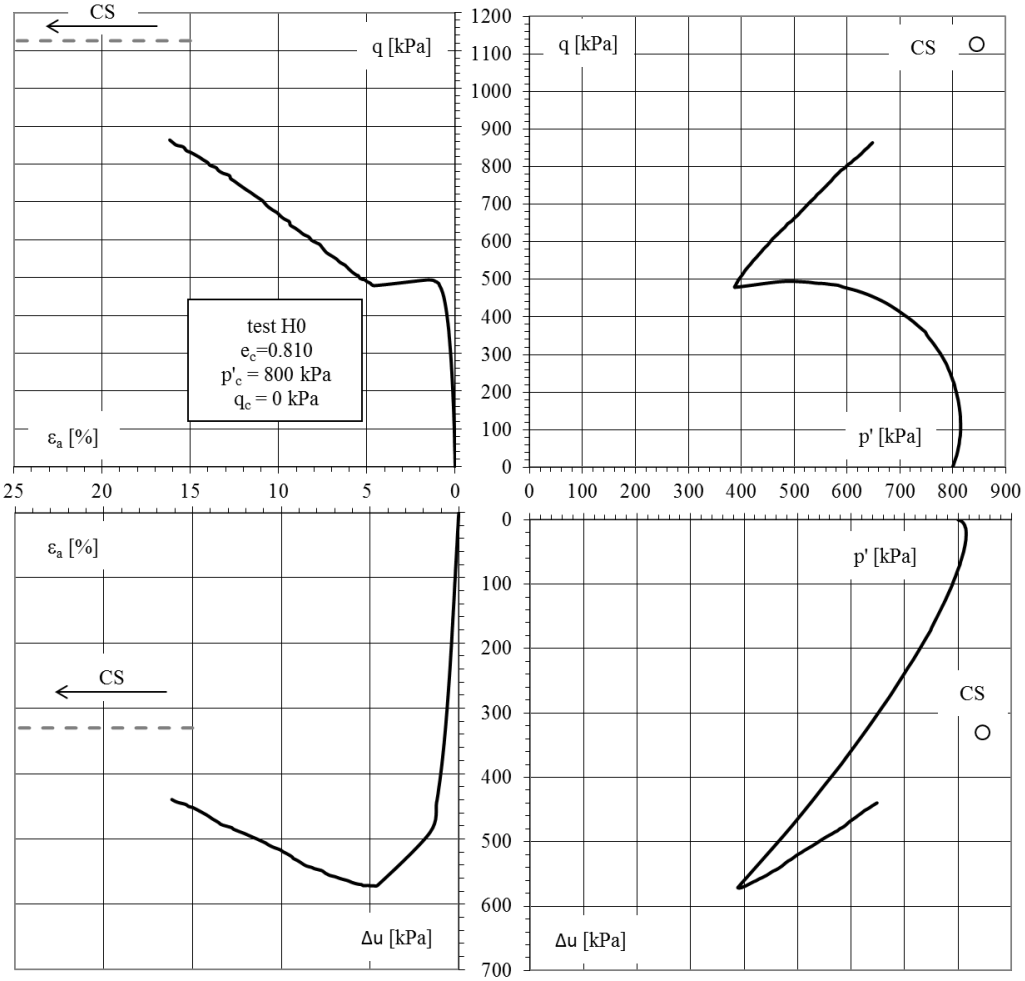

Critical State		
Δu [kPa]	q [kPa]	p' [kPa]
330	1126	845

Figure A.1-CIU-H0

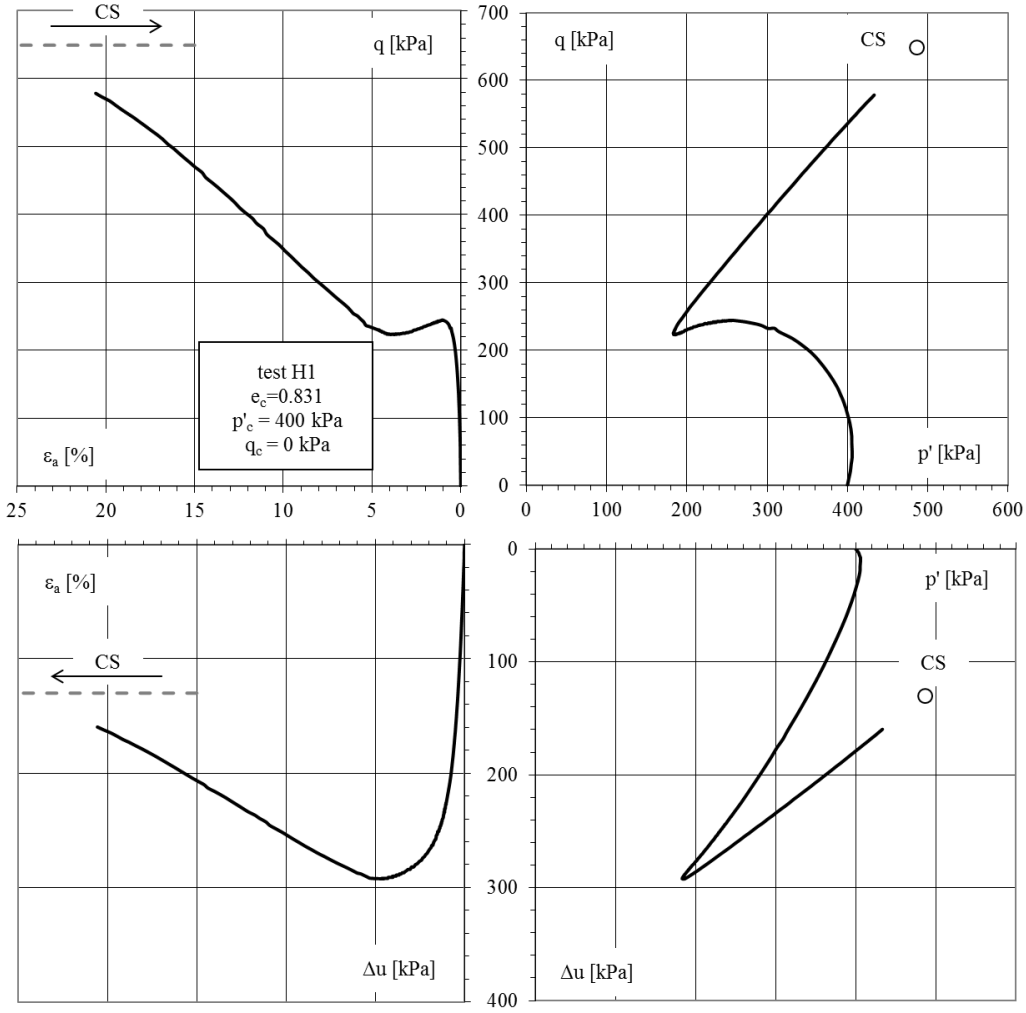

Critical State		
Δu [kPa]	q [kPa]	p' [kPa]
130	649	486

Figure A.2-CIU-H1

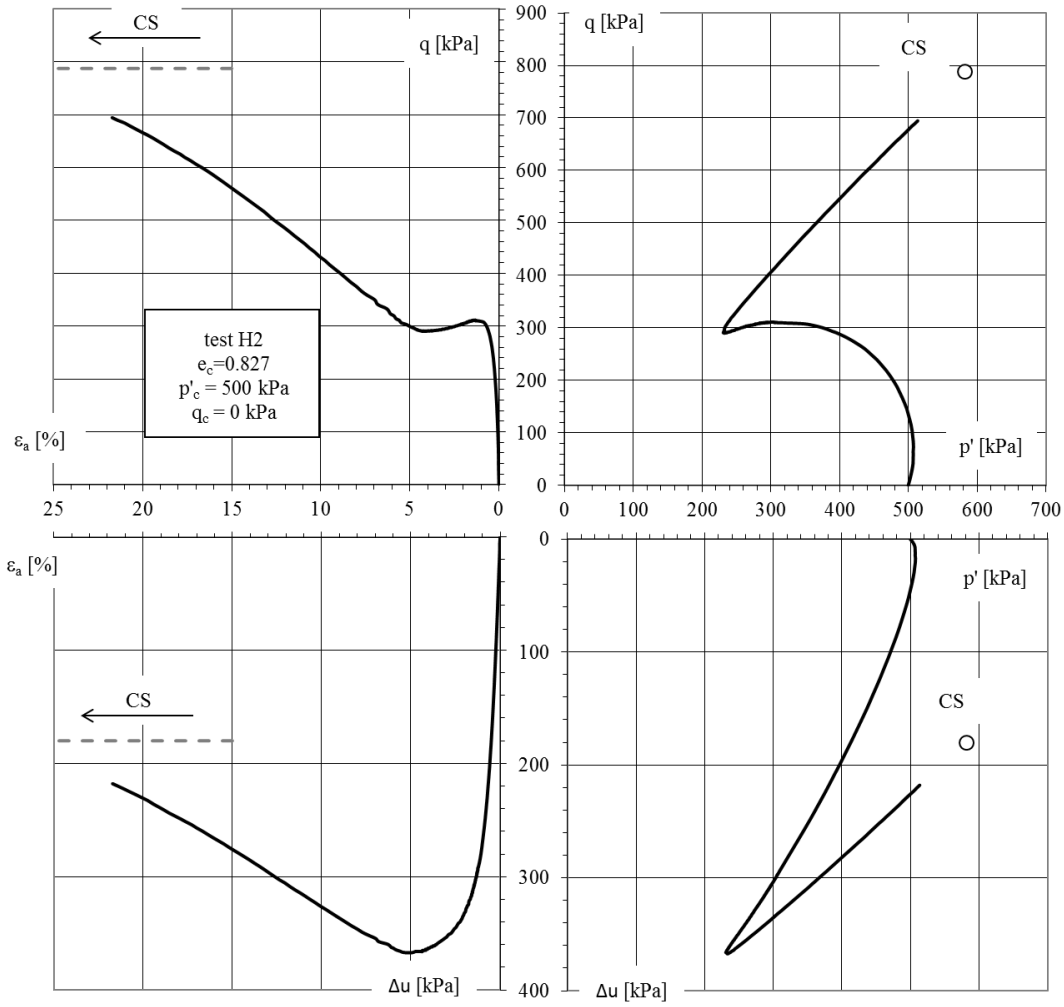

Critical State		
Δu [kPa]	q [kPa]	p' [kPa]
180	788	582

Figure A-CIU-H2

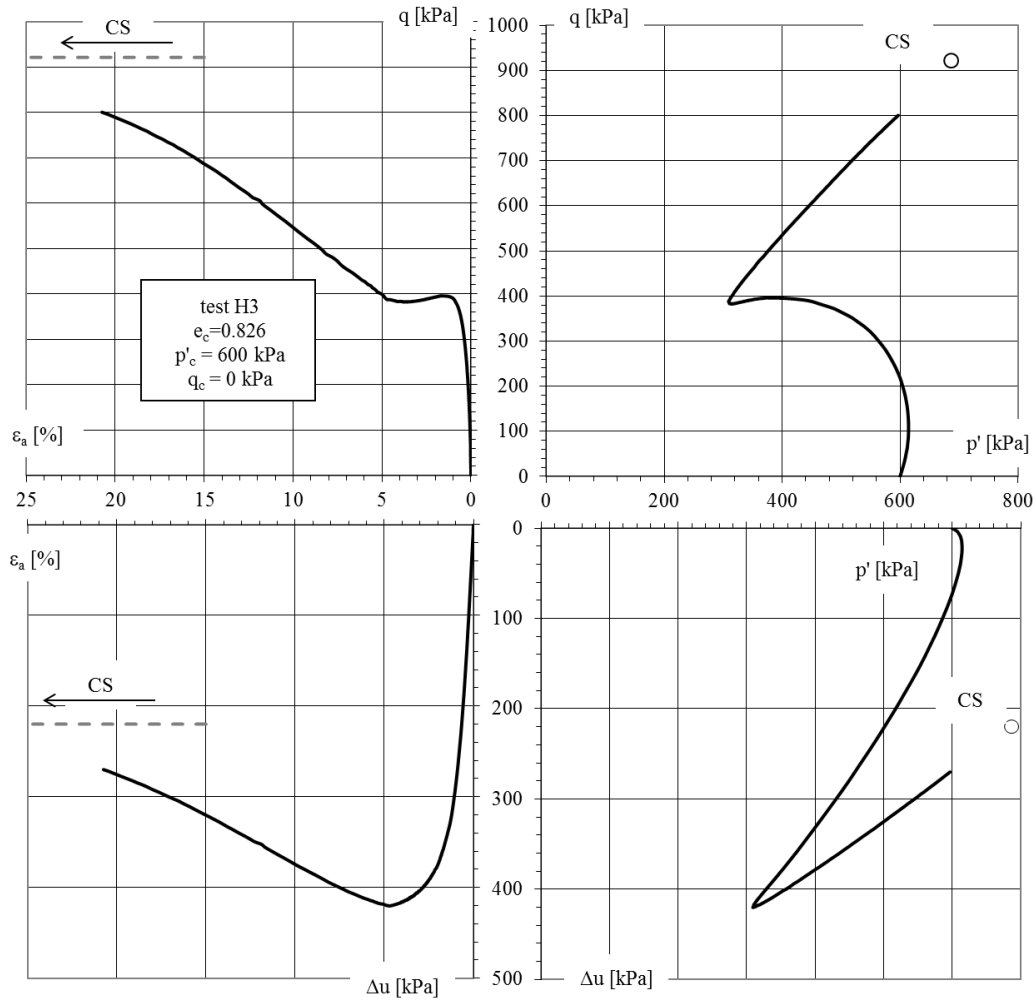

Critical State		
Δu [kPa]	q [kPa]	p' [kPa]
220	921	687

Figure A.3-CIU-H3

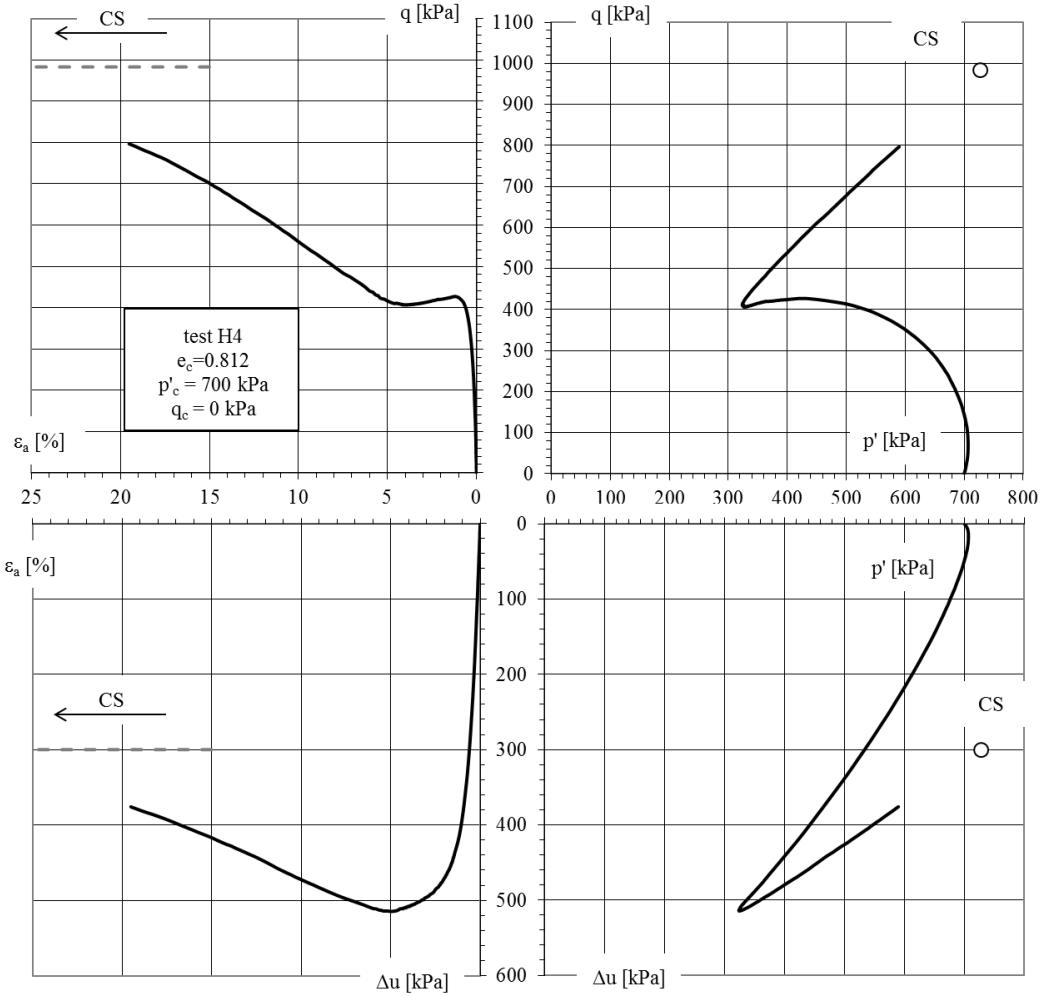

Critical State		
Δu [kPa]	q [kPa]	p' [kPa]
300	983	728

Figure A.4-CIU-H4

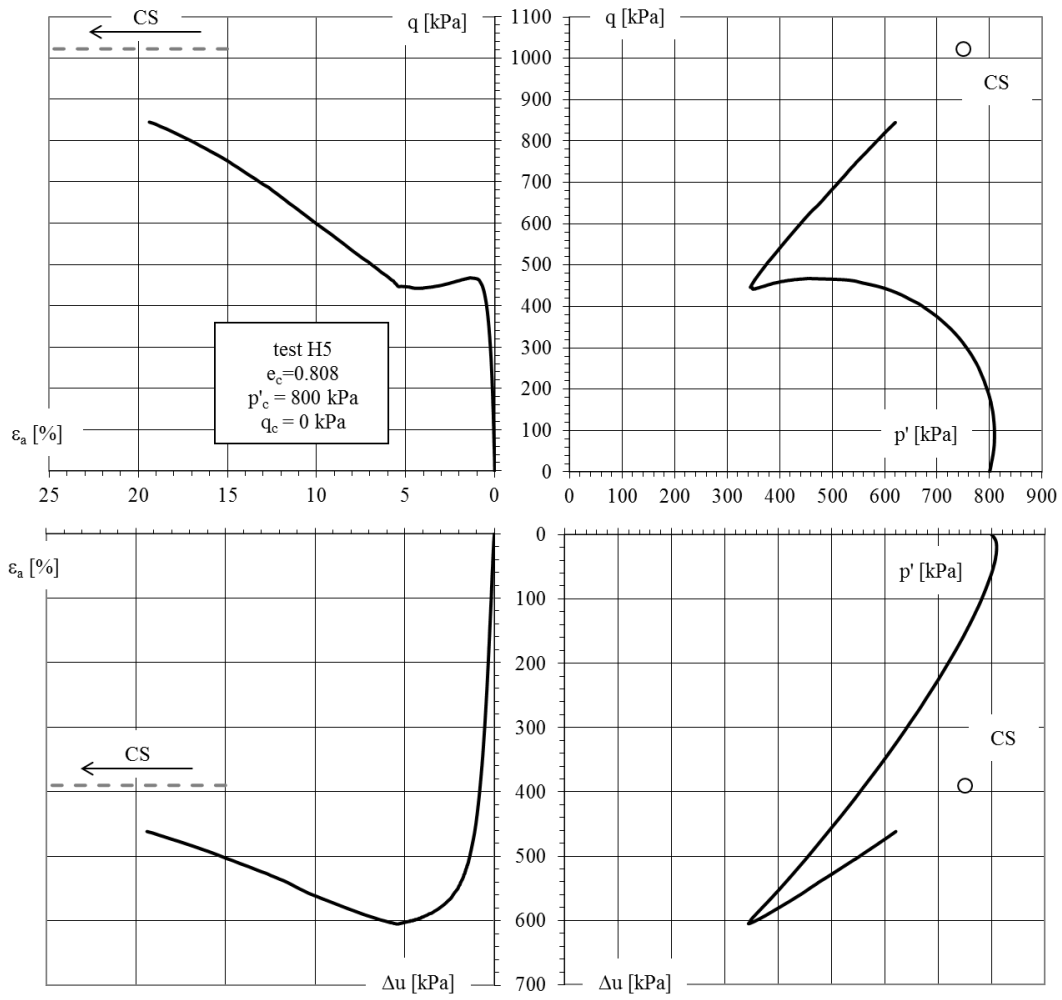

Critical State		
Δu [kPa]	q [kPa]	p' [kPa]
390	1022	751

Figure A.5-CIU-H5

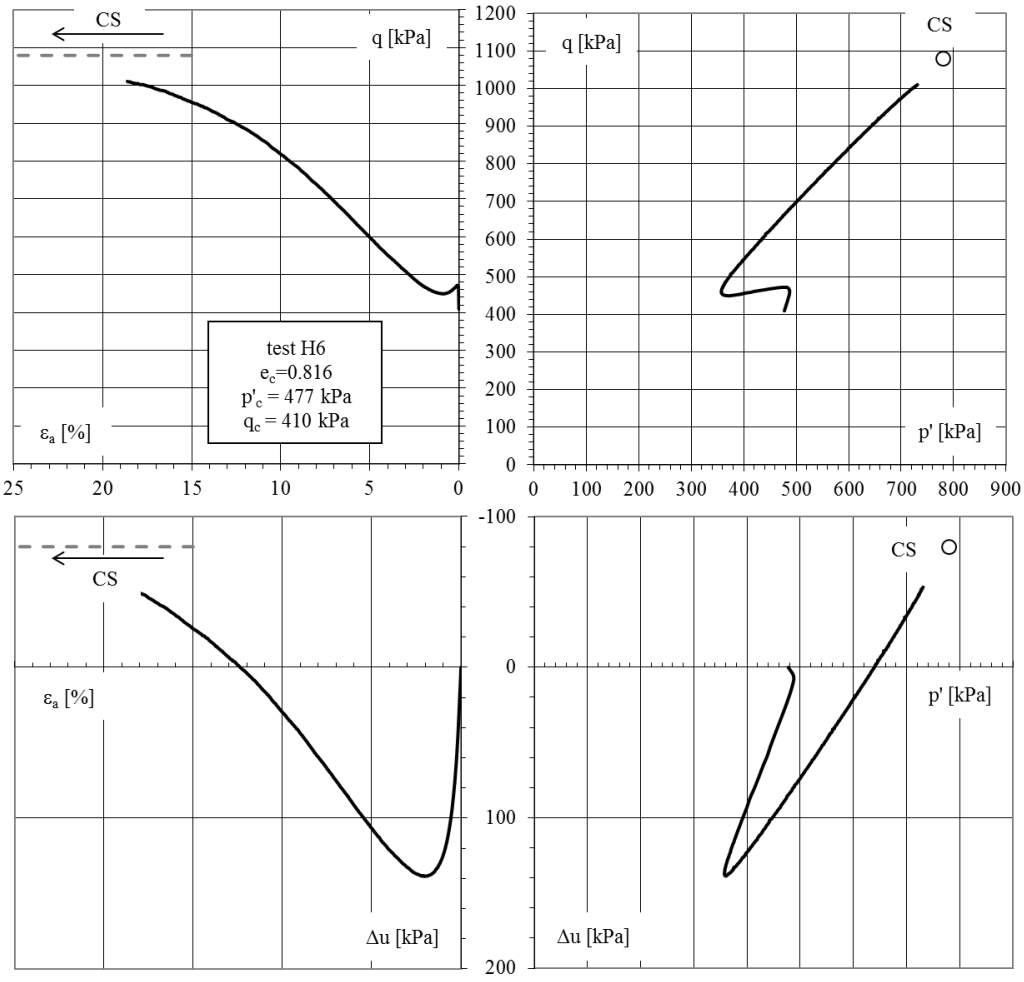

Critical State		
Δu [kPa]	q [kPa]	p' [kPa]
-80	1079	781

Figure A.6-CK0U-H6

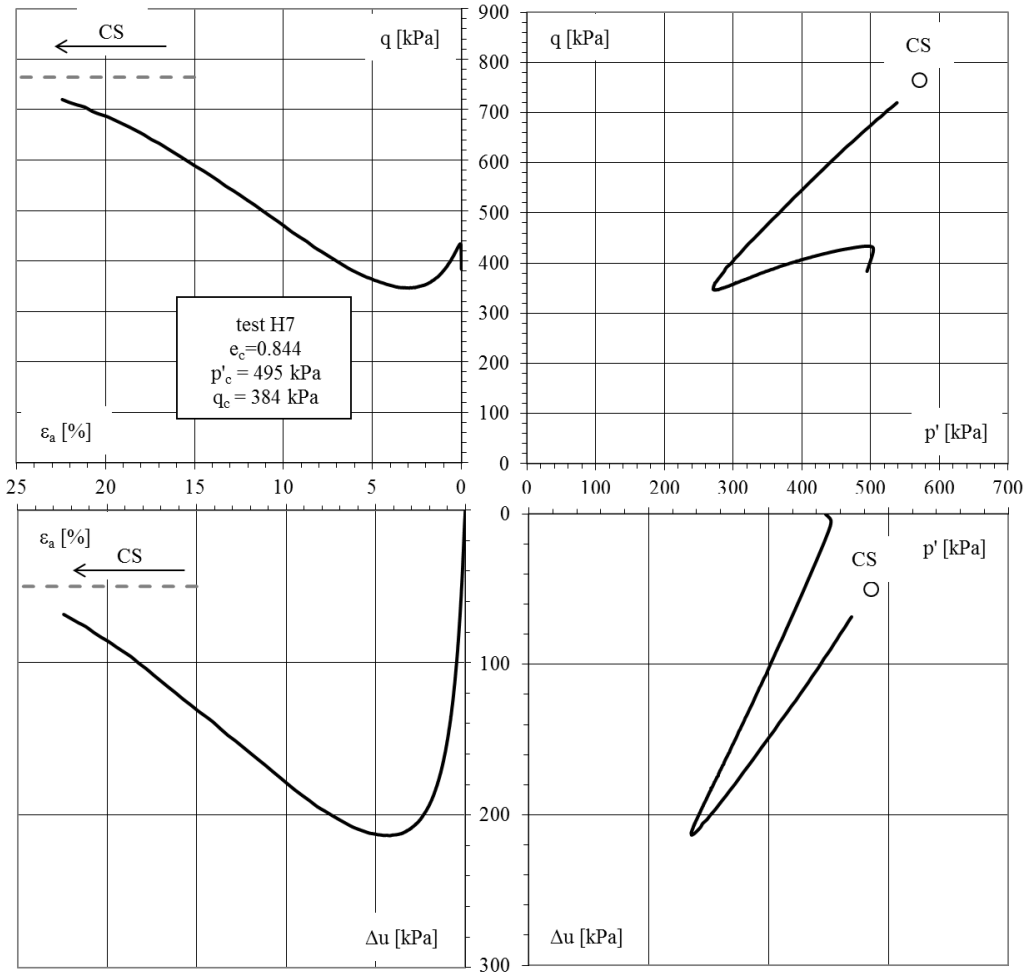

Critical State		
Δu [kPa]	q [kPa]	p' [kPa]
50	764	571

Figure A.7-CK0U-H7

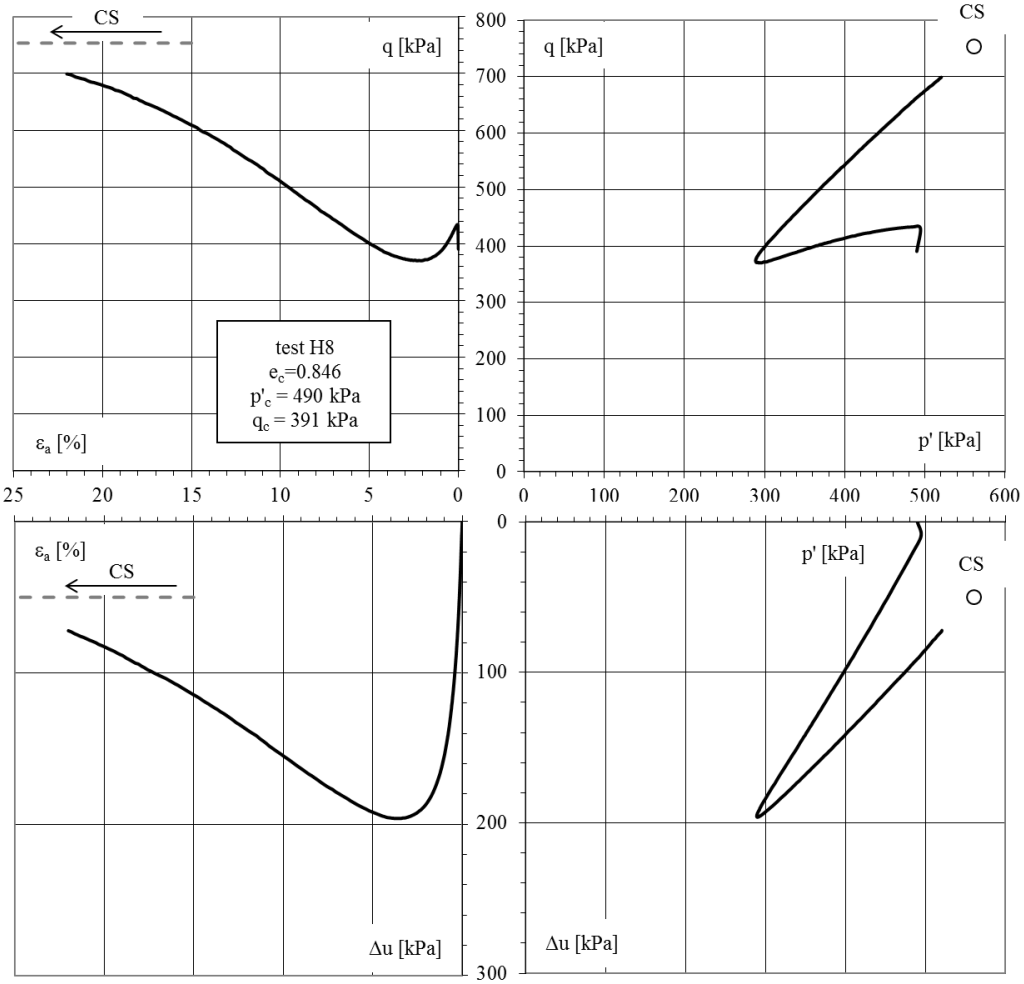

Critical State		
Δu [kPa]	q [kPa]	p' [kPa]
50	753	561

Figure A.8-CK0U-H8

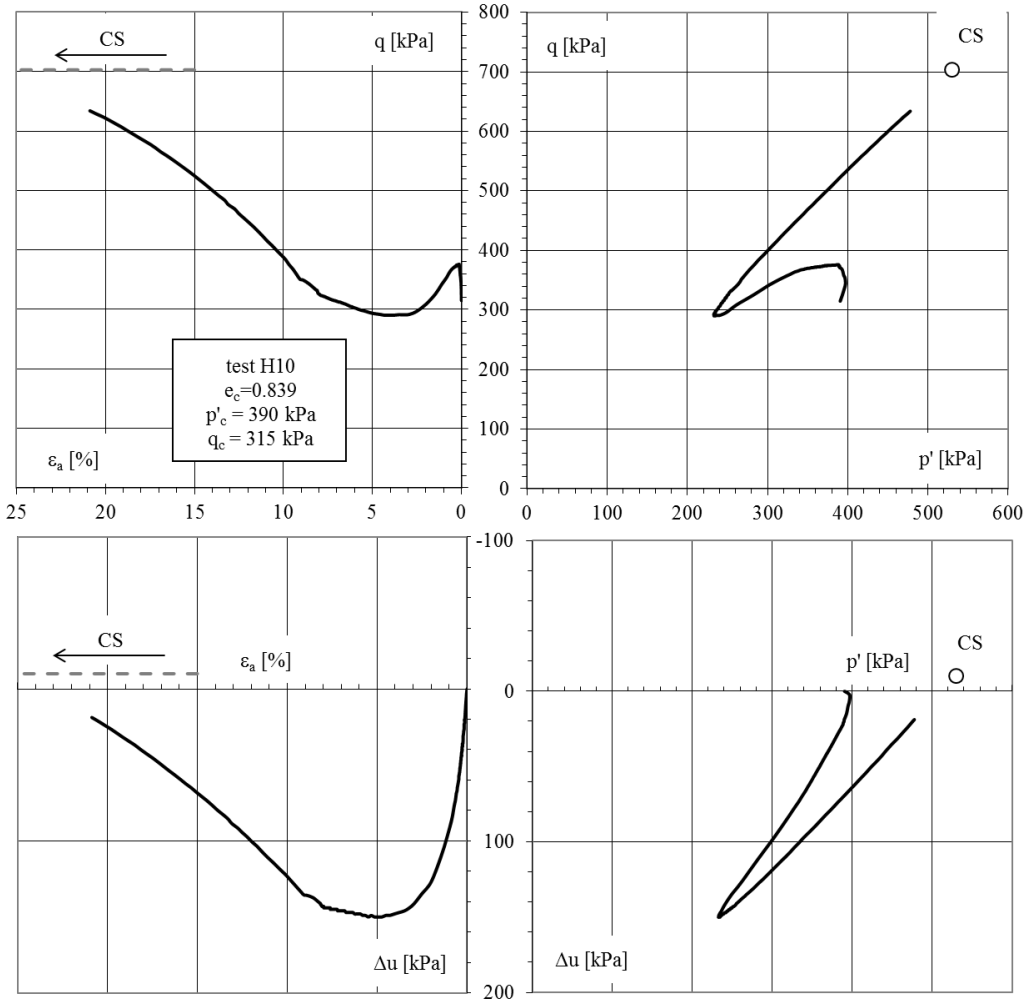

Critical State		
Δu [kPa]	q [kPa]	p' [kPa]
-10	703	530

Figure A.9-CK0U-H10

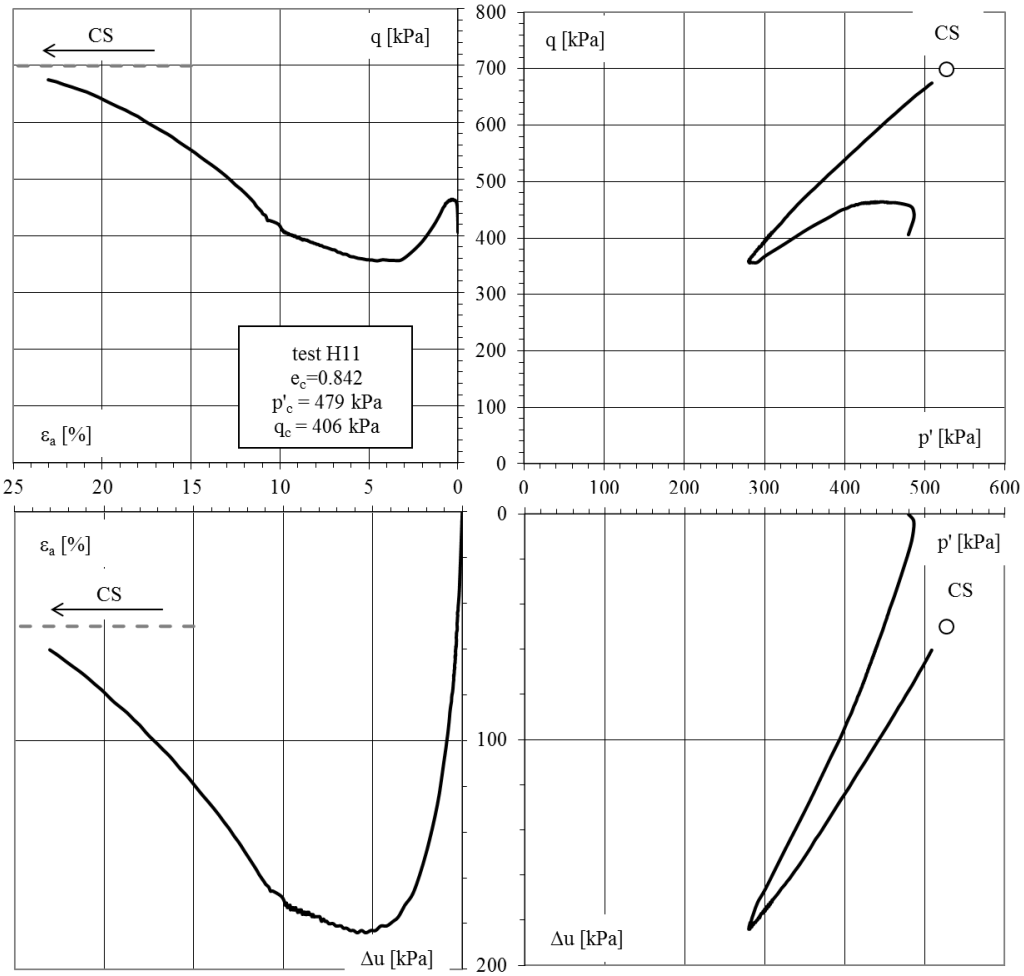

Critical State		
Δu [kPa]	q [kPa]	p' [kPa]
50	699	527

Figure A.10-CK0U-H11

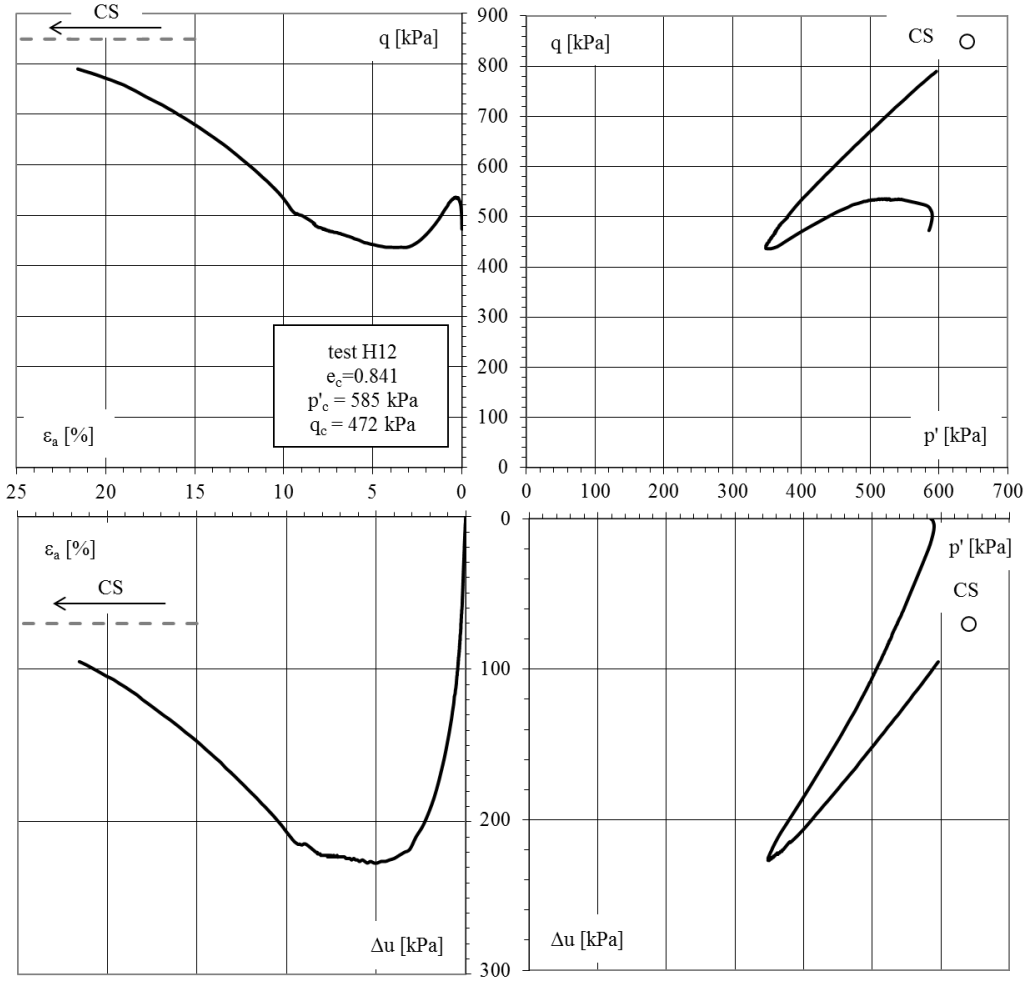

Critical State		
Δu [kPa]	q [kPa]	p' [kPa]
70	849	641

Figure A.11-CK0U-H12

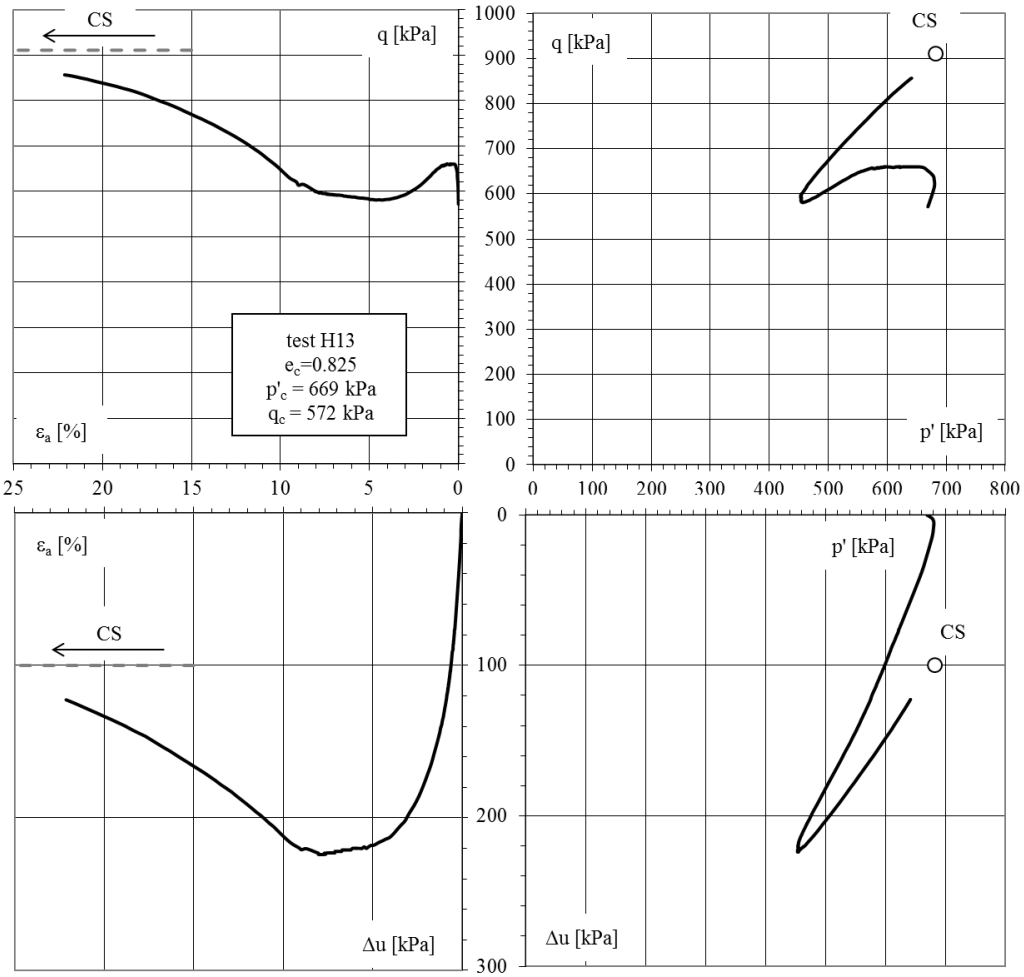

Critical State		
Δu [kPa]	q [kPa]	p' [kPa]
100	911	682

Figure A.12-CK0U-H13

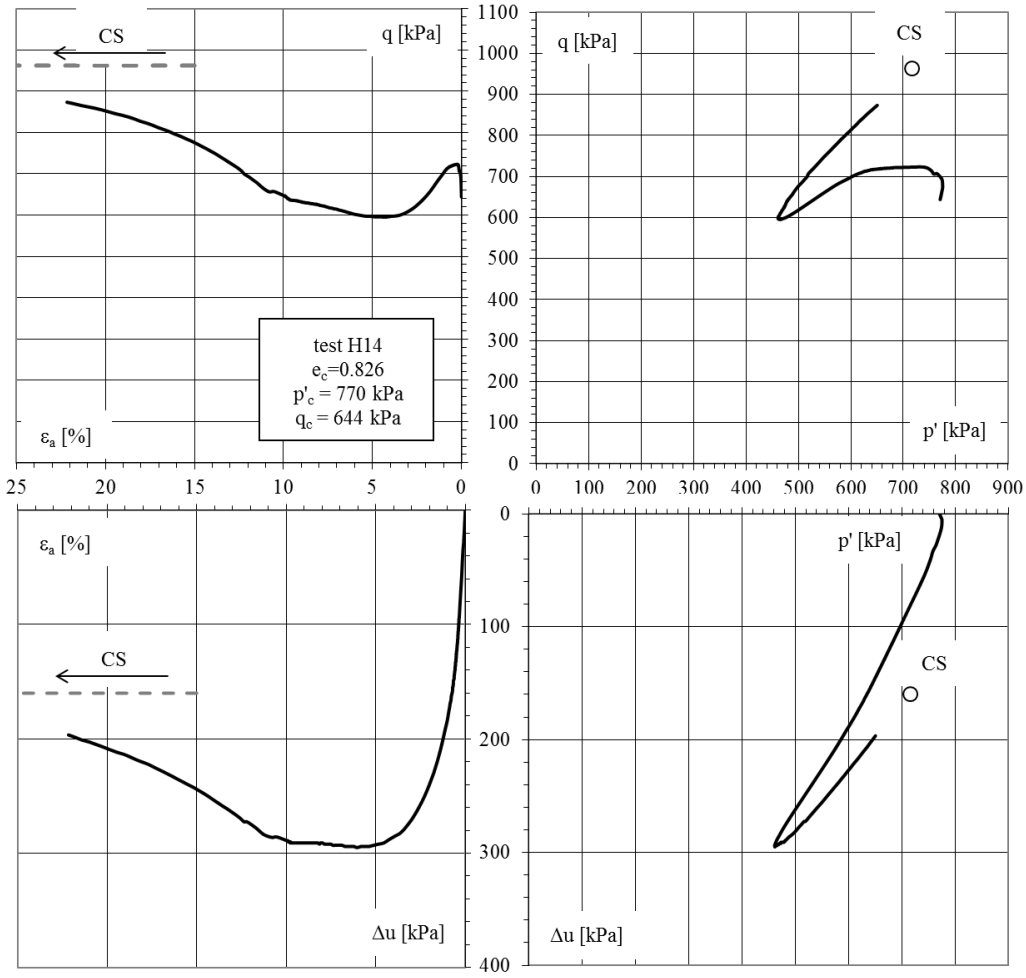

Critical State		
Δu [kPa]	q [kPa]	p' [kPa]
160	962	717

Figure A.13-CK0U-H14

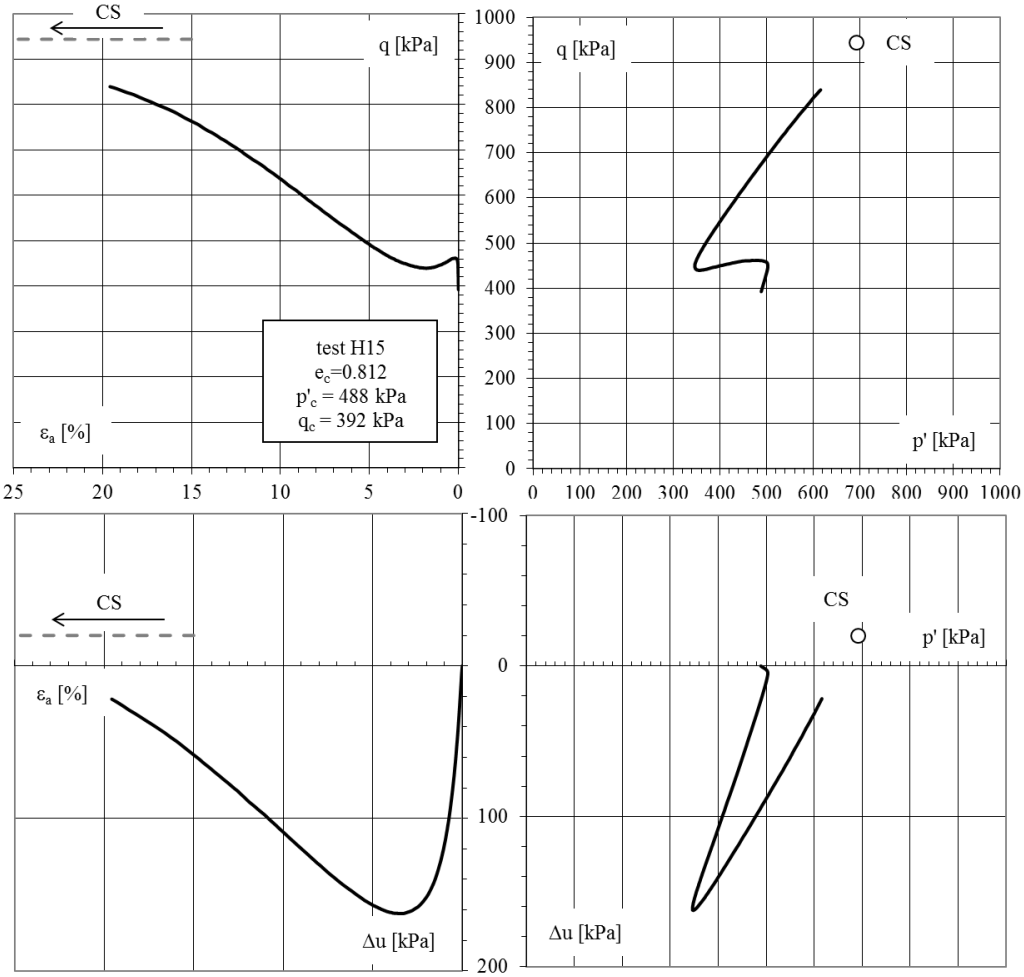

Critical State		
Δu [kPa]	q [kPa]	p' [kPa]
-20	944	692

Figure A.14-CK0U-H15

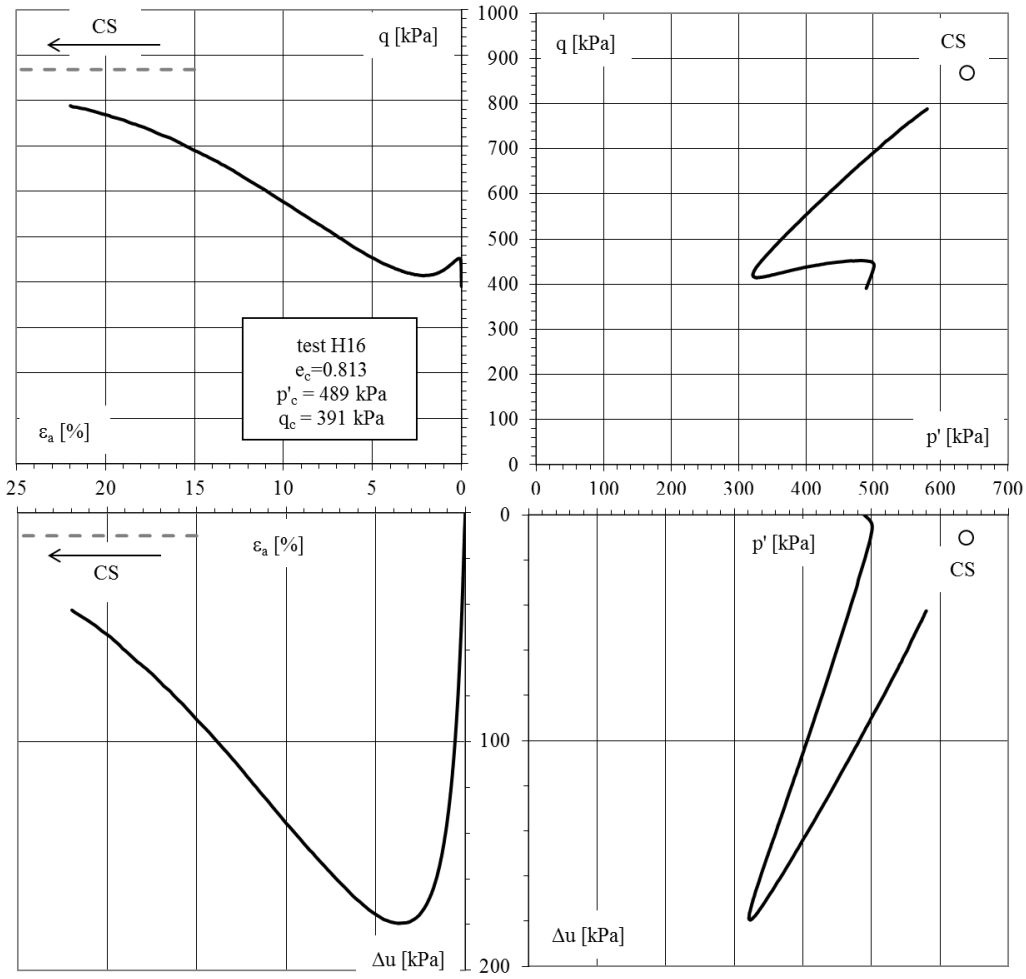

Critical State		
Δu [kPa]	q [kPa]	p' [kPa]
10	868	639

Figure A.15-CK0U-H16

DRAINED TESTs

A total of 14 drained monotonic triaxial tests were performed on Ticino sand on specimens reconstituted with air pluviation method.

The main data about the dimensions and the type of load, together with the initial state of samples are summarized in Table A.2.

Test	Sample B x H [cm x cm]	Type	Stress path	Sourse	Depositional Method	Failure mode	e_c **** [-]	σ'_{vc} [kPa]	σ'_{hc} [kPa]	p'_c [kPa]	q'_c [kPa]	OCR/R [-]
171		CK0D	σ_3=cost	ISMES	AP *	def	0.759	500	235	324	265	1.2
172	7 x 14	CK0D	σ_3=cost	ISMES	AP *	def	0.773	401	221	281	180	1.5
CK5		CK0D	σ_3=cost	ISMES	AP**	def	0.790	877	370	539	507	1
K6	4 x 8	CK0D	σ_3=cost	ISMES	AP**	def	0.730	1447	581	870	866	1
K8		CK0D	σ_3=cost	ISMES	AP**	def	0.798	774	341	485	433	1
M32	7 x 14	CID	σ_3=cost	ISMES	AP**	def	0.640	800	800	800	0	1
R14		CK0D	p'=cost	ISMES	AP***	def	0.698	1200	507	738	693	1
U21		CK0D	σ_3=cost	ISMES	AP***	def	0.756	301	298	299	3	4
U22		CK0D	σ_3=cost	ISMES	AP**	def	0.796	125	124	124	1	4
U24		CK0D	σ_3=cost	ISMES	AP**	def	0.760	125	118	120	7	4
U36	4 x 8	CK0D	σ_3=cost	ISMES	AP**	def	0.751	200	246	231	-46	6
U38		CK0D	σ_3=cost	ISMES	AP**	def	0.760	50	59	56	-9	6
U50		CK0D	σ_3=cost	ISMES	AP**	def	0.785	75	94	88	-19	8
V9		CK0D	σ_3=cost	ISMES	AP**	def	0.687	1155	437	676	718	1

* miura depositional method, ** dep. Fixed meches; *** dep. Moving meches

**** e_{max} = 0.923; e_{min} = 0.574

Table A.2- Drained triaxial tests on Ticino sand

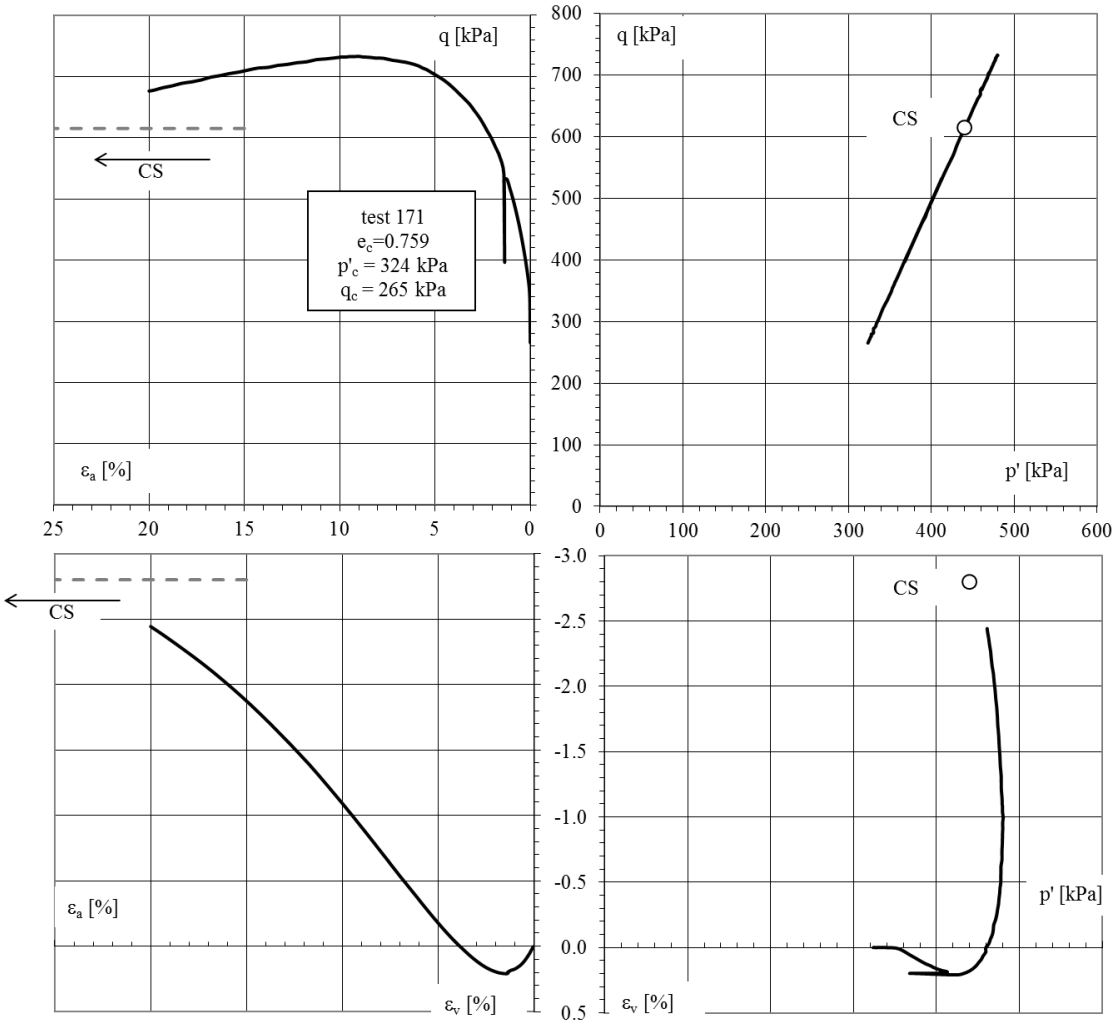

Critical State		
ε_v [%]	q [kPa]	p' [kPa]
-2.8	615	440

Figure A.16-CK0D-171

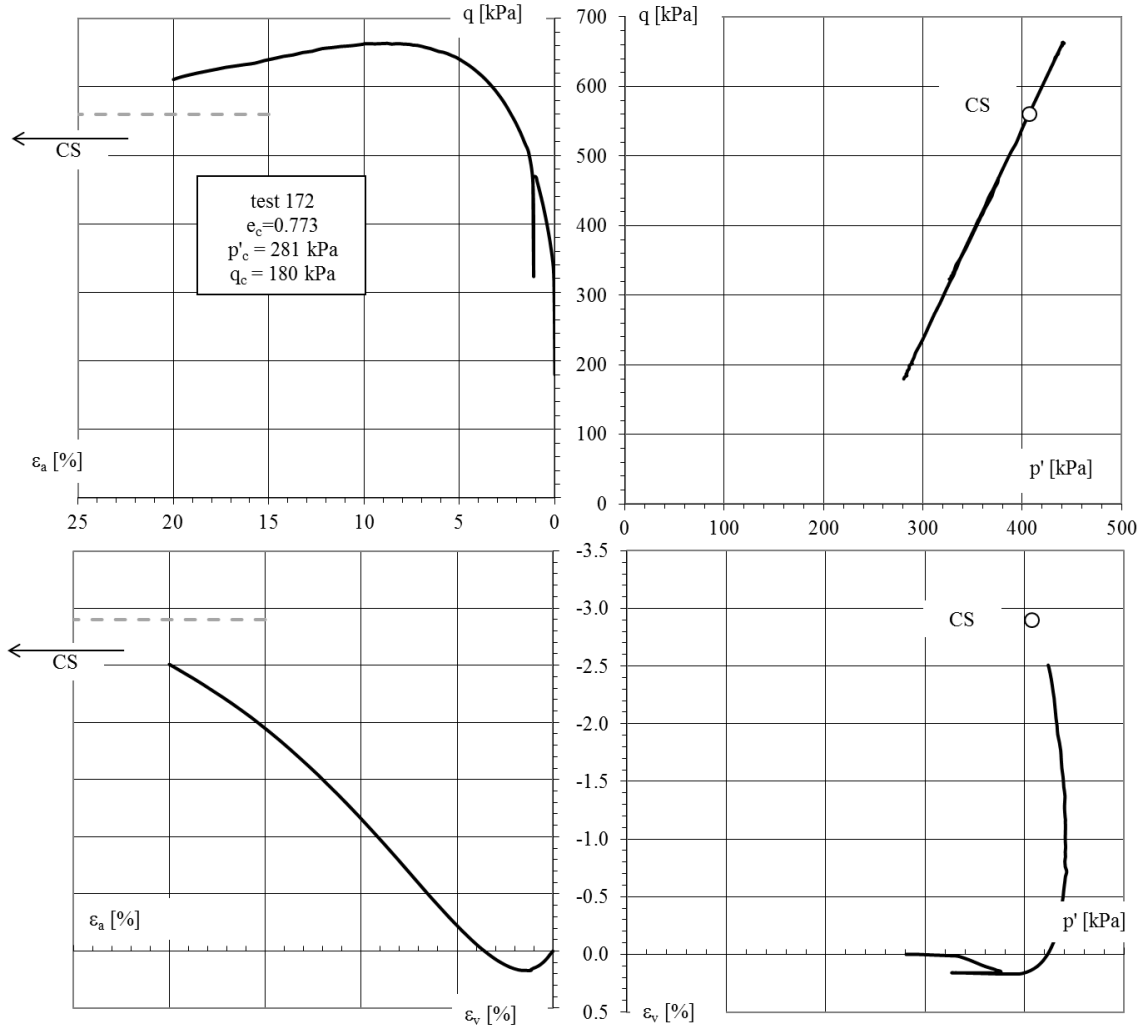

Critical State		
ε_v	q	p'
[%]	[kPa]	[kPa]
-2.9	560	407

Figure A.17-CK0D-172

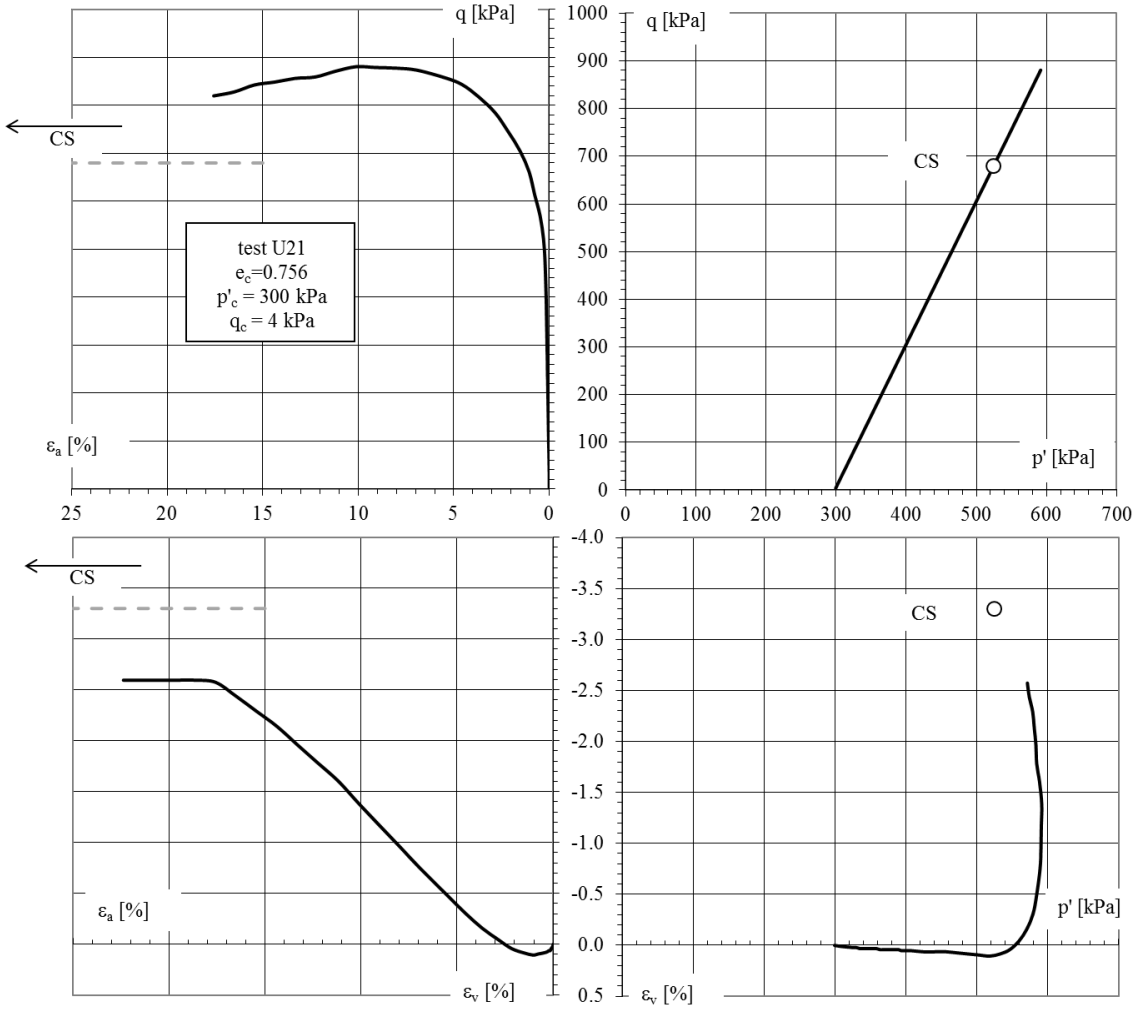

Critical State		
ε_v [%]	q [kPa]	p' [kPa]
-3.3	680	525

Figure A.18-CID-U21

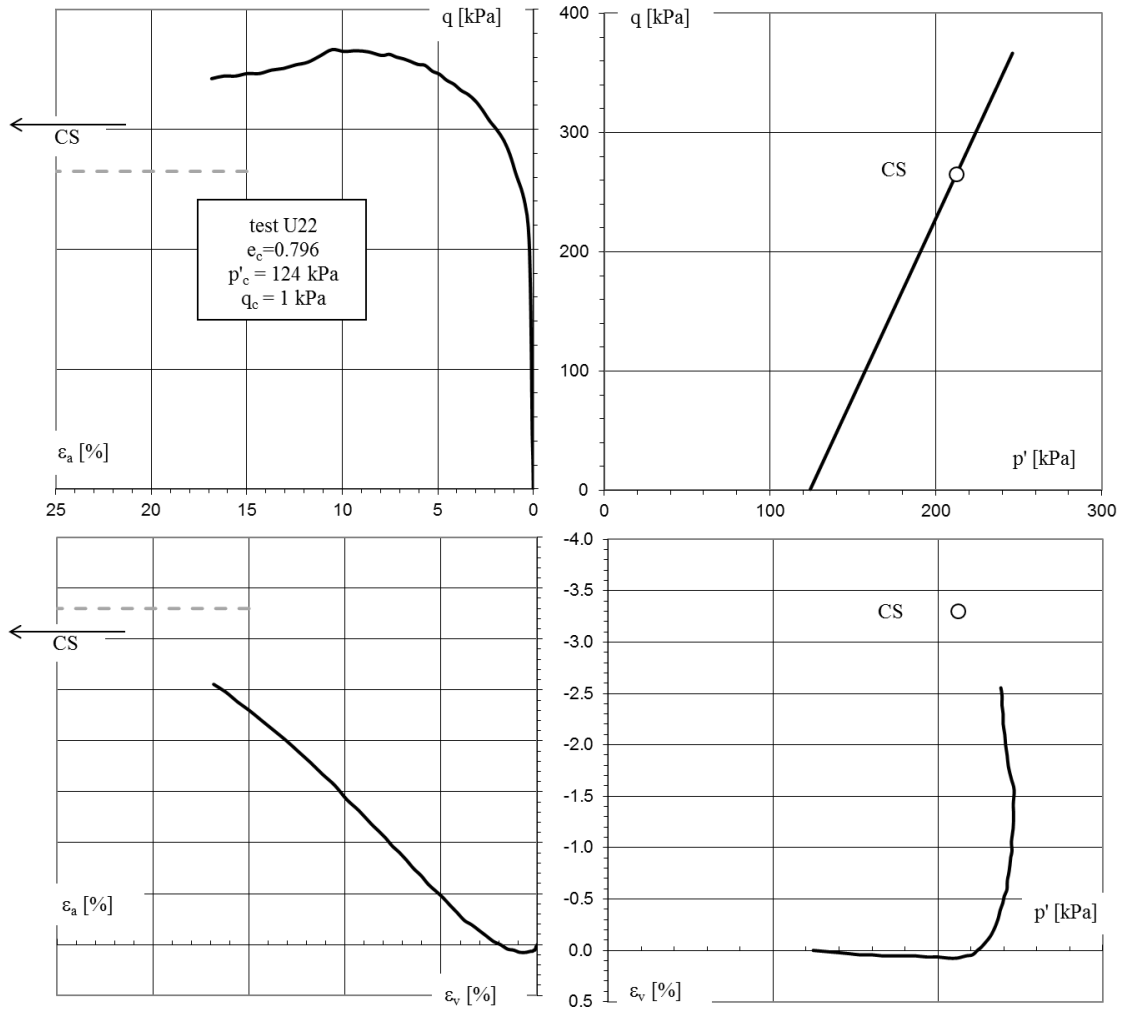

Critical State		
ε_v [%]	q [kPa]	p' [kPa]
-3.3	265	212

Figure A.19-CID-U22

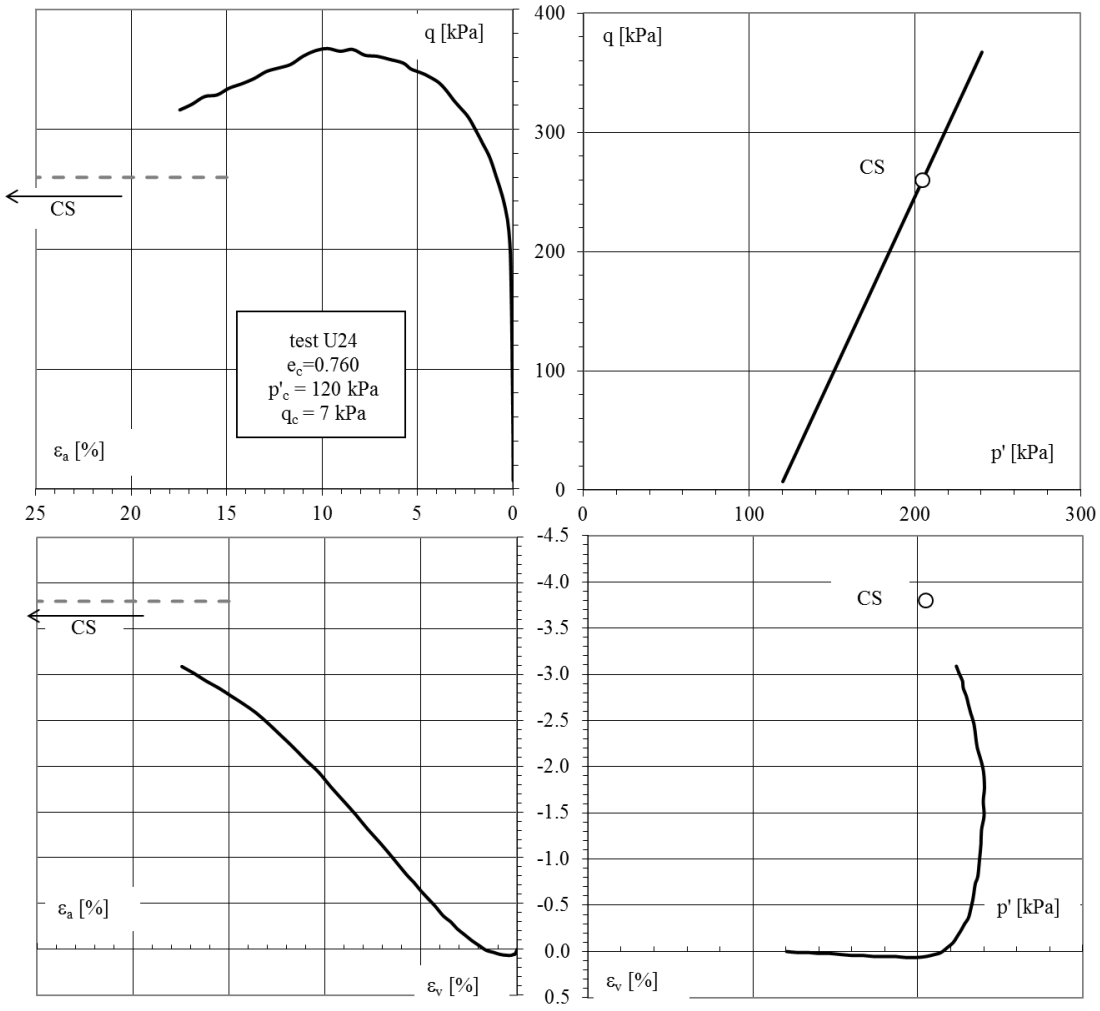

Critical State		
ε_v [%]	q [kPa]	p' [kPa]
-3.8	260	205

Figure A.20-CID-U24

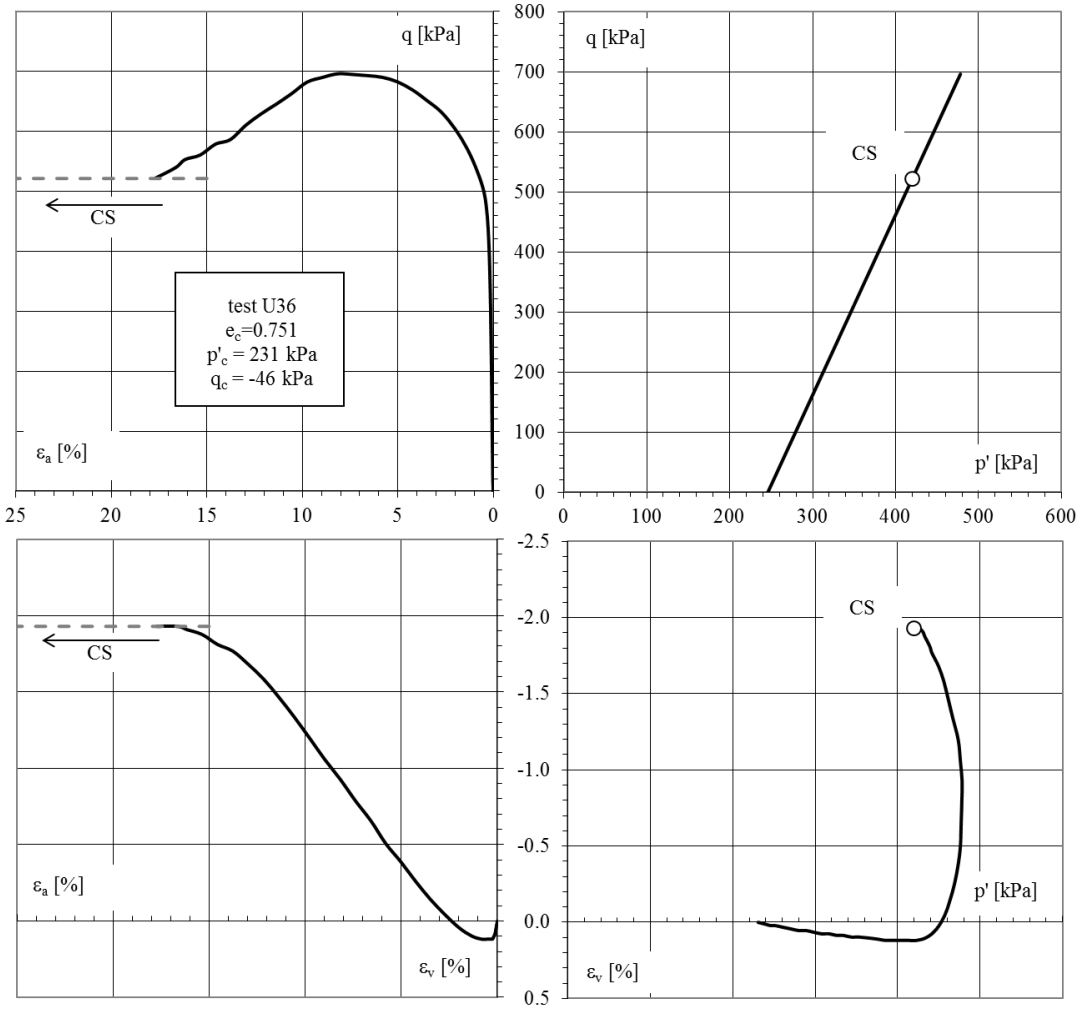

Critical State		
ε_v [%]	q [kPa]	p' [kPa]
-1.9	521	420

Figure A.21-CID-U36

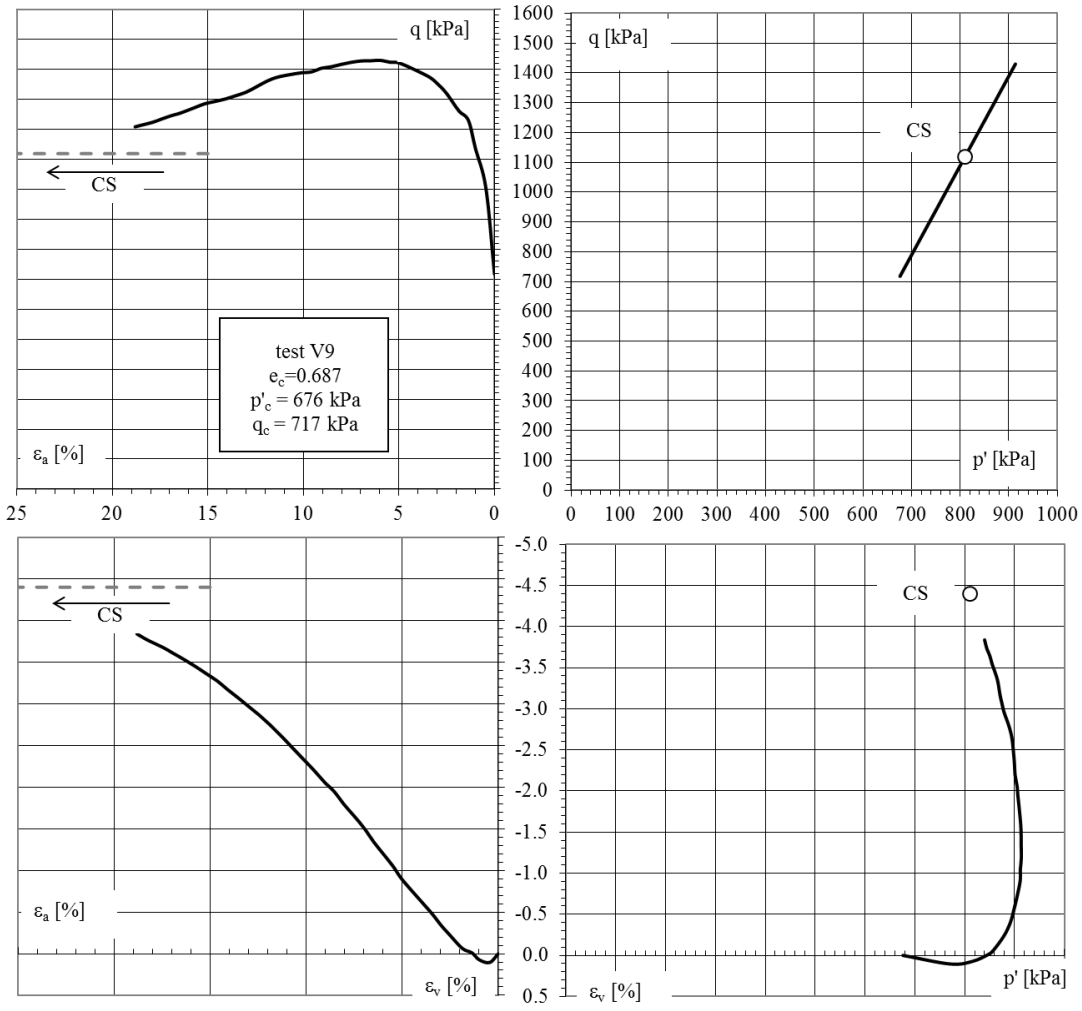

Critical State		
ε_v [%]	q [kPa]	p' [kPa]
-4.4	1119	810

Figure A.22-CK0D-V7

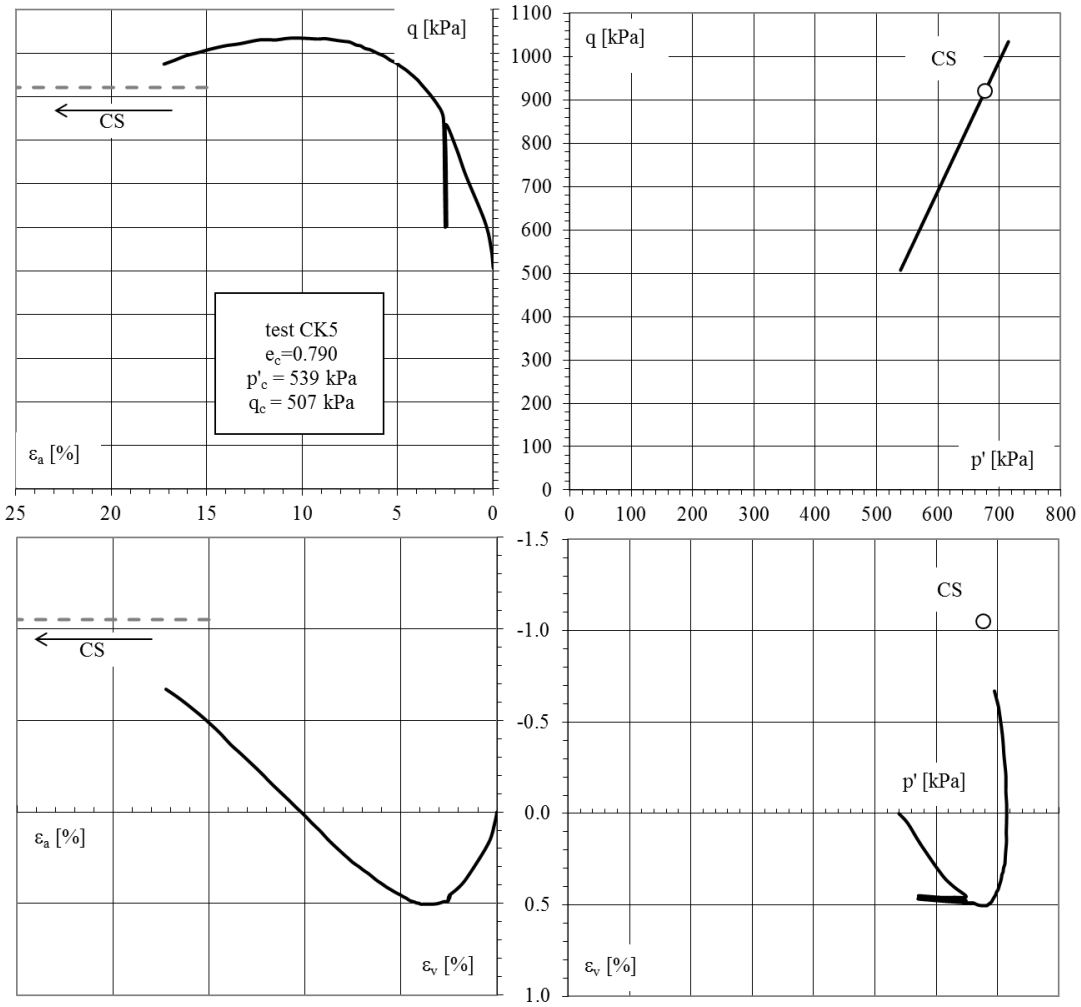

Critical State		
ε_v [%]	q [kPa]	p' [kPa]
-1.1	921	660

Figure A.23-CK0D-CK5

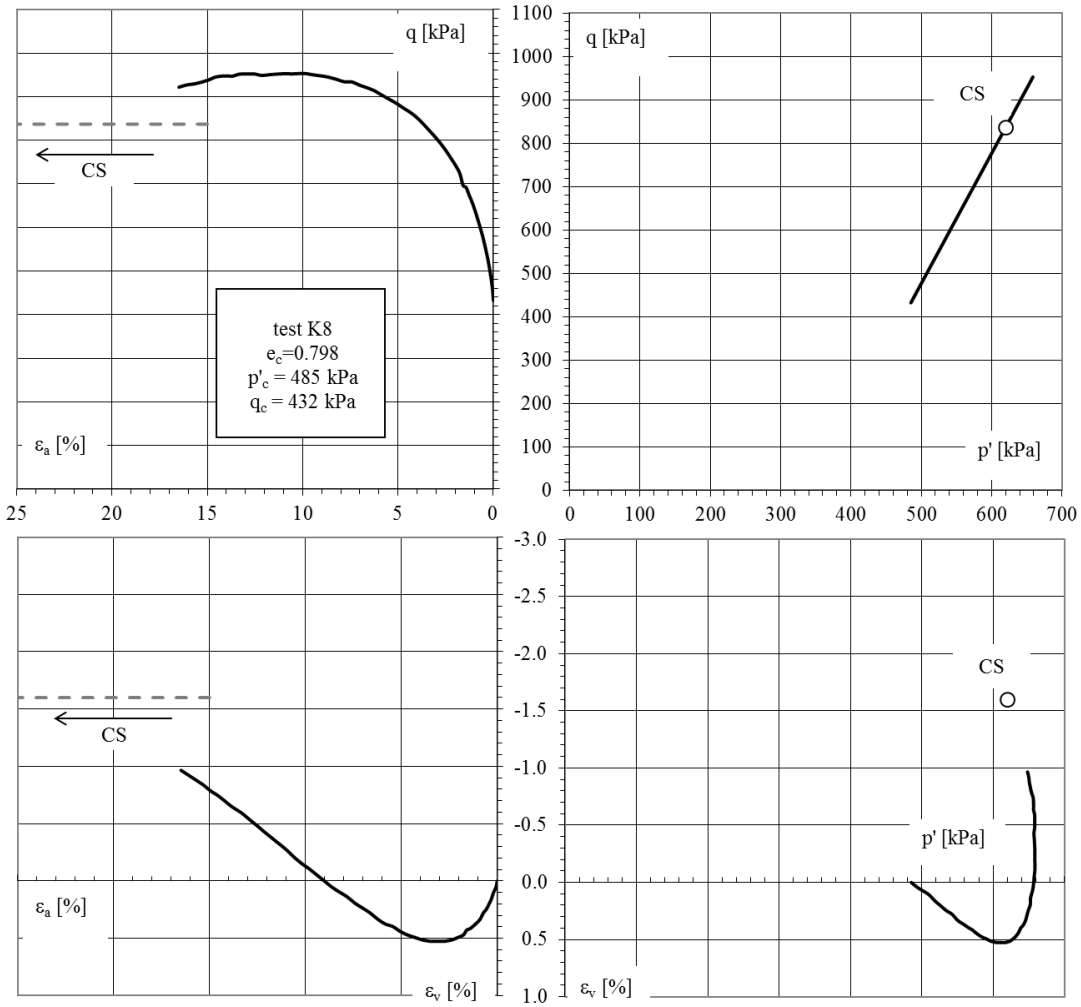

Critical State		
ε_v [%]	q [kPa]	p' [kPa]
-1.6	837	621

Figure A.24-CK0D-K8

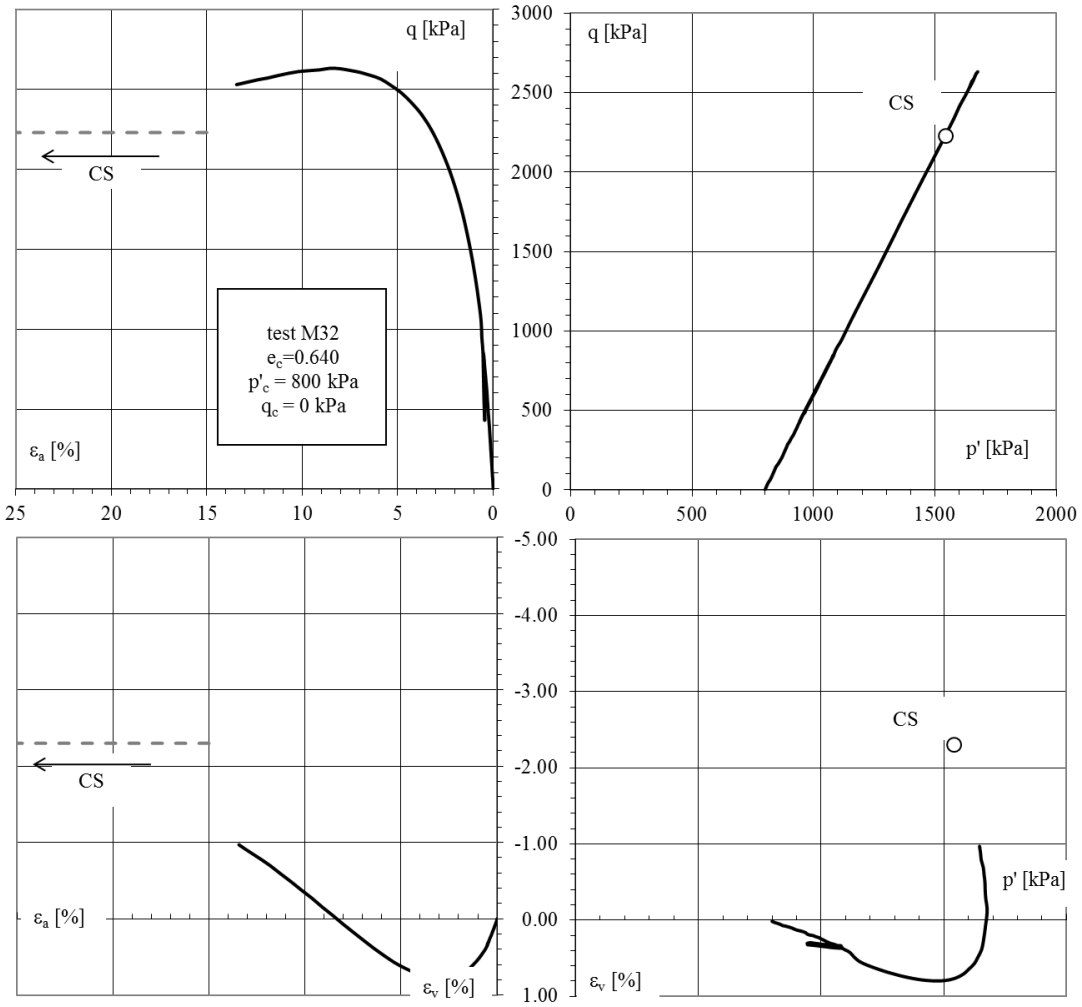

Critical State		
ε_v	q	p'
[%]	[kPa]	[kPa]
-2.3	2230	1543

Figure A.25-CID-M32

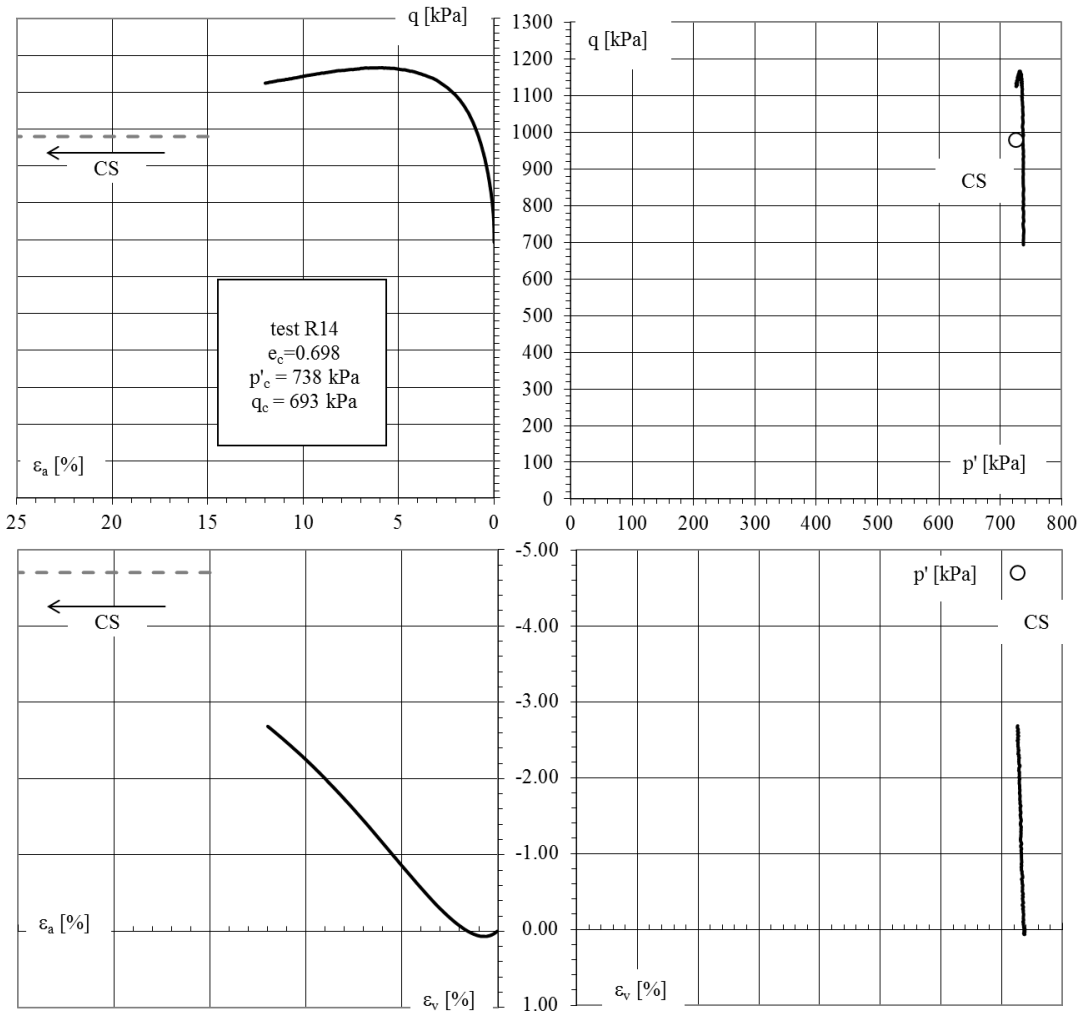

Critical State		
ε_v	q	p'
[%]	[kPa]	[kPa]
-4.7	980	726

Figure A.26-p’ cost-R14

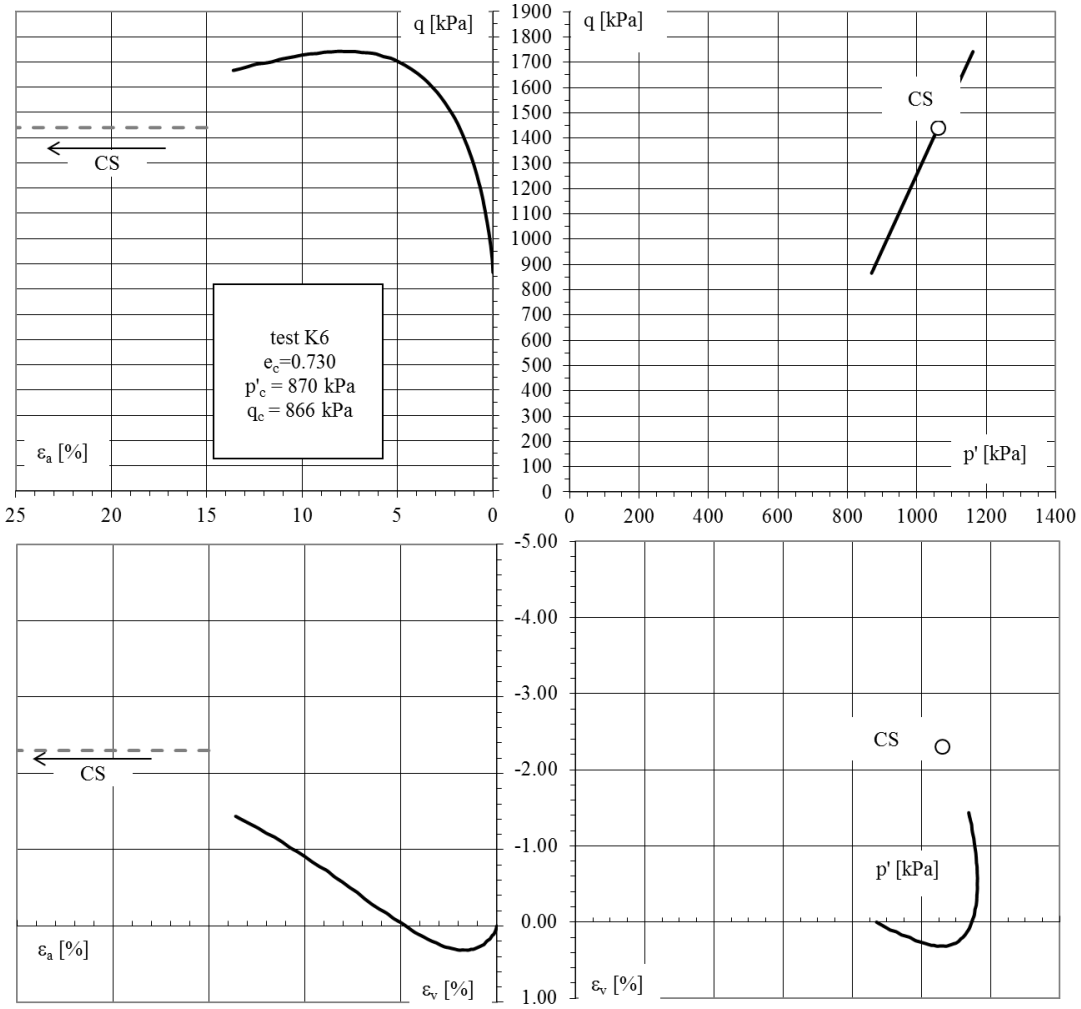

Critical State		
ε_v	q	p'
[%]	[kPa]	[kPa]
-2.3	1440	1061

Figure A.27-CK0D-K6

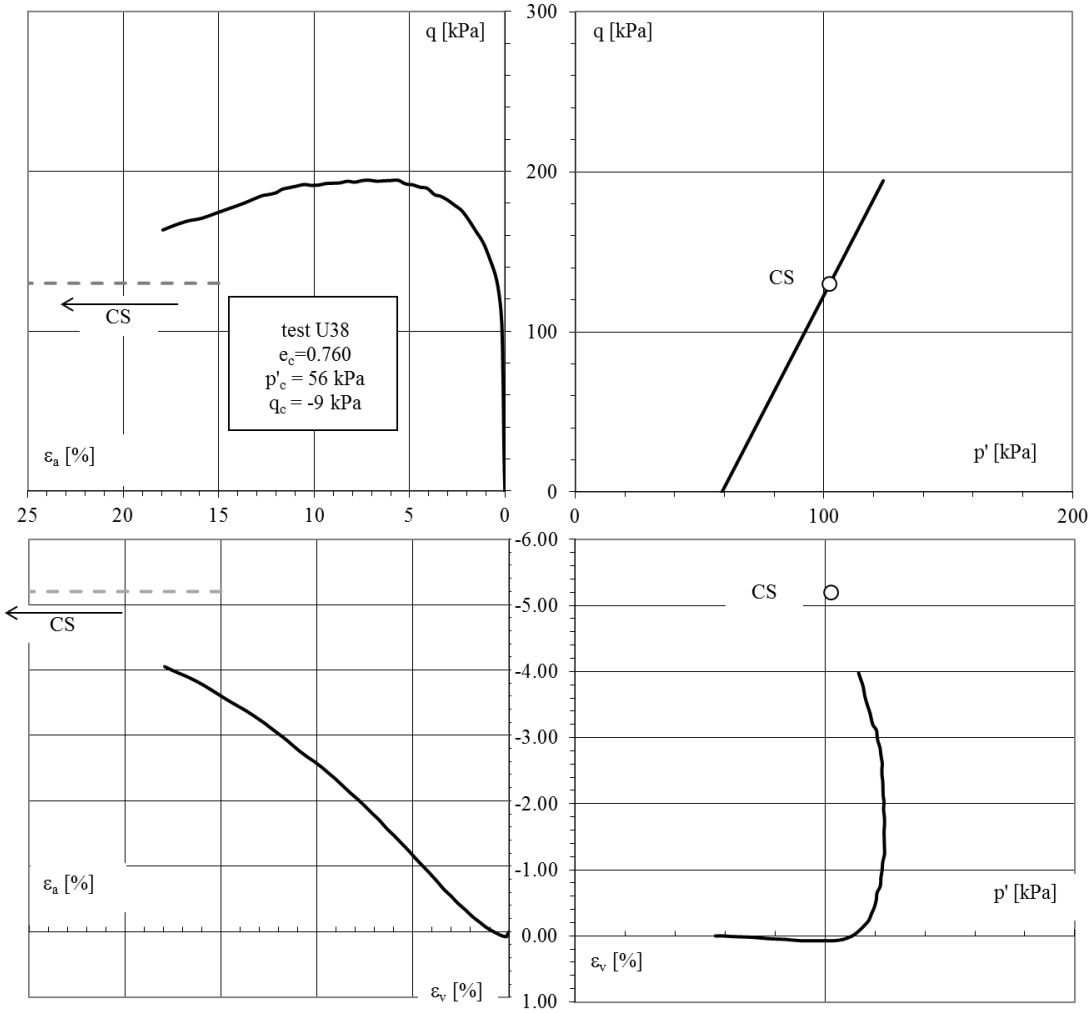

Critical State		
ε_v [%]	q [kPa]	p' [kPa]
-5.2	130	102

Figure A.28-CID-U38

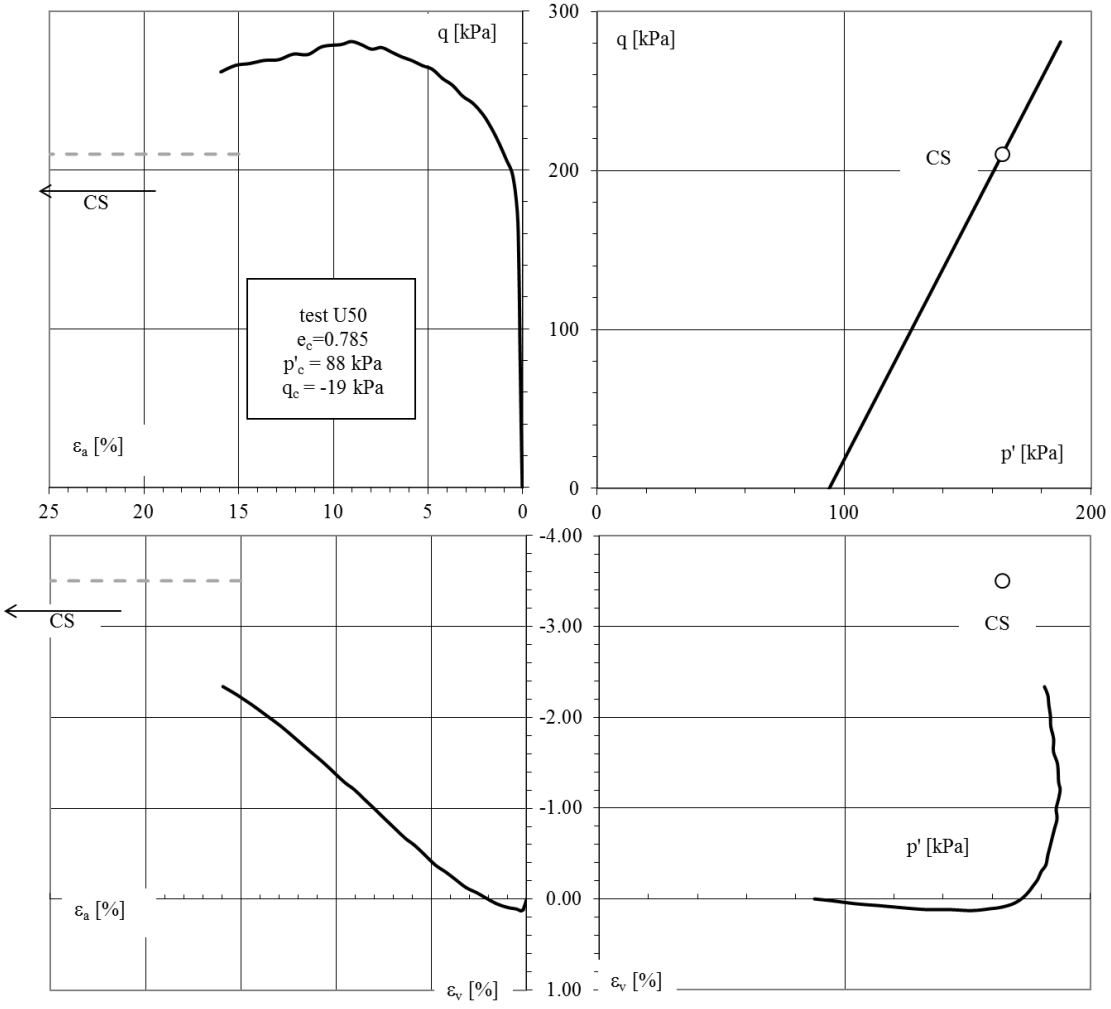

Critical State		
ε_v [%]	q [kPa]	p' [kPa]
-3.5	210	164

Figure A.29-CID-U50

DRAINED AND UNDREAINED GOLDER ASSOCIATED TESTs

Drained and undrained tests published by Been (1991) [Golder Associates] are used in the present thesis in order to determine the critical state line for Ticino sand. Two drained and four undrained tests are selected and the characteristics of the tests and the initial state conditions are reported in Table A.3.

Samples were reconstituted with the wet-tamping method, a reconstitution technique that closely simulates field compaction systems.

This methodology consists in pouring in the mold pre-weighed and oven-dried sand mixed with usually 5% of water. Sand is deposed by hand in five or six layers keeping the height of fall constant; at each stage of the lifts, tamping is applied lightly with a small flat tamper. The energy and the numbers of tamping determinate the variation of relative density in the sample: considering the capillarity effects and using a very small amount of energy, the moist sand can be placed in very loose configurations, well in excess of the maximum void ratio of the dry sand determined by ASTM or JSSMFE methods.

Test	Sample B x H [cm x cm]	Type	Stress path	Sourse	Depositional Method	Failure mode	e_c * [-]	σ'_{vc} [kPa]	σ'_{hc} [kPa]	p'_c [kPa]	q'_c [kPa]	OCR/R [-]
CID_C262	-	CID	σ_3=cost	GOLDER	MT	-	0.851	200	200	200	0	1
CID_C263		CID	σ_3=cost	GOLDER	MT	-	0.781	200	200	200	0	1
LIQ_1101	-	CIU	σ_3=cost	GOLDER	MT	-	0.867	308	308	308	0	1
LIQ_1103		CIU	σ_3=cost	GOLDER	MT	-	0.877	302	302	302	0	1
LIQ_1105		CIU	σ_3=cost	GOLDER	MT	-	0.898	279	279	279	0	1
LIQ_1106		CIU	σ_3=cost	GOLDER	MT	-	0.850	504	504	504	0	1

* e_{max} = 0.923; e_{min} = 0.574

Table A.3- Undrained and drained triaxial tests on Ticino sand [Been, 1991]

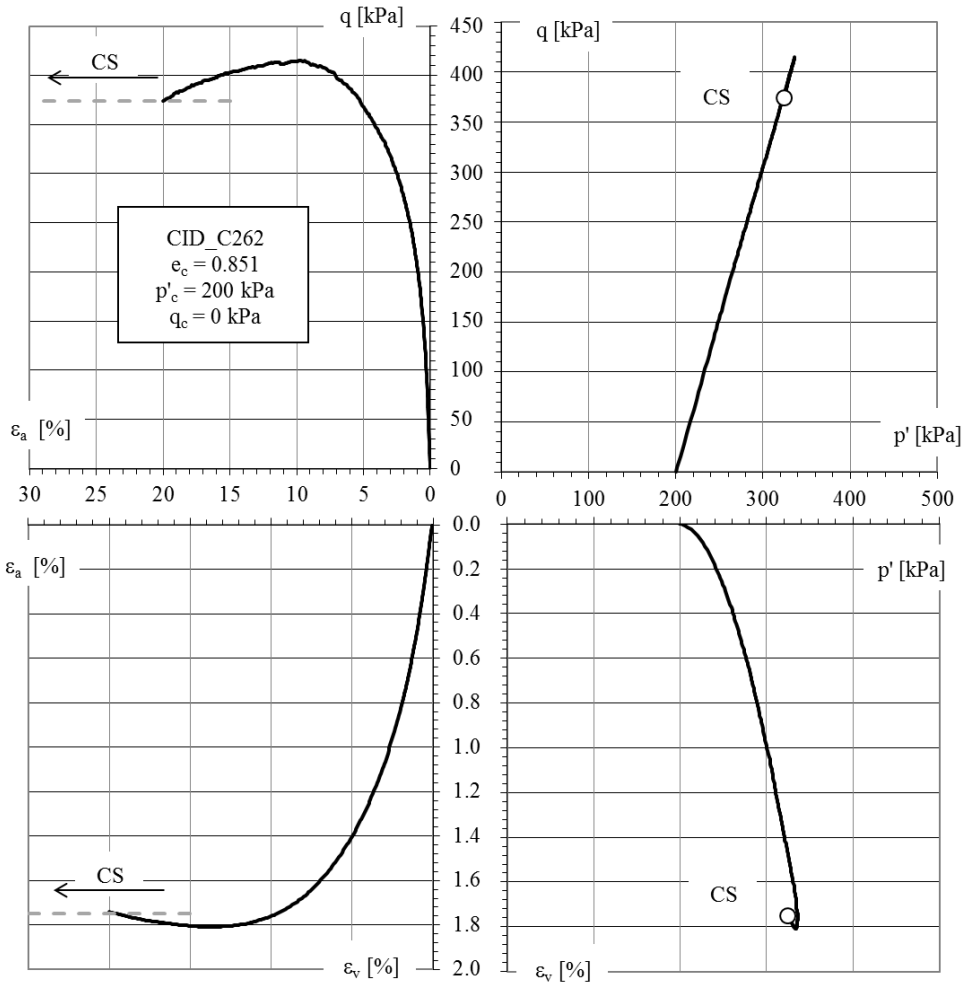

Critical State		
ε_v [kPa]	q [kPa]	p' [kPa]
1.75	374	325

Figure A.30-CID-C262

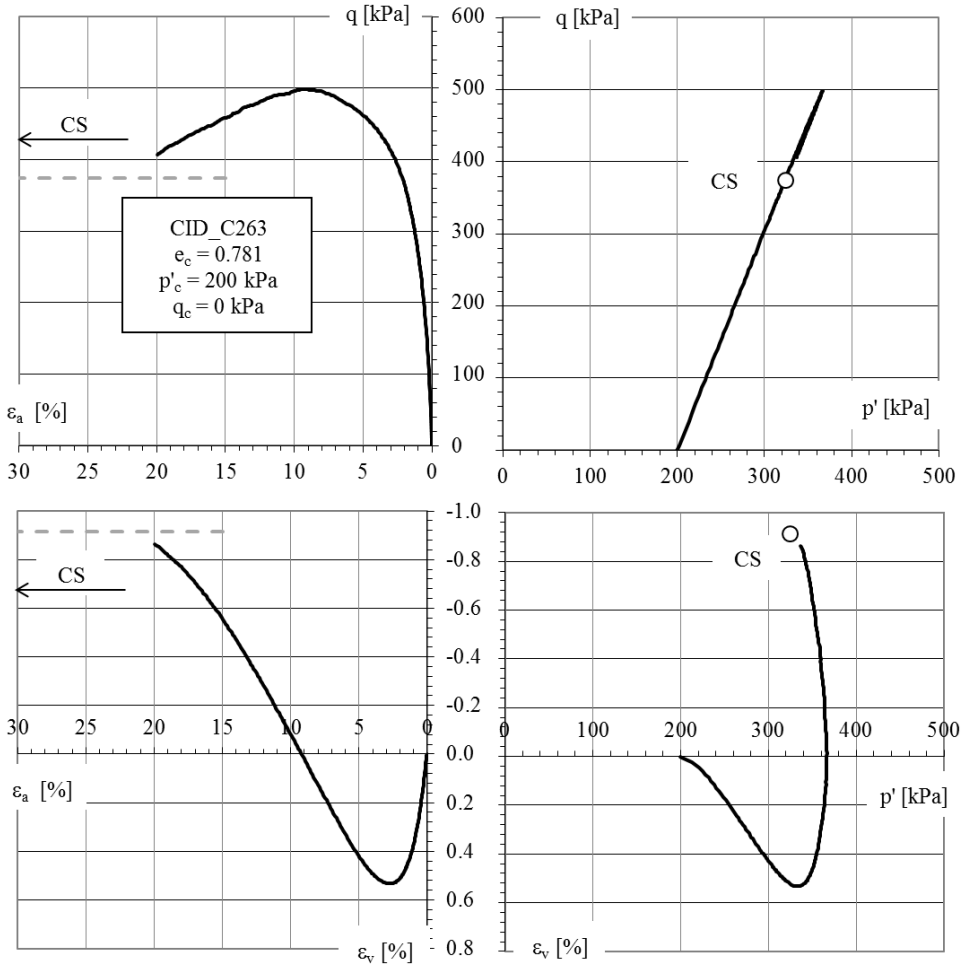

Critical State		
ε_v [kPa]	q [kPa]	p' [kPa]
-0.91	374	337

Figure A.31-CID-C263

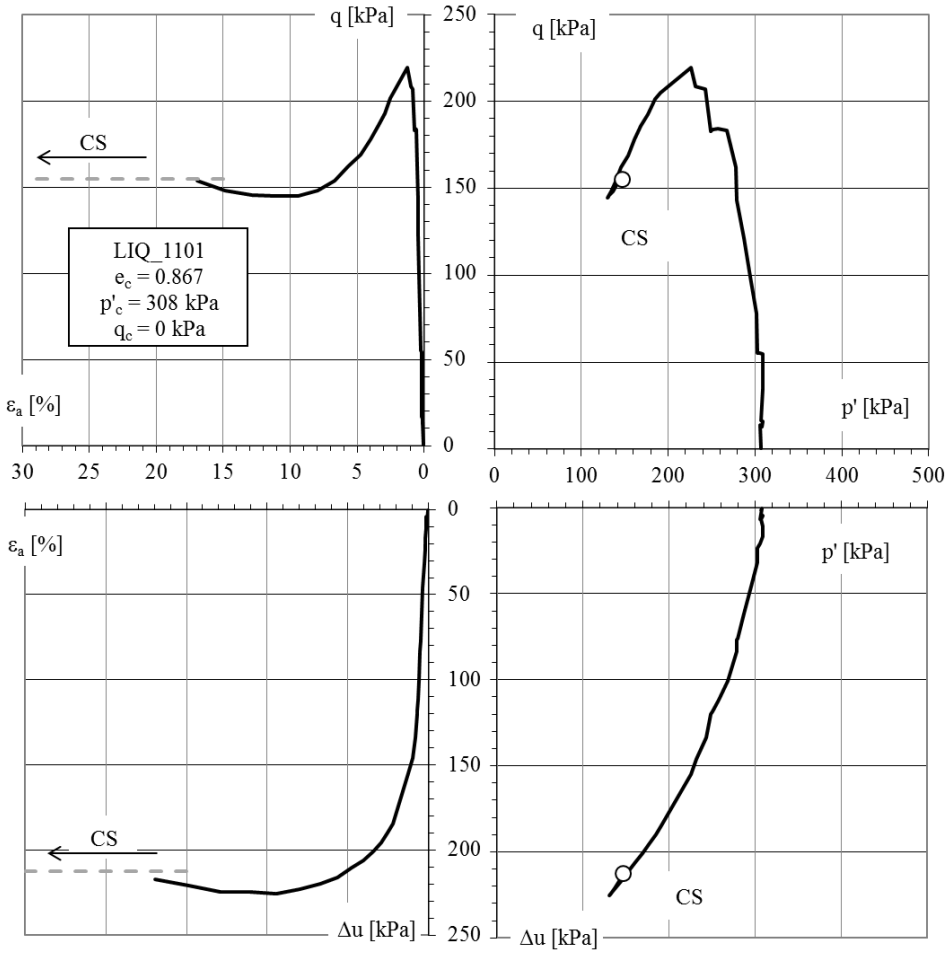

Critical State		
Δu [kPa]	q [kPa]	p' [kPa]
213	155	147

Figure A.32-LIQ-1101

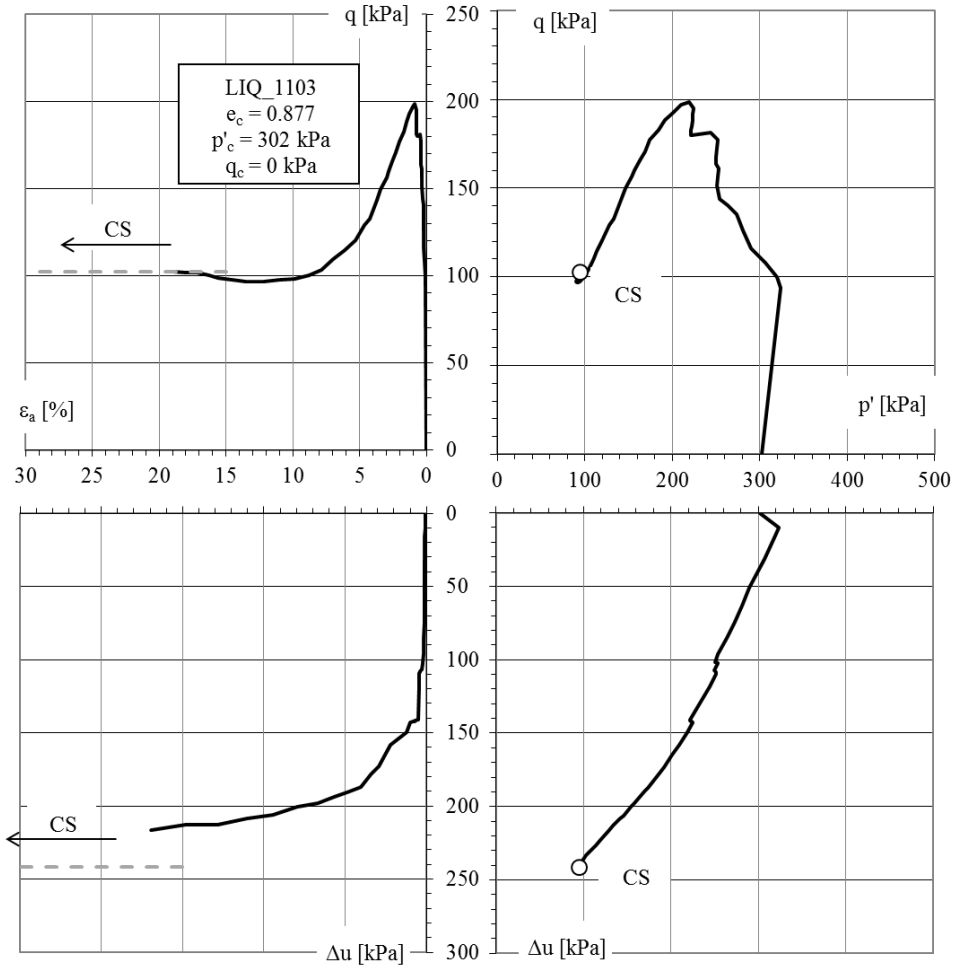

Critical State		
Δu [kPa]	q [kPa]	p' [kPa]
242	103	95

Figure A.33-LIQ-1103

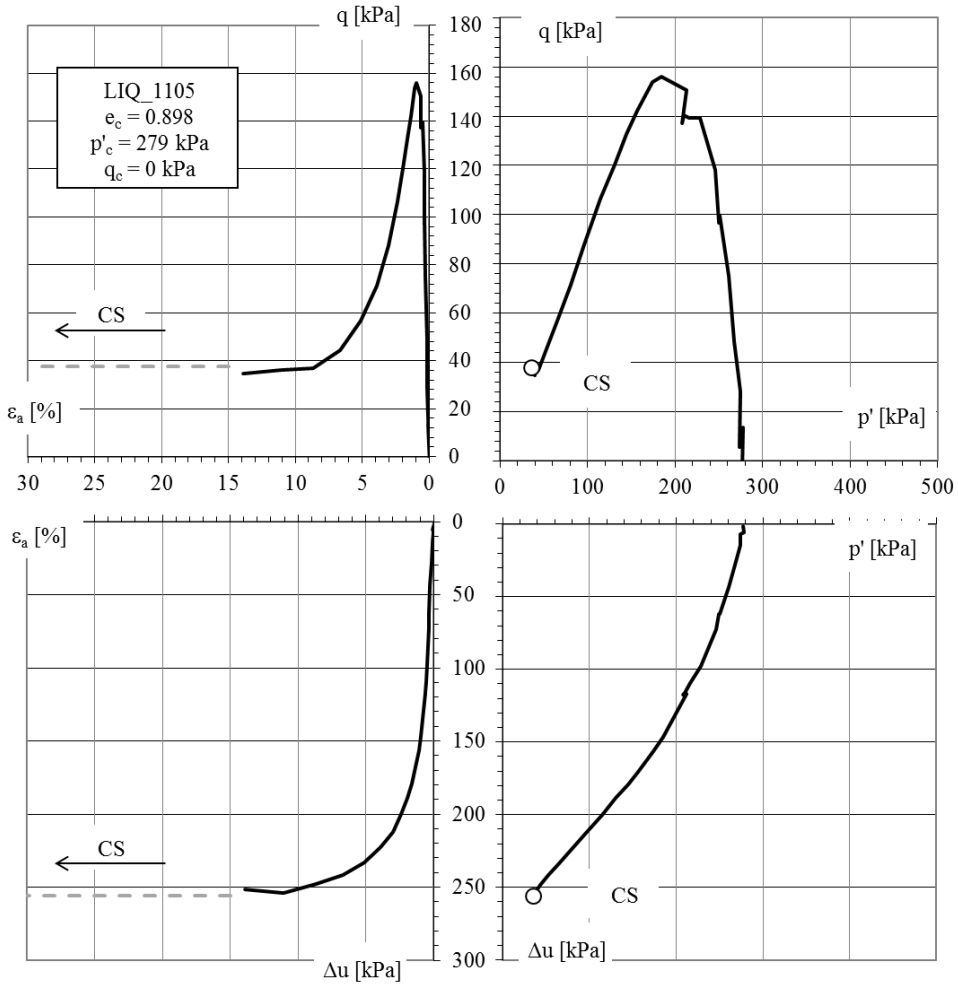

Critical State		
Δu [kPa]	q [kPa]	p' [kPa]
256	38	36

Figure A.34-LIQ-1105

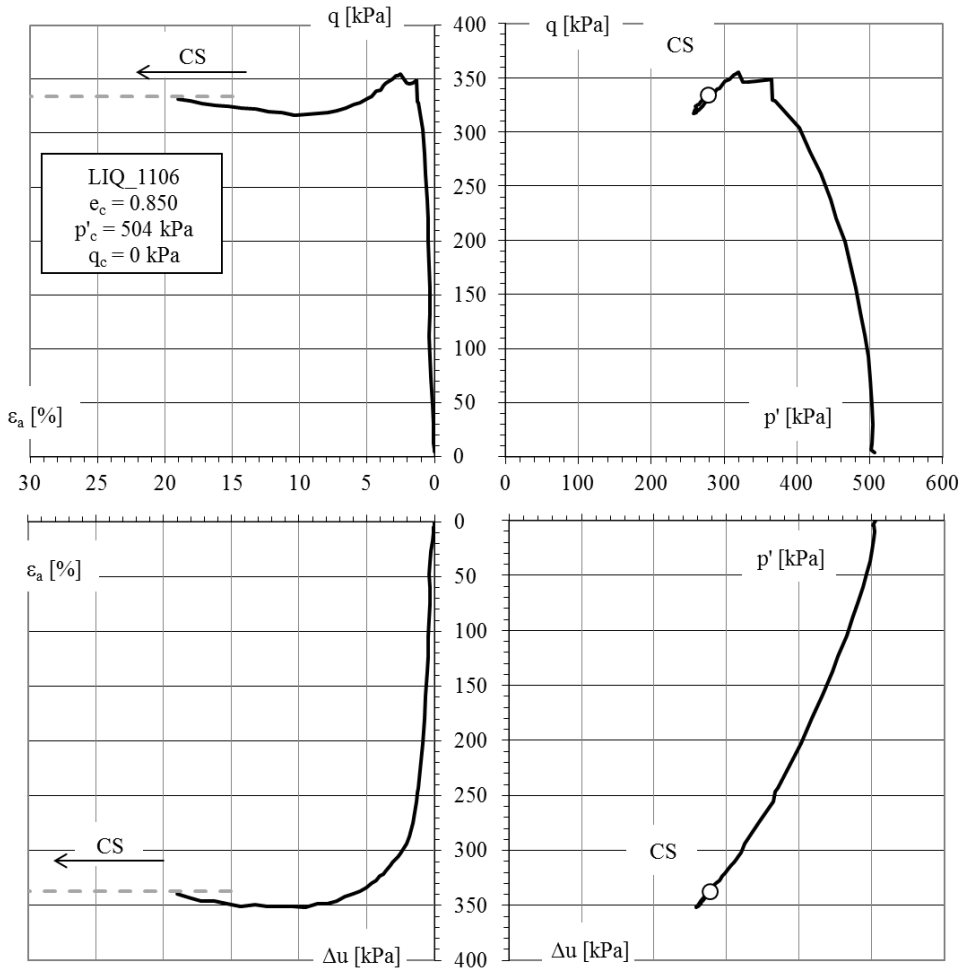

Critical State		
Δu [kPa]	q [kPa]	p' [kPa]
337	334	278

Figure A.35-LIQ-1106

APPENDIX B

Cyclic Triaxial Isotropical Consolidated tests
TICINO SAND

Symbols and abbreviations for triaxial condition:

$q = \sigma'_1 - \sigma'_3 = \sigma_1 - \sigma_3$	deviatoric stress	$[F/L^2]$
$p = (\sigma_1 + 2 \cdot \sigma_3)/3$	mean total stress	$[F/L^2]$
$p' = (\sigma'_1 + 2 \cdot \sigma'_3)/3$	mean effective stress	$[F/L^2]$
$\varepsilon_a = \Delta H/H_0$	axial deformation	[-]
Δu	overburden water pressure	$[F/L^2]$
N	number of cyclic liquefaction	[-]
$R_u = \Delta u/\sigma'_{3c}$	overburden pressure ratio	[-]
ψ_0	initial state parameter	[-]

AP	air pluviation method
WS	water sedimentation method
M_{tc} , M_{te}	critical state stress ratio in compression and extension in q – p' plain
CSR	cyclic stress ratio
CRR	cyclic resistance ratio
Summit "SS" and"TX"	simple shear and triaxial condition

CYCLIC TRIAXIAL TESTs

A total of 17 cyclic triaxial tests are performed on Ticino sand on specimens reconstituted with air pluviation method.

The main information about the dimensions and the source, the initial state of samples and dynamic stresses applied, together with the number of cyclic to liquefaction are summarized in Table B.1.

The results of tests are reported from Figure B.1 to Figure B.17 in four graphs:

- axial deformation ε_a versus number of cycles N;
- overburden water pressure Δu versus number of cyclic N;
- deviatoric stress q versus axial deformation ε_a;
- deviatoric stress q versus mean effective stress p'.

In all graphs are also superimposed with dot white symbol the liquefaction point derived from the analysis.

In Figure B.18 are reported the liquefaction points deduced from the cyclic triaxial tests conducted on Ticino sand: the results are plotted in cyclic stress ratio CSR^{TX} vs. number of cycles to liquefaction N.

Here after, some useful information about test results from Porcino's research. The void ratio at the end of consolidation stage e_c is deduced from the relative density and considering the maximum and minimum void ratio published in Porcino's articles. In order to determine the state parameter the critical state line determined in Chapter 3 is used. In Table B.2 are summarized the main characteristics of the tasted samples, underlined that some data are graphically deduced.

Specimens are reconstituted by water sedimentation method. In this technique mixture of sand and water is poured through the plastic tube in four layers at a constant speed, so that the surface of water is always coincident with that of sand sediment. The sand is deposited continuously under water without causing segregation but, if a denser specimen is to be prepared, compaction energy is applied by hitting the side of the mound.

Test	Sample B x H [cm x cm]	Type of test	Sourse	Depositional Method	e_c * [-]	σ'_{vc} [kPa]	σ'_{hc} [kPa]	p'_c [kPa]	ψ [-]	CSR^{TX} initial [-]	CSR^{TX} ** [-]	CSR^{SS} *** [-]	N [-]	criteria
TS4_13_1	5 x 10	CYC ISO	ISMGeo	AP	0.740	100	100	100	-0.137	0.234	0.201	0.126	6.5	*εa = 5%
TS4_13_4					0.730	100	100	100	-0.147	0.183	0.160	0.100	25.5	*εa = 5%
TS4_13_6					0.700	100	100	100	-0.177	0.181	0.161	0.101	150.5	*εa = 5%
TS4_13_7					0.700	100	100	100	-0.177	0.336	0.330	0.207	4.5	*εa = 5%
TS4_13_8					0.640	100	100	100	-0.237	0.304	0.310	0.194	14.5	*εa = 5%
TS4_13_9					0.640	100	100	100	-0.237	0.243	0.241	0.151	12.5	*Ru = 0.95
TS4_13_11					0.760	200	200	200	-0.099	0.285	0.288	0.180	1.5	*εa = 5%
TS4_13_13					0.760	100	100	100	-0.117	0.253	0.252	0.158	3.5	*εa = 5%
TS4_13_14					0.730	100	100	100	-0.147	0.207	0.157	0.098	15.5	*εa = 5%
TS4_13_15					0.730	100	100	100	-0.147	0.162	0.125	0.078	617.8	*εa = 5%
TS4_13_17					0.700	100	100	100	-0.177	0.330	0.320	0.201	8.5	*εa = 5%
TS4_13_20					0.644	100	100	100	-0.233	0.198	0.166	0.104	27.5	*Ru = 0.95
TS4_13_23					0.707	100	100	100	-0.171	0.244	0.220	0.138	8.5	*εa = 5%
TS4_14_01					0.586	100	100	100	-0.291	0.414	0.411	0.258	85.0	*Ru = 0.95
TS4_14_02					0.580	100	100	100	-0.297	0.288	0.278	0.175	220.0	*Ru = 0.95
TS4_14_03					0.581	100	100	100	-0.297	0.208	0.172	0.108	920.0	*Ru = 0.95
TS4_14_04					0.582	100	100	100	-0.295	0.391	0.385	0.242	120.0	*Ru = 0.95

* e_{max} = 0.923; e_{min} = 0.574

at ε_a = 5% or R_u = 0.95, *$CSR^{SS} = (1+2\,k_0)/3 \cdot CSR^{TX}$

Table B.1- ISMGeo cyclic triaxial tests

Test	Sample B x H [cm x cm]	Type	Sourse	Depositional Method	e_c * [-]	σ'_{vc} [kPa]	ψ ** [-]	CSR^{SS} [-]	N (SA 3.75%) [-]
1	8 x 2	CYC - K0	Reggio Calbria University	WS	0.000	100	-0.887	0.255	2.0
2					0.000	100	-0.887	0.195	4.0
3					0.000	100	-0.887	0.160	8.0
4					0.000	100	-0.887	0.100	80.0
5					0.000	100	-0.887	0.300	5.0
6					0.000	100	-0.887	0.250	5.1
7					0.000	100	-0.887	0.200	10.3
8					0.000	100	-0.887	0.160	65.0

* e_{max} = 0.905; e_{min} = 0.559, ** $\sigma'_{h0} = k_{0,field}\ \sigma'_{v0}$

Table B.2- Porcino's simple shear tests

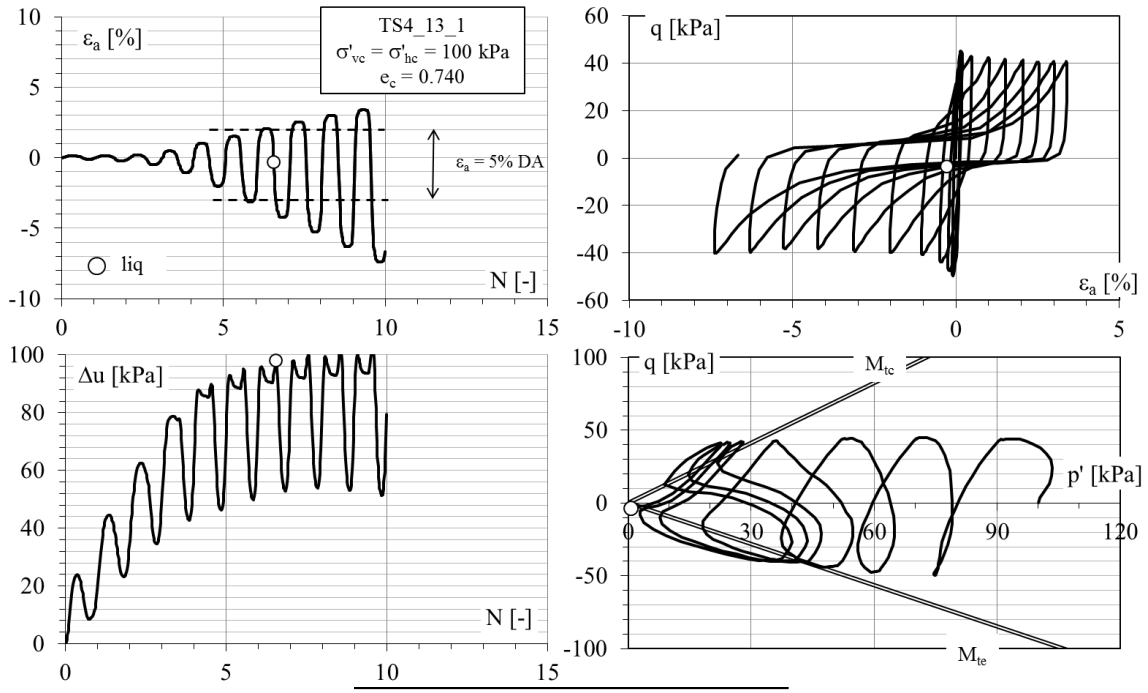

point of liquefaction		
CSR^{TX}*	N**	R_u**
-	-	-
0.201	6.5	0.97

*at cyclic liquefaction point,**DA 5%

Figure B.1-CYC ISO TS4_13_1

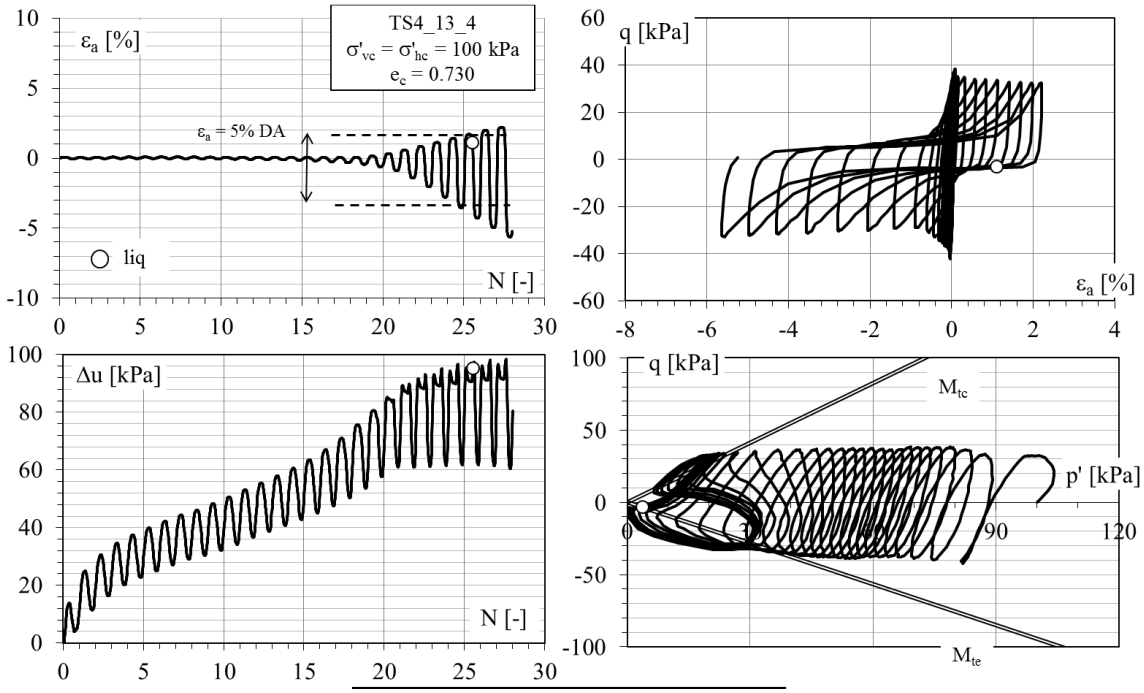

point of liquefaction		
CSR^{TX}*	N**	R_u**
-	-	-
0.160	25.5	0.97

*at cyclic liquefaction point,**DA 5%

Figure B.2-CYC ISO TS4_13_4

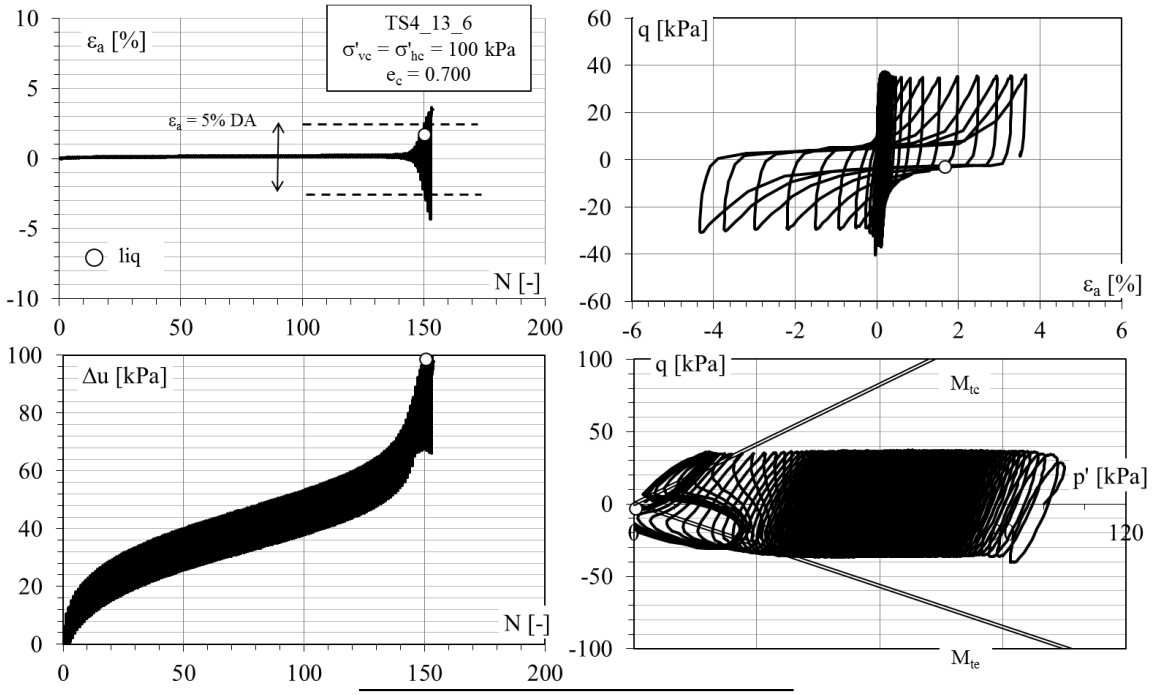

point of liquefaction		
CSR^{TX}*	N**	R_u**
-	-	-
0.161	150.5	1.00

*at cyclic liquefaction point,**DA 5%

Figure B.3-CYC ISO TS4_13_6

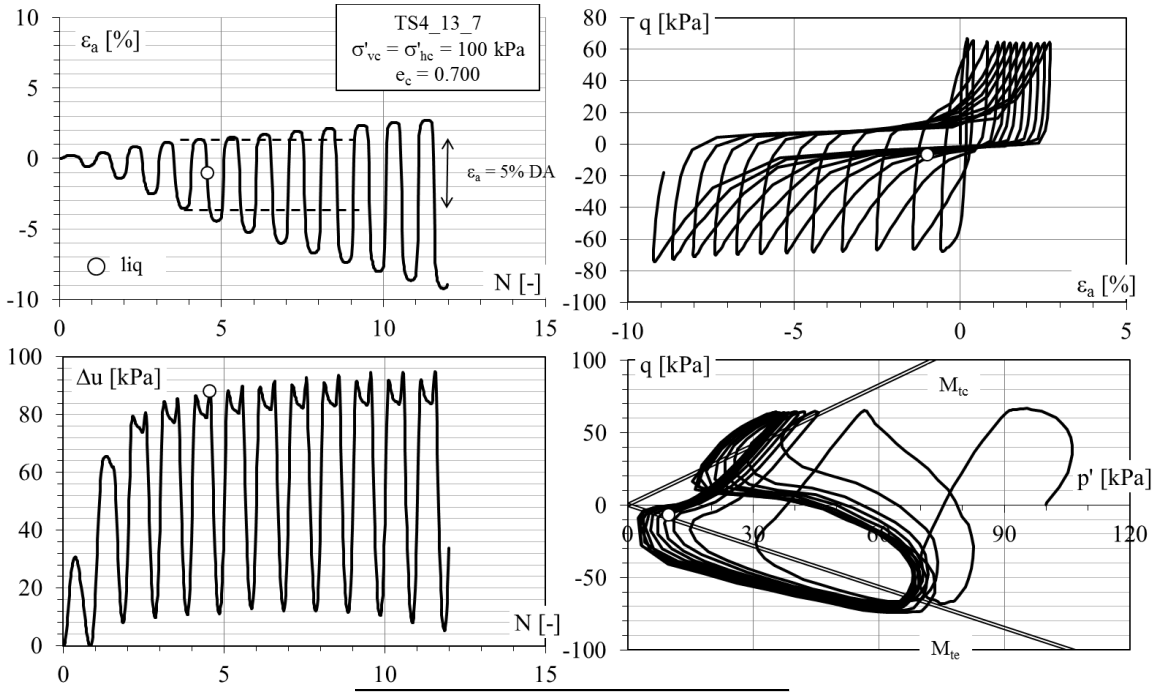

point of liquefaction		
CSR^{TX}*	N**	R_u**
-	-	-
0.330	4.5	0.88

*at cyclic liquefaction point,**DA 5%

Figure B.4- CYC ISO TS4_13_7

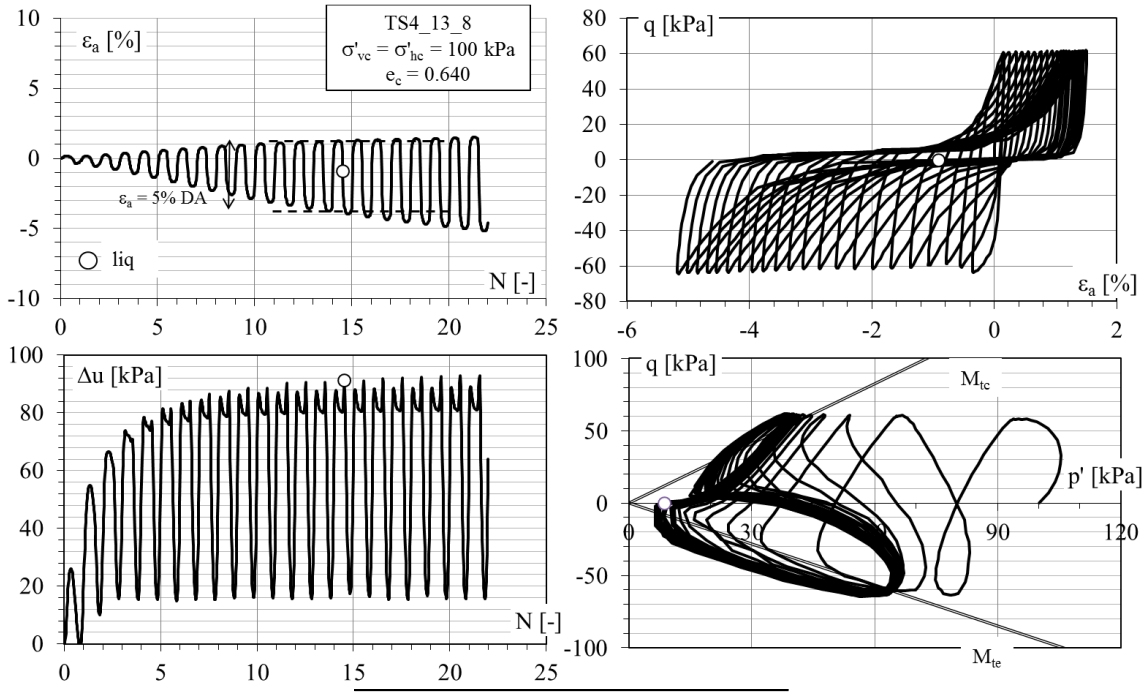

point of liquefaction		
CSR^{TX}*	N**	R_u**
-	-	-
0.310	14.5	0.91

*at cyclic liquefaction point,**DA 5%

Figure B.5-CYC ISO TS4_13_8

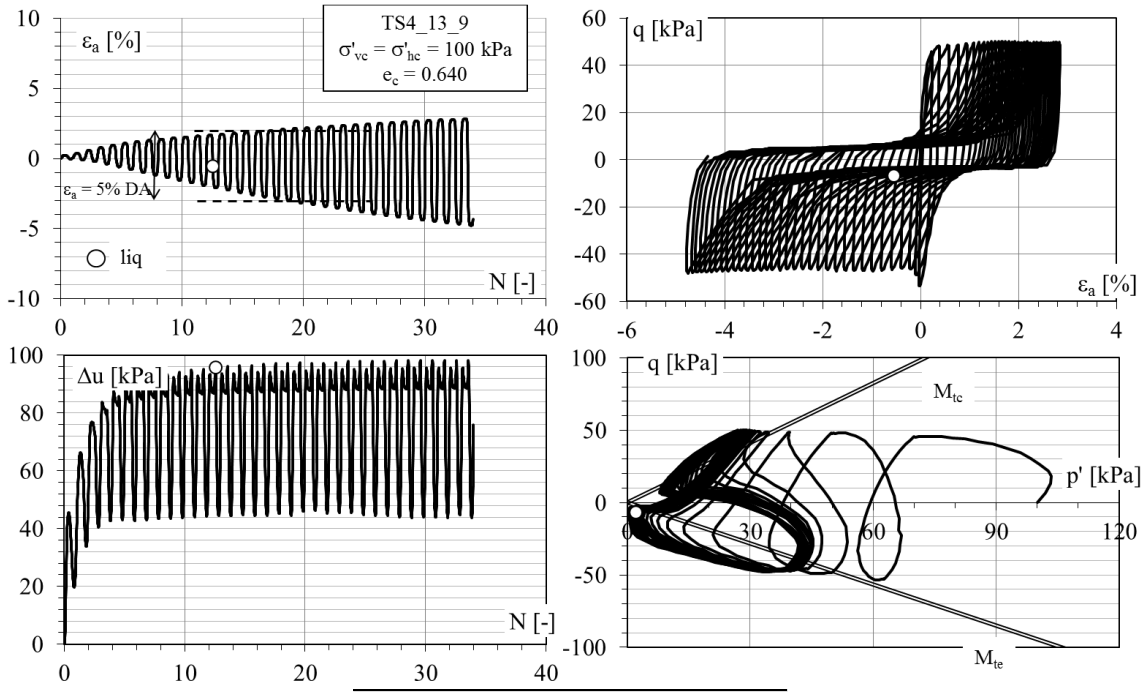

point of liquefaction		
CSR^{TX}*	N**	ε_a**
-	-	%
0.241	12.5	3.50

*at cyclic liquefaction point,**Ru = 0.95

Figure B.6-CYC ISO TS4_13_9

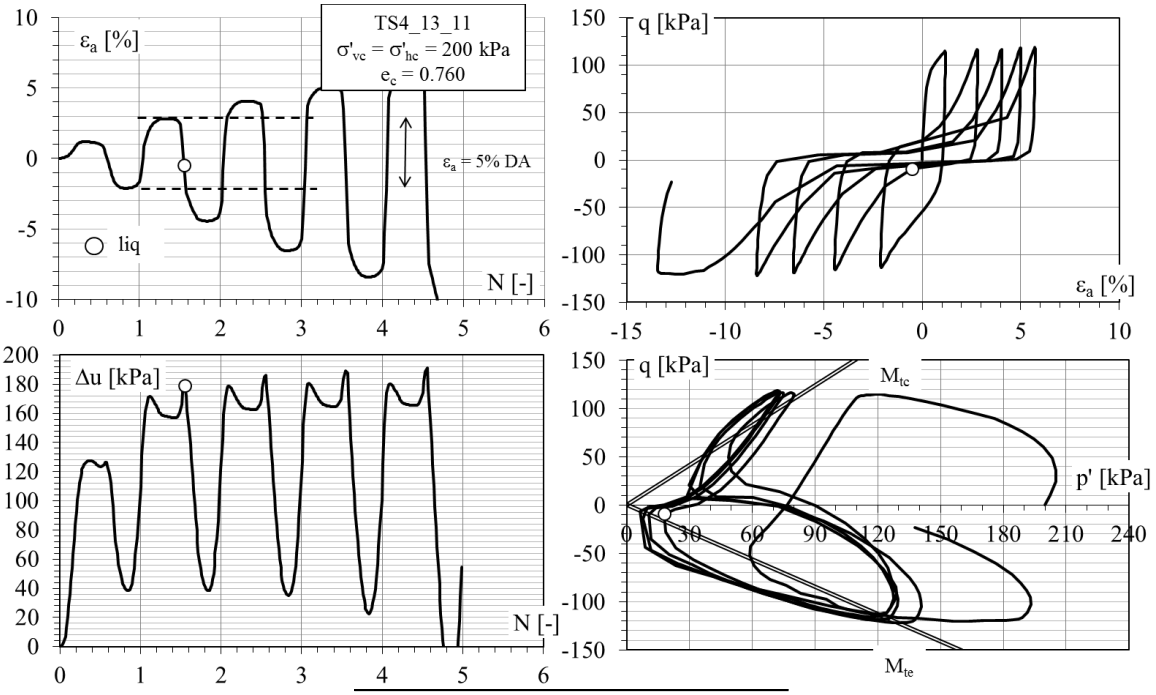

point of liquefaction		
CSR^{TX}*	N**	R_u**
-	-	-
0.288	1.5	0.80

*at cyclic liquefaction point,**DA 5%

Figure B.7-CYC ISO TS4_13_11

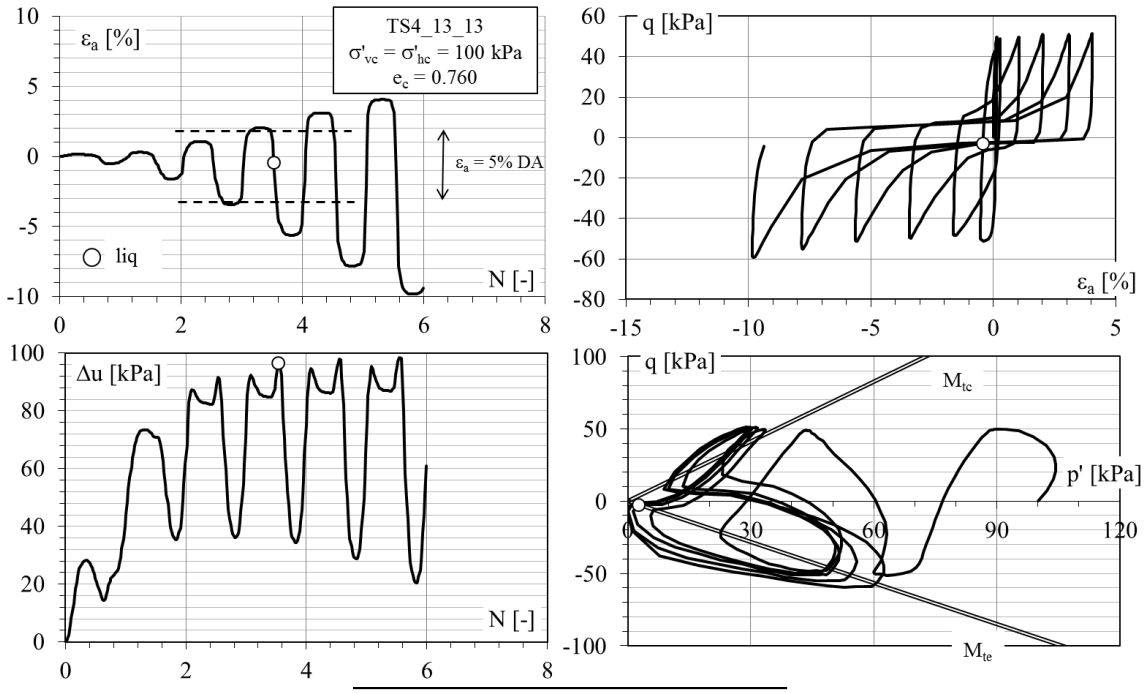

point of liquefaction		
CSR^{TX}*	N**	R_u**
-	-	-
0.252	3.5	0.96

*at cyclic liquefaction point,**DA 5%

Figure B.8-CYC ISO TS4_13_13

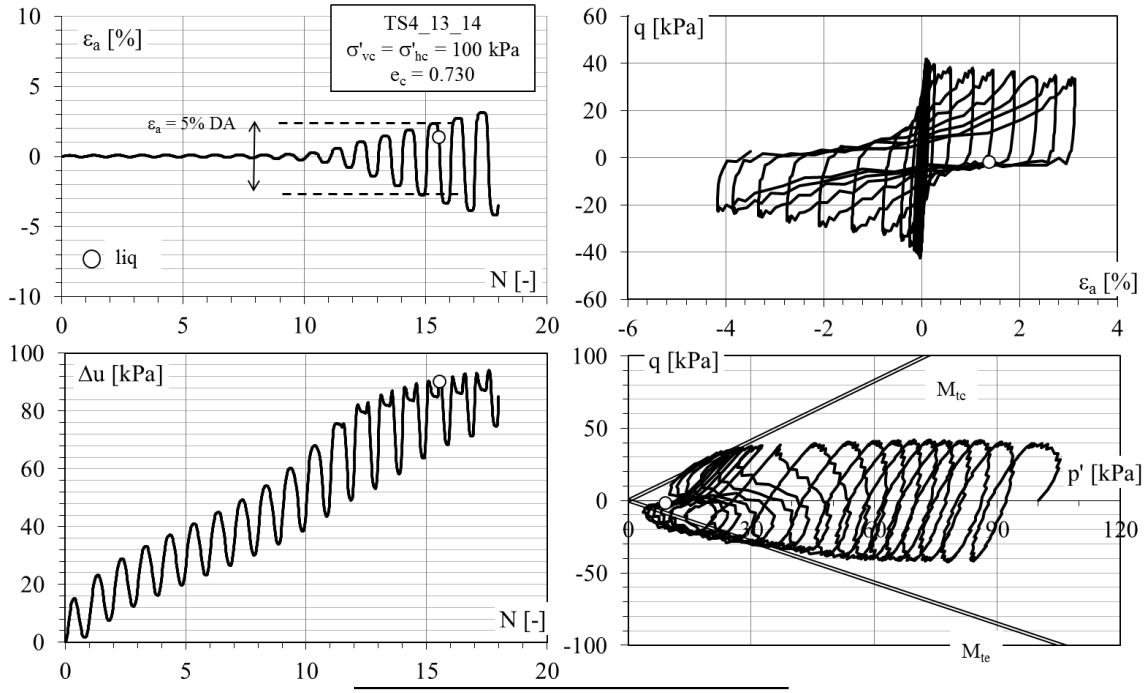

point of liquefaction		
CSR^{TX}*	N**	R_u**
-	-	-
0.157	15.5	0.90

*at cyclic liquefaction point,**DA 5%

Figure B.9-CYC ISO TS4_13_14

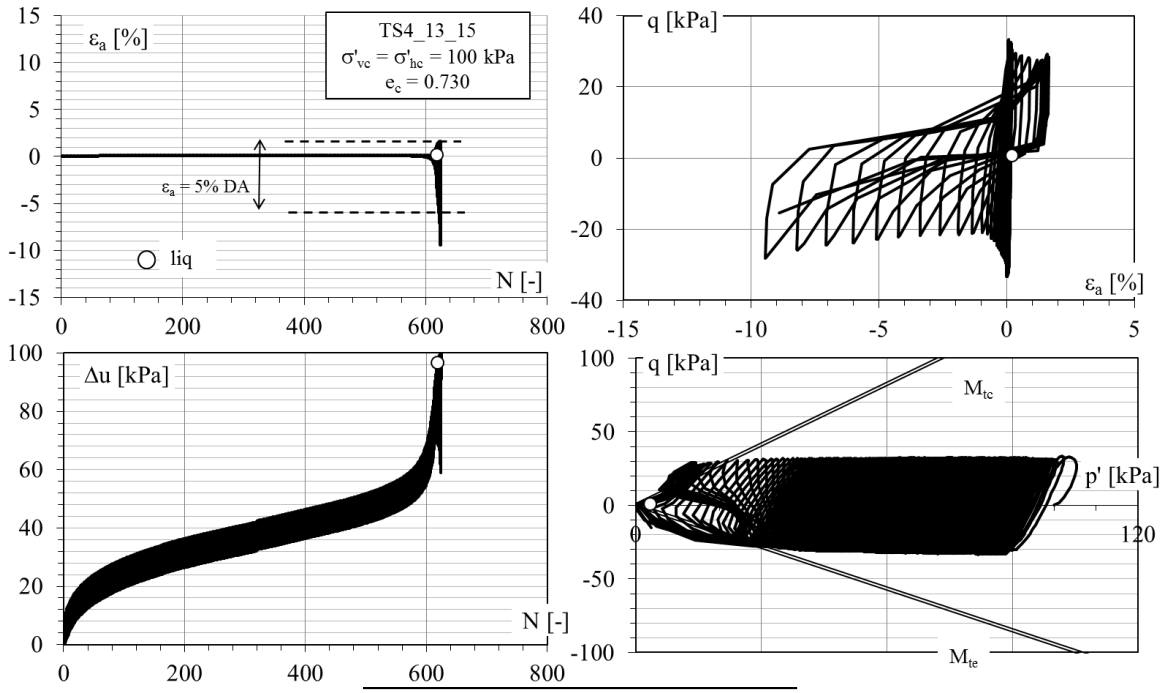

point of liquefaction		
CSR^{TX}*	N**	R_u**
-	-	-
0.125	617.8	0.95

*at cyclic liquefaction point,**DA 5%

Figure B.10-CYC ISO TS4_13_15

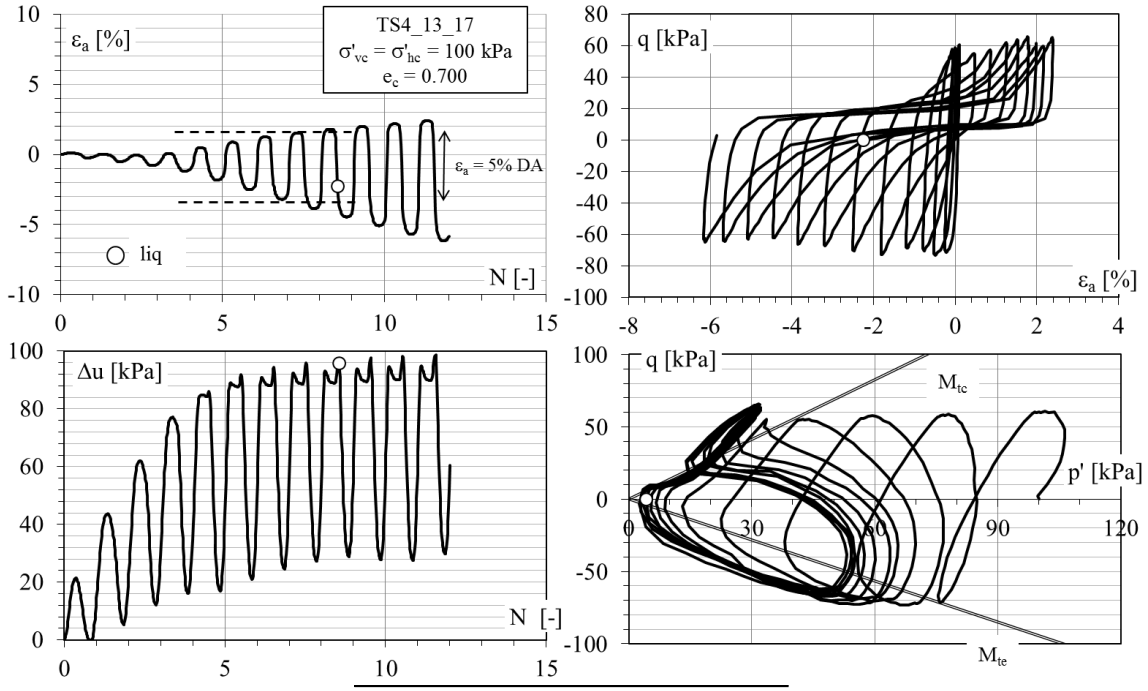

point of liquefaction		
CSR^{TX}*	N**	R_u**
-	-	-
0.320	8.5	0.95

*at cyclic liquefaction point,**DA 5%

Figure B.11-CYC ISO TS4_13_17

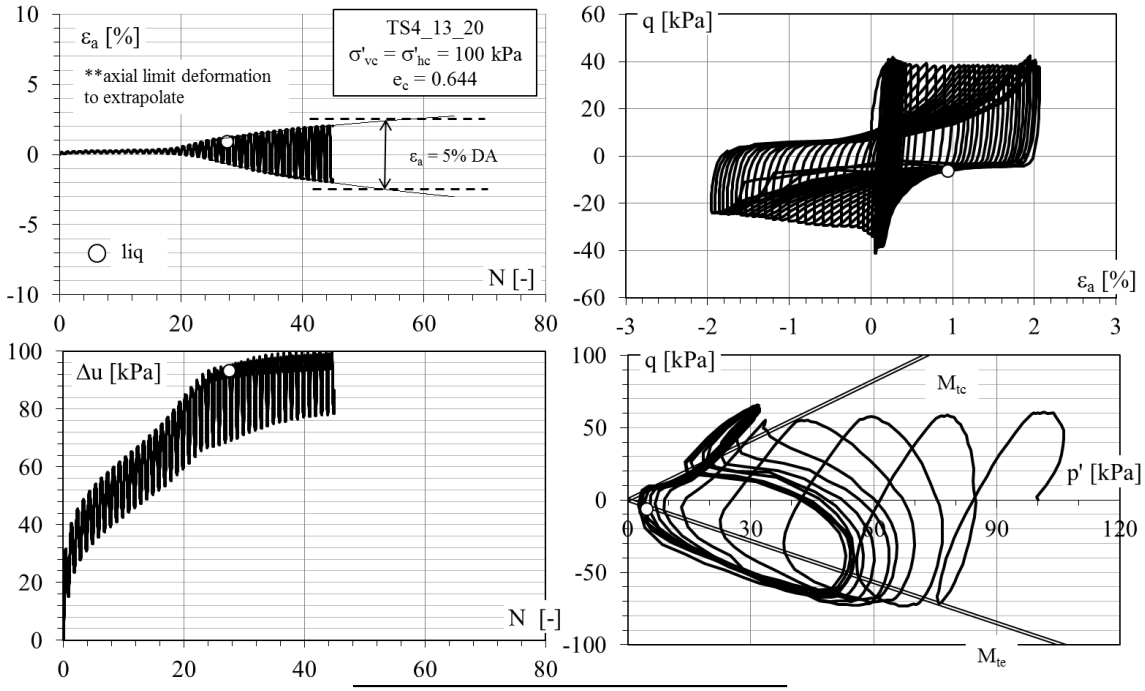

point of liquefaction		
CSR^{TX}*	N**	ε_a**
-	-	%
0.166	27.5	1.80

*at cyclic liquefaction point,**Ru = 0.95

Figure B.12-CYC ISO TS4_13_20

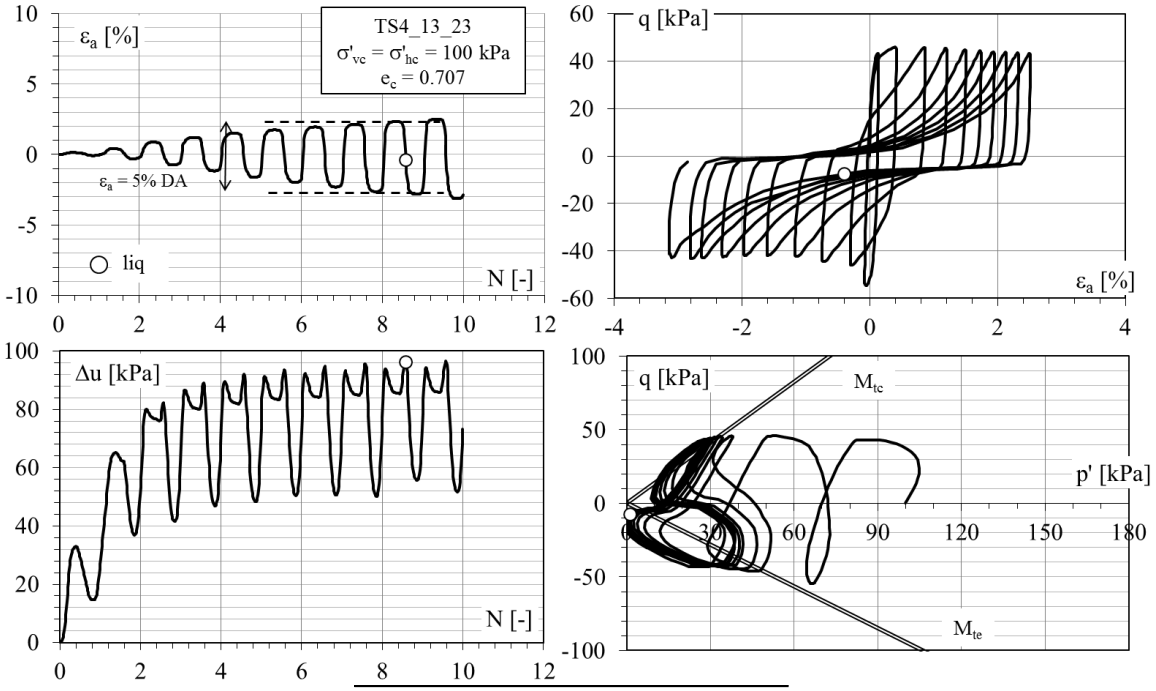

point of liquefaction		
CSR^{TX}*	N**	R_u**
-	-	-
0.220	8.5	0.96

*at cyclic liquefaction point,**DA 5%

Figure B.13-CYC ISO TS4_13_23

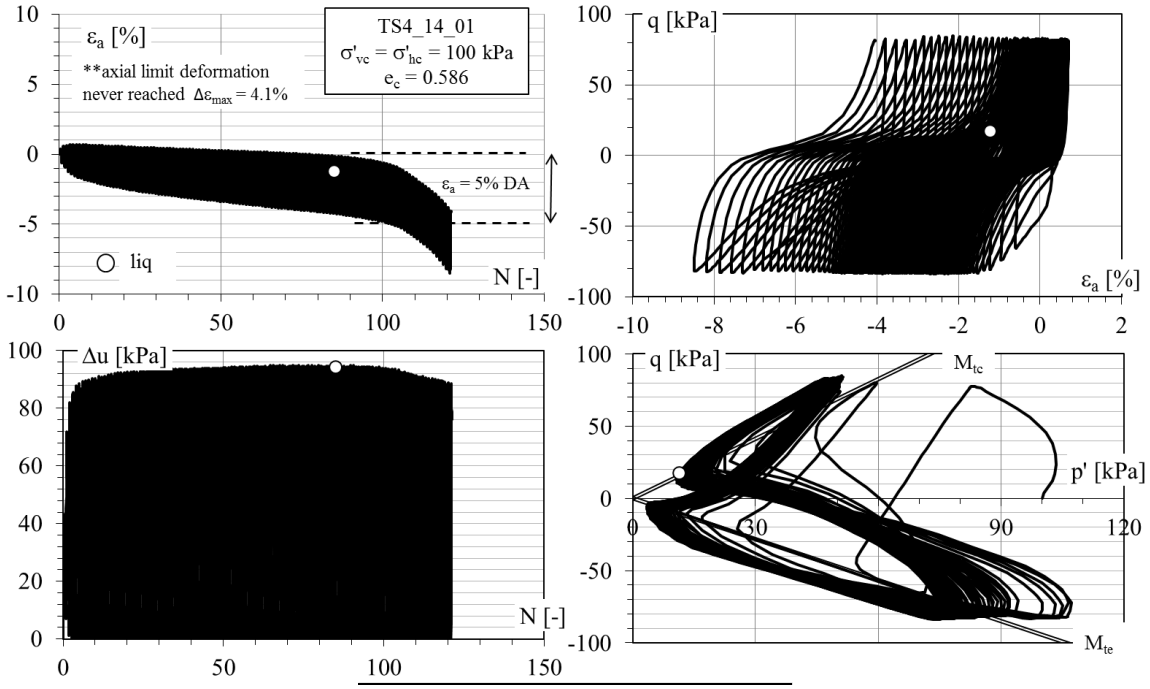

point of liquefaction		
CSR^{TX}*	N**	ε_a**
-	-	%
0.411	85.0	4.10

*at cyclic liquefaction point,**Ru = 0.95

Figure B.14-CYC ISO TS4_14_01

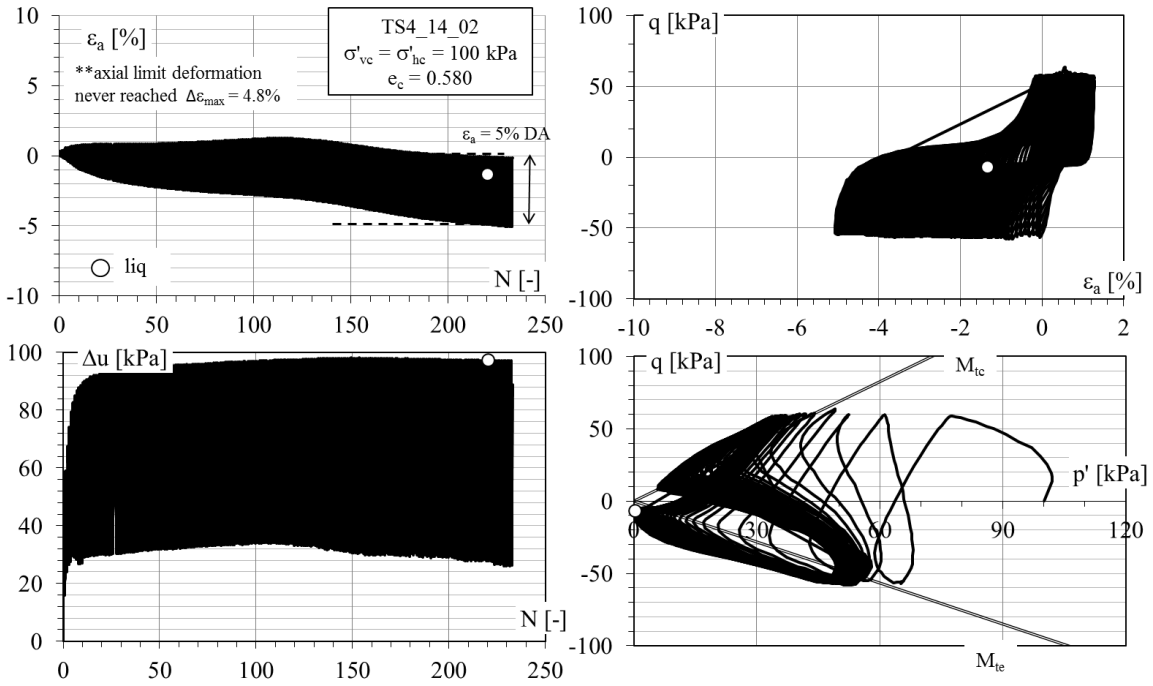

point of liquefaction		
CSR^{TX}*	N**	ε_a**
-	-	%
0.278	220.0	4.80

*at cyclic liquefaction point,**Ru = 0.95

Figure B.15-CYC ISO TS4_14_02

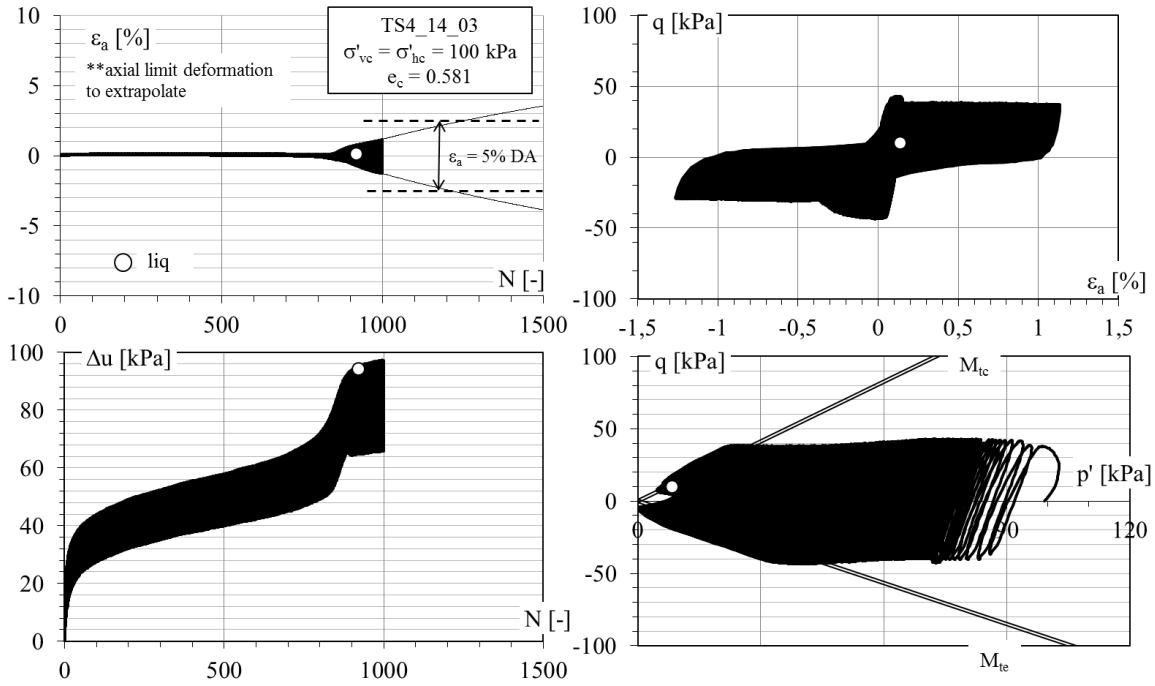

point of liquefaction		
CSR^{TX}*	N**	ε_a**
-	-	%
0.172	920.0	1.50

*at cyclic liquefaction point,**Ru = 0.95

Figure B.16-CYC ISO TS4_14_03

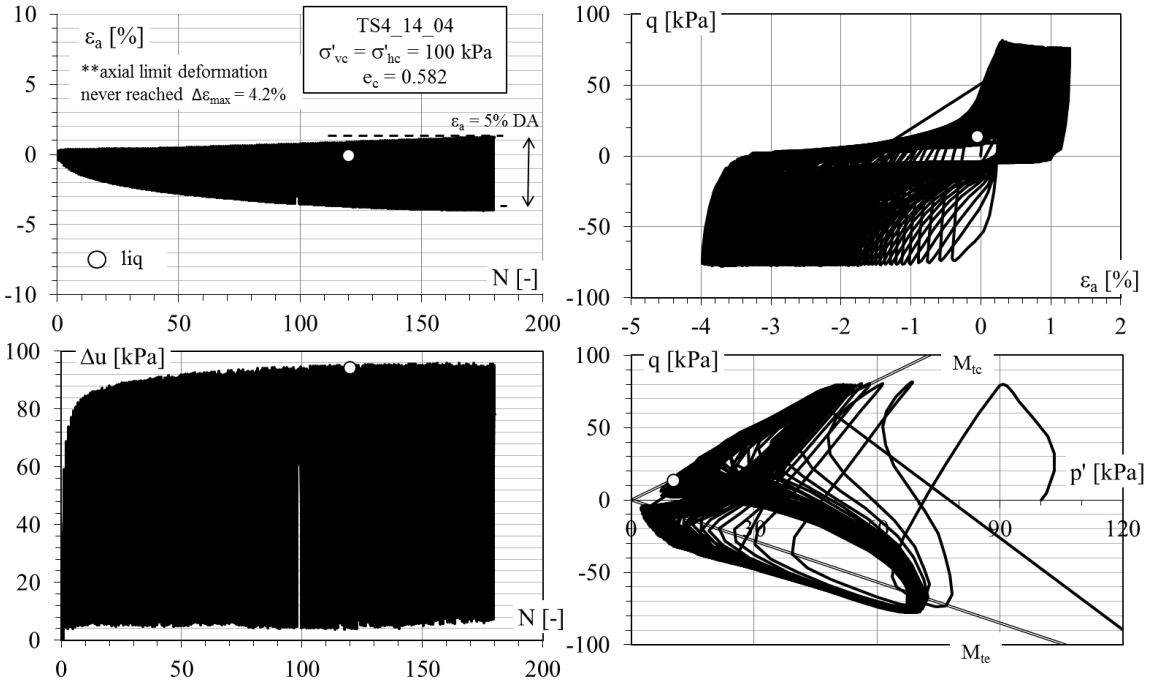

point of liquefaction		
CSR_{TX}*	N**	ε_a**
-	-	%
0.385	120.0	4.20

*at cyclic liquefaction point,**Ru = 0.95

Figure B.17-CYC ISO TS4_14_04

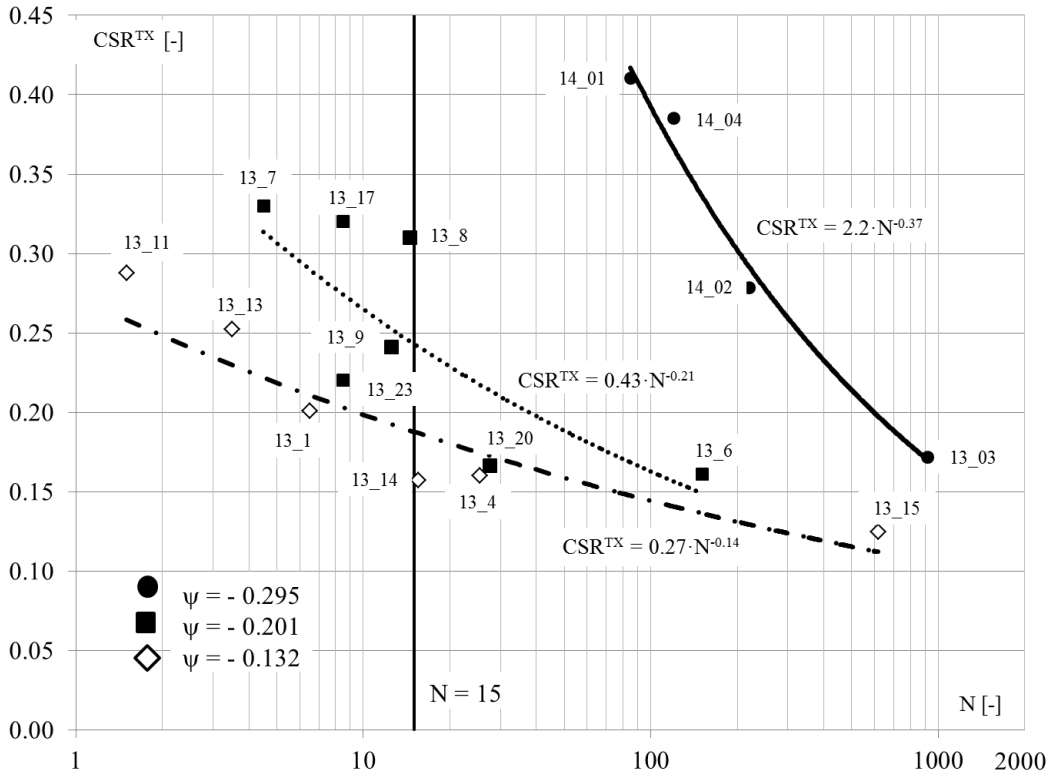

Figure B.18-Cyclic triaxial tests results for Ticino sand